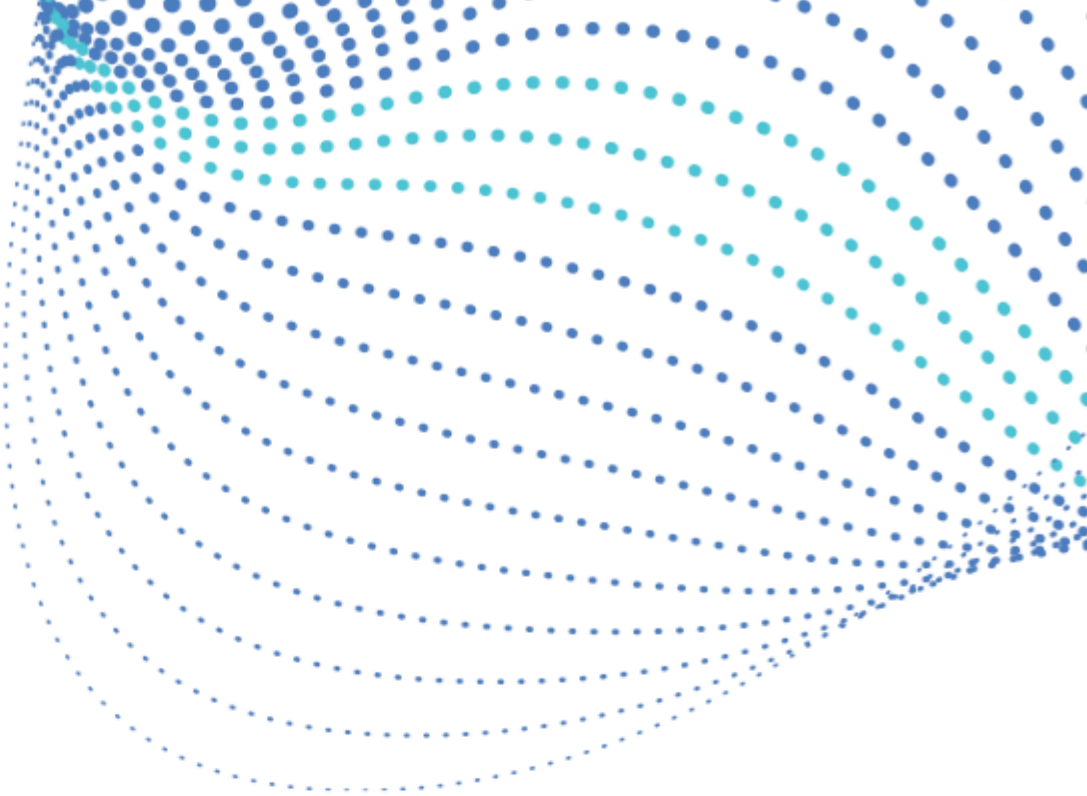

Verisk™

Verisk Severe Thunderstorm Model for the United States

Publication Date: July 2022

Revision History

Date	Description
June 2022	Original document release.
July 12, 2022	Updated the "Comparison of Verisk-modeled and PCS industry gross insured average AOL and occurrence return periods for the U.S., for all lines of business" figure.
February 8, 2023	Fixed two typos in Appendix B: Temporal Vulnerability Changes
March 10, 2023	Clarified details regarding the 10K cat-only stochastic catalog supported by Touchstone Re in Section 1.6, Section 8.1, and Appendix A.

Table of Contents

List of Figures

List of Tables

1 Facts at a Glance

1.1 Model abstract

The Verisk Severe Thunderstorm Model for the United States simulates losses resulting from straight-line winds, hail, and tornadoes on insured properties in the lower 48 states plus Washington D.C. The model captures the spatial extent of both large atmospheric systems and the highly localized effects of individual hailstorms, straight-line convective windstorms, and tornadoes by simulating daily activity based on realistic historical occurrence rates and weather patterns for a specific location and season.

The event generation module combines statistical and physical methods to determine the annual frequency, intensity, and location of simulated severe thunderstorms. The module is built based on historical data from the National Oceanic and Atmospheric Administration's (NOAA's) Storm Prediction Center (SPC), NOAA's National Weather Service (NWS) Radar Operations Center (ROC), and NOAA's National Centers for Environmental Information (NCEI).

The model's engineering component relates event intensity (wind speed or hail impact energy) to physical damage by means of damage functions, which provide an estimate of mean damage ratio as a function of event intensity. The financial module translates damage into financial loss. Ground-up losses are calculated by applying the appropriate damage function to the replacement value of the insured property, while gross insured losses are determined by applying policy conditions and take-up rates to the ground-up loss estimates. The Verisk model accounts for policy conditions specific to the United States and meets the wide spectrum of risk management needs of all stakeholders, including the insurance and reinsurance industry.

1.2 Model facts

Model Name	Verisk Severe Thunderstorm Model for the United States
Release Date	June 2022
Software Systems	• Touchstone 2022 (10.0) • Touchstone Re 2022 (10.0)
Model Domain	Conterminous United States (48 states plus D.C.)
Modeled Perils	• Hail • Convective straight-line winds • Tornadoes of at least EF-1 intensity (≥ 86 mph)

Non-Modeled Perils	The impacts of lightning and heavy rainfall (e.g., highly-localized flash flooding and water ingress) on modeled losses are implicitly modeled to the extent they are included in actual reported severe thunderstorm losses to which the model was validated.
Intensity Parameters	• Hail – Hail impact energy (J/m^2) • Convective straight-line winds – Average maximum wind speed (3-sec gust; mph) • Tornadoes – Maximum wind speed (3-sec gust; mph)
Secondary Risk Characteristics (SRCs) for Straight-Line Wind and Tornado Damage Estimation	• Appurtenant Structures • Average Adjacent Building Height • Building Condition • Building Foundation Connection • Certified Structures (IBHS) • Exterior Doors • Floor of Interest • Glass Percentage • Glass Type • Large Missile • Roof Anchorage • Roof Attached Structure • Roof Covering • Roof Covering Attachment • Roof Deck • Roof Deck Attachment • Roof Geometry • Roof Pitch • Roof Year Built • Seal of Approval • Small Debris • Terrain Roughness • Tree Exposure • Wall Attached Structure • Wall Siding • Wall Type • Window Protection

Secondary Risk Characteristics (SRCs) for Hail Damage Estimation	• Certified Structures (IBHS) • Glass Percentage • Glass Type • Roof Attached Structure • Roof Covering • Roof Deck • Roof Geometry • Roof Hail Impact Resistance • Roof Pitch • Roof Year Built • Wall Attached Structure • Wall Siding • Window Protection

Figure 1 shows the modeled conterminous United States (48 states plus D.C.) domain.

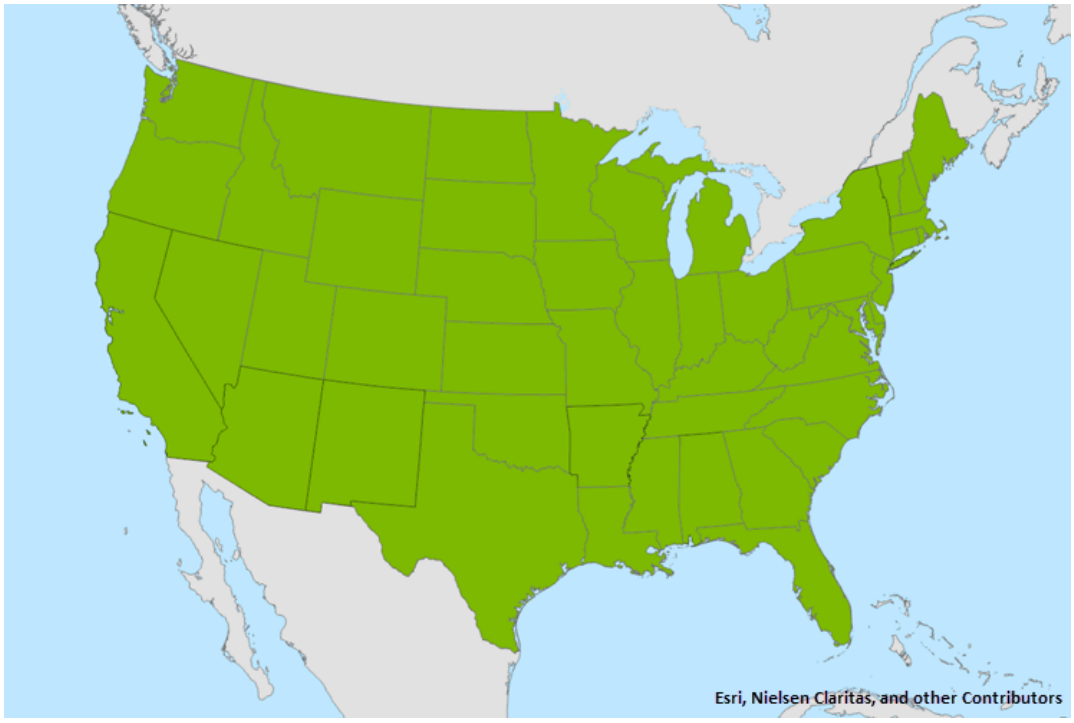

Figure 1. Severe Thunderstorm Model for the United States domain

1.3 Country facts - United States

The following table provides population and gross domestic product (GDP) statistics for the United States of America.[1]

Population	337.3 million (2022 estimate)
GDP	19.85 trillion USD (2020 estimate)
Per capita GDP	60,200 USD (2020 estimate)

The population density map shown in Figure 2 below shows the location of population centers across the United States.

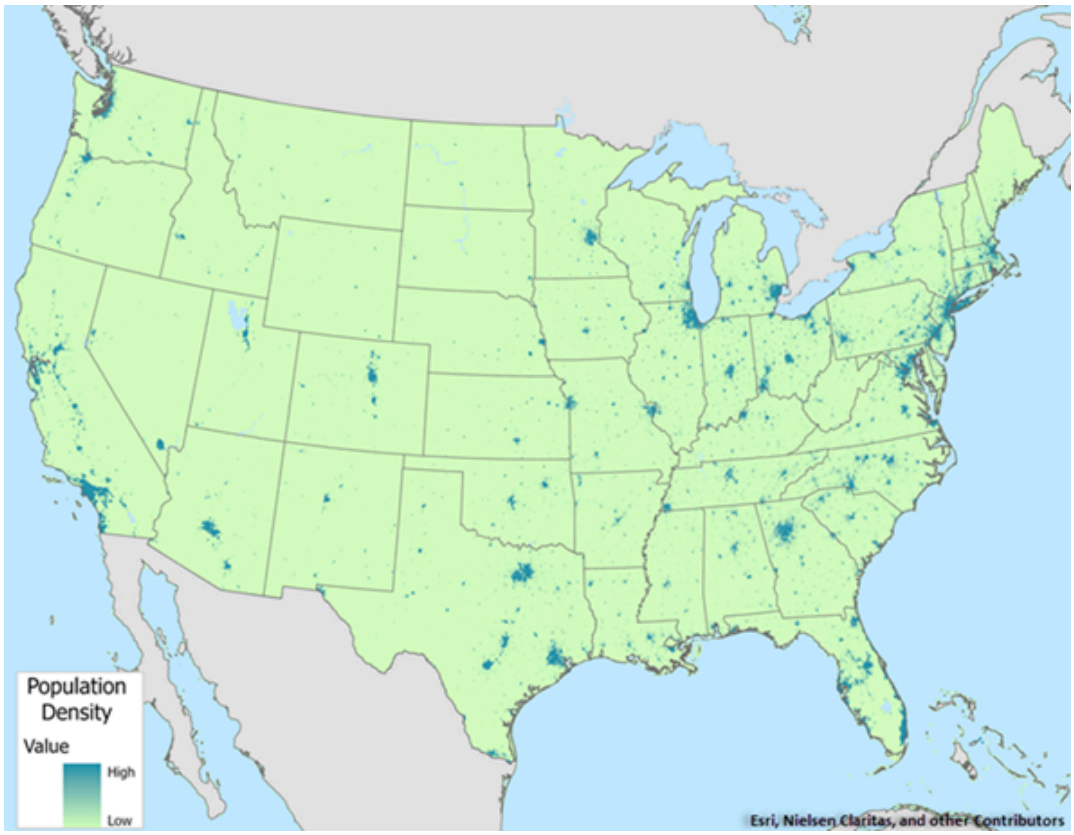

Figure 2. Population density in the continental United States

1.4 Data sources

Verisk used the data sources described below in the development of the Verisk Severe Thunderstorm Model for the United States. Additional details are presented in the component-specific sections of this document.

[1] Data from the CIA World Factbook

See Also
Event generation data sources

Historical catalog

The historical catalog for hail, straight-line winds, and tornadoes produced by severe thunderstorms in the United States includes events as described below. This catalog serves as a basis for the stochastic catalog. Additional details are presented in the component-specific sections of this document.

Number of Events and Date Range	Hundreds of thousands of reports from the: • Storm Prediction Center (SPC; 1979 - 2018) • Community Collaborative Rain, Hail, and Snow (CoCoRaHS) Network (1998 - 2018) • Severe Hazards Analysis and Verification (SHAVE) Project (2006 - 2015) • NOAA's Next Generation Radar (NEXRAD) Radar (Level III Data; 1996 - 2017)
Data Sources	• National Oceanic and Atmospheric Administration's (NOAA's) SPC • NOAA's National Centers for Environmental Information (NCEI) • NOAA's National Centers for Environmental Prediction (NCEP) • NOAA's National Weather Service (NWS) Radar Operations Center (ROC)
Additional Detail	Verisk is not releasing the full historical catalog but will make a subset of events available.

See Also
Event generation data sources

1.5 Industry Exposure Database

Verisk recommends using the Industry Exposure Database for the United States listed below when running the Verisk Severe Thunderstorm Model for the United States in Touchstone Re.

Release date	End of 2019
Resolution	90-m
Vintage	2019

Please refer to the *Verisk Industry Exposure Database for the United States* for details on data sources used to develop the Industry Exposure Database for the model. This document is available with login through the Client Portal.

1.6 Stochastic catalog

The Verisk Severe Thunderstorm Model for the United States supports two 10,000-year (10K), two 50,000-year (50K), and two 100,000-year (100K) stochastic catalogs of simulated severe thunderstorms, as detailed below. While all six catalogs are available in Touchstone, only the 10K cat-only catalog is available in Touchstone Re.[2]

Available Catalogs	• 10K All-events • 10K Cat-only • 50K All-events • 50K Cat-only • 100K All-events • 100K Cat-only
Total Number of Modeled Events (10K All-Events Catalog)	• 2,278,221 (2,216,817 of which impact Verisk's Industry Exposure Database) • Hail = 77,005,148 • Wind = 47,423,952 • Tornado = 11,977,679
Total Number of Modeled Events (10K Cat-Only Catalog)	• 839,363 (all impact Verisk's Industry Exposure Database) • Hail = 59,132,668 • Wind = 32,666,217 • Tornado = 9,688,168
Additional Info	The default catalog, known as the all-events catalog, consists of all simulated macroevents regardless of how much industry loss they cause. The other catalog, known as the cat-only catalog, consists of only those macroevents that result in gross insurable losses of at least 25 million USD.

Table 1 and Figure 3 show the distribution of annual simulated macroevents in the 10K cat-only catalog. Similarly, Table 2 and Figure 4 show the distribution of annual simulated macroevents in the 10K all-events catalog. Each bar in the two figures represents the relative frequency of the number of years in the stochastic catalog which contain the indicated number of simulated macroevents. Note that there are, on average, 83.9 cat-only macroevents per year in the 10K cat-only catalog as compared to approximately 221.7 macroevents per year in the 10K all-events catalog that cause insured loss.

[2] The Touchstone Re stochastic catalog contains industry losses for cat-only events and zero industry loss placeholders for non-cat events to support losses from detailed company loss files/company loss association files (CLF/CLA) that may include these non-cat events. They will not produce industry loss but will produce loss for non-cat events if they are present in the CLF/CLA.

Table 1. Annual simulated macroevent count and relative frequencies in the 10K cat-only catalog

Simulated Number of Annual Events	Number of Years with Event Count	Relative Frequency	Simulated Number of Annual Events	Number of Years with Event Count	Relative Frequency
58	2	0.0002	87	438	0.0438
60	2	0.0002	88	395	0.0395
61	12	0.0012	89	371	0.0371
62	9	0.0009	90	327	0.0327
63	17	0.0017	91	301	0.0301
64	37	0.0037	92	289	0.0289
65	30	0.0030	93	254	0.0254
66	31	0.0031	94	202	0.0202
67	57	0.0057	95	189	0.0189
68	65	0.0065	96	191	0.0191
69	89	0.0089	97	158	0.0158
70	125	0.0125	98	118	0.0118
71	134	0.0134	99	100	0.0100
72	169	0.0169	100	72	0.0072
73	236	0.0236	101	66	0.0066
74	247	0.0247	102	52	0.0052
75	292	0.0292	103	52	0.0052
76	329	0.0329	104	23	0.0023
77	355	0.0355	105	29	0.0029
78	392	0.0392	106	13	0.0013
79	416	0.0416	107	14	0.0014
80	437	0.0437	108	6	0.0006
81	463	0.0463	109	6	0.0006
82	515	0.0515	110	5	0.0005
83	464	0.0464	111	5	0.0005
84	493	0.0493	114	2	0.0002
85	444	0.0444	115	1	0.0001
86	459	0.0459			

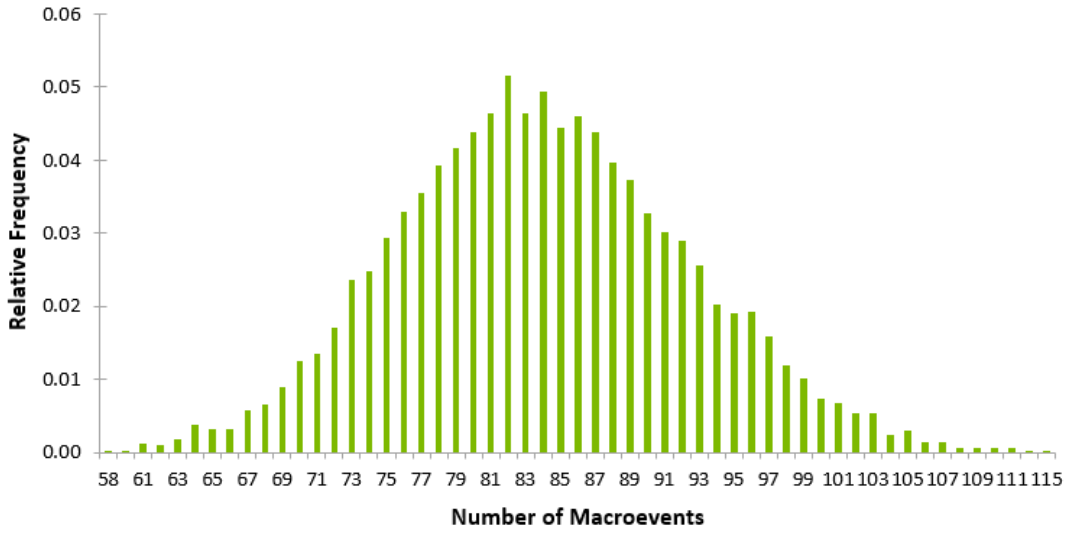

Figure 3. Frequency distribution of annual simulated macroevents in the 10K cat-only catalog

Table 2. Annual simulated macroevent count and relative frequencies in the 10K all-events catalog

Simulated Number of Annual Events	Number of Years with Event Count	Relative Frequency	Simulated Number of Annual Events	Number of Years with Event Count	Relative Frequency
161	1	0.0001	218	232	0.0232
168	1	0.0001	219	247	0.0247
169	1	0.0001	220	241	0.0241
170	1	0.0001	221	299	0.0299
171	1	0.0001	222	291	0.0291
172	3	0.0003	223	354	0.0354
173	2	0.0002	224	384	0.0384
174	4	0.0004	225	350	0.0350
175	1	0.0001	226	359	0.0359
176	2	0.0002	227	317	0.0317
177	2	0.0002	228	316	0.0316
178	3	0.0003	229	298	0.0298
179	1	0.0001	230	262	0.0262
180	2	0.0002	231	284	0.0284
181	4	0.0004	232	242	0.0242
182	5	0.0005	233	234	0.0234
183	7	0.0007	234	291	0.0291

Simulated Number of Annual Events	Number of Years with Event Count	Relative Frequency	Simulated Number of Annual Events	Number of Years with Event Count	Relative Frequency
184	5	0.0005	235	294	0.0294
185	8	0.0008	236	284	0.0284
186	4	0.0004	237	263	0.0263
187	7	0.0007	238	243	0.0243
188	4	0.0004	239	227	0.0227
189	7	0.0007	240	243	0.0243
190	10	0.0010	241	186	0.0186
191	4	0.0004	242	163	0.0163
192	7	0.0007	243	143	0.0143
193	5	0.0005	244	129	0.0129
194	7	0.0007	245	98	0.0098
195	8	0.0008	246	96	0.0096
196	4	0.0004	247	92	0.0092
197	7	0.0007	248	102	0.0102
198	10	0.0010	249	80	0.0080
199	19	0.0019	250	73	0.0073
200	22	0.0022	251	71	0.0071
201	18	0.0018	252	65	0.0065
202	30	0.0030	253	41	0.0041
203	28	0.0028	254	40	0.0040
204	32	0.0032	255	23	0.0023
205	47	0.0047	256	21	0.0021
206	65	0.0065	257	18	0.0018
207	58	0.0058	258	14	0.0014
208	81	0.0081	259	8	0.0008
209	90	0.0090	260	4	0.0004
210	104	0.0104	261	10	0.0010
211	107	0.0107	262	8	0.0008
212	134	0.0134	263	8	0.0008
213	137	0.0137	264	5	0.0005
214	157	0.0157	265	3	0.0003
215	200	0.0200	266	4	0.0004
216	226	0.0226	267	1	0.0001

Simulated Number of Annual Events	Number of Years with Event Count	Relative Frequency	Simulated Number of Annual Events	Number of Years with Event Count	Relative Frequency
217	246	0.0246			

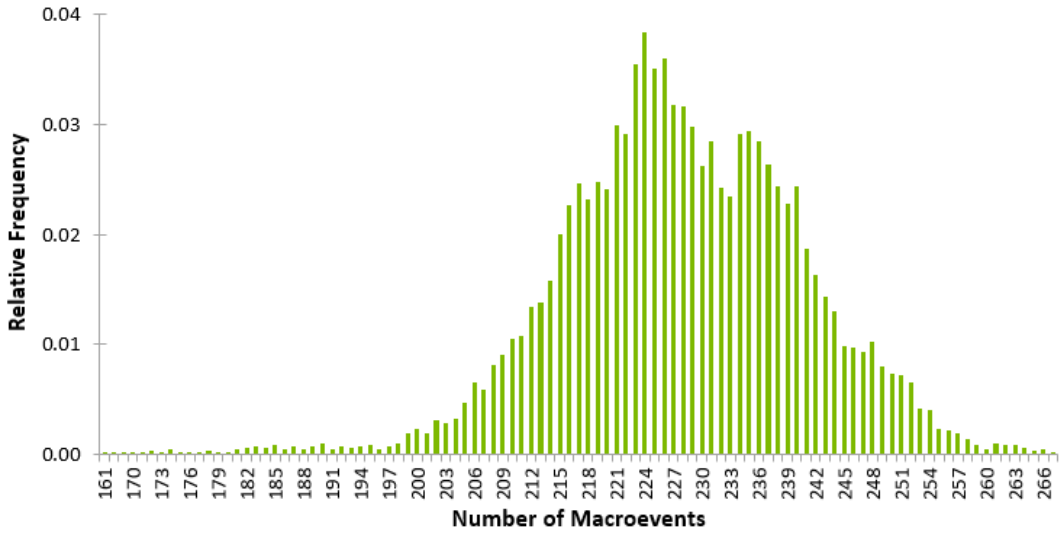

Figure 4. Frequency distribution of annual simulated macroevents in the 10K all-events catalog

Figure 5 and Figure 6 show the seasonal frequency distributions of simulated macroevents for the 10K cat-only and 10K all-events catalogs, respectively. The monthly number and relative frequency of microevents, by sub-peril, for the 10K cat-only and 10K all-events catalogs are detailed in Table 3 and Table 4, respectively. In addition, these monthly microevent frequency distributions are displayed in Figure 7 (10K cat-only catalog) and Figure 8 (10K all-events catalog). As expected, seasonal frequency distribution differences exist between the two catalogs because the "all-events" catalog includes a wide range of smaller, high-frequency (i.e., non-catastrophic or "non-cat") events in addition to a broad range of larger but lower-frequency (i.e., catastrophic or "cat") events.

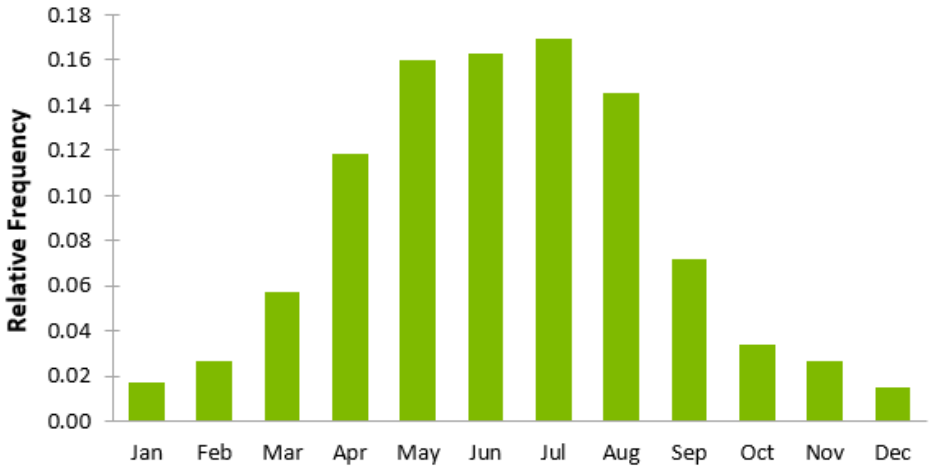

Figure 5. Seasonal frequency distribution of simulated macroevents using the 10K cat-only catalog

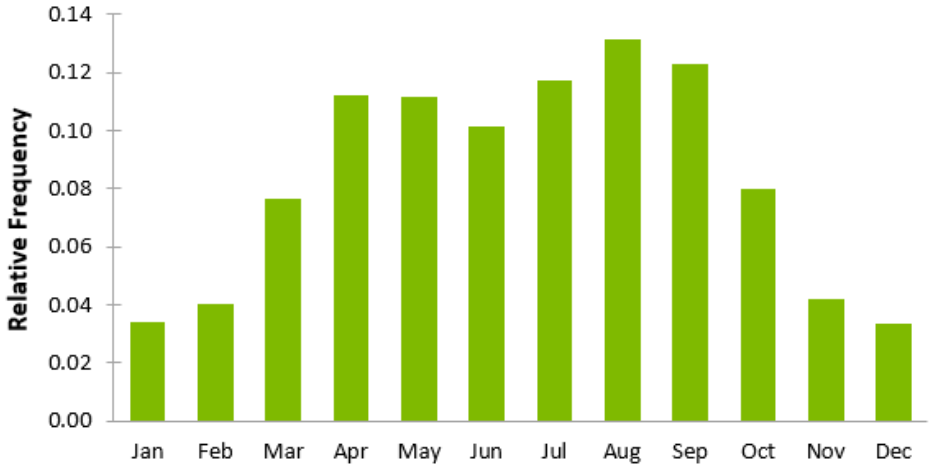

Figure 6. Seasonal frequency distribution of simulated macroevents using the 10K all-events catalog

Table 3. Monthly microevent counts and relative frequencies in the 10K cat-only catalog

	Monthly Event Counts				Relative Frequencies		
	Hail	Wind	Tornado		Hail	Wind	Tornado
Jan	414,461	336,980	269,383	**Jan**	0.007	0.010	0.028
Feb	743,797	508,376	280,962	**Feb**	0.013	0.016	0.029
Mar	3,424,554	1,214,968	687,711	**Mar**	0.058	0.037	0.071
Apr	7,486,558	2,496,955	1,571,483	**Apr**	0.127	0.076	0.162
May	13,004,805	4,769,422	2,312,274	**May**	0.220	0.146	0.239
Jun	14,763,861	8,105,591	1,985,491	**Jun**	0.250	0.248	0.205

	Monthly Event Counts				Relative Frequencies		
	Hail	Wind	Tornado		Hail	Wind	Tornado
Jul	10,326,746	8,163,932	961,499	**Jul**	0.175	0.250	0.099
Aug	5,489,696	4,425,835	421,253	**Aug**	0.093	0.135	0.043
Sep	1,734,799	1,145,844	179,234	**Sep**	0.029	0.035	0.019
Oct	903,826	599,221	302,560	**Oct**	0.015	0.018	0.031
Nov	617,870	625,965	503,765	**Nov**	0.010	0.019	0.052
Dec	221,695	273,128	212,553	**Dec**	0.004	0.008	0.022

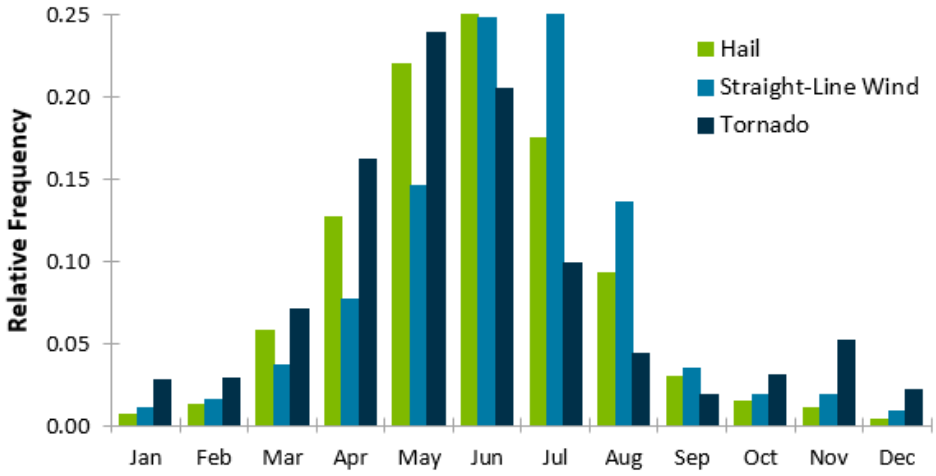

Figure 7. Seasonal frequency distribution of simulated microevents using the 10K cat-only catalog

Table 4. Monthly microevent counts and relative frequencies in the 10K all-events catalog

	Monthly Event Counts				Relative Frequencies		
	Hail	Wind	Tornado		Hail	Wind	Tornado
Jan	580,957	544,444	335,918	**Jan**	0.008	0.011	0.028
Feb	1,023,892	720,567	332,449	**Feb**	0.013	0.015	0.028
Mar	4,305,446	1,659,545	794,687	**Mar**	0.056	0.035	0.066
Apr	9,504,932	3,389,123	1,793,410	**Apr**	0.123	0.071	0.150
May	15,614,798	6,144,920	2,607,303	**May**	0.203	0.130	0.218
Jun	17,466,734	10,179,941	2,301,938	**Jun**	0.227	0.215	0.192
Jul	13,511,019	11,530,044	1,304,759	**Jul**	0.175	0.243	0.109
Aug	8,635,306	7,877,750	735,831	**Aug**	0.112	0.166	0.061
Sep	3,616,956	2,876,187	419,340	**Sep**	0.047	0.061	0.035
Oct	1,590,124	1,149,078	457,300	**Oct**	0.021	0.024	0.038
Nov	822,292	866,390	599,127	**Nov**	0.011	0.018	0.050

	Monthly Event Counts				Relative Frequencies		
	Hail	Wind	Tornado		Hail	Wind	Tornado
Dec	332,692	485,963	295,617	**Dec**	0.004	0.010	0.025

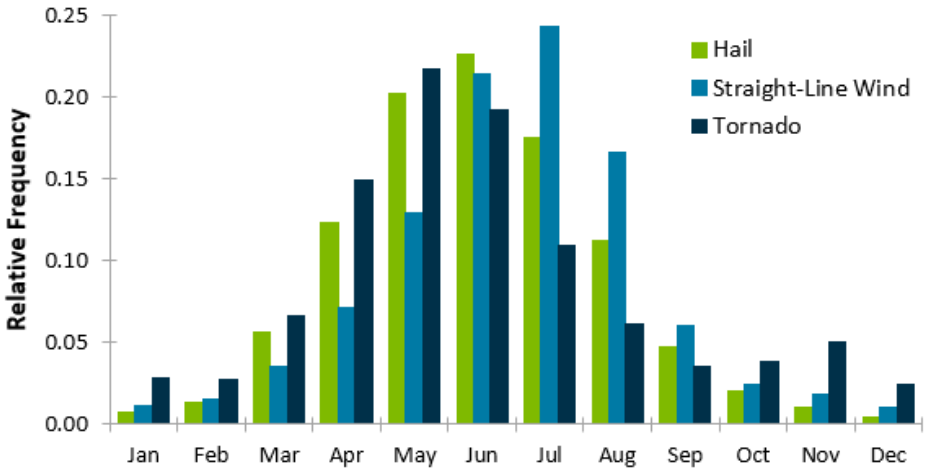

Figure 8. Seasonal frequency distribution of simulated microevents using the 10K all-events catalog

1.7 Historical event set

The model includes a historical event set (also known as the marquee event set) consisting of 35 events. These 35 events consist of 5 perturbations of 7 events listed in Table 5. Note that the five realizations of each event contain the same number of events by sub-peril and are of the same duration. They do, however, differ in terms of modeled variables, such as starting location, length, width, storm track direction, and intensity, with the amount of perturbation depending upon the degree of uncertainty. The path length, width, and intensity of the Joplin tornado (part of the May 20-27, 2011 outbreak), for example, are more certain than for any particular straight-line wind swath in that outbreak. Verisk's cluster analyses lead to different counts than the SPC provides for these events.

Table 5. Historical event set with sub-peril counts

Event	Hail Count	Straight-Line Wind Count	Tornado Count
May 10, 2010	76	21	95
May 12-16, 2010	517	196	15
June 10-16, 2010	615	413	10
October 4-6, 2010	96	13	6
April 22-28, 2011	1,187	560	707

Event	Hail Count	Straight-Line Wind Count	Tornado Count
May 20-27, 2011	1,280	600	199
June 28-July 2, 2012	424	228	0

See Also
Significant historical U.S. severe thunderstorms
Historical event set

1.8 Model resolution

The Verisk Severe Thunderstorm Model for the United States resolution is provided below, along with supported resolutions in Touchstone and Touchstone Re. Specific datasets may be available at a higher resolution, as described in component-specific sections of this document.

General model resolution

Model Resolution	Location-level covering the exact footprint of each sub-peril (hail, straight-line winds, and tornadoes)

Touchstone model resolution

Touchstone supports the following geographic resolutions for this model.

Supported Geographic Resolutions	• County • ZIP Code • Complete address (including street, city, and state) • User-specified latitude/longitude

Touchstone Re model resolution

In Touchstone Re, industry exposure files and input/output data for this model are supported at the resolution listed below.

Industry Exposure Loss Files Resolution	90-m
Input/Output (Losses) Resolution	• State • County

1.9 Modeled lines of business

Touchstone Re supports the following lines of business and their associated primary risk characteristics for reporting modeled losses.

Residential	• Building • Contents • Time Element
Manufactured (Mobile) Home	• Building • Contents • Time Element
Commercial/ Industrial	• Building • Contents • Time Element
Automobile	

1.10 Construction and occupancy classes

The Verisk Severe Thunderstorm Model for the United States supports numerous construction and occupancy classes, as listed below.

Construction Classes	140
Occupancy Classes	112 (of which 62 classes are large industrial facilities)

For a complete list of construction classes, occupancy classes, and supported combinations, see the *Verisk Severe Thunderstorm Model for the United States Supplement* available with login on the Client Portal.

See Also

Construction and occupancy classes, year built and height bands, and relative vulnerabilities

1.11 Modeled industry losses

It is important to distinguish between insurable and insured losses when modeling the industry exposure.

Insurable exposure	Total replacement value and number of properties (risk counts) that are eligible for insurance.

Insured exposure	Although eligible for insurance, "take-up" or purchase of insurance coverage for eligible properties varies by peril and region. For example, coverage for some natural perils may be mandatory in a region, and consequently the insurance take-up rate would be 100%. For other natural perils, insurance may be voluntary, and take-up may be in single-digit percentage values. Based on available information, Verisk provides estimates of take-up rates for each modeled region and simulated peril. Insured exposure is calculated by multiplying the take-up rate by the insurable risk count and replacement values.
Insurable losses	Estimated losses to insurable exposures.
Insured losses	Estimated losses to insured exposures.

Note: The losses presented in this document include demand surge. In addition, they were generated using the *filtered* 10K cat-only catalog available in Touchstone Re. This filtered 10K cat-only catalog is a subset of events from the unfiltered 10K all-events catalog used to increase the model's computational efficiency in Touchstone Re. It was created by removing the following from the unfiltered 10K all-events catalog:

- Counties that experience minimal loss from a given severe thunderstorm event, and
- Macroevents that result in gross insurable losses of less than 25 million USD.

See Also

Supported take-up rates and policy conditions

Modeled occurrence losses

Conterminous United States hail, straight-line wind, and tornado (combined) modeled gross insured and insurable occurrence loss estimates for the 1% (100-year) and 0.4% (250-year) exceedance probabilities are provided below. These losses were calculated using the filtered 10K cat-only catalog as well as the 2019 Industry Exposure Database. These losses include demand surge and were calculated using Touchstone Re.

Modeled Insured Occurrence Losses (10K Cat-Only Catalog)

1% Exceedance Probability (100-year)	21,332,334,375 USD
0.4% Exceedance Probability (250-year)	28,960,260,725 USD

Modeled Insurable Occurrence Losses (10K Cat-Only Catalog)

1% Exceedance Probability (100-year)	22,248,521,768 USD
0.4% Exceedance Probability (250-year)	31,051,977,232 USD

See Also
Analysis Settings

Modeled aggregate loss estimates

Combined hail, straight-line wind, and tornado average annual gross insured aggregate loss (AAL) estimates for the conterminous United States, the eight regions, and the ten states with the highest total losses using the filtered 10K cat-only catalog are shown in Figure 9. These loss estimates include demand surge and were calculated using the 2019 Industry Exposure Database. Touchstone Re was run to obtain these modeled losses.

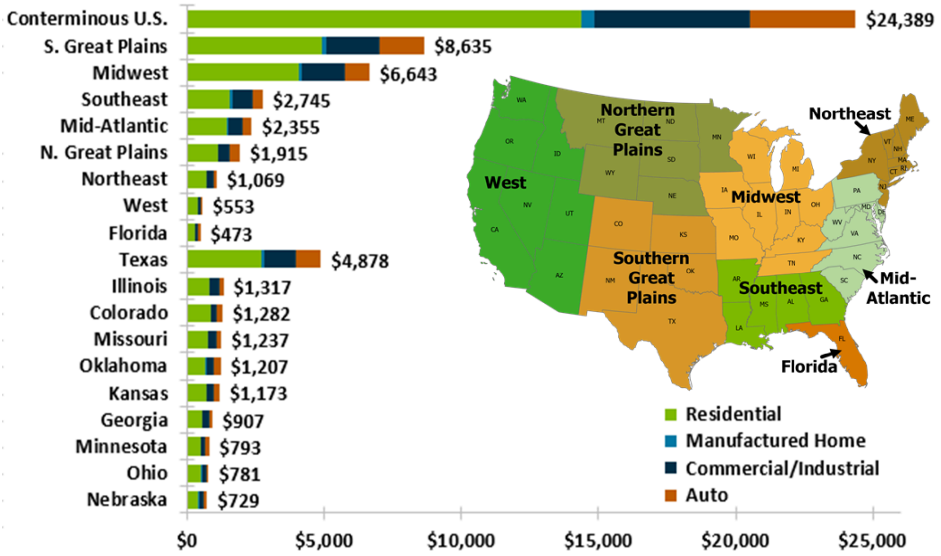

Figure 9. Modeled hail, straight-line wind, and tornado (combined) average annual gross insured aggregate losses (in USD millions), by line of business, using the 10K cat-only catalog.
Total insured losses are labeled to the right of each horizontal bar. The eight geographical regions are defined in the inset map.

Combined hail, straight-line wind, and tornado average annual gross insurable aggregate loss estimates for the conterminous United States, the eight regions, and the ten states with the highest total losses using the filtered 10K cat-only catalog are shown in Figure 10. These loss estimates include demand surge and were calculated using the 2019 Industry Exposure Database. Touchstone Re was run to obtain these modeled losses.

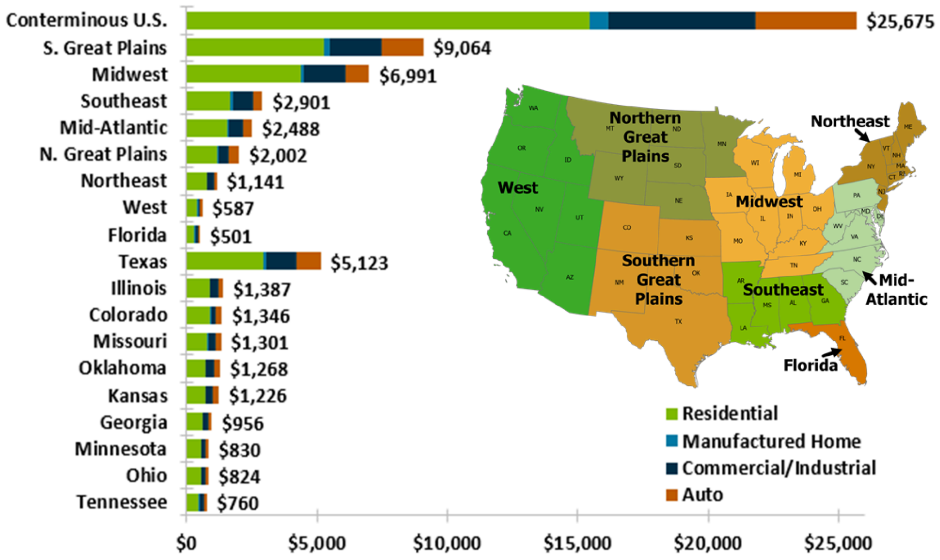

Figure 10. Modeled hail, straight-line wind, and tornado (combined) average annual gross insurable aggregate losses (in USD millions), by line of business, using the 10K cat-only catalog.
Total insurable losses are labeled to the right of each horizontal bar. The eight geographical regions are defined in the inset map.

Table 6 provides the contribution of each sub-peril to the total gross insurable aggregate loss for the conterminous United States and for each state, using the filtered 10K all-events catalog in Verisk's Research Model. These percent contributions do not include demand surge. The sub-peril percent contribution to the total aggregate loss is provided for the aggregate average annual loss (AAL) and for the aggregate loss exceedance probabilities of 50%, 1%, and 0.4%. These losses were generated by dividing each sub-peril loss by the total loss at each return period or AAL.

Note that the sub-peril percent contributions do not add up to 100% because the losses are generated from separate EP curves for each sub-peril, and for all sub-perils combined. Each event does not necessarily contain all three sub-perils; therefore, to generally show which sub-peril is contributing the most to the loss at a given return period, Verisk scientists calculated percent contributions using losses from each sub-peril's EP curve. Also note that while the sub-peril loss percentages presented in Table 6 were calculated using total gross insurable aggregate losses, due to the high insurance take-up rates in the United States, sub-peril loss percentages calculated using total gross insured aggregate losses would result in very similar values as shown in this table.

Table 6. Contribution of each sub-peril to the total gross insurable aggregate loss for the contiguous U.S. and for each state using the 10K all-events catalog

State	EP	Hail	Tornado	Wind	State	EP	Hail	Tornado	Wind
All U.S.	**50.0%**	50%	22%	23%	MT	**50.0%**	53%	0%	29%
	1.0%	47%	50%	23%		**1.0%**	92%	3%	21%
	0.4%	45%	57%	21%		**0.4%**	93%	6%	17%

State	EP	Hail	Tornado	Wind	State	EP	Hail	Tornado	Wind
	AAL	50%	27%	23%		**AAL**	71%	2%	27%
AL	**50.0%**	27%	25%	24%	**NC**	**50.0%**	40%	6%	27%
	1.0%	29%	86%	11%		**1.0%**	40%	84%	17%
	0.4%	30%	93%	10%		**0.4%**	40%	90%	15%
	AAL	29%	52%	19%		**AAL**	42%	36%	23%
AR	**50.0%**	40%	13%	27%	**ND**	**50.0%**	61%	0%	22%
	1.0%	42%	80%	15%		**1.0%**	87%	22%	14%
	0.4%	37%	84%	12%		**0.4%**	83%	34%	10%
	AAL	41%	36%	23%		**AAL**	72%	7%	20%
AZ	**50.0%**	15%	0%	38%	**NE**	**50.0%**	64%	1%	19%
	1.0%	87%	4%	37%		**1.0%**	74%	48%	12%
	0.4%	93%	9%	29%		**0.4%**	70%	65%	10%
	AAL	58%	5%	38%		**AAL**	69%	14%	17%
CA	**50.0%**	6%	0%	27%	**NH**	**50.0%**	7%	0%	63%
	1.0%	72%	27%	51%		**1.0%**	68%	36%	34%
	0.4%	75%	41%	46%		**0.4%**	66%	54%	29%
	AAL	45%	15%	40%		**AAL**	44%	18%	39%
CO	**50.0%**	77%	0%	8%	**NJ**	**50.0%**	11%	0%	55%
	1.0%	87%	28%	11%		**1.0%**	48%	68%	20%
	0.4%	92%	39%	11%		**0.4%**	44%	86%	19%
	AAL	83%	7%	10%		**AAL**	37%	32%	32%
CT	**50.0%**	3%	0%	60%	**NM**	**50.0%**	71%	0%	13%
	1.0%	44%	64%	21%		**1.0%**	93%	13%	16%
	0.4%	44%	87%	17%		**0.4%**	95%	19%	12%
	AAL	35%	34%	31%		**AAL**	82%	4%	14%
DC	**50.0%**	N/A	N/A	N/A	**NV**	**50.0%**	0%	0%	40%
	1.0%	57%	2%	17%		**1.0%**	78%	0%	51%
	0.4%	50%	36%	11%		**0.4%**	94%	0%	39%
	AAL	32%	57%	11%		**AAL**	52%	2%	46%
DE	**50.0%**	0%	0%	68%	**NY**	**50.0%**	22%	0%	45%
	1.0%	44%	57%	19%		**1.0%**	51%	59%	27%
	0.4%	47%	81%	14%		**0.4%**	55%	76%	23%
	AAL	33%	33%	33%		**AAL**	39%	28%	33%
FL	**50.0%**	22%	12%	27%	**OH**	**50.0%**	27%	2%	43%
	1.0%	31%	90%	14%		**1.0%**	51%	67%	28%

State	EP	Hail	Tornado	Wind	State	EP	Hail	Tornado	Wind
	0.4%	33%	98%	13%		**0.4%**	58%	81%	25%
	AAL	28%	52%	21%		**AAL**	37%	23%	40%
GA	**50.0%**	33%	14%	24%	**OK**	**50.0%**	53%	7%	24%
	1.0%	37%	85%	12%		**1.0%**	67%	66%	14%
	0.4%	36%	95%	10%		**0.4%**	67%	74%	12%
	AAL	35%	47%	18%		**AAL**	57%	22%	21%
IA	**50.0%**	52%	4%	27%	**OR**	**50.0%**	9%	0%	16%
	1.0%	65%	53%	19%		**1.0%**	61%	5%	32%
	0.4%	71%	68%	17%		**0.4%**	80%	15%	32%
	AAL	56%	18%	26%		**AAL**	57%	12%	31%
ID	**50.0%**	10%	0%	52%	**PA**	**50.0%**	26%	1%	43%
	1.0%	73%	9%	41%		**1.0%**	39%	78%	22%
	0.4%	81%	19%	36%		**0.4%**	38%	81%	19%
	AAL	43%	10%	47%		**AAL**	34%	34%	33%
IL	**50.0%**	33%	4%	35%	**RI**	**50.0%**	0%	0%	78%
	1.0%	60%	55%	21%		**1.0%**	66%	19%	27%
	0.4%	58%	72%	16%		**0.4%**	61%	45%	21%
	AAL	45%	24%	30%		**AAL**	33%	30%	37%
IN	**50.0%**	32%	4%	36%	**SC**	**50.0%**	39%	4%	27%
	1.0%	53%	66%	23%		**1.0%**	41%	82%	14%
	0.4%	51%	79%	19%		**0.4%**	36%	88%	12%
	AAL	41%	26%	33%		**AAL**	42%	37%	21%
KS	**50.0%**	59%	4%	22%	**SD**	**50.0%**	70%	0%	18%
	1.0%	69%	56%	14%		**1.0%**	86%	25%	13%
	0.4%	64%	74%	11%		**0.4%**	93%	39%	11%
	AAL	62%	17%	20%		**AAL**	76%	7%	18%
KY	**50.0%**	34%	10%	28%	**TN**	**50.0%**	31%	16%	24%
	1.0%	42%	79%	17%		**1.0%**	33%	84%	11%
	0.4%	39%	90%	13%		**0.4%**	37%	96%	10%
	AAL	37%	40%	23%		**AAL**	32%	49%	19%
LA	**50.0%**	23%	24%	25%	**TX**	**50.0%**	53%	11%	19%
	1.0%	28%	93%	10%		**1.0%**	59%	72%	13%
	0.4%	25%	95%	8%		**0.4%**	56%	75%	12%
	AAL	26%	56%	18%		**AAL**	56%	26%	18%
MA	**50.0%**	5%	0%	59%	**UT**	**50.0%**	2%	0%	60%

State	EP	Hail	Tornado	Wind	State	EP	Hail	Tornado	Wind
	1.0%	62%	46%	28%		**1.0%**	72%	1%	66%
	0.4%	59%	62%	26%		**0.4%**	81%	7%	53%
	AAL	41%	26%	34%		**AAL**	29%	9%	61%
MD	**50.0%**	21%	0%	41%	**VA**	**50.0%**	35%	2%	35%
	1.0%	42%	81%	17%		**1.0%**	46%	80%	16%
	0.4%	36%	92%	12%		**0.4%**	43%	90%	12%
	AAL	38%	39%	23%		**AAL**	42%	33%	25%
ME	**50.0%**	7%	0%	61%	**VT**	**50.0%**	10%	0%	61%
	1.0%	78%	20%	52%		**1.0%**	65%	40%	50%
	0.4%	78%	26%	44%		**0.4%**	73%	61%	42%
	AAL	44%	9%	47%		**AAL**	39%	13%	48%
MI	**50.0%**	29%	1%	42%	**WA**	**50.0%**	11%	0%	26%
	1.0%	62%	49%	38%		**1.0%**	66%	2%	42%
	0.4%	68%	65%	30%		**0.4%**	80%	9%	54%
	AAL	43%	16%	40%		**AAL**	57%	5%	37%
MN	**50.0%**	54%	2%	22%	**WI**	**50.0%**	52%	1%	25%
	1.0%	83%	32%	17%		**1.0%**	80%	48%	22%
	0.4%	77%	45%	13%		**0.4%**	76%	62%	19%
	AAL	66%	13%	21%		**AAL**	61%	14%	25%
MO	**50.0%**	44%	7%	30%	**WV**	**50.0%**	31%	0%	45%
	1.0%	52%	73%	17%		**1.0%**	54%	66%	26%
	0.4%	48%	77%	14%		**0.4%**	52%	84%	21%
	AAL	47%	26%	27%		**AAL**	42%	20%	38%
MS	**50.0%**	28%	28%	23%	**WY**	**50.0%**	65%	0%	18%
	1.0%	29%	87%	11%		**1.0%**	95%	10%	10%
	0.4%	31%	91%	10%		**0.4%**	91%	23%	9%
	AAL	29%	53%	18%		**AAL**	81%	4%	15%

See Also
Analysis Settings

Loss cost

Loss cost is the aggregate AAL normalized by the asset replacement cost. Figure 11, Figure 12, Figure 13, and Figure 14 depict the loss cost (risk) for severe thunderstorms, hail, tornado, and straight-line wind activity, respectively, in the conterminous United States. These maps represent the AAL to Coverage A (buildings) of a uniform exposure type (construction class 101, occupancy class 302, 1-story building height, and unknown building age) with a

uniform exposure value and were calculated at 5-km grid resolution. Note that the 5-km grid underestimates the risk due to tornadoes both in the severe thunderstorm loss costs map and in the tornado-specific loss cost map because a tornado's narrow swath may miss the 5-km grid point.

The lost cost maps do not include demand surge. To obtain data for the loss cost maps, Verisk ran a detailed loss analysis on the gridded exposure in Touchstone.

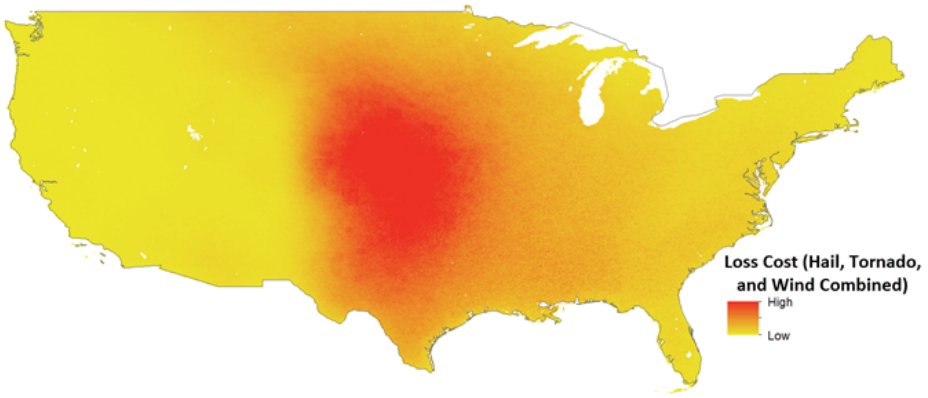

Figure 11. Severe thunderstorm (hail, straight-line wind, and tornado, combined) risk (loss costs) in the United States

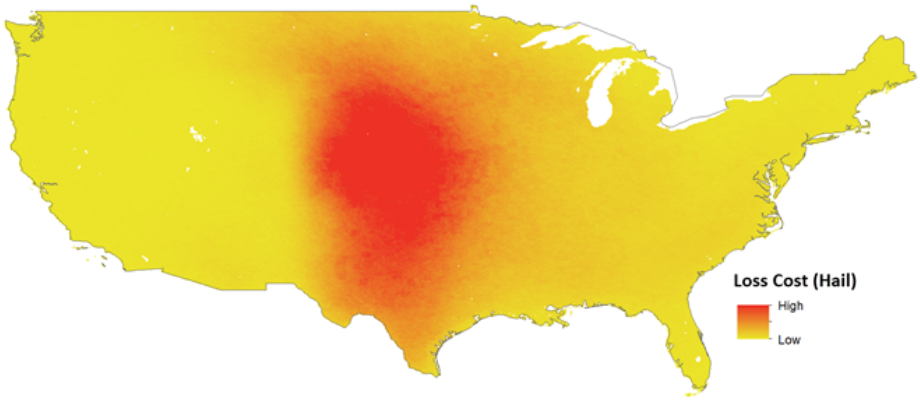

Figure 12. Hail risk (loss costs) in the United States

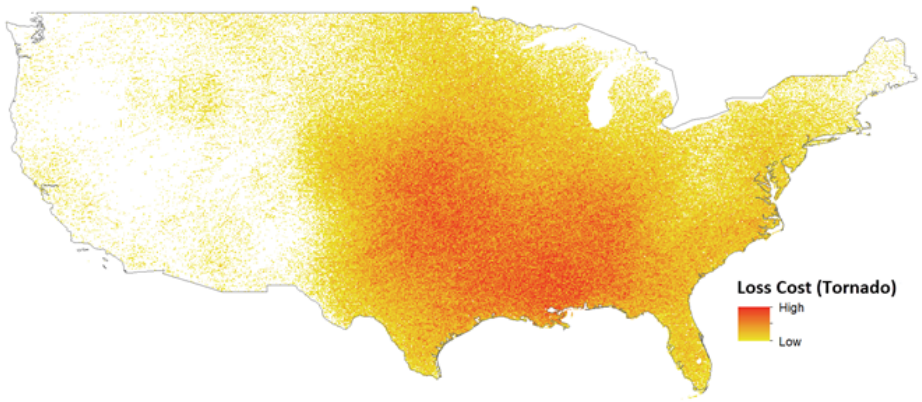

Figure 13. Tornado risk (loss costs) in the United States

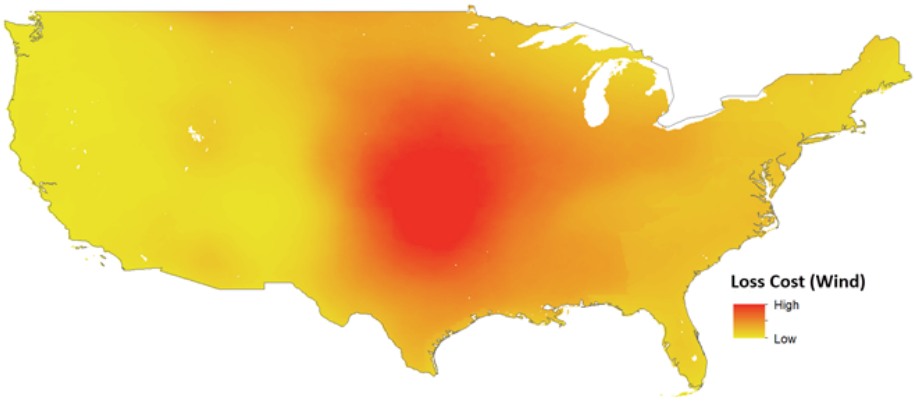

Figure 14. Straight-line wind risk (loss costs) in the United States

See Also
Analysis Settings

Modeled losses for historical severe thunderstorms

Table 7 and Table 8 list the modeled gross insured and insurable loss estimates, respectively, for significant historical severe thunderstorms affecting the conterminous United States, based on Verisk's 2019 United States Industry Exposure Database. Modeled losses include property and contents, business interruption, and additional living expenses. These loss estimates include demand surge and were calculated using Touchstone Re. Note that there are five values for each category because Verisk released five realizations of each event.

Table 7. Modeled gross insured losses for historical severe thunderstorms (2019 Exposure, USD)

Event	Residential	Manufactured Home	Commercial/ Industrial	Auto	Total
May 10, 2010	512,825,137	24,463,411	180,511,047	104,999,200	822,798,795
May 10, 2010	569,579,460	26,887,983	168,844,683	130,709,660	896,021,786
May 10, 2010	576,437,229	30,134,438	204,240,053	132,158,137	942,969,857
May 10, 2010	653,717,010	28,804,005	163,379,450	134,175,117	980,075,583
May 10, 2010	776,470,751	33,483,391	173,591,152	138,124,517	1,121,669,811
May 12-16, 2010	1,775,664,179	38,100,114	640,565,139	768,410,225	3,222,739,657
May 12-16, 2010	1,880,016,688	34,473,146	647,134,049	800,960,957	3,362,584,840
May 12-16, 2010	1,914,126,008	36,347,063	655,261,024	816,549,310	3,422,283,404
May 12-16, 2010	1,944,363,812	34,459,615	700,031,442	828,106,325	3,506,961,194
May 12-16, 2010	2,117,856,067	35,340,334	691,465,422	857,983,316	3,702,645,139
June 10-16, 2010	577,278,106	21,528,740	182,275,260	270,734,255	1,051,816,361
June 10-16, 2010	598,805,874	22,014,266	191,809,171	280,016,384	1,092,645,695
June 10-16, 2010	609,097,960	23,652,045	194,303,305	292,019,406	1,119,072,717
June 10-16, 2010	630,097,771	24,331,956	201,751,415	307,656,050	1,163,837,192
June 10-16, 2010	654,233,021	27,137,609	212,087,304	305,229,914	1,198,687,848
October 4-6, 2010	2,139,257,657	33,905,743	644,362,026	927,495,955	3,745,021,381

Event	Residential	Manufactured Home	Commercial/ Industrial	Auto	Total
October 4-6, 2010	2,221,919,534	36,449,957	695,378,924	942,354,688	3,896,103,103
October 4-6, 2010	2,256,397,607	34,353,796	718,079,419	948,785,350	3,957,616,172
October 4-6, 2010	2,351,712,221	39,697,147	716,629,170	958,486,583	4,066,525,121
October 4-6, 2010	2,391,761,127	42,329,352	734,215,053	996,340,000	4,164,645,532
April 22-28, 2011	6,158,143,063	412,629,995	2,889,989,960	1,962,748,938	11,423,511,956
April 22-28, 2011	6,275,821,398	398,753,624	3,107,251,646	1,995,013,880	11,776,840,548
April 22-28, 2011	6,403,271,294	413,135,042	3,120,613,221	2,055,370,879	11,992,390,436
April 22-28, 2011	6,571,221,924	440,496,971	3,306,882,759	2,043,763,980	12,362,365,634
April 22-28, 2011	6,637,739,447	414,783,468	3,687,997,895	2,112,886,047	12,853,406,857
May 20-27, 2011	6,006,324,795	194,253,043	2,227,799,463	1,706,686,389	10,135,063,690
May 20-27, 2011	6,036,695,378	187,232,866	2,758,155,773	1,737,420,692	10,719,504,709
May 20-27, 2011	5,883,848,358	183,546,210	3,093,109,279	1,772,559,389	10,933,063,237
May 20-27, 2011	5,595,893,041	194,142,542	3,636,066,792	1,793,837,179	11,219,939,554
May 20-27, 2011	5,875,011,130	197,867,951	4,128,432,839	1,792,410,465	11,993,722,386
June 28-July 2, 2012	1,819,678,700	76,682,419	611,500,972	394,890,641	2,902,752,732
June 28-July 2, 2012	1,861,478,341	77,909,579	624,627,676	399,744,097	2,963,759,694

Event	Residential	Manufactured Home	Commercial/ Industrial	Auto	Total
June 28-July 2, 2012	1,894,793,381	77,764,016	634,116,478	394,277,105	3,000,950,981
June 28-July 2, 2012	1,928,765,135	78,902,664	651,243,742	392,969,664	3,051,881,205
June 28-July 2, 2012	1,960,708,393	81,160,075	654,838,038	420,549,921	3,117,256,427

Table 8. Modeled gross insurable losses for historical severe thunderstorms (2019 Exposure, USD)

Event	Residential	Manufactured Home	Commercial/ Industrial	Auto	Total
May 10, 2010	548,655,369	34,880,102	180,720,476	104,999,200	869,255,147
May 10, 2010	609,073,175	38,333,978	169,029,639	130,709,660	947,146,452
May 10, 2010	616,519,345	43,003,400	204,437,803	132,158,137	996,118,685
May 10, 2010	699,036,988	41,077,060	163,551,519	134,175,117	1,037,840,684
May 10, 2010	830,148,771	47,747,406	173,779,660	138,124,517	1,189,800,354
May 12-16, 2010	1,897,936,624	54,156,832	641,304,097	768,410,225	3,361,807,778
May 12-16, 2010	2,008,445,350	49,023,486	647,877,024	800,960,957	3,506,306,817
May 12-16, 2010	2,044,560,848	51,720,062	656,044,872	816,549,310	3,568,875,092
May 12-16, 2010	2,077,104,612	49,015,818	700,828,490	828,106,325	3,655,055,245
May 12-16, 2010	2,262,565,047	50,279,048	692,297,497	857,983,316	3,863,124,908
June 10-16, 2010	618,675,217	30,544,565	182,461,339	270,734,255	1,102,415,376
June 10-16, 2010	641,722,178	31,274,578	192,007,844	280,016,384	1,145,020,984

Event	Residential	Manufactured Home	Commercial/ Industrial	Auto	Total
June 10-16, 2010	652,554,097	33,546,333	194,502,779	292,019,406	1,172,622,615
June 10-16, 2010	675,004,736	34,471,489	201,960,199	307,656,050	1,219,092,474
June 10-16, 2010	701,009,190	38,512,968	212,294,994	305,229,914	1,257,047,066
October 4-6, 2010	2,297,801,787	47,667,734	645,452,936	927,495,955	3,918,418,412
October 4-6, 2010	2,386,623,453	51,246,808	696,557,522	942,354,688	4,076,782,471
October 4-6, 2010	2,423,697,956	48,298,428	719,297,145	948,785,350	4,140,078,879
October 4-6, 2010	2,526,055,594	55,805,266	717,844,103	958,486,583	4,258,191,546
October 4-6, 2010	2,569,353,970	59,590,561	735,460,461	996,340,000	4,360,744,992
April 22-28, 2011	6,596,646,478	587,372,586	2,892,223,337	1,962,748,938	12,038,991,339
April 22-28, 2011	6,724,433,227	567,581,044	3,109,650,398	1,995,013,880	12,396,678,548
April 22-28, 2011	6,859,723,769	588,038,621	3,123,015,764	2,055,370,879	12,626,149,033
April 22-28, 2011	7,039,847,132	626,792,705	3,309,402,827	2,043,763,980	13,019,806,643
April 22-28, 2011	7,112,577,755	590,233,803	3,690,738,095	2,112,886,047	13,506,435,700
May 20-27, 2011	6,445,310,549	275,284,326	2,229,665,635	1,706,686,389	10,656,946,898
May 20-27, 2011	6,477,874,081	265,338,787	2,760,209,271	1,737,420,692	11,240,842,831
May 20-27, 2011	6,314,291,915	260,265,046	3,095,298,670	1,772,559,389	11,442,415,020

Event	Residential	Manufactured Home	Commercial/ Industrial	Auto	Total
May 20-27, 2011	6,003,571,172	275,238,891	3,638,374,306	1,793,837,179	11,711,021,546
May 20-27, 2011	6,304,212,948	280,664,872	4,130,919,270	1,792,410,465	12,508,207,555
June 28-July 2, 2012	1,954,805,196	108,604,537	612,290,146	394,890,641	3,070,590,520
June 28-July 2, 2012	1,999,358,247	110,425,407	625,403,932	399,744,097	3,134,931,683
June 28-July 2, 2012	2,035,559,288	110,224,203	634,907,743	394,277,105	3,174,968,339
June 28-July 2, 2012	2,071,368,324	111,870,227	652,061,407	392,969,664	3,228,269,622
June 28-July 2, 2012	2,105,555,162	114,959,831	655,655,494	420,549,921	3,296,720,408

See Also

Significant historical U.S. severe thunderstorms

Analysis Settings

1.12 Navigating the document

Figure 15 illustrates the components of the Verisk model and how they are related.

Figure 15. Components of the Verisk model

2 Severe Thunderstorms in the United States

This section provides an overview of severe thunderstorms and introduces some important concepts in severe thunderstorm modeling.

2.1 Severe thunderstorms: An overview

Thunderstorms are one of the most common natural hazards in the world. Severe thunderstorms can cause loss of life, property and crop damages, and large insured losses.

The Verisk Severe Thunderstorm Model for the United States includes the hail, straight-line wind, and tornado sub-perils. As defined by the NWS, a thunderstorm is classified as severe if it produces at least one of the following: 1-inch or greater diameter hail, 58-mph or greater straight-line wind gusts, or a tornado of any intensity. However, the weakest (EF-0) tornadoes, as classified using the Enhanced Fujita Scale (EF Scale), are excluded from the Verisk model due to the large degree of uncertainty in reporting consistency and accuracy in the historical record and their low loss potential.

Prerequisites for thunderstorm formation are warm, moist air, atmospheric instability, environmental wind shear (change in wind speed or direction with height), and a mechanism that will cause air near the ground to be lifted. Storm initiation may be triggered by various mechanisms, such as an air mass boundary (e.g., cold front), unequal heating of the earth's surface, upslope flow over hills and mountains, or diverging upper-level winds.

The life cycle of a thunderstorm includes three stages, each of which may last between several minutes and several hours:

1. In the **cumulus** stage, storm initiation occurs, and allows for moist, unstable air to rise. As this air rises, it cools to its saturation point and condenses into cloud droplets. This condensation fuels greater growth of the cloud through the release of latent heat and is supported by a constant inflow of warm air into the cloud through the cloud updraft.
2. In the **mature** stage, the storm cell takes on the familiar towering cumulonimbus shape, often with a large stratus anvil. Condensation further encourages strong growth, as more latent heat is released into the near cloud environment, while evaporation of falling precipitation produces a cold storm outflow, or downdraft. In the absence of considerable wind shear, this downdraft can outrun the storm's forward propagation, cutting off the cloud's warm updraft and leading to the demise of the storm. The presence of wind shear allows the storm to develop a balance between the storm's inflow and outflow, promoting storm longevity and severity. Moderately-sheared environments may result in the development a squall line (i.e., a linear complex of storms). These storms could further develop into fast moving, far-reaching windstorms called derechos, which are long-lived and typically associated with strong wind gusts. In highly sheared environments, the storm may develop into a supercell with a rotating updraft known as a mesocyclone.

These types of storms are typically associated with larger hailstones, strong winds, and an increased risk of tornadoes.

3. In the **dissipation** stage, the storm cell becomes outflow dominated, cutting off the storm's source of warm, unstable air and resulting in its demise.

Thunderstorms may occur singly, in clusters, or in lines. Thunderstorms often do not fall neatly into categories, but generally, the four main types are single-cell, multicell cluster, multicell line, and supercell storms. A single-cell storm is an isolated event that has a single updraft. These storms usually pose little threat of property damage and are typically associated with moderate to heavy rainfall and the possibility of small hail or brief strong wind gusts. A multicell cluster thunderstorm, which poses a moderate risk of damage, is a cluster of cells that evolves into an organized storm. They are the most common type of thunderstorm and are associated with moderate to heavy precipitation and the possibility of hail and short-lived tornadoes. Multicell lines are multicell storms in linear formation with a continuous gust front. These storms are also called squall lines or derechos. Supercells are rare but highly organized severe thunderstorms with strong, long-lasting, and vertically-rotating updrafts (known as mesocyclones). Supercells, although rare, pose a high threat of damage to life and property and are the most likely type of storms to be accompanied by large hail, high winds, and violent tornadoes.

In the United States, severe thunderstorms can occur any time of the year and in any state, but they are most common during the spring and summer months in the area between the Rocky and Appalachian Mountains due to the greater prevalence of favorable atmospheric conditions.

Hailstorms

A hailstone forms when an existing ice particle collides with supercooled liquid water within a thunderstorm. As the hailstone is repeatedly lifted and dropped by updrafts within the storm clouds, water collects and freezes on the hailstone, and the hailstone grows. When the hailstone becomes too heavy to be suspended aloft by the storm updraft, it will fall to the ground, partially melting as it passes through warmer layers of the atmosphere. Larger hailstones can also form by collisions of two smaller hailstones, which create odd, non-spherical shapes sometimes observed.

Table 9 compares hail size to the size of common objects and demonstrates damage potential at a variety of hail sizes. Note that due to these objects being used for reference, 1.75- and 2.5-inch hail reports are more common than 2-inch reports, a bias that must be accounted for using non-parametric smoothing in the local intensity calculation. Hail measuring at least one inch in diameter is associated with severe thunderstorms.

Table 9. Estimating hailstone size and damage potential

Hailstone Diameter (in)	Object for Comparison	Damage Potential
0.25	Pea	Very Light
0.5	Marble	Light
0.75	Penny	Moderate

Hailstone Diameter (in)	Object for Comparison	Damage Potential
0.875	Nickel	Moderate
1.0	Quarter	Moderate (severe thunderstorm definition threshold)
1.5	Ping-Pong Ball	Considerable
1.75	Golf Ball	Considerable
2.5	Tennis Ball	Severe
2.75	Baseball	Severe
3.0	Teacup	Devastating
4.0	Softball	Incredible
4.5	Grapefruit	Incredible

Usually, the largest observed hailstone is recorded from a given thunderstorm, but that alone does not determine hail damage potential. Other factors, such as the size distribution of all hailstones that fall, hailfall duration, and horizontal wind speed, help determine hail damage potential. High winds can increase the kinetic energy of hailstones and blow them at angles significantly off the vertical, thus increasing the likelihood of broken windows and cladding damage. Larger hailstones generally create more damage than smaller stones because they can fall at higher speeds (up to 100 mph). Significant property damage usually occurs when hailstones are golf-ball size and larger.

The heaviest and largest authenticated hailstone to fall in the U.S. was found in Vivian, South Dakota on July 23, 2010. The stone weighed nearly 2 pounds (1 pound 15 ounces), was 8.0 inches in diameter, and had a circumference of 18.625 inches. The previous record for the heaviest documented hailstone was 1.67 pounds for a stone that fell in Coffeyville, Kansas on September 3, 1970. The previous record for hailstone diameter was 7 inches, which was found in Aurora, Nebraska on June 22, 2003. Note that this Aurora hailstone still holds the record for largest circumference at 18.75 inches.[3]

Straight-line windstorms

As precipitation falls and evaporates or melts, it cools the air around it. This cold air forms the storm downdraft and outflow as descending wind reaches the surface and spreads out. An area of particularly strong wind is often called a downburst. Downbursts less than 2.5-mi wide are known as microbursts and greater than 2.5-mi wide are macrobursts. Severe straight-line wind is defined as a 3-sec gust exceeding 58 mph (50 knots). While rare, thunderstorm wind gusts can exceed 100 mph and cause damage similar to strong tornadoes.

Severe straight-line winds occur on a variety of temporal and spatial scales. While a single location may experience high winds for only a few minutes, the parent thunderstorm that produces them may persist for hours and cover hundreds of miles in its lifetime. One such

[3] National Oceanic and Atmospheric Administration (NOAA) National Weather Service Aberdeen, SD Weather Forecast Office. *Record Setting Hail Event in Vivian, South Dakota on July 23, 2010.* https://www.weather.gov/abr/vivianhailstone

wind event, known as a derecho, is a long-lasting straight-line windstorm that can traverse more than 250 miles.

Losses from large-scale straight-line wind events can be very significant in terms of both damage intensity and quantity. The damage path of a severe straight-line windstorm can extend across hundreds of miles and may include toppled trees, downed power lines, and destroyed homes and automobiles.

Tornadoes

Severe thunderstorms may produce tornadoes, which are rapidly rotating columns of air connected to the base of the thunderstorm and in contact with the ground. Due to its geography, the United States experiences the most tornadoes of any country, with an average of 1,253 tornadoes occurring each year.[4] These storms are some of the most destructive forces in nature, causing an average of 70 deaths and 1,500 injuries per year.[5]

The development of a tornado is referred to as tornadogenesis and is an active area of academic research. It is generally accepted that tornadogenesis occurs when rotational momentum from the parent storm becomes stretched and concentrated. Just as ice skaters increase their rotation through the contraction of their arms, a tornado gains rotational momentum as the updraft and downdraft of the storm stretch and contract the rotating air parcel into a thin column. The strong upward motions within this column of air typically result in the formation of a dark condensation funnel, which is attached to the cloud base. When the funnel cloud makes contact with the ground, a tornado has officially formed. Debris and dust are often lifted into the air around the tornado, forming a debris cloud. Often this debris cloud is visible on radar in the form of a 'radar debris ball.'

Most tornadoes rotate cyclonically (counterclockwise in the Northern Hemisphere) with forward speeds ranging from stationary to about 70 mph. Tornadoes generally have rotational wind speeds ranging from 40 to 110 mph, although they can have winds over 300 mph. Weaker tornadoes generally last only minutes and travel only short distances, while the strongest tornadoes can last for hours and can travel hundreds of miles.

Tornadoes vary in intensity regardless of shape, size, or location, although stronger tornadoes tend to be larger than weaker ones. Longer track tornadoes also tend to be stronger than those that have a shorter track; however, these correlations are quite weak given the considerable complexity of severe weather systems.

It is difficult to directly measure tornado wind speeds by conventional methods because the storms are usually small, brief, and occur out of range of weather stations or anemometers. Also, instruments in a tornado's path are often destroyed by the wind intensity. The Fujita Scale, or F-Scale, was developed in 1971 as an indirect method for classifying tornado intensity based upon observed damage. In 2007, this scale was updated to the Enhanced Fujita Scale, or EF-Scale, by a panel of meteorologists and engineers who believed the original F-Scale overestimated winds for F-3 and higher tornadoes.

[4] National Oceanic and Atmospheric Administration (NOAA) Climate.gov (2021). *Average Annual and Monthly Numbers of Tornadoes by State - Maps.*. https://www.climate.gov/

[5] Missouri Storm Aware. *Tornado Facts & History.* https://stormaware.mo.gov/tornado-facts-history/

The EF-scale is a set of wind speed estimates, in terms of three-second gusts, based on the observed degree of damage to 28 types of structures called damage indicators. These damage indicators consist of 23 types of buildings, including schools, homes, barns, apartments, retail buildings, and warehouses, and 5 additional objects, including trees, towers, and poles. The degrees of damage range from the threshold of visible damage to total destruction (Table 10). In the United States, approximately 80% of reported tornadoes are EF-0 or EF-1.

Table 10. The Enhanced Fujita Tornado Damage Scale

Scale	3-Second Gust (mph)	Potential Damage
EF-0	65-85	Light damage to roofs, gutters, and siding. Tree branches broken. EF-0 tornadoes can also mean unknown intensity. In rural areas, EF-0 tornadoes could actually be stronger as there isn't as much property to damage, while in urban areas, it is more likely that an EF-0 tornado is actually an EF-0.
EF-1	86-110	Moderate damage to roofs. Mobile homes badly damaged. Exterior doors and windows lost. Glass broken.
EF-2	111-135	Considerable damage to buildings. Roofs torn off well-constructed houses, foundations of frame homes shifted, and mobile homes destroyed. Large trees snapped or uprooted, light-object missiles generated, and cars lifted off the ground.
EF-3	136-165	Severe damage to well-constructed homes and large buildings, trains overturned, and trees debarked. Heavy cars lifted off the ground and structures with weak foundations blown some distance.
EF-4	166-200	Devastating damage to well-constructed houses, whole frame houses leveled. Cars thrown and small missiles generated.
EF-5	Over 200	Incredible damage as strong frame houses leveled off foundations and automobile-sized missiles are airborne. Steel reinforced concrete structures badly damaged and high-rise buildings have significant structural deformation.

2.2 Severe thunderstorm risk in the United States

Losses from individual severe thunderstorms in the United States are generally not as great as those from individual hurricanes or earthquakes, but the annual aggregate losses from severe thunderstorms have accounted for more than half of all U.S. catastrophic insured losses since 2011.[6] In terms of state rankings of natural catastrophe loss potential, Texas severe thunderstorm risk ranks third, following only California earthquake and Florida hurricane risk.

[6] National Oceanic and Atmospheric Administration (NOAA) National Centers for Environmental Information (NCEI; 2021). *U.S. Billion-Dollar Weather and Climate Disasters (2021).*

Thunderstorms that produce hail occur throughout the U.S., but severe activity is particularly common in the Great Plains, Midwest, and Southeast. This activity is, in part, due to the proximity of these regions to the Atlantic Ocean, Gulf of Mexico, Rocky Mountains, and the Mexican Plateau. Florida also has a high rate of thunderstorm occurrence, however, many of these thunderstorms fail to meet the official severe criteria. Severe thunderstorms most frequently occur during the spring and summer months in North America, although in southern California, storms are more common during the winter and spring due to temperature inversions.

While tornadoes can affect all 50 states, tornadoes are particularly common in an area termed "Tornado Alley." This area encompasses the lowland areas of the Missouri, Mississippi, and Ohio River Valleys and includes regions in Texas, Nebraska, Kansas, and Oklahoma. In recent years, a secondary peak in tornado occurrence has been observed throughout much of Mississippi, Alabama, Georgia, and Tennessee (as discussed in the "Accounting for Climate Change" chapter of this document); however, this region exhibits a wide degree of variability.

Hail is most common in mid-latitude regions and along mountain ranges between May and August, although it can occur anywhere throughout the world at any time of year. In the United States, hailstorms occur most frequently throughout the Central Great Plains.

During the months of May through August, severe windstorms are most common from the upper Mississippi to Ohio River valleys and from the mid-Mississippi River valley to the Southern Plains. During September through April, severe windstorms are seen most frequently from eastern Texas to the southeastern U.S.

See Also

Historical trends in tornado activity
Historical trends in hail activity
Historical trends in straight-line wind activity

2.3 Significant historical U.S. severe thunderstorms

Seven significant historical U.S. severe thunderstorms supplement the model's stochastic catalog. These events occurred on May 10, 2010; May 12-16, 2010; June 10-16, 2010; October 4-6, 2010; April 22-28, 2011; May 20-27, 2011; and June 28-July 2, 2012.

See Also

Historical event set
Modeled losses for historical severe thunderstorms

1953 Worcester Tornado

On June 9, 1953, an F-4 tornado struck the city of Worcester, MA, and surrounding areas. The tornado touched down near Petersham, moved across Barre, and then finally entered Worcester, where it reached a width of 1 mile. There was extensive damage in Worcester; Assumption College (now home to Quinsigamond Community College) was nearly destroyed,

and homes in nearby neighborhoods were flattened. In one neighborhood, a 12-ton bus was thrown against an apartment building.

The Worcester tornado was part of the Flint-Worcester tornado outbreak, which occurred over a three-day period from June 6-9, 1953. The tornado caused 94 fatalities, over 1,000 injuries, damaged or destroyed over 4,000 buildings, and left over 10,000 people homeless. The storm stayed on the ground for nearly 90 minutes and traversed a 48-mi long path across Central Massachusetts. The Worcester tornado was one of only four F-4 tornadoes reported in New England to date (2021).

1974 Super Outbreak

The "Super Outbreak" of April 3-4, 1974 was the worst tornado outbreak of the 20th century with 148 tornadoes produced in just 18 hours. Over half of these tornadoes were classified as significant/strong at F-2 strength or higher, including 23 F-4s and 7 F-5s. The tornadoes struck Illinois, Indiana, Michigan, Ohio, Kentucky, Tennessee, Alabama, Mississippi, Georgia, North Carolina, Virginia, West Virginia, and New York and damaged 900 square miles.

The outbreak began in Morris, Illinois around 1 pm on April 3rd. The storm system intensified as it moved east into more unstable air. By the time this outbreak finally ended in Caldwell County, North Carolina around 7 am on April 4th, a total of 319 people had lost their lives. One of the most deadly and damaging tornadoes struck Xenia, Ohio where 32 people perished, and a significant portion of the town was destroyed. Apartment buildings, homes, businesses, churches, and schools, including Xenia High School, were destroyed. Another tornado produced F-5 damage when it struck Brandenburg, Kentucky and leveled or swept away numerous homes and caused 18 fatalities. In addition, grass was completely torn out of the ground; cars were thrown hundreds of miles and were found mangled and wrapped around trees.

Many comparisons have been made between this outbreak and the April 25-28, 2011 outbreak that resulted in 354 fatalities. While the 2011 outbreak featured many more tornadoes than the 1974 outbreak and occurred over a longer time period, the impacted area was smaller compared to the 1974 Super Outbreak.

Outbreak of May 5-6, 1995

On the evening of May 5, 1995, a devastating supercell struck the Dallas-Fort Worth, Texas area. These storms produced grapefruit-sized hailstones, damaging winds, and heavy rains as they passed over Tarrant County. The hail swath included the bank of the Trinity River where an outdoor festival, Mayfest, was in progress. These storms resulted in no fatalities at the festival, but 60 people suffered serious injuries that required hospitalization.

As the storms moved eastward, the supercell merged with a squall line to produce extensive rainfall, including flash floods, over eastern Tarrant County and much of Dallas County. In northern Dallas County, rainfall rates approached 23 cm/hr (9 in./hr). Over 350 cars sustained weather-related damage, including hail and water damage. Hail also damaged the sidings, windows, and roofs of hundreds of homes and businesses. Strong winds measuring 60-70 mph ripped the roofs off buildings, causing many buildings to collapse. Over 50,000 homes

were left without power in Tarrant County. This outbreak caused 20 fatalities, 17 of which were attributed to flash flooding.

Outbreak of May 15-16, 1998

A rapidly-moving line of violent thunderstorms spawned 5 tornadoes, generated high winds, and produced large hailstones across much of Minnesota during May 15-16, 1998. In St. Paul/Minneapolis, Minnesota, 90 mph winds and golf ball-sized hail caused extensive damage to residences, commercial buildings, and vehicles; hailstones up to three inches in diameter were reported in the International Falls area. This outbreak resulted in one fatality.

Outbreak of May 3-7, 1999

Starting in the late afternoon of May 3, 1999, a severe thunderstorm outbreak produced many large and damaging tornadoes in central Oklahoma. This outbreak was the most prolific in Oklahoma history as 70 tornadoes were observed across the region, 16 of which were classified as strong or violent (F-2 or higher). At one point, there were four tornadoes on the ground at the same time in Oklahoma.

The storm's most destructive tornado was an F-5. This storm tracked for nearly 90 minutes along a 38-mi path from Chickasha through south Oklahoma City and the suburbs of Bridge Creek, Newcastle, Moore, Midwest City, and Del City. This tornado alone was responsible for 36 fatalities and over 500 injuries.

Oklahoma's May 3-7, 1999 outbreak caused a total of 48 fatalities and destroyed over 10,500 buildings and 47 businesses.

Outbreak of March 28-29, 2000

On March 28, 2000, a tornado touched down west of downtown Fort Worth and created a 4-mi path of destruction through the city during the evening rush hour. Although the storm lasted only ten minutes, it demolished several high-rise buildings and significantly damaged many homes, office buildings, vehicles, and a church. The tornado, which caused F-2 damage at its peak, had weakened by the time it entered the downtown area, but it still caused thousands of broken windows in buildings and high-rises due to wind-borne debris (Figure 16).

The same storm system spawned another tornado near Arlington and Grand Prairie, Texas, destroying roughly 150 buildings. The storm started as an F-3 and varied from an F-2 to an F-0 along its 6.5-mi path. Many homes were completely devastated, leaving approximately 80 people homeless. Heavy rains flooded streets, and glass was shattered by hailstones that measured up to 2.75 in. in diameter. Five people lost their lives during this storm, and an estimated ninety more were injured.

Figure 16. Tornado Damage to Commercial Buildings in Fort Worth, Texas, on March 28, 2000 (Source: Verisk)

Outbreak of April 6-12, 2001

From April 6-12, 2001, severe thunderstorms produced tornadoes across 14 states, including Arkansas, Colorado, Iowa, Illinois, Indiana, Kansas, Michigan, Minnesota, Nebraska, Ohio, Oklahoma, Pennsylvania, and Texas. The storms also produced widespread straight-line winds. In Oklahoma alone, a network of environmental monitoring stations recorded winds in excess of 50 mph at 46 different sites.

The storms also produced hail swaths; the largest of which had a length of approximately 245 mi and a width of 22 mi as it moved east through the highly populated Interstate 70 corridor from southeast of Kansas City through St. Louis, Missouri on April 10th. The most damaging hail in this swath ranged between 1.00 and 3.00 in. in diameter. However, even hailstones with diameters between 0.75 in. and 1.00 in. caused considerable damage when they were propelled by a downward rush of air (i.e., a downburst) in excess of 70 mph. Northern St. Louis County experienced the brunt of the impact as nearly every home and business were damaged. In addition to widespread damage, there were 4 fatalities and 18 injuries that resulted from these storms.

Outbreak of May 2-11, 2003

Between May 2nd and 11th, multiple supercell thunderstorms developed and produced numerous tornadoes, hailstorms, and straight-line windstorms. These storms pummeled 20 states throughout the eastern half of the United States, including Alabama, Arkansas, Colorado, Georgia, Illinois, Indiana, Iowa, Kansas, Kentucky, Mississippi, Missouri, Nebraska, North Carolina, Ohio, Oklahoma, South Carolina, South Dakota, and Tennessee. The intense outbreak set a record for the most tornadoes (334) in a week.

May 4th was one of the worst days of the outbreak with 81 tornadoes, 26 of which were F-2 or greater. In addition, 15 of these tornadoes tracked distances ranging between 15 and 80 mi across southeast Kansas and the Missouri Ozarks. These tornadoes produced extensive

damage as more than 3,000 homes and businesses were impacted. One of the hardest hit towns was Pierce City in Lawrence County, Missouri, which was impacted by a tornado that remained on the ground for 30 minutes. This tornado damaged virtually every home and business in the town and leveled the National Guard Armory where several people had taken shelter.

There were reports of major damage in Kansas, Tennessee, and Arkansas. In Kansas, at least four tornadoes touched down, the largest of which reached a width of 500 yards, prompting the governor to declare a state of emergency in seven southeastern counties. In Madison County, Tennessee, a possible F-4 tornado with winds topping 207 mph left a 65-mi path of destruction that included 1,600 homes and businesses. In Arkansas, there were reports of extensive structural damage in Woodruff County, some 70 mi northeast of Little Rock.

Over 40 lives were claimed, greater than 2,300 homes and businesses were destroyed, and 11,200 additional homes and businesses were damaged during this event.

Outbreak of May 4-8, 2007

In May 2007, a storm system emerged out of the central Rockies to ignite powerful thunderstorms in several Great Plains states. This violent system generated hail that measured up to three inches in diameter, damaging wind gusts, downpours, and intense tornadoes, including a massive tornado that devastated the town of Greensburg in Kiowa County, Kansas on the night of May 4th.

The Greensburg tornado was declared an EF-5 by the NWS with approximately 205 mph winds. The twister was nearly 2-mi wide and left a damage trail nearly 22-mi long. Every business on the main street of Greensburg was demolished, churches lost their steeples, trees were stripped of their branches, and neighborhoods were flattened. Officials reported that 95% of the businesses and homes in Greensburg, a town of about 1,800 people, were destroyed and the remaining 5% were damaged. There were 11 fatalities and 60 injuries as a result of this tornado. Outside of Kiowa County, farm sheds, house windows, and shingles were blown out. The Greensburg tornado was one of 22 tornadoes that touched down in southern and central Kansas as a result of the same severe storm system.

Outbreak of February 5-6, 2008

During the Super Tuesday Tornado Outbreak of February 5-6, 2008, a massive storm system spawned deadly tornadoes throughout Arkansas, Alabama, Kentucky, and Tennessee. This system caused massive destruction when it swept through highly populated areas, such as Memphis, Nashville, and Jackson, Tennessee. The Storm Prediction Center received more than 130 reports of tornadoes, and 10 tornadoes were ranked as EF-3 or EF-4 events. The NWS reported that a single tornado in Tennessee was on the ground for nearly 40 mi. In Arkansas, a tornado with 200-mph winds had a track that measured approximately 123-mi long.

There were 250 reports of straight-line wind events throughout the southern states; in Indiana, gusts measuring up to 82 mph were recorded during one storm. There were also 128 reports of hailstorms, some of which had softball-sized hailstones. Portions of Illinois, New

York, Kentucky, Ohio, and Indiana experienced significant flooding due to heavy rains and melting snow, while areas in Michigan, Illinois, and Wisconsin were hit with heavy snow and freezing rains.

Numerous businesses, homes, churches, mobile homes, tractor trailers, and cars were destroyed throughout the southern United States during the outbreak. Thirty-one buildings on the campus of Union University in Jackson, Tennessee, were damaged, including two dormitories that were rendered uninhabitable (Figure 17). Fifty-seven people across four states were killed, and hundreds more were injured, during the event.

Figure 17. Tornado damage inflicted on February 5-6, 2008, at Union University in Jackson, Tennessee.
Images include: (a) Roof damage to Jennings Hall, (b) damage to Bancorp South, (c) destruction of the Jelks Dormitory, and (d) cars in a campus field. (Source: Verisk)

Outbreak of March 14-16, 2008

On March 14, 2008, the first tornado recorded in Atlanta since recordkeeping began (the 1880s) touched down in the city's center. The EF-2 tornado was 200 yards wide and tore a path 6 miles long. The storm was atypical because it was not associated with a squall line or a group of severe thunderstorms, but rather it was an isolated supercell drifting well ahead of the main storm system.

The tornado caused widespread damage in Atlanta's commercial district (Figure 18), including the CNN Center and the Georgia Dome. East of Atlanta's center, an auto parts warehouse collapsed, and a Georgia State University dormitory was seriously damaged. Numerous cars were overturned, windows were blown out, and buildings were flooded during the storm. The tornado continued into the residential neighborhood of Cabbagetown, where

the top floor of an old industrial building collapsed. Numerous single-family, wood-frame houses in the neighborhood sustained heavy damage from overturned trees.

The severe weather continued into March 15th, when the Storm Prediction Center received 38 tornado reports, 160 hail reports, and more than 70 reports of straight-line winds across northern Georgia and South Carolina. Two deaths were reported in northwest Georgia.

Figure 18. Tornado damage inflicted in downtown Atlanta on March 14-16, 2008 (Source: Verisk)

Outbreak of May 10, 2010

On May 10, 2010, long track supercell thunderstorms triggered 56 tornadoes over a large part of northern, central, and southern Oklahoma. The tornado damage paths were spread over 200 mi from near the Kansas-Oklahoma border to near Red River. Hail up to the size of softballs was also reported in several locations.

The first round of tornadoes developed around mid-afternoon near northern and western Oklahoma. One of these tornadoes was rated an EF-3 and traveled from near Wakita to Braman. By evening, tornadoes had also struck the Oklahoma City metro area and were about to break out across southwest and south-central Oklahoma.

The storms produced a total of 2 EF-4, 4 EF-3, and 2 EF-2 tornadoes. The tornadoes that occurred near the metro area caused significant damage to numerous structures, including vehicles, trees, and power lines. One of the more intense tornadoes moved across Lake Thunderbird east of Norman destroying numerous boats. There were 3 fatalities and over 450 injuries, most of which were minor.

Outbreak of May 12-16, 2010

A stationary front that developed from the Atlantic Seaboard westward produced a series of severe storms that rattled parts of Maryland, Pennsylvania, Oklahoma, Texas, and Illinois. Along this frontal boundary, severe weather outbreaks produced damaging winds with gusts nearing 60-85 mph in some locations, hail up to the size of softballs, tornadoes, and torrential rain and flooding. As a result, there were widespread reports of damaged buildings and cars, shattered windows, and downed trees and power lines.

A large supercell thunderstorm developed over Major County in Oklahoma, quickly became severe, and moved towards the southeast producing baseball-sized hail west of Fairview and up to softball-sized hail west of Okeene. A larger area of at least golf ball-sized hail developed from south of Kingfisher to northwest Oklahoma City, with embedded areas of larger than baseball-sized hail. Near Oklahoma City, hail as large as 4.25 in. caused widespread damage. Wind speeds also averaged around 50 mph, with some locations measured winds in excess of 60 mph. As the supercell moved through the heart of the Oklahoma City metro area, there were hundreds of reports of damaged automobiles, trees, and vegetation. Hail drifts reached several feet deep over some areas with hail still on the ground more than 12 hours later. The reported hail sizes became smaller as the storm moved into Seminole, Hughes, and Atoka counties.

Elsewhere, in Texas, storms produced damaging hail and dumped as much as 4.45 in. of rain causing widespread flooding. Storms in the Mid-Atlantic region produced damaging hail, torrential rain, and damaging winds in several areas. In Illinois, wind gusts nearing 60 mph in some locales damaged buildings, shattered windows, and downed trees and power lines. Some cities and towns also received over two inches of rain.

Outbreak of June 10-16, 2010

On June 10, 2010, a slow-moving frontal system triggered severe storms from northeastern Colorado through several states. The storms produced hail up to 2 to 3 in. in diameter and damaging wind gusts. Two tornadoes also touched down in northeastern Colorado. Some of the storms unleashed downpours that led to localized flash flooding.

In eastern New Mexico, the counties of Quay, Curry, Eddy, Roosevelt, Chaves, and Leah were especially hard hit with hail and winds that gusted to over 60 mph. These winds caused downed power lines and blowing dust in several areas.

As the frontal system moved eastward, it continued to generate severe weather over portions of the southern Plains, the Lower Midwest, and the Carolinas. The storms were particularly violent in parts of Kansas where golf ball to baseball-sized hail shattered windows and destroyed crops. In addition, wind gusts of up to 80 mph produced widespread damage and several tornadoes were spotted. Several inches of rain fell in a matter of hours over areas that were already saturated, which resulted in widespread flash flooding. Indiana was also struck hard with grapefruit-sized hail.

The southern states were impacted by these violent thunderstorms, which unleashed strong damaging winds, hail, and flooding throughout North Carolina, South Carolina, and Georgia. The storm brought down trees and tree limbs leading to damaged homes and power outages.

The storm also blew debris into homes and vehicles and caused structural damages to many properties. In South Carolina, Anderson County was especially hard hit, where large hail was reported as was damage from lightning strikes.

Outbreak of October 4-6, 2010

The combination of a strong low pressure system in Southern California and moisture-rich air from Mexico caused severe thunderstorms to break out across the Phoenix metro area on October 5, 2010. These storms produced baseball-sized hail in Maricopa County, Arizona where the hardest hit areas were Scottsdale and West Chandler. These storms continued to develop as they moved northward during the night. As a result, there were 8 confirmed tornadoes in northern Arizona on Wednesday, October 6, 2010. These 8 confirmed tornadoes were the most to strike Arizona in a single day. They caused significant damage as they followed long paths, one of which exceeded 30 mi. Another tornado was strong enough to earn a rating of EF-3. There were also 4 EF-2 tornadoes and 1 EF-3 tornado.

This major hail event, a relatively rare occurrence in the Metro Phoenix area, caused significant damage to homes and automobiles. Specifically, windows were smashed, and roof tiles and shingles were blasted apart. In addition, approximately 40 telephone poles in southwest Mesa fell during the storm causing damage to 20 to 30 homes. Also noteworthy was the temperature drop from the mid-80s to the mid-50s in just 15 minutes.

Outbreak of April 22-28, 2011

In late April of 2011, a severe thunderstorm outbreak ravaged the southeastern United States. The outbreak included over 300 tornadoes, 15 of which were classified as violent (i.e., EF-4 or higher), straight-line winds, and baseball-sized hailstones. Also, a record was set for the most tornadoes in a 24-hour period as 190 touched down between April 27th and April 28th. The outbreak caused the most loss of life from a natural disaster since Hurricane Katrina in 2005 with 354 fatalities. The damage resulting from these tornadoes was extensive; whole neighborhoods were destroyed, and power was cut to over a million households.

Alabama was the most affected state as 9 violent tornadoes touched down on April 27th. The city of Tuscaloosa (population of about 95,000) was especially hard hit when it sustained a near-direct hit from a high-end EF-4 tornado with winds of at least 190 mph. This tornado had a base approximately 1.5-mi wide and tore an 80.3-mi path through the city. The tornado caused catastrophic damage as thousands of homes, businesses, schools, and other structures were severely damaged or destroyed (Figure 19).

Two massive EF-5 tornadoes impacted other areas of Alabama as well. One of these tornadoes followed a 25.2-mi path through Marion, Franklin, Lawrence, Limestone, and Madison counties. This tornado devastated the town of Hackleburg in Marion County, where an estimated 75% of the town was destroyed. The other EF-5 tornado ripped a path through Dekalb County.

The damage in Alabama prompted the governor to declare both a state emergency and classify 38 of 67 counties disaster areas. A federal emergency declaration was also declared, which activated 2,000 members of the state national guard for rescue and recovery efforts.

Figure 19. Tornado damage inflicted to a small business in Tuscaloosa, Alabama on April 27-28, 2011 (Source: Verisk)

Outbreak of May 20-27, 2011

May 2011, normally the most active month for tornadoes, began quietly. For three weeks, only a handful of isolated tornadoes were reported. But on May 20th, severe thunderstorms in eastern Texas and parts of Arkansas and Oklahoma brought high winds, hail, and five reported tornadoes. Over the next seven days, more than 150 confirmed tornadoes raged across the heart of the country. The severe weather funneled across a corridor that stretched from Lake Superior to central Texas and east through Missouri, Tennessee, Kentucky, Ohio, and to the East Coast, impacting more than 20 states in all. Thousands of buildings were damaged, hundreds more were destroyed, and more than one thousand people were injured. There were more than 160 fatalities with most occurring in Joplin, Missouri.

Missouri was the most severely hit as several tornadoes touched down on May 22nd. The city of Joplin, located in the southwestern corner of the state just a few miles from the Kansas border, experienced an extraordinarily violent tornado that was later rated an EF-5. This tornado touched down just inside the Missouri border and cut straight across Joplin before continuing to the east. The tornado left a 0.75-mi wide and 14-mi long flattened path through Joplin. In nine minutes, more than 8,000 homes and apartment units, and more than 500 commercial properties, were heavily damaged or destroyed.

There was also significant damage in Minnesota, Kansas, northern Texas, and southern Indiana. In Minnesota, more than 100 houses and several commercial properties were damaged, and many trees and power lines were knocked down. In Kansas, 14 reported tornadoes touched down on May 21st, and some locales were hit with hail as large as

baseballs. In Texas, tennis ball-sized hail fell across the Dallas and Fort Worth areas through the early evening of May 24th. This hail smashed car windows, damaged roofs, and left nearly 70,000 homes and businesses without electricity. Eight confirmed tornadoes also touched down in Texas. In Indiana, the small town of Bedford sustained significant damage with several homes destroyed.

Outbreak of June 28, 2012 - July 2, 2012

This severe thunderstorm outbreak spawned one of the most destructive derechos in North American history. This fast-moving derecho tracked across a large section of the Midwestern United States, across the central Appalachians, and into the Mid-Atlantic states during the afternoon and evening of June 29th and into the early morning of June 30, 2012.

The storm began as a small thunderstorm in central Iowa, developed into a mesoscale convective system as it tracked into Illinois, and then evolved into a derecho as it moved eastward into Indiana. Wind gusts increased to as high as 91 mph in Fort Wayne, Indiana.

Damage was widespread and extensive along the derecho's entire path, especially in northern Indiana and the Fort Wayne metro area, central and western Ohio, northeastern Kentucky, southwestern Pennsylvania, West Virginia, northern, central, and southwestern Virginia, Maryland, Washington, D.C., Delaware, and southern New Jersey. The damage included millions of power outages; siding torn off houses; roofs removed from houses, businesses, and apartment buildings; mobile homes heavily damaged; barns and garages destroyed; and airplanes flipped. The storm also resulted in 22 fatalities across the entire affected region.

May 20, 2013 Moore, Oklahoma Tornado

A devastating EF-5 tornado struck Moore, Oklahoma, and adjacent areas on the afternoon of May 20, 2013. This event was part of a tornado outbreak that capped-off a three-day stretch of significant severe weather. Peak wind gusts from this event were estimated at 210 mph. The tornado touched down west of Newcastle and stayed on the ground for 39 minutes over a 17-mi path. Within minutes of touching down, the tornado became violent and proceeded to track in an east-northeast direction across the city of Moore and parts of south Oklahoma City before finally dissipating near Lake Stanley Draper.

The tornado destroyed entire subdivisions in its path, which included 1,150 homes. There were 24 fatalities. Among the fatalities were 7 children at Plaza Towers Elementary School, one of two elementary schools that were in the hardest hit areas. At the Plaza Towers Elementary School, the maximum wind of the EF-5 tornado caused structural failure of the main frame and completely destroyed the roof system (Figure 20). As seen in Figure 21, just two blocks north of the school, structures sustained significant damage but were not leveled by the tornado.

Moore Medical Center was also heavily damaged. There were more than 61,500 power outages related to the tornado. Oklahoma governor Mary Fallon declared a state of emergency, and President Obama declared a major disaster in the state, ordering federal aid into the affected counties, which include Cleveland, Lincoln, McClain, Oklahoma, and Pottawatomie.

Figure 20. Remains of the Plaza Towers Elementary School (Source: Verisk)

Figure 21. Just two blocks north of the Plaza Towers Elementary School, structures sustained significant damage but were not leveled. (Source: Verisk)

3 Event Generation

The event generation module combines statistical and physical methods to determine the annual frequency, intensity, and location of simulated severe thunderstorms. The motivation for employing both methods in the model is to (1) apply the large amount of meteorological research that suggests that parameters (index values) can be used to determine when conditions are favorable for severe thunderstorm formation, and (2) address the significant reporting biases that exist in the SPC data. The approach Verisk researchers followed to evaluate historical data, develop damage footprints, augment the data, and validate the catalog are all discussed in this chapter.

3.1 Model domain

The Verisk Severe Thunderstorm Model for the United States' model domain in the event generation module, shown in Figure 22, includes the conterminous United States and most of Canada's southernmost provinces. Note that events are not generated over the Atlantic or Pacific Oceans.

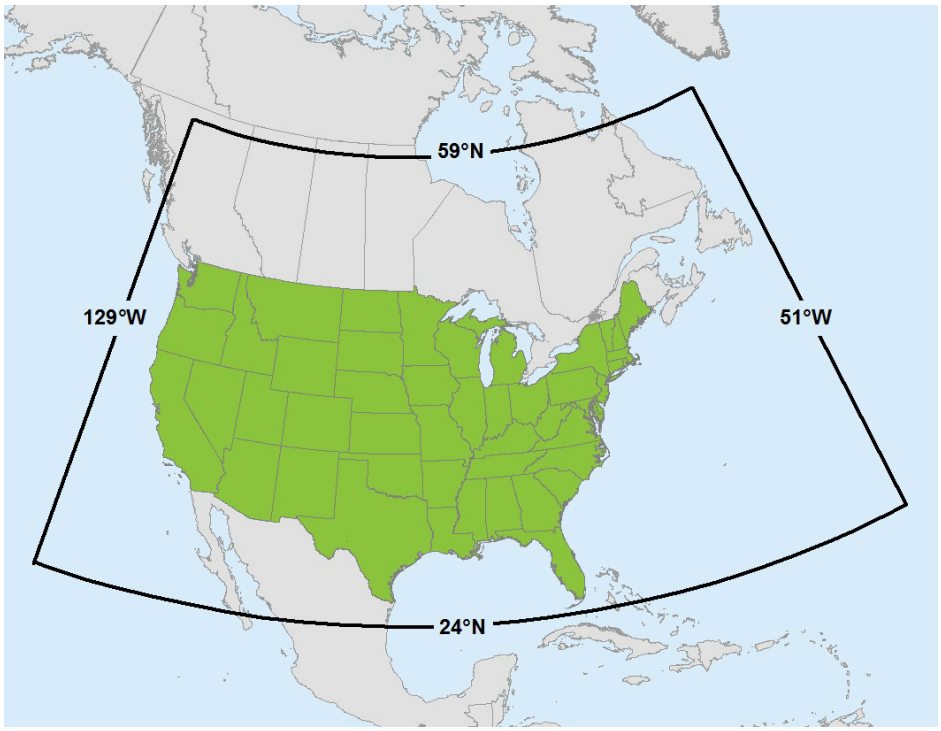

Figure 22. Event generation module model domain for the Verisk Severe Thunderstorm Model for the United States

3.2 Event definition

Verisk's event generation module captures both the highly-localized effects of individual tornadoes, hailstorms, and convective straight-line windstorms, as well as the effects of large severe thunderstorm events, known as microevents and macroevents, respectively.

A microevent is a single simulated convective straight-line wind, hail, or tornado event (a single "swath" or "footprint") and is modeled as a discrete ellipse object with no artificial grid. Each microevent has the following properties:

- Starting/"Touchdown" location
- Spatial extent
- Orientation/Direction
- Date of occurrence
- Intensity

A location is impacted by a microevent if it is inside the ellipse and missed if it is outside the ellipse. This modeling approach best represents the binary nature of severe thunderstorm damage footprints, as there is often an abrupt change from little or no damage to severe damage over a short distance.

Macroevents represent large-scale atmospheric systems that cause outbreaks of severe weather. A macroevent can be any one of the following:

- A single microevent
- A collection of microevents that occur on the same day
- A collection of microevents that occur over multiple days, where multiple storms pass in very close succession to one another

The Verisk model splits the total number of macroevents produced in a year into individual events and outbreaks. Daily activity is simulated based on realistic historical occurrence rates and weather patterns for a specific location and season. The algorithm that determines macroevent length depends only on the hazard frequency, not on any loss or duration threshold. Thus, these events and outbreaks can range from one day with just a single swath to over one week with thousands of swaths. All microevents that occur on a unique date are always part of the same macroevent (i.e., the Verisk model does not split a given day into separate macroevents).

The model classifies severe thunderstorm outbreaks based on whether they produce gross insurable losses of at least 25 million USD, which is similar to Verisk's ISO Property Claims Services' (PCS's) definition of a catastrophic event (i.e., events that result in gross insured losses of at least 25 million USD). As a result, Verisk releases two versions of their stochastic catalog to clients: the all-events catalog and the cat-only catalog. The all-events catalog consists of all severe thunderstorm events that meet the modeled intensity thresholds, while the cat-only catalog consists of only those events that produce gross insurable losses of at least 25 million USD. These catalogs enable Verisk's clients to see the impact of both small and large events on their risks.

See Also

Hail impact energy

3.3 Event generation data sources

To thoroughly analyze risk in the conterminous United States, Verisk researchers use information from several agencies, which are listed below.

NOAA's Storm Prediction Center (SPC) and National Centers for Environmental Information (NCEI) Storm Reports	Historical hail, convective straight-line wind, and tornado point data https://www.spc.noaa.gov/wcm/#data Dates: 1979 to 2018
Community Collaborative Rain, Hail, and Snow (CoCoRaHS) Network	Historical hail point data https://www.cocorahs.org/ViewData/ Dates: 1998 to 2018
Severe Hazards Analysis and Verification (SHAVE) Project	Historical severe weather point data https://www.nssl.noaa.gov/projects/shave/ Dates: Mid-spring through late summer, 2006 to 2015
Climate Forecast System Reanalysis (CFSR)	Various meteorological variables combined into composite severe weather indices https://climatedataguide.ucar.edu/climate-data/climate-forecast-system-reanalysis-cfsr Dates: 1979 to 2018 Resolution: 0.5° latitude x 0.5° longitude; 6-hr time intervals
NOAA's Next Generation Radar (NEXRAD) Level III Data	Individual radar site reflectivity data, storm cell ID, predicted probability of hail, predicted probability of severe hail, predicted maximum hail size, and hail index overlay products https://www.ncdc.noaa.gov/nexradinv/ Dates: 1996 to 2017 Resolution: 2-km grid spacing; 10-min time intervals
National Lightning Detection Network (NLDN)	Daily cloud-to-ground lightning flash counts https://www.ncei.noaa.gov/maps/swdi/ Dates: 1992 to 2017 Resolution: 0.10-degree

SPC Storm Reports

Historical point data on tornadoes, hailstorms, and straight-line windstorms are available in a severe thunderstorm database maintained by NOAA's SPC and the NCEI known as the SPC Storm Reports. This extensive database includes information on more than 55,000 tornadoes, 345,000 hailstorms, and 366,000 convective straight-line windstorms from 1950

to the present for tornadoes and from 1955 to the present for hailstorms and straight-line windstorms. The SPC maintains this database by collecting storm event reports from local authorities, trained weather spotters, the media, and local citizens.

The SPC Storm Reports contain valuable information about the frequency, geographical distribution, and intensity of individual microevents that are a crucial part of evaluating severe thunderstorm risk across the United States. However, there are several reporting biases in the SPC data that must be corrected by the model. These biases include:

- Population - Since someone must witness an event to report it, reports are more common in and around population centers. In addition, as the population grows over time, so does the event reporting frequency.
- Location - Some areas within the U.S. have a more robust trained spotter network and data collection methods than others and, therefore, receive more reports than other areas.
- Intensity estimation - There can be significant uncertainty in reported hail size and wind speed because these measurements are frequently estimated by the person reporting the event. For example, individuals often compare hailstones to common objects (e.g., golf balls). As a result, diameters associated with common objects appear more frequently in the report databases than in reality, causing large peaks and valleys in the reported intensity distribution. In addition, tornado damage surveys potentially bias intensity low if a given tornado touched down over a rural area (e.g., corn field) and did not impact any significant structures, for example. Finally, most straight-line wind reports in the SPC data include estimated, rather than measured, wind speeds. These estimated wind speeds are typically biased high compared to actual wind speeds.
- Event classification - Wind reports can include wind speeds from various types of weather systems (e.g., extratropical cyclones) and not just severe thunderstorm-produced convective straight-line winds. These wind reports must be filtered to eliminate non-convective straight-line wind events. Similarly, SPC tornado reports include all reports, including those tornadoes produced by tropical cyclones. These non-convective storm-produced tornadoes need to be removed from the Verisk severe thunderstorm event generation database.

Verisk researchers determined that reporting biases were most severe between 1955 and the early 1970s when no formal reporting system existed. For this reason, and the lack of CFSR data (discussed in a subsequent section) prior to 1979, Verisk researchers did not directly include any SPC data collected prior to 1979. However, the Verisk model uses hundreds of thousands of SPC reports from 1979 to 2018.

Severe thunderstorm event reporting rose beginning in the 1970s due to several reasons. First, the NWS launched a campaign in the 1970s to recruit volunteers to report spot observations. This campaign consisted of the establishment of a formal training program known as SKYWARN®. This program greatly improved the quality of event reporting by providing severe weather spotters with essential information for identifying and describing local storms. In addition, the development of an internationally accepted standard for measuring tornado severity by Ted Fujita in 1971 led to considerable improvements in the quality of tornado survey data.

Further increases in reports ensued in the 1980s because the NWS started issuing severe thunderstorm warnings, which increased event awareness and interest among the general public. Also, the installation of Doppler radar systems at local and regional weather forecast offices in the 1990s dramatically expanded the coverage density and observance of events. There were further increases in event reporting in the 1990s and 2000s due to advances in technology (including the expansion of cell phone networks, making it easier to report severe weather), social media, and the blockbuster 1996 movie "Twister," which resulted in a greater interest in severe weather and storm reporting. Lastly, there were increases over the entire time period due to population growth (i.e., the number of reports increased as the population grew).

Verisk researchers employ a combination of statistical and physical methods to correct for all these reporting biases to ensure full spatial coverage of storm potential, including in locations where no severe weather events have been observed in the past, and generate a stochastic catalog. In addition, hail and wind reports are spatially clustered on a daily resolution to combine reports that were likely from the same storm. A hierarchical clustering algorithm is used with single linkage and cut heights of 0.3 and 0.5 for hail and wind, respectively. Minimum bounding ellipses are computed for each cluster of reports to estimate swath dimensions. Swath intensities are based on the maximum reported hail size and the average wind gust.

See Also

Hailstorms
Straight-line windstorms
Tornadoes

Additional observational datasets

Additional historical observational data are obtained from the Community Collaborative Rain, Hail, and Snow (CoCoRaHS) network and the Severe Hazards Analysis and Verification (SHAVE) project. The CoCoRaHS network began in 1998 and is comprised of volunteer weather enthusiasts who measure and report precipitation (i.e., rain, hail, and snow) in their local communities. As a result, these data are limited to static locations. In addition, the density of this network varies throughout the country, with higher density in the High Plains region, particularly Colorado. The amount of information that accompanies each observation is typically greater than SPC Storm Reports, but there are much fewer CoCoRaHS reports overall.

The SHAVE project was an effort to collect additional targeted storm reports through phone surveys and blend these reports with radar data. This project collected thousands of additional storm reports while it ran (from mid-spring through late summer, 2006-2015). Both the CoCoRaHS network and SHAVE project provide additional but limited data for use in Verisk-model validation.

Climate Forecast System Reanalysis

In 2010, NOAA's NCEP completed a climate study that provided a high-resolution coupling of the atmosphere, ocean, land surface, and sea ice systems around the globe. The goal of

the project, called the Climate Forecast System Reanalysis (CFSR) Project, is to provide the best currently available estimate of the state of these connected systems over a historical period at a higher spatial and temporal resolution than had been done in past climate studies.[7] Version 1 CFSR data (also known as CFSv1) are available from 1979 to 2011. This dataset has been extended to the present using the same climate model run with real-time observations and is known as CFS, version 2 (i.e., CFSv2).

Reanalyses, which produce datasets for climate research, use dynamical models and observation data to produce best estimates of the state of the atmosphere at regular time intervals (usually every 6-12 hours). The raw data used as input come from various sources including satellite, radiosonde (i.e., weather balloon), and reported observations from sea vessels, aircraft, and land-based stations. These data vary, as would be expected, but the amount of data input and thorough validation has shown reanalysis data to be extremely valuable.

CFSR data (i.e., CFSv1 and CFSv2) are available on a global grid at a resolution of 0.5° latitude x 0.5° longitude, four times a day, and at six-hour time intervals. Thus, these datasets provide a higher spatial and temporal resolution than previous well-known and established reanalyses (e.g., NCEP/NCAR Reanalysis). They are widely believed to provide the best available state of the interaction between the ocean and the atmosphere for use in climate research. They are used by NCEP's Climate Prediction Center (CPC) to calibrate operational climate forecasts and to provide estimates and evaluations of the Earth's climate. In addition, a large amount of meteorological research suggests that composite indices calculated from the CFSR data can be used to determine when historical atmospheric conditions were favorable for the occurrence of hail, tornado, and/or straight-line wind events.

To supplement the SPC data, Verisk researchers extract 6-hourly meteorological variables from the CFSR dataset over the Verisk Severe Thunderstorm Model for the United States domain from 1979 to 2018. These variables are combined into composite severe weather indices known to be correlated with severe thunderstorm activity at each 0.5° latitude x 0.5° longitude grid cell and include:

- Convective Available Potential Energy (CAPE)
- Vertical wind shear
- Mid-level lapse rate
- 500 mb temperature
- Significant Hail Parameter (SHiP)
- Energy Helicity Index (EHI)
- Significant Tornado Parameter (STP)

Finally, these indices are aggregated to represent daily (maximum, minimum, or mean, depending on the index) values, which are used to inform the stochastic microevent locations.

[7] "Climate Forecast System Reanalysis (CFSR)." Climate Data Guide. NCAR/UCAR, 2017. Web. 08 Nov. 2017. https://climatedataguide.ucar.edu/climate-data/climate-forecast-system-reanalysis-cfsr

Atmospheric indices

There is extensive research showing that meteorological parameter values can indicate whether atmospheric conditions are favorable for severe thunderstorm activity. For example, historically lower parameter values over mountainous terrain and the leeward side of the Great Lakes is consistent with lower levels of severe thunderstorm activity in those regions. Variations in parameter values within an air mass are also indicative of differences in the stability of the air mass, which sometimes explains why some locales experience more severe thunderstorm activity than others even though both locales are influenced by the same air mass. In other cases, the lack of severe thunderstorm activity is due to an insufficient storm initiation mechanism.

In the Verisk Severe Thunderstorm Model for the United States, parameter values are an integral part of enabling the model to (1) account for risk in regions that have not experienced major severe thunderstorm activity in the brief historical record, and (2) simulate major outbreaks similar to those that occurred outside the historical record used in model development. Two outbreak examples include the 1974 Super Outbreak, in which over 60 F-3 or greater tornadoes struck, and the late season EF-4 tornado that struck Illinois in November 2013.

The parameter values chosen for the analysis are the Significant Hail Parameter (SHiP) for hail,[8] the Significant Tornado Parameter (STP) for tornadoes,[9] and the Energy Helicity Index (EHI) for straight-line winds.[10] These parameter values are known as composite indices because they are composed of meteorological variables (i.e., Convective Available Potential Energy (CAPE), lapse rates, moisture content, and wind shear, amongst others) that are considered ingredients for severe thunderstorm formation. The equations for these parameters are as follows:

$$SHiP = \left[\left(CAPE_{MU}\ J/kg\right)\times\left(Mixing\ \ Ratio\ \ of\ \ MU\ \ PARCEL\ \ g/kg\right)\times\left(LAPSE\ RATE_{700\text{-}500\,mb}\ ^{\circ}C/km\right)\times\left(-TEMP_{500\,mb}\ \ ^{\circ}C\right)\times\left(Shear_{0\text{-}6\,km}\ \ m/s\right)\right]\div 44,000,000$$

$$STP = \left(CAPE_{SB}/1,500\ \ J/kg\right)\times\left(\left(2,000-LCL_{SB}\right)/1,000\ \ m\right)\times\left(SRH_{0\text{-}1\,km}/150\ \ m^2/s^2\right)\times\left(6BWD/20\ \ m/s\right)$$

$$EHI = \left(CAPE_{SB}\times SRH_{0\text{-}1km}\right)-160,000$$

"MU," "ML," and "SB" denote the type of air parcels used to calculate CAPE or Lifting Condensation Level (LCL). "MU" refers to the "Most Unstable" parcel found in the lowest 300 mb of the atmosphere, "ML" refers to the "Mean Layer" conditions in the lowest 100 mb of the atmosphere, and "SB" (i.e., "Surface Based") refers to a parcel found at the surface. Note that for the STP and EHI calculations, Verisk researchers substituted a surface-based ("SB") parcel for all instances of "MU" or "ML" to simplify the calculation of the composite indices. Also, the STP calculation follows the parameter as defined by the SPC for the "fixed layer" formulation, where "6BWD" represents the 0-6 km Bulk Wind Difference, and "SRH" represents Storm Relative Helicity.

[8] http://www.spc.noaa.gov/exper/soundings/help/ship.html
[9] https://www.spc.noaa.gov/exper/soundings/help/stp.html
[10] http://www.stormtrack.org/library/forecast/ehi.htm

Data for these variables are available in the form of the CFSR data for the period of 1979 to the present. For those variables that were not present in the data, Verisk researchers made the appropriate substitutions. Verisk researchers used these data to calculate maximum daily values (06 UTC – 06 UTC) for each of the chosen parameters for the entire historical record used in model development.

Radar reflectivity

Additional historical data are obtained from 22 years of raw NEXRAD Level III radar data from individual radar sites across the contiguous United States from 1996 to 2017. These data are combined into gridded composite radar reflectivity data at 2-km grid spacing and 10-min time intervals. The reflectivity value in each mosaic grid cell is determined using the maximum reflectivity from the nearest neighbor of each contributing radar.

Verisk researchers use these data to identify thunderstorms and to characterize these storms. Radar measures the strength of reflected microwave pulses, which depend, in part, on the average size and state of the precipitation particles. Hail is a better reflector of microwaves than liquid water primarily because hail particles have larger diameters than raindrops but also because water-coated ice particles have a very high reflectivity as compared to liquid water. As a result, hail is usually measured on a radar scan as an anomalously high area of reflectivity. Thus, Verisk researchers developed a storm tracking algorithm that tracks these areas of high reflectivity, which represent the severe portion of the storm's precipitation and often coincide with hail reports and claims that are overlaid.

The Verisk-developed storm tracking algorithm identifies thunderstorms with the potential for large hail as contiguous grid cells with reflectivity values exceeding a 50-dBZ threshold. The algorithm calculates each storm's centroid and then predicts each storm's position for the next timestep based on the current centroid position, movement direction, and speed (new storms are assigned a speed of zero for this timestep).

At the next timestep, storms are again identified and then matched between timesteps. A storm identified at the second timestep is considered to be the same storm identified at the first timestep if: 1) its centroid is the closest to its predicted location, and 2) it has traveled a realistic distance from one timestep to another. Storm movement direction and speed are updated based on the difference in centroids between the first and second timesteps. Storms identified during the first timestep that do not match a storm at the second timestep are terminated. Likewise, storms identified during the second timestep that do not match a storm from the first timestep are initiated as new. This process is repeated every 10 minutes for every day. At the end of each day, all grid cells that were affected ("hit") by a storm are saved. From these data, storm footprints are created by computing the minimum bounding ellipse around the grid cells hit by each storm. Several radar maximum reflectivity statistics (e.g., mean, median) at each grid cell in a footprint are saved. In addition, various other parameters are attached to each footprint such that appropriate filter analyses can be performed by Verisk researchers, including:

- Several meteorological indices (e.g., CAPE, freezing level, SHiP, shear) extracted from CFSR data
- National Lightning Detection Network (NLDN) cloud-to-ground lightning flashes

- NEXRAD Level III hail signatures (e.g., probability of hail, probability of severe hail, maximum hail size)
- SPC, CoCoRaHS, and SHAVE storm report summaries

The full set of radar-based storm swaths is filtered to retain only those that 1) have a predicted maximum hail size of at least 1.75 in. and occur in an environment with a freezing level less than 4,000 m above ground level, or 2) have a reported (SPC, CoCoRaHS, or SHAVE) maximum hail size of at least 0.75-in. The 1.75-in. threshold is based on Verisk's analysis of predicted and observed hail sizes in populated areas where most severe hail would likely be reported. This 1.75-in. hail size threshold is the best discriminator that maximizes the probability of detection and minimizes the false positive rate when predicting whether a radar-based swath contains severe hail. In addition, radar-based storm swath widths are divided by two before generating distributions based on Verisk's internal analysis and results from various field studies that have found actual hail swaths are narrower than radar-based storm swaths (e.g., Changnon, 1970; Giammanco and DeCiampa, 2018; Nisi et al., 2018).

See Also

Hail

3.4 Microevents

Microevents must be generated before they can be grouped into macroevents that comprise storm outbreaks. During Verisk's microevent-generation process, both the frequency and location of severe thunderstorm events are determined based on historical years 1979 - 2017. In addition, SPC's storm reports are augmented for underreporting, the false linear time trend, and frequency discontinuities present in the data using statistical detrending, hybrid smoothing, and Generalized Additive Models (GAMs). This microevent-generation process is discussed in further detail in the following subsections.

Event frequency

Generation

The microevent-generation process begins with randomly selecting a historical seed year to represent a base year at the start of each stochastic year. Both the frequency and locations of simulated events are based on days of the randomly-selected historical seed year, with noise to avoid being too constrained by the historical record.

Next, each stochastic day is simulated separately, based on the corresponding day of that historical seed year. For example, if historical year 2005 is randomly selected as the seed year for stochastic year 1, then 1 January of stochastic year 1 will be based on 1 January 2005, 2 January of stochastic year 1 will be based on 2 January 2005, and so forth.

The simulated number of microevents for each sub-peril is calculated from the modified historical count plus noise to account for variability. About 30% of the simulated years are skewed, meaning that there is an additional factor applied to daily counts that further

inflates or deflates all days in the year. Skewing some simulated years produces a more comprehensive stochastic catalog that allows the model to include years that experience more or less severe thunderstorms than average. The annual skew factors are based on historical clustered SPC Storm Report counts on the date of interest in each seed year. Modifications are made to these storm report counts and include adjustments to account for the lack of severe storm reports in neighboring Canada and detrending to account for growth in the number of severe days and reports over time.

Statistical detrending of SPC Storm Reports

Prior to simulating microevent frequency, Verisk researchers statistically detrend the annual severe hail and convective straight-line wind days and clustered reports in the SPC data to remove the false linear time trend present in the earlier years of this dataset. There is no clear time trend in the EF-1 or greater tornado reports, so no detrending is performed with the observed tornado dataset. The detrending process for hail and wind reports is accomplished using a piecewise model fit to the data that assumes a positive linear trend in the early years and no trend in the later years. In addition, adjustments are made to account for known deficiencies in the database.

For example, Figure 23 shows a time series of the annual number of reported hail days in the SPC Storm Reports database from 1979 to 2017. It is evident that there is a general increase in reported hail days with time from 1979, which levels off around 1998 (green line). If this false trend is not corrected, then simulated years based on the 1979-1997 historical years would have fewer severe days than post-1997 years because the daily count is based on what was reported. These earlier years likely had more severe weather days, but the severe weather was never reported. After statistically detrending these data, the false linear trend is significantly reduced (blue line).

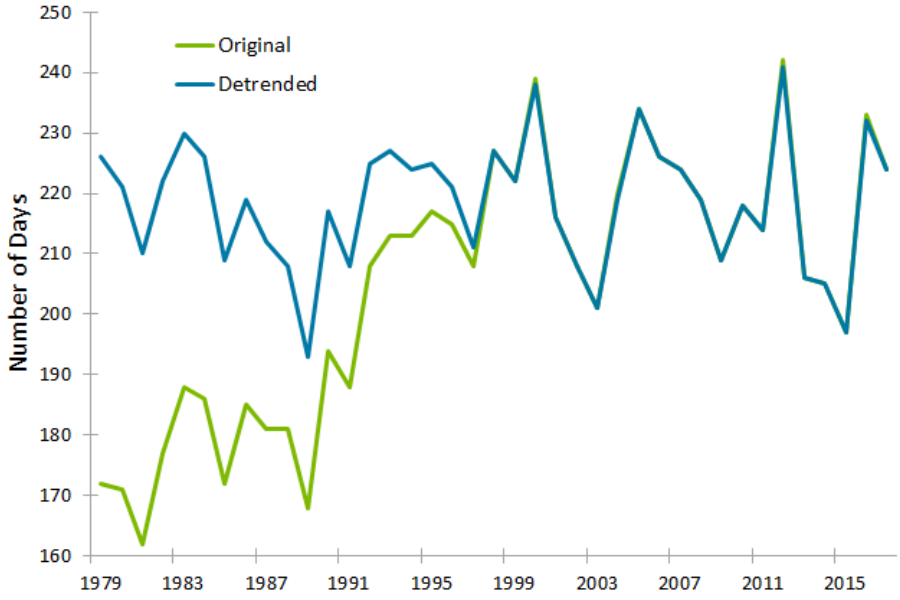

Figure 23. Historical (green line) and detrended (blue line) annual reported number of hail days from SPC's Storm Reports database from 1979 to 2017

As seen in Figure 23, even with adding severe days to the early years, there is still a positive trend in the number of severe hail reports with time. To correct for this false positive trend, Verisk researchers perform the following additional processing steps to the data. First, as seen in Figure 24, hail reports are added to the raw annual number of clustered severe hail reports (green line) to produce the "adjusted" light blue line. This step is performed to account for days that were added during the previous detrending step and to compensate for the lack of data in neighboring Canada. Next, the "adjusted" time series is detrended by using the same piecewise model fit to the data where early years are explained by a linear increase, and no trend is assumed after 2010. The dark blue line in the figure represents this resulting "detrended" time series. Finally, this "detrended" time series is multiplied by two for hail (no inflation factor is used for wind or tornado) and represents the "final" model hail count (orange line). This final step is performed because clustered hail reports and radar data often combine two or more actual separate narrow hail swaths into one swath. If not corrected, a low bias in hail swath frequency would exist in the Verisk model.

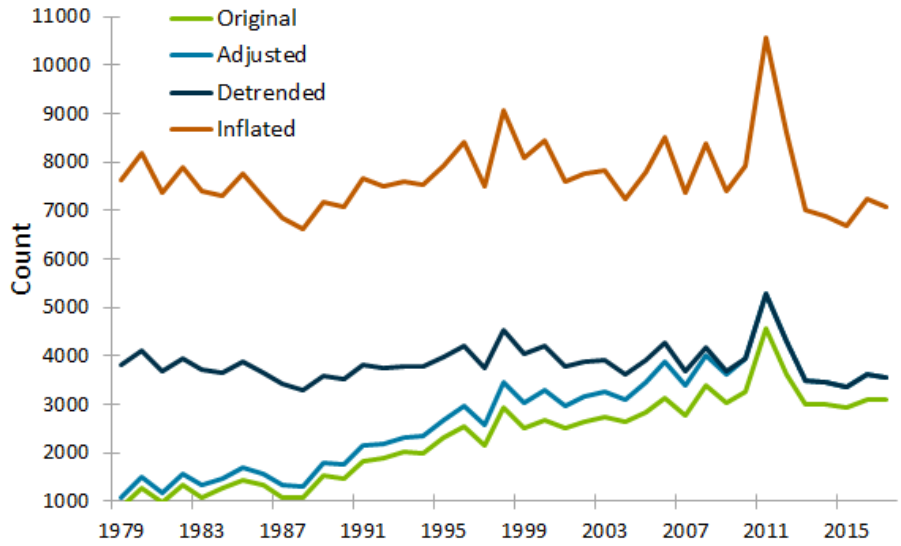

Figure 24. Example of the Verisk statistical detrending methodology used for SPC hail reports.
Plotted in this time series include historical raw annual number of clustered severe hail reports (green line), annual clustered hail reports plus detrended days added (light blue line), detrended version of the light blue line (dark blue line), and the inflated version of the dark blue line (orange line) that accounts for the difference between the actual hail swath shape and what clustered storm reports and radar data indicate. Raw data are from SPC's Storm Reports from 1979 to 2017.

The resulting dataset produces an average number of microevents used to simulate for each historical date and sub-peril. Each time a historical date is used as a seed for a simulated date, this average number is determined, and some noise is added for variability in the dataset. The detrending process ensures that simulated years that use earlier historical years as their seeds do not suffer from lower frequencies than recent years of data would indicate is the true frequency.

See Also
Hazard footprints for historical events

Event placement

Similar to microevent frequency, microevent locations are based on where historical storms occurred. For each historical seed date, Verisk researchers use atmospheric reanalysis data to identify severe storm environments. In addition, Verisk researchers use hybrid smoothing of SPC reports and environmental conditions derived from CFSR (for wind and tornadoes) and hybrid smoothing of SPC reports and environmental conditions captured by Generalized Additive Models (GAMs; for hail) to account for the geographical differences in sub-peril frequency and variability across the U.S. From these resulting data, the model creates gridded probability surfaces representing possible locations where severe thunderstorms could have occurred. These surfaces are sampled hundreds of times (for a 10K catalog) to generate events that are realistic but have not occurred in the relatively short historical record.

Wind and tornado event placement: Hybrid smoothing

To address the observed discontinuities in historical straight-line wind and tornadic storm frequency among neighboring grid cells in some regions, Verisk researchers statistically smooth the data using high-resolution CFSR-based meteorological parameter indices (i.e., EHI and STP, respectively) in a process that can aptly be called "hybrid statistical-meteorological smoothing" to produce a probability surface. This surface represents the chance that a randomly simulated microevent will occur within a 0.5-degree grid cell. This statistical smoothing (via kernel density estimation) allows historical storms to occur in areas where they were meteorologically plausible but not recorded, while the parameter values ensure that the storms are smoothed to physically realistic locations. Since probability surfaces are based on historical storm reports and meteorological variables, the grid cells with the highest probability are locations where storms were observed or where the atmospheric conditions were conducive for storms.

Verisk researchers chose to use the EHI and STP indices for microevent placement location after performing extensive research including analyzing 40 years of CFSR data alongside SPC data for the same time period. They concluded that, on a given day, when the chosen parameters were above certain threshold values, there was a high number of SPC reports for the respective sub-perils. However, when the parameter values were below certain threshold values, there could still be SPC reports for the respective sub-perils. Similarly, there were often areas that seemed favorable for severe storm development according to the indices, but storms never formed. For these and other reasons (e.g., CAPE values tend to inflate the indices over warm bodies of water, like the Gulf of Mexico, leading to results that were not physically realistic), Verisk researchers concluded that the stochastic catalog should be built using a combination of index values and SPC data.

A probability surface for a specific sub-peril is created by first taking the storm reports from a historical date of interest and summing the number that occur within each grid cell. Based on extensive meteorological research, Verisk researchers chose both minimum and maximum

cutoff values for the EHI and STP indices to compare against the calculated daily maximum values for each of the indices as follows:

- If the maximum daily value at a location falls below the minimum cutoff point, Verisk researchers do not smooth the historical reports into that area.
- If the maximum daily value at a location falls below the minimum cutoff point **and** there are historical reports in that area, Verisk researchers spatially smooth the historical reports into that area. This smoothing is performed because low index values do not necessarily indicate that severe thunderstorm activity is not possible.
- If the maximum daily value at a location is greater than the maximum cutoff point **and** there are no historical reports in that area, Verisk researchers allow the probability of events to generate in that location. The amount of probability added is proportional to the difference between the cutoff value and maximum daily value at that location. These gridded data are then smoothed spatially.

The case study shown in Figure 25 shows how this process works for a collection of SPC tornado reports from May 10, 2010. Notice that just statistical smoothing of the SPC reports as shown in (b) does not allow the probability of events to generate in central and eastern parts of Texas. Conversely, a probability function based solely on the index values as shown in (c) could overestimate the probability of events being generated in those locales. By combining SPC reports and parameter values, the final probability function shown in (d) realistically captures the probability of events generated in Texas, which is supported by the NWS's tornado watches for that day shown in Figure 26. The resulting probability surface allows for the generation of plausible, physically realistic, alternative scenarios that did not actually happen, but could have, had conditions been slightly different.

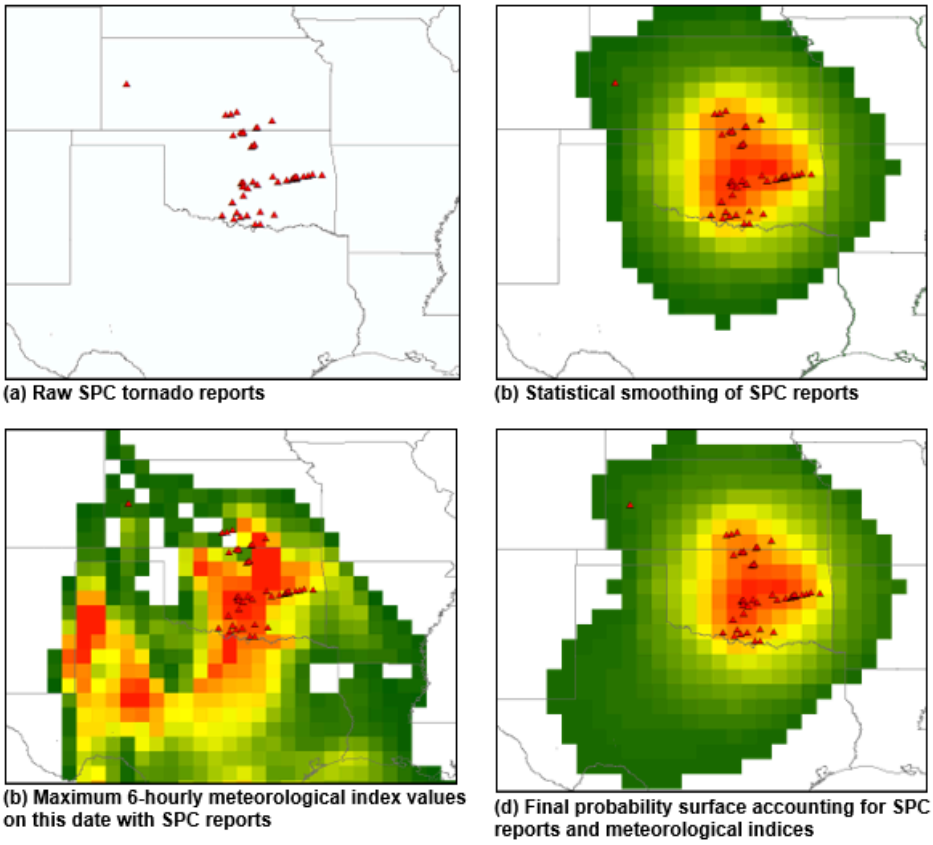

Figure 25. An example of the hybrid smoothing process using the May 10, 2010 historical event

Shown above include: a) raw SPC tornado reports, b) statistically-smoothed SPC reports (with SPC report point data overlaid), c) maximum 6-hrly STP (with SPC report point data overlaid); and d) final probability surface that accounts for SPC reports and the STP index (with SPC report point data overlaid)

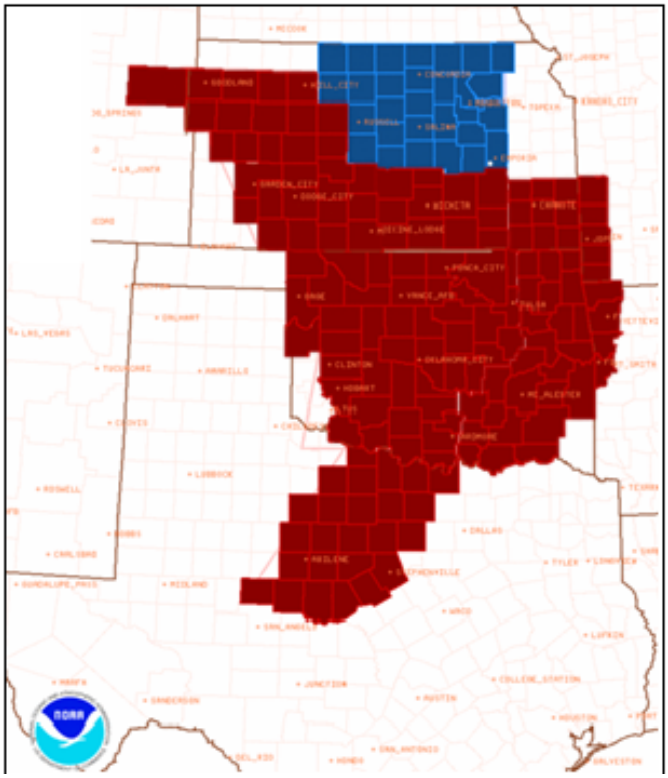

Figure 26. Tornado watches from May 10, 2010 show the potential for activity well into Texas (Source: NOAA)

Hail event placement using Generalized Additive Models

While the "hybrid statistical-meteorological smoothing" technique for determining probable straight-line wind and tornado event locations on a given day validates well, this technique's dependence on a single threshold atmospheric value (i.e., SHiP) for probable hailstorm locations has limited success. This dependence ignores the fact that SHiP is a better indicator of hail in certain regions of the U.S. (e.g., the Great Plains) than others (e.g., the Northeast and the Rocky foothills) because many of its constituent components (e.g., CAPE, shear, lapse rate, and 500-mb temperature) are more important in specific regions and/or elevations than others.

To address both reporting discontinuities in hailstorm events and the varying appropriateness of using a single SHiP threshold value as an indicator of hail activity across the U.S., Verisk researchers use spatially-varying Generalized Additive Models (GAMs) trained separately for each month with equally-weighted observational data and individual SHiP parameters to generate daily hail probability surfaces across the U.S. GAMs allow Verisk researchers to fit a relationship between hail occurrence and environmental parameters while maintaining the flexibility of accounting for regional differences, term interactions, and non-linear relationships. Observational data includes SPC Storm Reports, CoCoRaHS, SHAVE, various claims, and radar data. The individual SHiP parameters are obtained from the maximum and minimum CFSR values for their respective variables on a given day and include:

- CAPE
- Temperature lapse rate (700 - 500 mb)
- 500 mb temperature
- Vertical wind shear
- Elevation
- CAPE-elevation interaction
- Shear-elevation interaction
- CAPE-shear interaction

All data are preprocessed on a 0.5-degree grid, which aligns with the native CFSR grid. The GAMs' results are processed through a sigmoid transform function to produce a grid point-specific probability of hail occurrence on a given day for every day from 1979 to 2017 and for every grid cell in the model domain. These hail probability surfaces were blended with smoothed observational surfaces using a method similar to that for straight-line wind and tornado, but with more equal weights given to each dataset for hail. The results were further calibrated to correct state frequency biases in the data. The final resulting daily hail probability surfaces more accurately capture the hail frequency and variability across the U.S. than using a single SHiP threshold value alone.

Adaptive clustering sampling

To create realistic, spatially-grouped severe thunderstorm events that would not be possible using random sampling alone, the model employs a method called adaptive clustering sampling. This method determines a microevent's location by randomly selecting a grid cell from the appropriate probability surface for a given sub-peril and seed date. It also ensures that subsequently-placed microevents of the same sub-peril are likely to fall near that first microevent.

Adaptive clustering sampling was introduced and developed by Steven K. Thompson in 1990 (Thompson, 1990) as a method of sampling for rare events. This sampling strategy is often used by botanists to sample for rare plant species suspected of forming clusters within the larger population. For botanists, the strategy involves searching for a rare plant until one is found and then focusing the search near the discovered plant, as one would expect that there would be more of this plant species nearby. This sampling strategy is considered adaptive because the design is not completely predictable but rather adapts to the search as it happens.

Adaptive cluster sampling can be applied to severe thunderstorm microevents because, like rare plants, microevents often occur in clusters. That is, a localized area favorable for severe convection will likely generate multiple severe weather-producing cells. The cluster sampling strategy is implemented using the model's daily smoothed and augmented probability distributions as the seeds for stochastic events. First, a point is drawn at random from the distribution and placed according to the original probability surface. Areas immediately surrounding the "touchdown" location of the first stochastic microevent then have an increased probability of hosting a subsequent microevent. Each sub-peril uses separate clustering parameters, which were based on comparisons of modeled results with storm

reports. The procedure continues, each time increasing the probability around each placed microevent.

The combination of using meteorological and statistical smoothing with adaptive cluster sampling allows meteorologically plausible, yet unrecorded, outbreaks to occur.

As an example, Figure 27 shows four stochastic simulations for the May 10, 2010 seed date previously discussed. The black dots show the locations of the microevents for each simulation. The simulation shown on the bottom right is possible because meteorological and statistical smoothing created the probability of generating events in eastern and central Texas and adaptive cluster sampling allowed for realistic outbreak patterns.

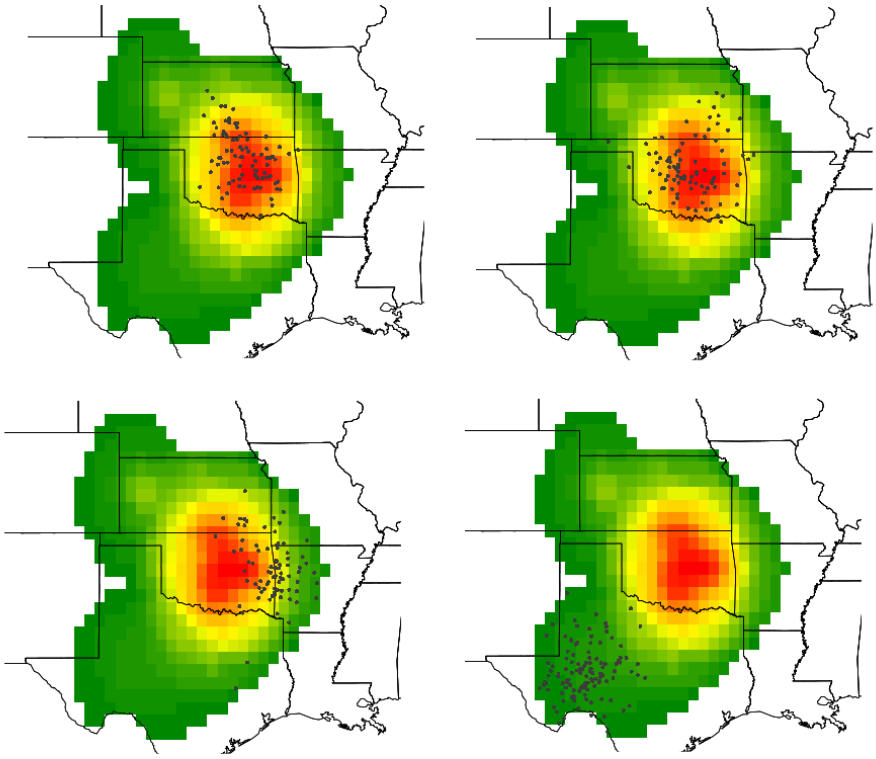

Figure 27. Four stochastic tornado simulations based on the May 10, 2010 seed date.

Note that the stochastic events generated in Figure 27 constitute samples from the smoothed distributions for this particular historical day. As the number of simulation years increases, the spatial distribution of simulated microevents will approach the distribution shown in the background of the figure.

Storm-track direction

The direction of each microevent depends on its starting location. Daily predicted storm motion vectors are calculated from CFSR data using the right-moving supercell motion equation from Bunkers et al. (2000). Since CFSR data is available on a 6-hourly time resolution, the daily average of each vector component (x and y) is calculated, and the direction is calculated from the average components. The model assumes that the most

likely direction is similar to that of the storm motion vector at the microevent's starting location. This direction given by the reanalysis is then perturbed slightly to obtain each microevent's unique simulated storm track direction.

3.5 Modeled storm variables

Verisk's stochastic catalog is built based on detailed historical frequency and storm track information for the three modeled severe thunderstorm sub-perils. Attributes (length, width, direction, and intensity) for all microevents are randomly drawn from distributions developed from the historical data (for hail, these data include radar data) to create a complete range of possible scenarios. The simulated microevents are then clustered to create macroevents. Each event in Verisk's resulting stochastic catalog contains storm parameters specific to each sub-peril and includes a starting location, storm track direction, storm length and width, and intensity.

See Also
Local Intensity Calculation

Hazard footprints for historical events

Hazard footprints, or swath sizes, are derived from the dimensions of historical severe thunderstorm microevents. For wind and tornado, these dimensions were derived from clustered SPC reports; for hail, the radar dataset was used.

Footprint length and width

Footprint length is the distance along the axis of storm motion, and footprint width is the cross-swath distance. They are determined through empirically fit cumulative distribution functions (CDFs) developed using historical observed swaths and vary by sub-peril, location, and season. Unlike microevent frequency and location, these distributions are not specific to the historical seed date, but some vary seasonally and spatially, which allows for realistic variation in microevent attributes.

See Also
Swath length
Swath width

Hail

To define hail microevent footprint length, width, and intensity, Verisk researchers create empirical CDFs from filtered radar-based swaths for each 0.5-degree grid cell in the model domain and for each month of the year. These filtered radar-based swaths are generated using 2-km national gridded composite radar reflectivity imagery from 1996-2017 along with SPC reports, as discussed earlier. This Cumulative Distribution Function-generation (CDF-generation) process involves both spatial and temporal smoothing as well as additional inverse distance weighted (IDW) interpolation to further spatially-smooth the CDFs.

Specifically, for a given grid cell during a given month, radar-based swaths that occurred within 2 degrees of the grid cell and within plus or minus one month of the selected month are used to create empirical CDFs if the number of swaths exceeds 250. This process allows for a higher number of hail swaths to be sampled for creating the microevent attribute CDFs than using a single 0.5-degree grid cell alone. An example is shown in Figure 28 below.

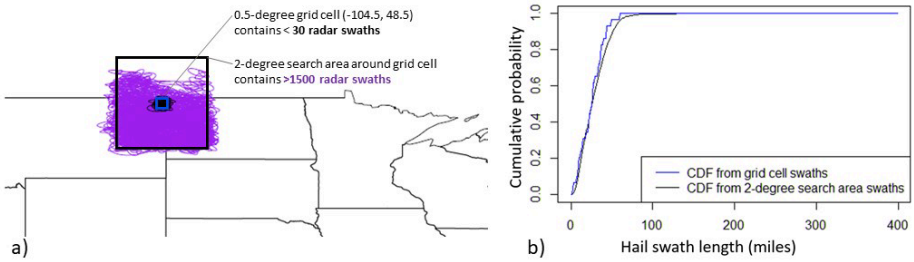

Figure 28. Example showing how using a 2-degree search area around a sample grid cell instead of a single 0.5-degree grid cell alone allows a much higher number of hail swaths to be sampled for creating the microevent attribute CDFs
a) A single 0.5-degree grid cell may contain too few radar swaths to create smooth hail swath length, width, and intensity CDFs. By adding a 2-degree search window around each grid cell, many more radar swaths are available to create hail swath length, width, and intensity CDFs. b) Hail microevent attribute CDFs are much smoother when they are created from many swaths (black) pulled from the 2-degree search area than from few swaths (blue) pulled from the grid cell alone.

If fewer than 250 swaths are identified in a given grid cell, then that grid cell's CDF is temporarily assigned as "NA" but later filled in using IDW interpolation of the surrounding grid cells' distributions. Verisk researchers determined the appropriate swath threshold number (N = 250) to use by dividing the hail swath length, width, and intensity standard error by the mean for each month according to:

$$N = \left(\frac{stdev}{0.05 \times mean} \right)^2$$

For hail swath, width, and intensity in each month, N ranges from 200 to 300 swaths. As a result, a 250-swath target was selected.

For grid cells that contain greater than 250 swaths, radar-based swaths are first used to compute kernel density estimates of the probability density function (PDF) for hail length, width, and intensity for the given grid cell. Then, these PDFs are cumulatively summed to result in monthly CDFs for each hail attribute for each grid cell in the model domain. The smooth CDFs created closely follow the observational data but avoid introducing biases due to data scarcity.

For grid cells that contain fewer than 250 swaths, empirical CDFs are created by spatially smoothing each bin of the monthly CDFs in the surrounding grid cells using IDW interpolation. The resulting hail swath length, width, and intensity empirical CDFs for each month and grid cell in the model domain are uncontaminated by biases due to small sample sizes and reflect both seasonal and spatial variation.

Since hail swath length and width are correlated, Verisk researchers use a Gaussian copula method to simulate them in a three-step process. First, random correlated variables are

generated from standard normal distributions by generating a random standard normal. Then, a second, correlated random standard normal is generated using the equation:

$$x_2 = r \times x_1 + \sqrt{(1 - r^2)} \times N(0, 1),$$

where x_1 and x_2 are the correlated standard normal variables, r is the correlation coefficient, and N(0,1) is a random standard normal. The correlation coefficient used is 0.585 and was determined by calculating the Spearman correlation coefficient from the radar-based storm swath lengths and widths. Once these correlated standard normals are generated, their probabilities are calculated using the standard normal cumulative distribution function. Finally, the empirical marginal CDFs created from the radar-based swaths are used as quantile functions to transform probability to the length and width of a hail swath.

See Also

Radar reflectivity

Straight-line winds

To define convective straight-line wind footprint length and width, Verisk researchers create empirical CDFs from clustered storm reports. These distributions are created by kernel density smoothing the observed lengths and widths for each month for non-derecho dates, and for the whole year for derecho dates. The same method of simulating correlated hail length and width swaths is used for straight-line wind swath simulation. A correlation coefficient of 0.714 is used and was determined from clustered SPC reports' swaths.

See Also

Hail

Tornadoes

To define tornado footprint length and width, Verisk researchers create empirical CDFs from filtered SPC tornado reports. Tornado intensity distributions vary spatially and seasonally for the EF-1 and EF-2 intensity categories. EF-3 to EF-5 tornado probabilities are the same for all seasons, but they do differ between the U.S. and Canada.

EF-1 and EF-2 probabilities are created by rasterizing the seasonal counts of EF-1, EF-2, and all tornadoes of known intensity in each grid cell, locally smoothing these rasters, and dividing the EF-1 and EF-2 rasters by the "all tornadoes" rasters to yield probability intensity rasters for EF-1 and EF-2 tornadoes. Note that empty grid cells in the EF-1 probability rasters are filled with a probability of one, while empty grid cells in the EF-2 probability rasters are filled with a zero. A daily skew factor also modifies the simulated tornado intensity, which is based on the average tornado intensity on the respective historical seed date. When the average intensity is less than EF-2, tornadoes are skewed, on average, to be weaker. When the average intensity is greater than EF-2, simulated tornadoes are skewed to be stronger, on average. However, there is still a random component to this daily tornado intensity skew factor. Even though a historical date may cause simulated dates to be skewed weaker or stronger, on average, it is still possible to skew in the opposite direction so that not all simulated days based on a specific historical date are skewed in the same direction or by the same amount.

To develop realistic swath sizes for tornadoes, Verisk researchers use either the length and width measurements taken at detailed storm surveys or those provided in the SPC database. Note that unlike hail and straight-line wind events, the SPC does provide approximate footprint dimensions for tornadoes along with their maximum EF Scale rating. Thus, simulated lengths and widths are randomly drawn from Weibull probability distributions fit to the reports, which vary by month and intensity. There is no simulated correlation between tornado length and width.

Figure 29 shows the Verisk historical tornado counts. Note that the yearly drop in tornado counts for the Verisk model as compared to the SPC is because Verisk does not model EF-0 tornadoes. Verisk researchers also eliminate any duplicate reports within the SPC database and do not include tornadoes that were produced by hurricanes.

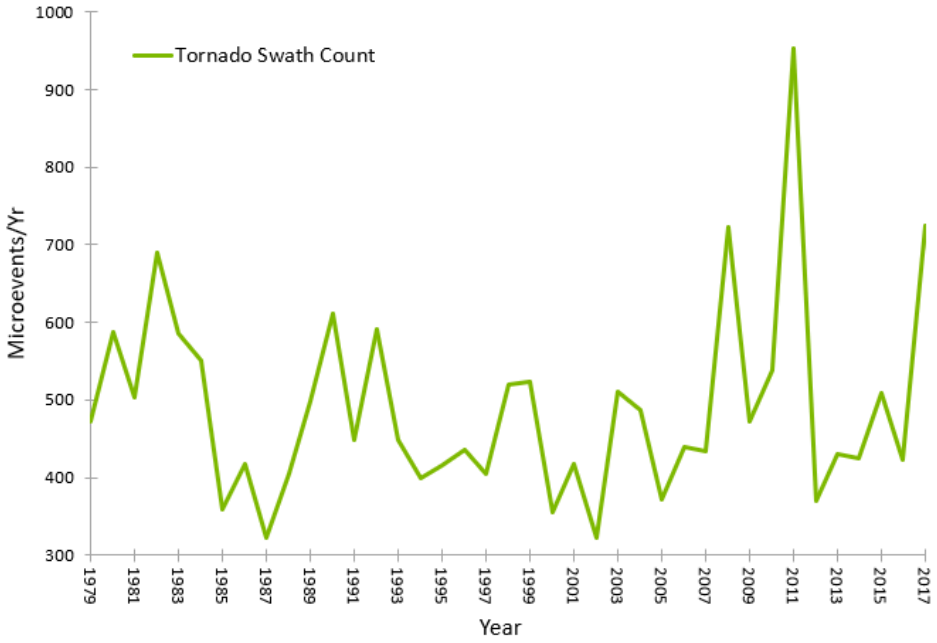

Figure 29. Verisk historical tornado microevent counts

Footprint shape

While the rectangular swath shown in Figure 30 realistically captures the size of the historical microevents, the shape is not necessarily representative of a microevent's true hazard footprint. Therefore, when generating swath sizes for the simulated events, the model translates the rectangular dimensions into those of ellipses. As shown schematically in Figure 30, the length of the ellipse's minor axis is set equal to the length of the short side of the rectangle and the length between the ellipse's two foci (light blue dots) is set equal to the length of the long side of the rectangle. Note for many historical tornado events, Verisk researchers manually split the tornado tracks into pieces based upon their intensity at different points along the track and whether they follow a curved path. Then, multiple ellipses were used for sections with either different EF Scale ratings or different path directions.[11]

[11] However, note that each stochastic tornado track is represented by a single ellipse.

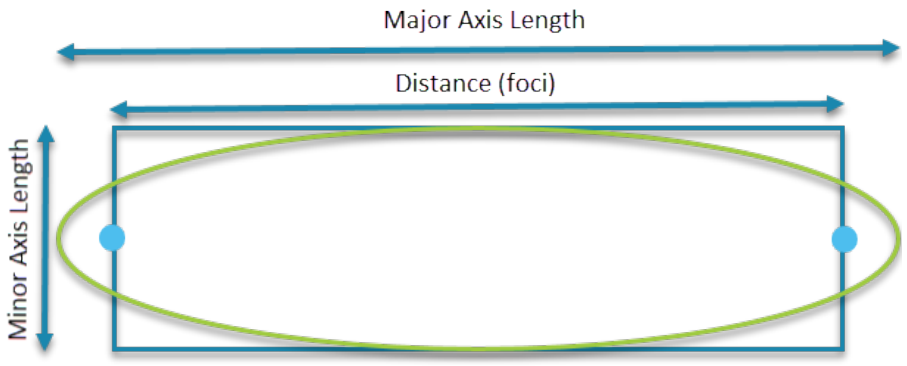

Figure 30. Schematic drawing of an ellipse placed around a microevent (Source: Verisk)

Derechos

Derechos are a subset of convective straight-line winds modeled by the Verisk Severe Thunderstorm Model for the United States. A derecho is defined as a long-spanning and long-lasting convective straight-line wind event that produces over a 240-mi damage swath with wind gusts of at least 58 mph (50 kts) along most of its length. The Verisk Severe Thunderstorm Model for the United States accounts for days in which derechos may occur stochastically by drawing ellipses from historical dates in which a derecho or large wind event occurred. To correctly simulate derecho days, the model must first have a robust set of historical days (i.e., stochastic seed days) for which it assumes a derecho may occur. This derecho dataset is generated using a derecho detection algorithm developed by Verisk researchers based on the scientific research in the detection of derechos.

The Verisk Severe Thunderstorm Model for the United States' derecho detection algorithm constructs a list of derecho event days using SPC wind reports between 1979 and 2018 based on the work of Coniglio and Stensrud (2004). Specifically, the algorithm first filters out all SPC daily wind speed reports below 58 mph (i.e., the threshold criteria for severe weather). Next, for each day in the historical record, hierarchical clustering is performed to spatially group wind reports. This clustering algorithm is similar to that used by the Verisk model when estimating hail and wind ellipses' parameters.

Once daily wind clusters are defined, each cluster is classified as a derecho if it and all its reports meet the following requirements:

- All occur within 2.5 hr of each other (i.e., temporally continuous)
- All occur within 200 km (124 mi) of one another (i.e., spatially continuous)
- The cluster contains three or more wind speed reports greater than 65 mph; each of these reports must also be separated by more than 64 km (40 mi)
- The total cluster length is at least 400 km (250 mi)

This procedure has two parameters: the hierarchical clustering cut height and the gust threshold. Verisk researchers performed sensitivity tests to determine the optimal values to use for these two parameters to best match observed derechos and their trends over time.

While the Verisk derecho detection algorithm is highly skilled at detecting both individual historical events as well as the overall U.S. derecho climatology, there are a few important caveats to consider. First, there is an obvious increasing trend in derecho activity since the late 1990s, similar to the trends seen in other severe thunderstorm sub-perils. This trend is most likely attributed to increased severe weather reporting post-1990, rather than an actual uptick in derecho events. In addition, while Coniglio and Stensrud (2004) used both SPC storm reports and radar data analysis, the Verisk algorithm relies solely on SPC storm reports. As a result, the Verisk algorithm may result in an underestimation of weak events or an earlier ending to an event. Alternatively, Verisk's methodology also includes long squall lines and possible multiple complex/cellular events, whereas, by incorporating radar, many of these events are omitted from the Coniglio and Stensrud (2004) study. It is advantageous to include these events as they represent longer duration events that occurred on given dates that the Verisk Severe Thunderstorm Model for the United States captures.

See Also

Historical trends in straight-line wind activity

3.6 Macroevents

Macroevents are generated on the fly as each day is simulated. At the end of each day, the number of microevents for each sub-peril is counted. If any of the counts exceed their predefined thresholds, then a multi-day macroevent is triggered. As each new day is processed, as long as one of the count thresholds continues to be exceeded, the multi-day macroevent continues and all microevents on those days are given the same macroevent ID. If the count thresholds are not exceeded after the first day, then the macroevent is classified as a single-day macroevent. A macroevent will also be terminated if it reaches 10 days and the total number of microevents on the current day is less than the previous day. Thus, macroevents are allowed to extend past 10 days if the daily count of microevents continues to increase each day.

Each sub-peril's predefined macroevent count threshold varies by day of the year. This threshold is determined from a piecewise function that uses different thresholds during the winter and summer and ramps up or down in short periods between these two seasons. The "winter" thresholds are used from October 15th through March 17th (i.e., days 1-76 and 288-365), and the "summer" thresholds are used from April 16th through September 15th (i.e., days 106-258). The linear ramp up or down exists between these ranges of days. Low and high thresholds for winter and summer are listed in Table 11.

Table 11. Daily microevent threshold used to define a macroevent

Sub-peril	Low Threshold Count (Winter)	High Threshold Count (Summer)
Hail	12	86
Straight-line Wind	12	56
Tornado	4	12

Sub-peril	Low Threshold Count (Winter)	High Threshold Count (Summer)
All Combined	20	120

Figure 31 shows the distribution of macroevent duration, in days, that result from this algorithm for cat-only events. Note that the duration of these events is both realistic and consistent with PCS events.

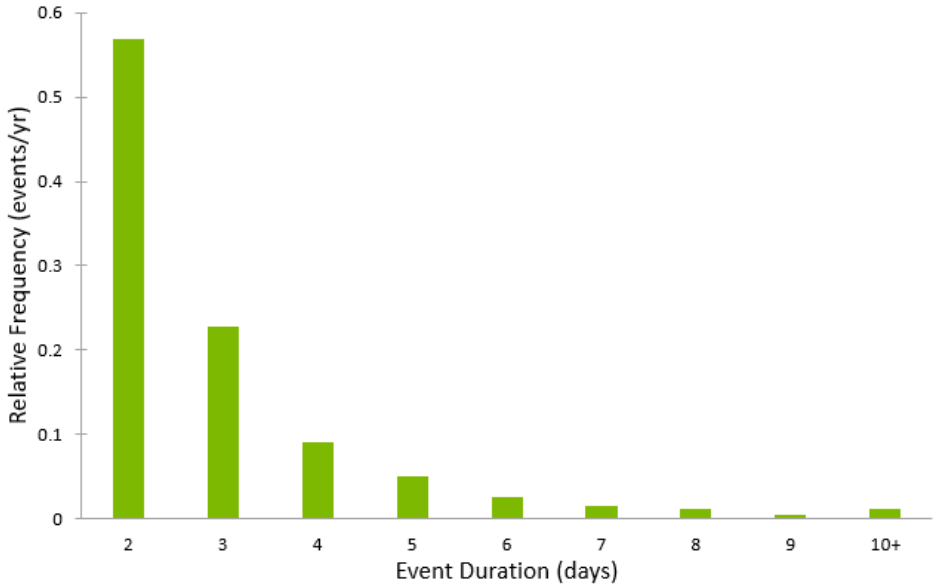

Figure 31. Distribution of simulated cat-only macroevent durations

3.7 Validating event generation

The Verisk Severe Thunderstorm Model for the United States has been extensively validated against the available historical data. This section provides validation of the model's spatial event frequency distributions, seasonality, and microevent attribute correlations.

Spatial frequency distributions

Average Annual Days

A common method used to measure severe thunderstorm frequency is by days per year. By definition, a location or area experiences a severe day if there is at least one occurrence of severe weather on a given day. The number of days is then summed for the year to determine the annual count. This calculation is performed over a defined number of years to determine the average annual severe days for the defined time period.

Verisk researchers validate the Verisk Severe Thunderstorm Model for the United States by comparing the model-simulated average annual severe days by state and sub-peril to the

number of severe days in the clustered SPC storm reports. Due to the stability in the reported number of severe days in the last couple decades, reports between 2000 and 2018 are used to create the observed severe days. Since it is very computationally intensive to compute the full ellipse to state polygon intersections, only the ellipse centroids are used to assign an ellipse to a state. This methodology leads to an underestimate in severe weather days assigned to a given state because an ellipse can intersect multiple states, but the centroid would only be inside one of these states. However, this underestimate is small for most states, and because the same method is used for both modeled and observed days, it is a fair comparison.

Figure 32, Figure 33 and Figure 34, below are scatter plots of model versus observed average annual severe hail, tornado days, and straight-line wind, respectively, with each point in the plot representing a state. As evident in these figures, there is good agreement between Verisk-modeled and observed average annual severe days. In the hail plot (Figure 32), the blue dots represent model validation against a second set of observations derived from radar swaths for the periods 1996-2002 and 2005-2017 (2003 and 2004 are missing). Hail (Figure 32) and tornado (Figure 33) average annual days show no clear bias, with all points distributed around the y=x (1:1) line. Average annual straight-line wind days (Figure 34) shows a small low bias, meaning the model simulates fewer days than observed. This behavior is expected because the observed SPC data has a noted high bias in estimated gusts and many wind reports may actually be less than severe intensity. Thus, the true severe wind frequency may actually be lower than what is reported.

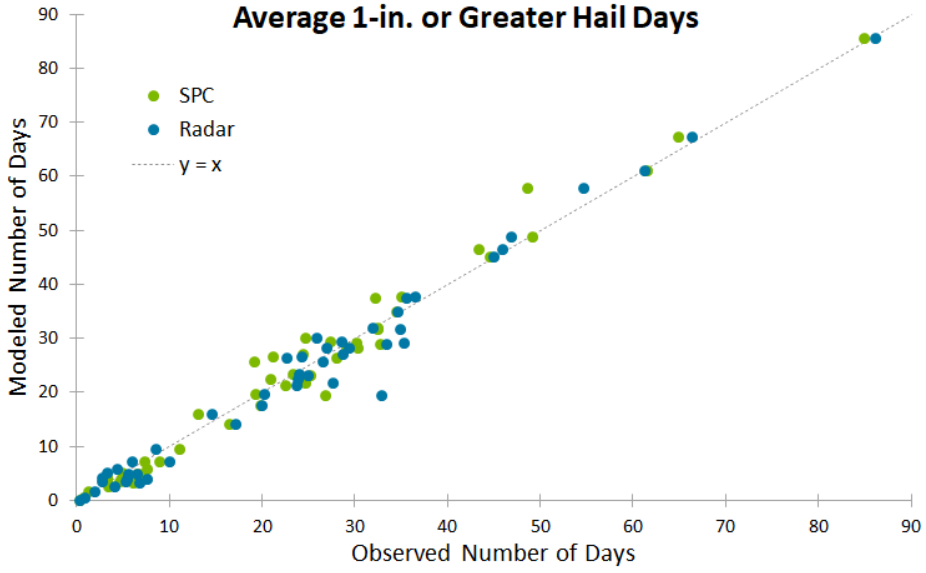

Figure 32. Verisk-Modeled versus observed average annual severe hail days (1-in. or greater) by state
Green dots represent model simulated versus 2000-2018 SPC observations. Blue dots represent model simulated versus 1996-2017 radar observations. Note: Each state's annual average value is represented by a dot.

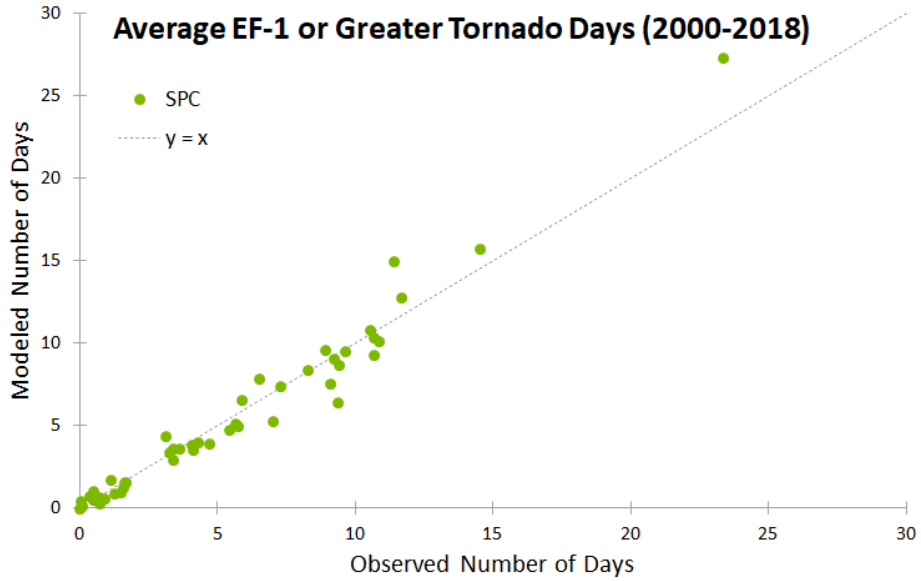

Figure 33. Verisk-modeled versus observed (SPC storm reports; 2000-2018) average annual EF-1 or greater tornado days by state
Note: Each state's annual average value is represented by a dot

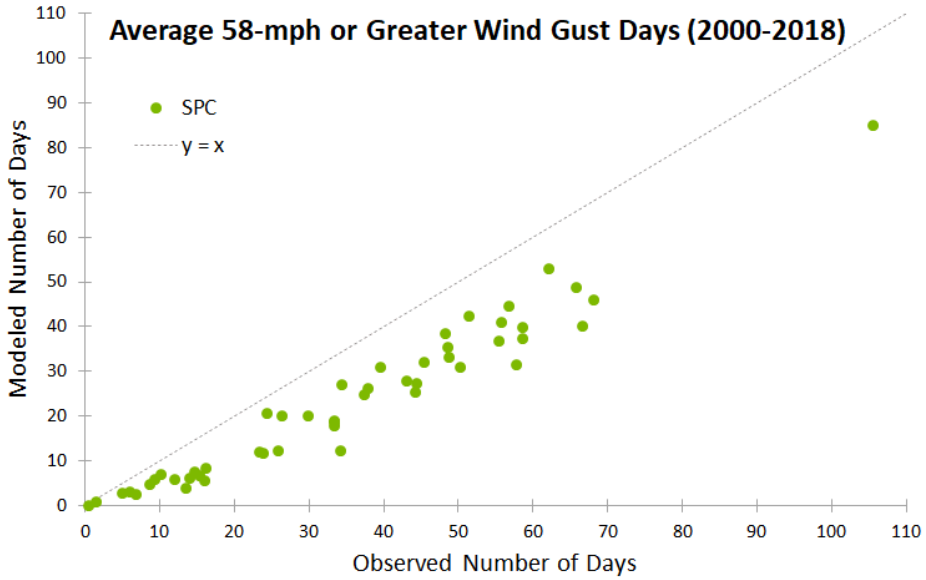

Figure 34. Verisk-modeled versus observed (SPC storm reports; 2000-2018) average annual severe straight-line wind days (58-mph or greater) by state
Note: Each state's annual average value is represented by a dot

Hits

The following set of images shows the spatial variation in average annual severe thunderstorm days by sub-peril on a regular 0.5-degree latitude/longitude grid ("hit" maps). Verisk model simulated hit maps are based on the 10K stochastic catalog, and observed hits are based on SPC reports from 2000 to 2018. As a result, the observed maps are much

noisier than the modeled maps and show the previously-described population biases. Overall, there is good agreement between these model-simulated and observed spatial frequency maps.

The Verisk model-simulated average annual severe hail (1-in. or greater) days (Figure 35) depicts an area of greatest hail activity that extends from Texas northward into the Dakotas, with a maximum in Kansas and Nebraska. A local maximum also exists in North and South Carolina, east of the Appalachian Mountains. Hail frequency rapidly decreases west of the Rocky Mountains and in the Northeast. The observed spatial pattern (Figure 36) looks very similar to the model but with magnitudes being notably lower. These lower magnitudes are a result of underreporting, particularly in many locations where hail occurs most frequently.

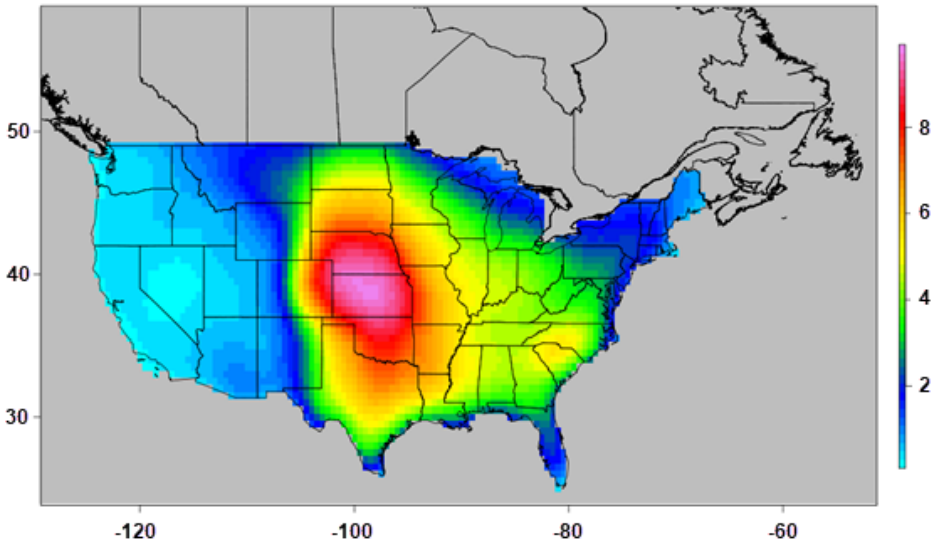

Figure 35. Verisk model-simulated average annual severe hail days (1-in. or greater) based on the 10,000-year stochastic catalog

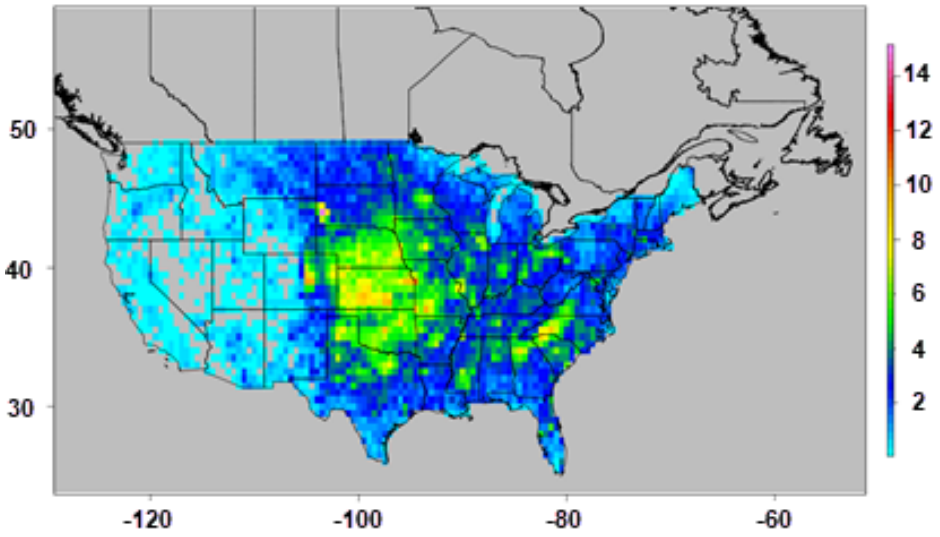

Figure 36. Observed average annual severe hail days (1-in. or greater) based on the SPC Storm Reports database from 2000 to 2018

The Verisk model-simulated average annual significant hail (2-in. or greater) days (Figure 37) has a very similar pattern as the modeled average annual severe hail frequency (Figure 35) but with lower magnitudes. The location of maximum frequency is shifted northwestward slightly toward the Kansas/Nebraska/Colorado intersection. The observed significant hail frequency spatial pattern (Figure 38) has its maximum farther south than the modeled significant hail frequency, but the magnitudes are similar in that area.

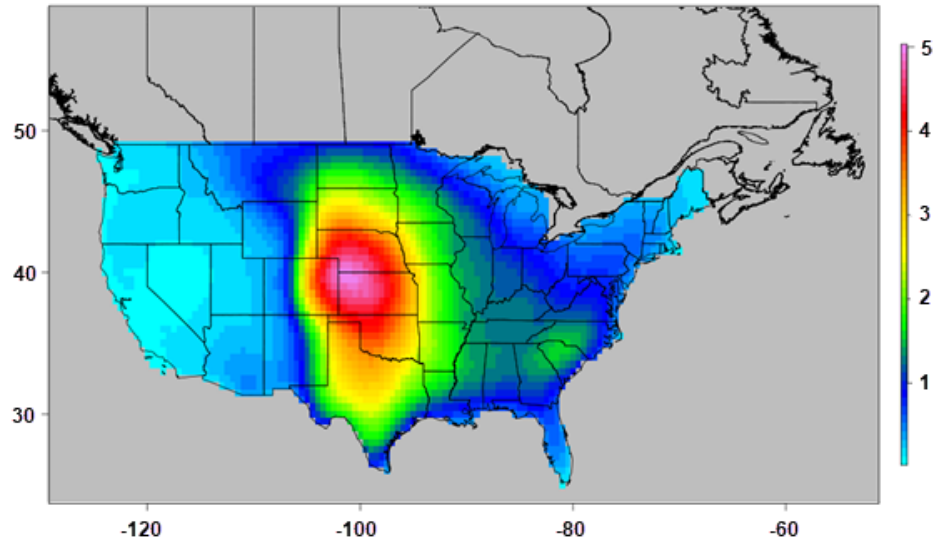

Figure 37. Verisk model-simulated average annual significant hail days (2-in. or greater) based on the 10,000-year stochastic catalog

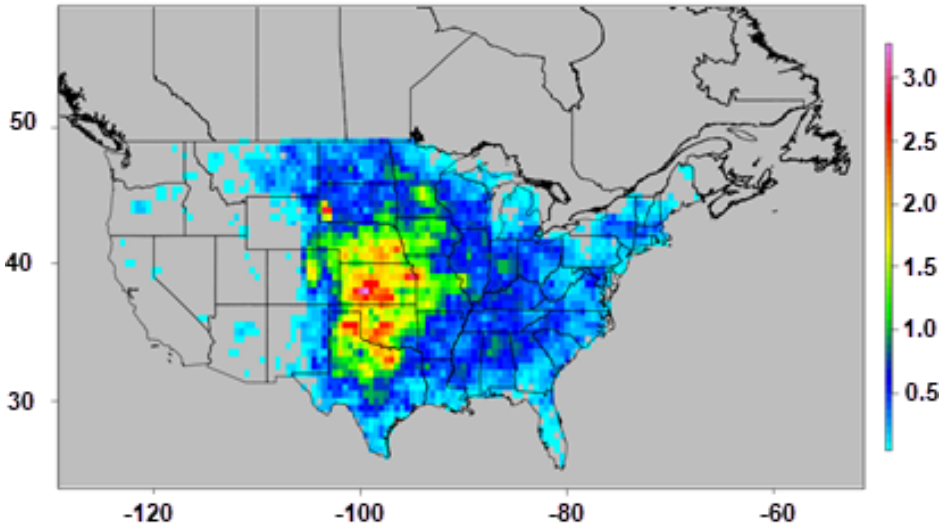

Figure 38. Observed average annual significant hail days (2-in. or greater) based on the SPC Storm Reports database from 2000 to 2018

The Verisk model-simulated average annual severe 58-mph or greater convective straight-line wind speed days (Figure 39) depicts a large area of greatest wind activity that encompasses much of the South and the southern portion of the Midwest. The observed 58-mph or greater wind speed frequency spatial pattern (Figure 40) also has a large area of maximum wind frequency across much of the South and southern portion of the Midwest, but with its maximum frequency expanded slightly farther north into the Mid-Atlantic.

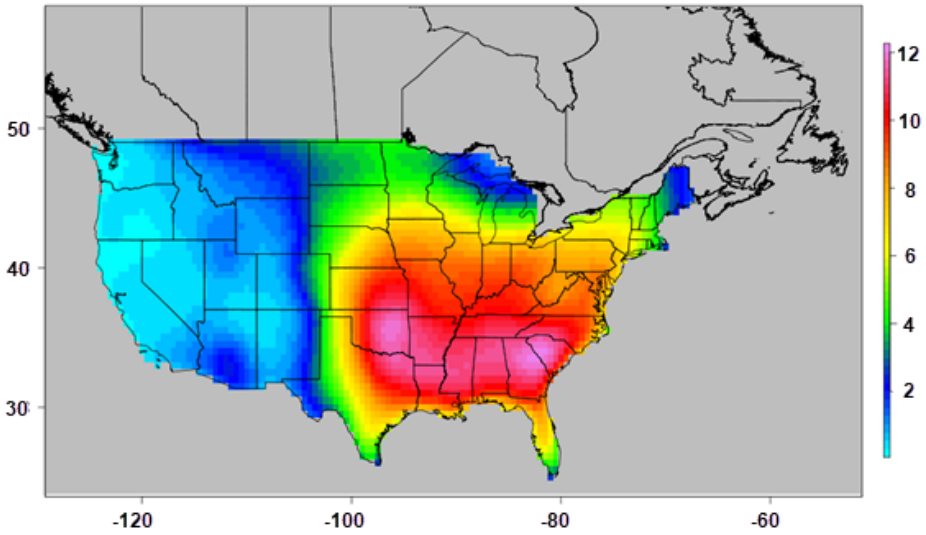

Figure 39. Verisk model-simulated average annual severe convective straight-line wind speed days (58 mph or greater) based on the 10,000-year stochastic catalog

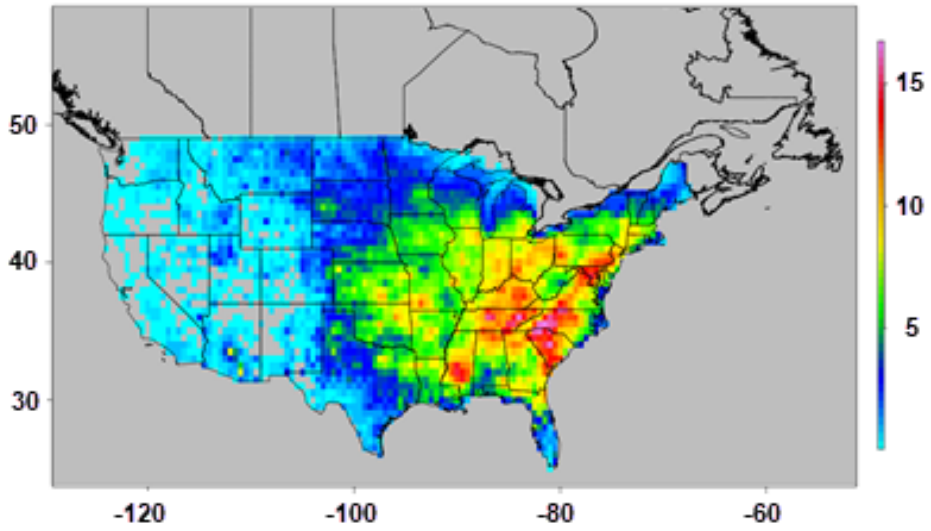

Figure 40. Observed average annual severe convective straight-line wind speed days (58 mph or greater) based on the SPC Storm Reports database from 2000 to 2018

The Verisk model-simulated average annual severe 75-mph or greater convective straight-line wind speed days (Figure 41) depicts an area of greatest wind activity that extends from Texas northward into the Dakotas, with a maximum in Kansas and northern Oklahoma. The observed 75-mph or greater wind speed frequency spatial pattern (Figure 42) shows a similar area of high wind frequency but with maxima over western Kansas (instead of central Kansas) and over Montana and North Dakota.

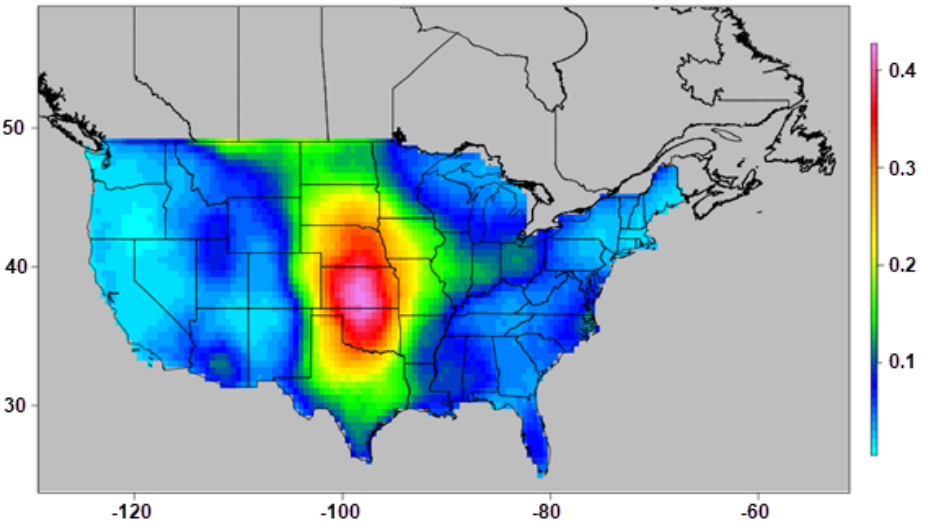

Figure 41. Verisk model-simulated average annual 75-mph or greater convective straight-line wind speed days based on the 10,000-year stochastic catalog

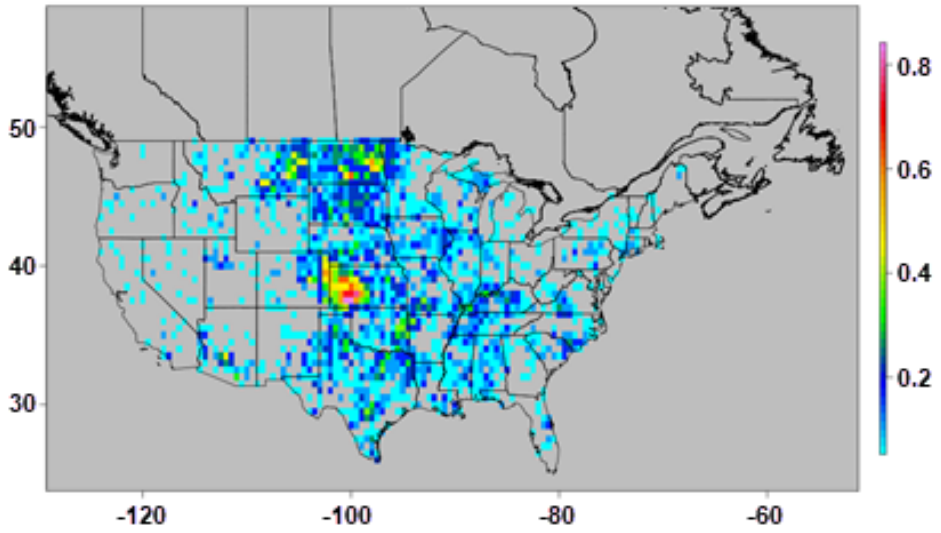

Figure 42. Observed average annual 75-mph or greater convective straight-line wind speed days based on the SPC Storm Reports database from 2000 to 2018

The Verisk model-simulated average annual EF-1 or greater tornado days (Figure 43) shows a large area of relatively high annual tornado frequency across much of the western two-thirds of the South and western half of the Midwest, with one maximum over Louisiana and Mississippi and a second maximum over Oklahoma and Kansas. The relatively high and maximum annual tornado frequency areas align well with observations (Figure 44).

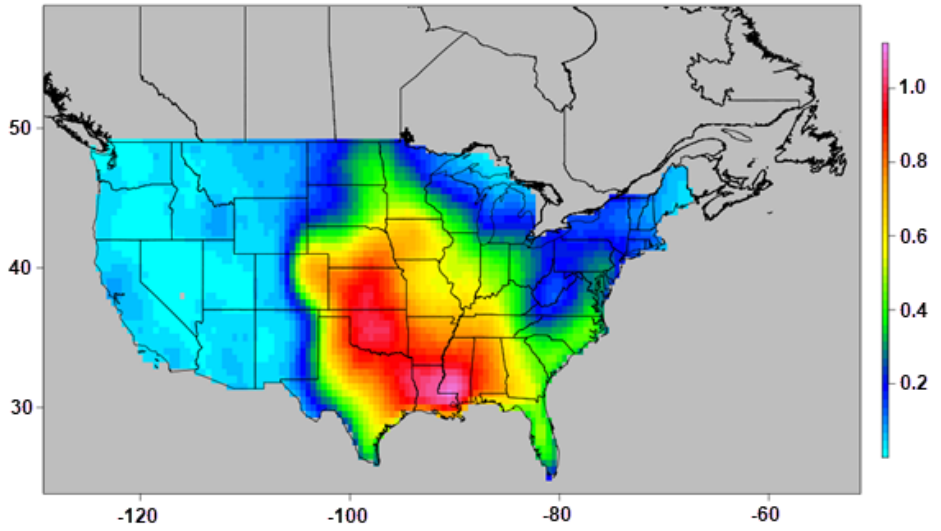

Figure 43. Verisk model-simulated average annual tornado days (EF-1 or greater) based on the 10,000-year stochastic catalog

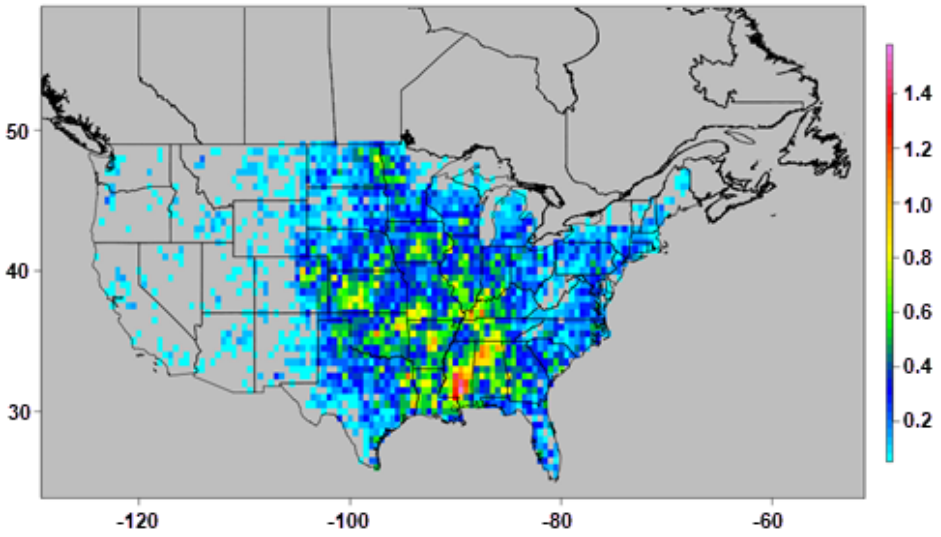

Figure 44. Observed average annual tornado days (EF-1 or greater) based on the SPC Storm Reports database from 2000 to 2018

The Verisk model-simulated average annual significant tornado (EF-3 or greater) days (Figure 45) has a very similar pattern as the modeled average annual EF-1 or greater tornado frequency (Figure 43) but with lower magnitudes. The relatively high and maximum modeled annual significant tornado frequency areas align well with observations (Figure 46).

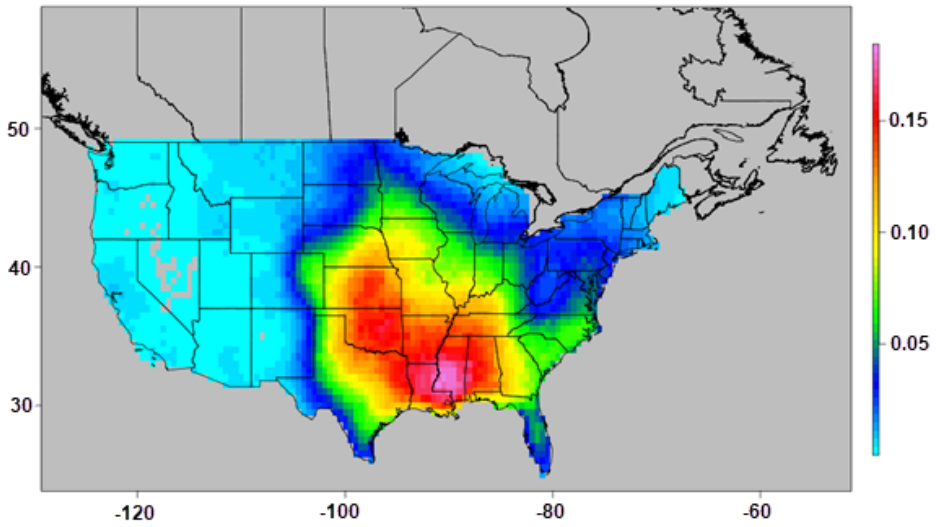

Figure 45. Verisk model-simulated average annual significant tornado days (EF-3 or greater) based on the 10,000-year stochastic catalog

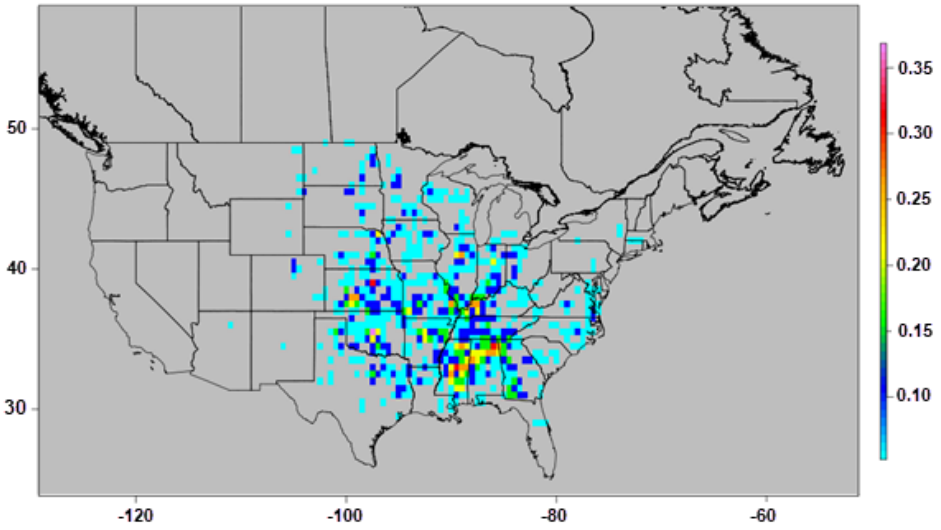

Figure 46. Observed average annual significant tornado days (EF-3 or greater) based on the SPC Storm Reports database from 2000 to 2018

Seasonality

Verisk researchers validated Verisk model-simulated seasonality by comparing model-simulated to observed monthly sub-peril relative occurrence frequencies. The observed monthly frequencies are based on SPC's Storm Reports database from 2000 to 2018, and the Verisk-modeled monthly frequencies are based on Verisk's 10K all-events catalog. In addition, a second set of observations derived from radar swaths for the periods 1996-2002 and 2005-2017 (2003 and 2004 are missing) is available for the hail sub-peril. The Verisk model, SPC's Storm Reports data, and radar-derived seasonality show similar frequencies in sub-peril activity throughout the year with 1-in. or greater diameter hail and EF-1 or greater tornado activity peaking in May and June (Figure 47 and Figure 49, respectively) and 58-mph or greater convective straight-line wind activity peaking in June and July (Figure 48).

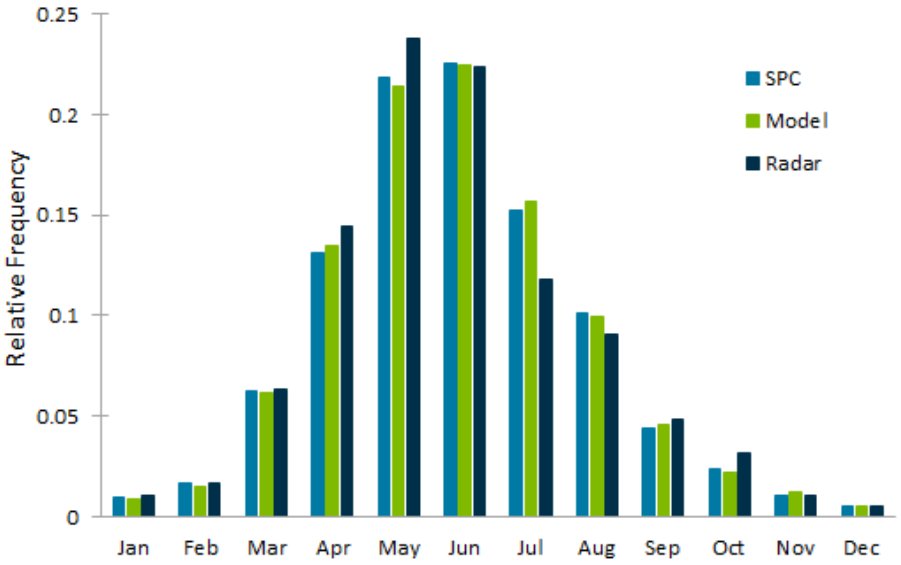

Figure 47. Seasonal distribution of 2000-2018 SPC-observed (light blue bars), 1996-2002 and 2005-2017 radar-derived (dark blue bars), and Verisk model-simulated (10K all-events catalog; green bars) 1-in. or greater hail counts

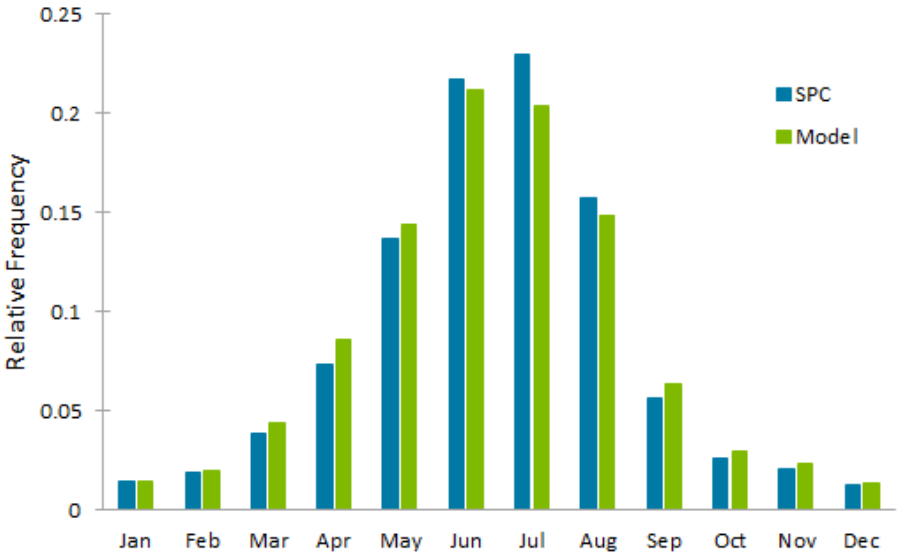

Figure 48. Seasonal distribution of 2000-2018 SPC-observed (light blue bars) and Verisk model-simulated (10K all-events catalog; green bars) 58-mph or greater convective straight-line wind counts

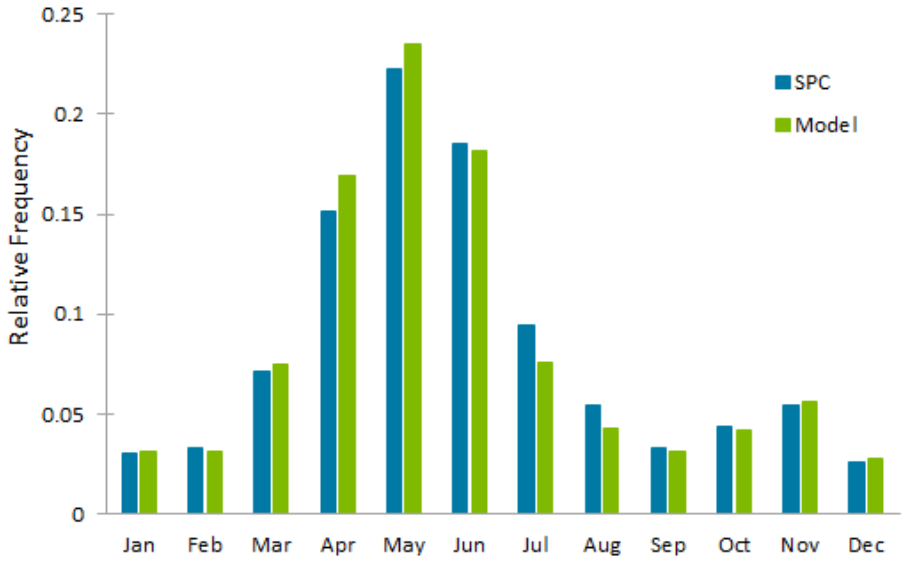

Figure 49. Seasonal distribution of 2000-2018 SPC-observed (light blue bars) and Verisk model-simulated (10K all-events catalog; green bars) EF-1 or greater tornado counts

Swath length

Verisk researchers validated Verisk model-simulated swath length by comparing model-simulated to observed swath length relative occurrence frequencies for the individual hail, tornado, and straight-line wind sub-perils (Figure 50, Figure 51, and Figure 52, respectively). The observed frequencies are based on SPC's Storm Reports database from 2000 to 2018, and the Verisk-modeled frequencies are based on Verisk's 10K all-events catalog. In addition, a second set of observations derived from radar swaths for the periods 1996-2002 and 2005-2017 (2003 and 2004 are missing) is available for the hail sub-peril. As seen in these figures, in general, the straight-line wind and tornado values compare well to those in the historical record.

For the hail sub-peril, there are reasonable patterns among the Verisk-modeled, reported (SPC), and radar-derived hail swath lengths. Specifically, for hail swaths of moderate to long lengths (20-30 mi and longer), the modeled swath length relative frequency is lower than radar but higher than SPC reports. This relationship is expected because, in general, SPC-reported swath lengths may underestimate the true swath length (due to difficulty in resolving the ends of the swath where hailstones are sparse), while radar-derived swath lengths represent overestimates of the true swath dimensions (Giammanco and DeCiampa, 2018). In addition, the high relative frequency of shorter swath lengths (0-10 mi and 10-20 mi in length, specifically) in the SPC data reflect the fact that reported swath lengths are underestimates of the true swath lengths. It would be expected that some of the 'true' longer swath lengths (>20 mi) have had their length underestimated in the SPC data and are therefore reflected in a smaller bin than they would have been if the true swath length had been observed. Similarly, the overestimation of swath length relative frequencies present in the radar-derived data result in some of the 'true' shorter swath lengths (0-10 mi and 10-20 mi in length, specifically)

being overestimated in the radar-derived data. Therefore, these 'true' shorter swath lengths are classified into a larger bin than they would have been if the true swath length had been derived.

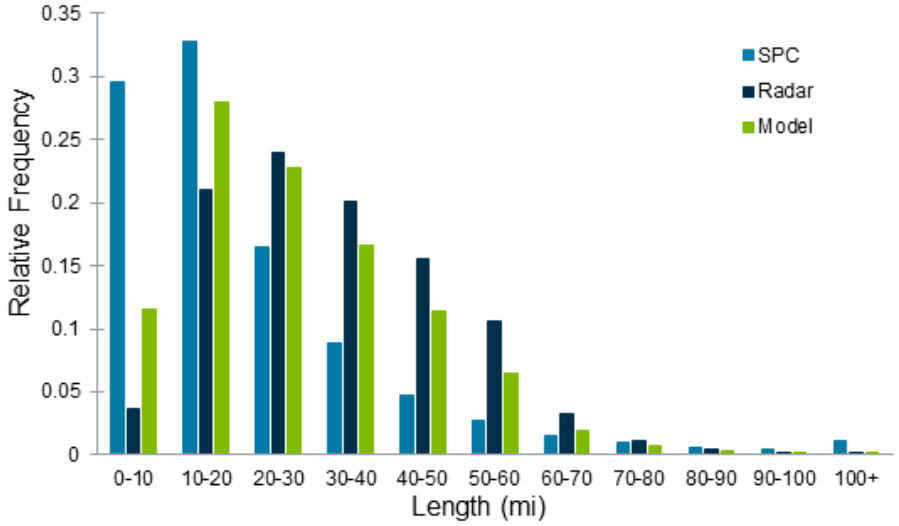

Figure 50. Comparison of the relative occurrence frequency of 1-in. or greater hail swath length distributions between Verisk model-simulated (10K all-events catalog; green bars), 2000-2018 SPC-observed (light blue bars), and 1996-2002 and 2005-2017 radar-derived (dark blue bars) events

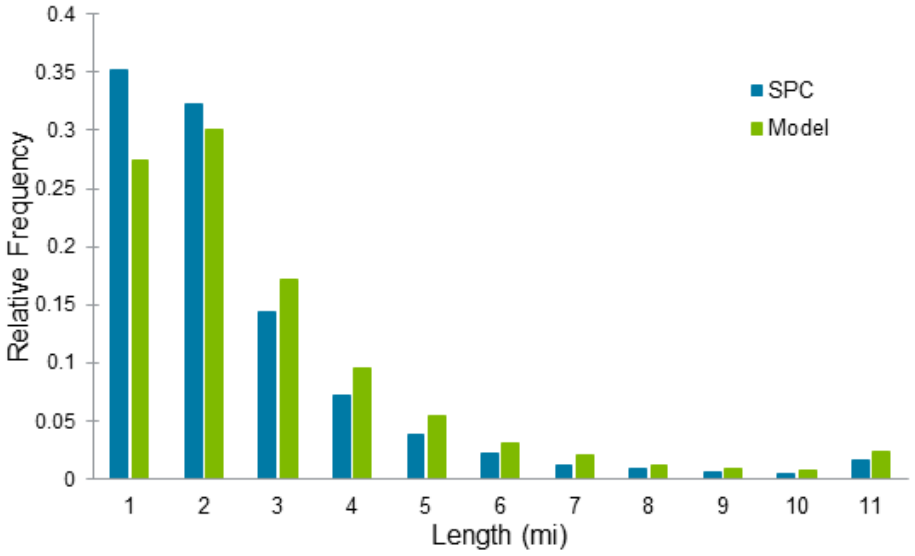

Figure 51. Comparison of the relative occurrence frequency of 58-mph or greater convective straight-line wind swath length distributions between Verisk model-simulated (10K all-events catalog; green bars) and 2000-2018 SPC-observed (light blue bars) events

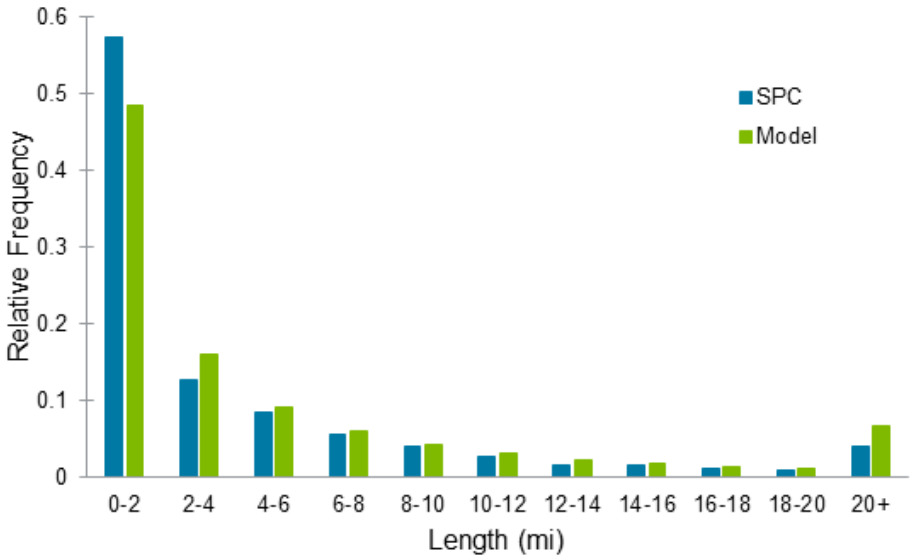

Figure 52. Comparison of the relative occurrence frequency of EF-1 or greater tornado swath length distributions between Verisk model-simulated (10K all-events catalog; green bars) and 2000-2018 SPC-observed (light blue bars) events

Swath width

Verisk researchers validated Verisk model-simulated swath width by comparing model-simulated to observed swath width relative occurrence frequencies for the individual hail, tornado, and straight-line wind sub-perils (Figure 53, Figure 55, and Figure 54, respectively). The observed frequencies are based on SPC's Storm Reports database from 2000 to 2018, and the Verisk-modeled frequencies are based on Verisk's 10K all-events catalog. In addition, a second set of observations derived from radar swaths for the periods 1996-2002 and 2005-2017 (2003 and 2004 are missing) is available for the hail sub-peril. As seen in these figures, overall, the values compare well to those in the historical record.

There are reasonable patterns among the Verisk-modeled, reported (SPC), and radar-derived hail swath widths. Specifically, for narrower hail swaths (≤10 mi), the modeled swath width relative frequency is higher than SPC reports whereas, for moderate to wide hail swath widths (>10 mi), the modeled swath width relative frequency is lower than SPC reports. This relationship is expected because, in general, swath widths derived from SPC reports may actually be a combination of more than one swath. As a result, some of the 'true' narrower swath widths (≤10 mi) have had their width overestimated in the SPC data and are therefore reflected in a larger bin than they would have been if the true swath width had been observed. While the Verisk-modeled and radar-derived hail swath width relative frequencies compare well overall, the radar-derived wide bias (i.e., actual hail swaths tend to be narrower than radar-based storm swaths) is evident when comparing the relative frequencies of the 0 - 5 mi bin to the 5 - 10 mi bin.

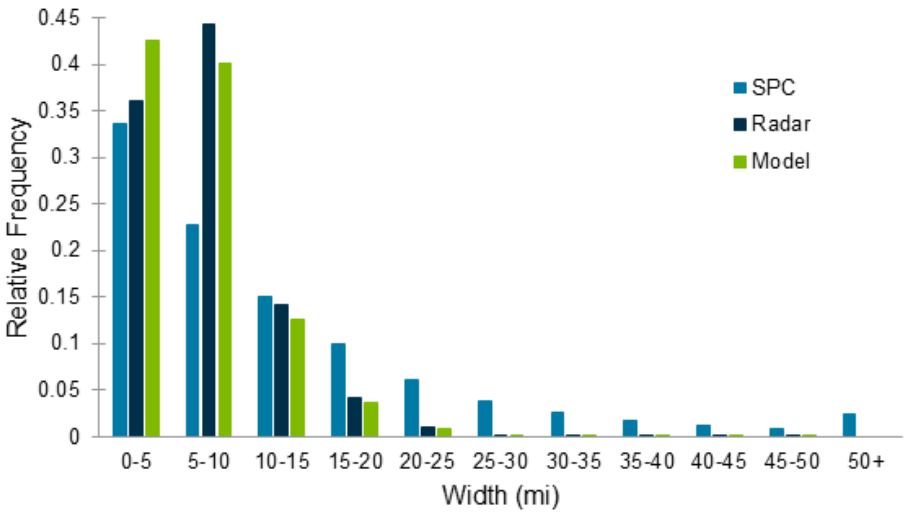

Figure 53. Comparison of the relative occurrence frequency of 1-in. or greater hail swath width distributions between Verisk model-simulated (10K all-events catalog; green bars), 2000-2018 SPC-observed (light blue bars), 1996-2002 and 2005-2017 radar-derived (dark blue bars) events

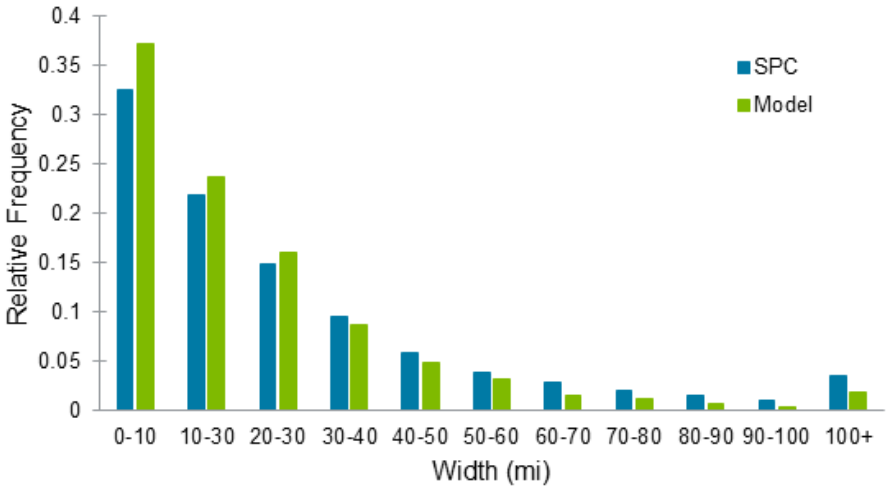

Figure 54. Comparison of the relative occurrence frequency of 58-mph or greater convective straight-line wind swath width distributions between Verisk model-simulated (10K all-events catalog; green bars) and 2000-2018 SPC-observed (light blue bars) events

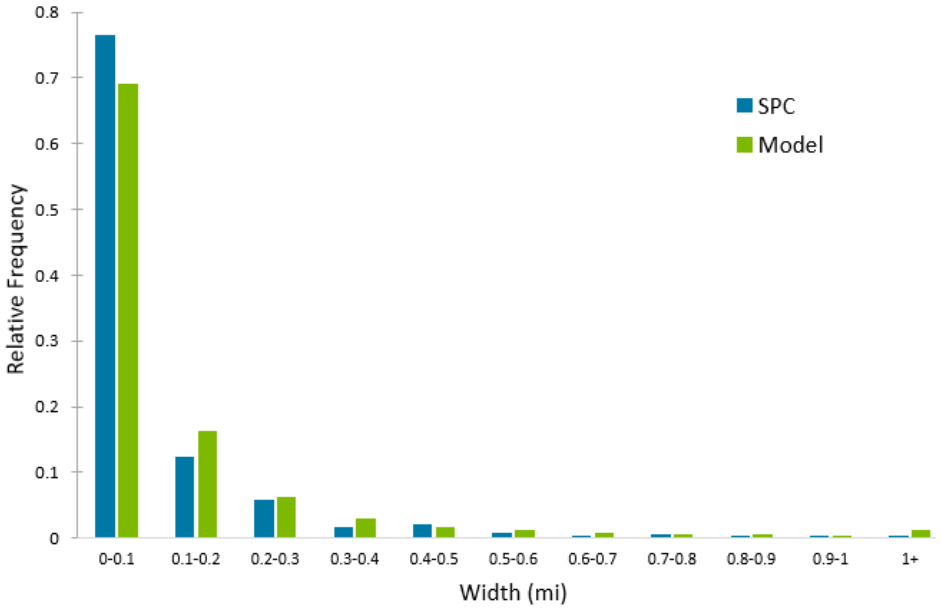

Figure 55. Comparison of the relative occurrence frequency of EF-1 or greater tornado swath width distributions between Verisk model-simulated (10K all-events catalog; green bars) and 2000-2018 SPC-observed (light blue bars) events

Multi-day macroevents

Verisk researchers validated Verisk model-simulated multi-day macroevent duration by comparing model-simulated to observed macroevent duration relative occurrence frequencies for all three sub-perils combined. The observed frequencies are based on Verisk's ISO Property Claims Services (PCS®) database from 1970 to 2018, and the Verisk-modeled frequencies are based on Verisk's 10K all-events catalog. Since PCS includes only catastrophic events (i.e., events that cause at least 25 million USD in insured loss), Verisk researchers used only multi-day macroevents for validation because single-day macroevents may not meet the catastrophic loss threshold due to their limited duration.

As seen in Figure 56, in general, the values compare well to those in the historical record. There are still differences between the model-simulated and PCS-observed relative frequencies for shorter duration macroevents, but they more closely align for longer duration macroevents. These differences are likely a result of some of the simulated shorter (2-3 day) macroevents present in the Verisk model do not meet the catastrophic loss threshold and, hence, would not be included in the PCS data. While the Verisk macroevent splitting algorithm seeks to create PCS-like events, the algorithm is completely based on the severe thunderstorm frequency, not loss. Therefore, differences between the two datasets are likely.

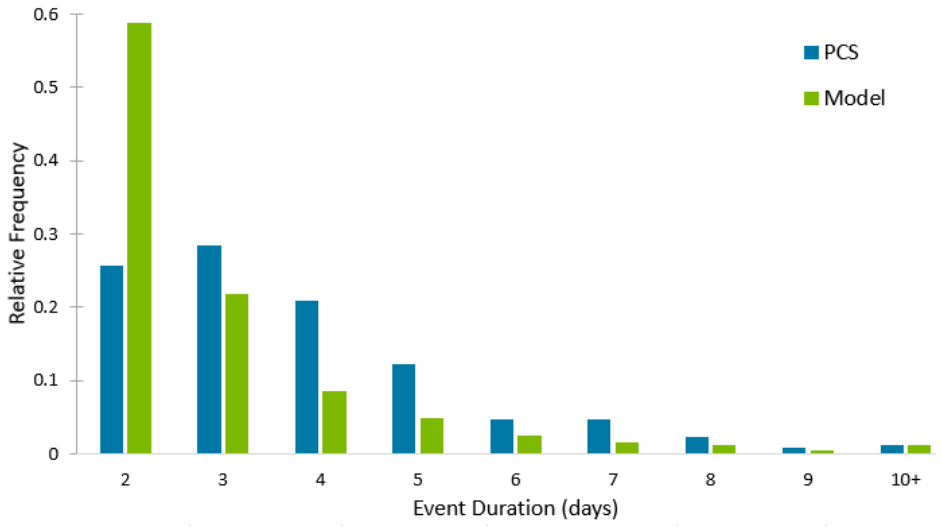

Figure 56. Comparison of the relative occurrence frequency of multi-day macroevent durations between Verisk model-simulated (10K all-events catalog; green bars) and 1970 - 2018 observed data using the PCS database (light blue bars) for all sub-perils combined

Derechos

Verisk researchers compared their model-simulated derecho climatology (Figure 57) to results from Coniglio and Stensrud (2004) and found the two datasets compare very well overall but vary slightly in location of maximum derecho activity. Also, Verisk's algorithm detects approximately 14.8 derechos per year, while Coniglio and Stensrud (2004) report around 15.3 events per year from 1980 to 2001.

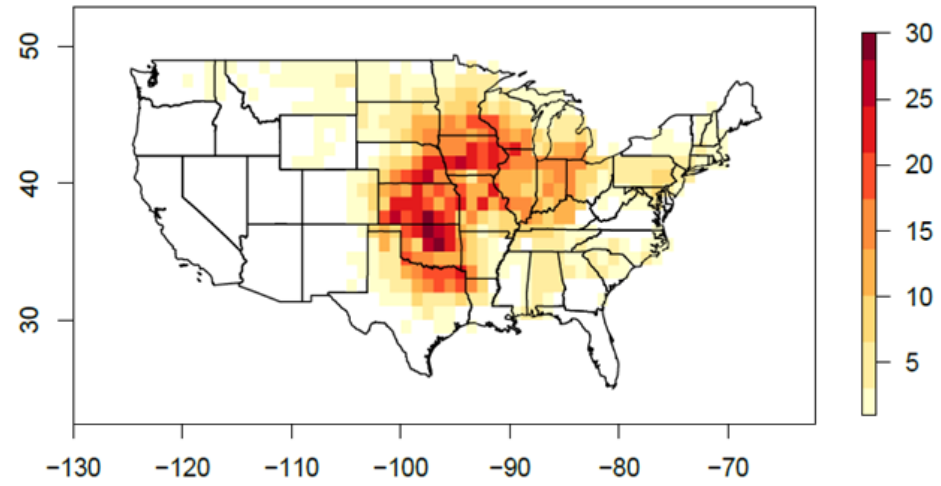

Figure 57. Spatial distribution of derechos produced by Verisk's derecho detection algorithm from 1980 to 2001

Figure 58 and Figure 59 are two examples of Verisk's ability to correctly detect notable derecho events. Figure 58 is of the June 29, 2012 North American derecho, which developed

in Iowa, moved east across the Appalachian Mountains, and then finally offshore early in the morning on June 30th. This derecho caused significant damage, with nearly 3 billion USD in loss and 22 fatalities. As seen in Figure 58, Verisk's algorithm is able to accurately capture the 2012 North American derecho's large longitudinal extent and spatial distribution, with reports extending from Des Moines, Iowa (western extent) to Washington D.C. (eastern extent). In addition, the model correctly identifies derecho wind reports from northern Indiana to southern Virginia.

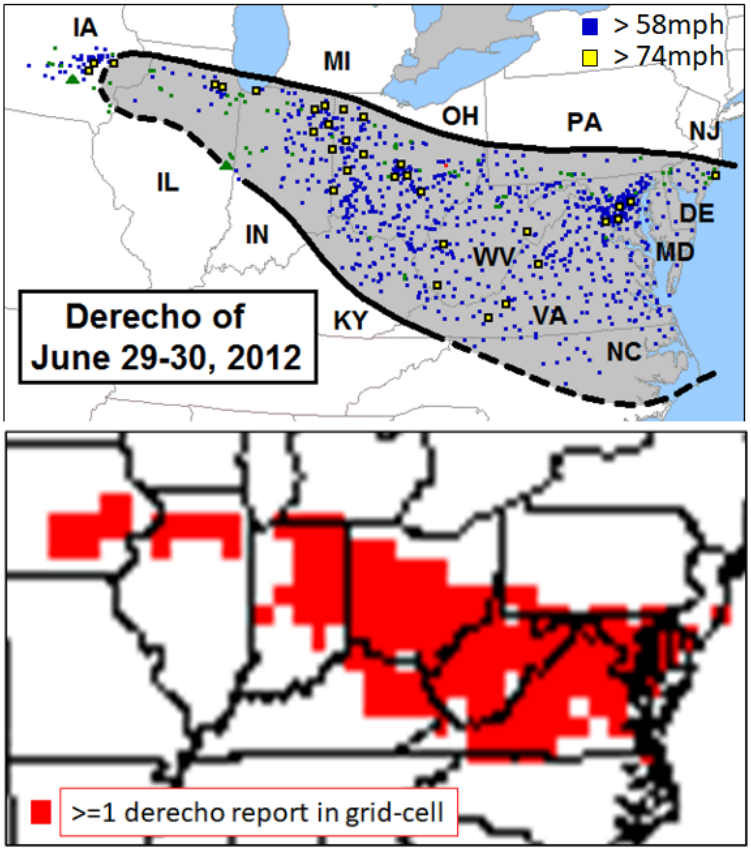

Figure 58. June 29, 2012 derecho example
The top image is SPC storm reports and the bottom image shows the grid cells in the Verisk derecho detection algorithm in which an SPC report is identified as being part of a derecho.

Figure 59 shows Verisk derecho detection algorithm's representation of the May 8, 2009 derecho event, which developed over western Kansas and moved eastward across multiple states before weakening over the mid-Atlantic states. This derecho was particularly strong regarding the number of tornadoes it produced (39); the unique wake low, which developed behind the initial line of storms; and the baseball-sized hail it generated; all of which are rare in derecho events. Verisk's algorithm correctly captures the coverage of this derecho across Kansas, Missouri and farther east through Kentucky and Tennessee.

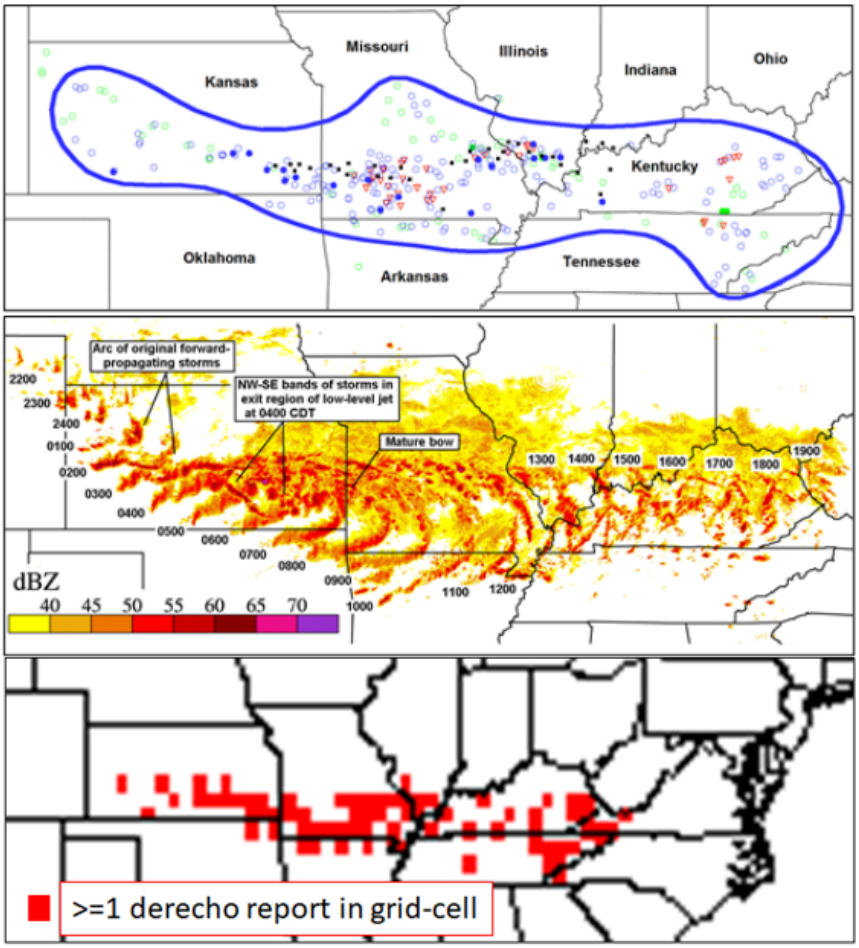

Figure 59. May 8, 2009 derecho example
The top and middle images are SPC storm reports and the corresponding radar reflectivity, respectively, and the bottom image shows the grid cells in the Verisk derecho detection algorithm in which an SPC report is identified as being part of a derecho.

4 Local Intensity Calculation

In the local intensity component of the Verisk model, hailstorm intensity is represented by hail impact energy (J/m^2) (a measure of total kinetic energy), derived from the maximum reported hail diameter. For tornadoes, intensity is expressed as the maximum 3-sec wind speed gust (mph). For convective straight-line winds, intensity is represented as an average 3-sec wind speed gust (mph), derived from the mean reported 3-sec gust from all the SPC reports within the footprint. An average wind speed is used because the clustered wind footprints tend to be quite large, but only a small fraction of the footprint experiences the highest of reported wind speeds. Using a 3-sec average gust allows the wind footprints to be reasonably large but still produce realistic loss estimates.

For each of these intensity parameters, cumulative distribution functions (CDFs) are fit on a moving 0.5° by 0.5° grid by season based on the clustered SPC reports and radar-based footprints. To account for uncertainty around the reported values, kernel density estimation was used to smooth the clustered reports into other-sized bins using a 5° by 5° moving window. SPC hail reports, for example, are typically given in terms of objects more familiar to observers (e.g., baseballs, golf balls, quarters, etc.), which leads to inexact measurements.

To simulate events that are stronger or weaker than what is represented in the CDFs, correlation is imposed within outbreaks by making daily, yearly, and microevent adjustments to intensity and swath counts. These adjustments and the reasoning for each adjustment are as follows:

- Yearly adjustments are made because some years have a higher frequency of severe convective weather events than other years.
- Daily adjustments are made because some historical seed days tend to have more significant (EF-3 intensity and higher) tornadoes than could be drawn from a CDF, so these days are enhanced. Similarly, the weaker days tend to be weaker, so these days are reduced.
- Daily adjustments are made because, regardless of the seed day, a simulated day may be more or less convectively-active than expected.
- Microevent adjustments are made because individual microevents may occur in convectively-favorable or convectively-unfavorable areas (according to the severe weather index values), and it is necessary to account for this behavior.
- Once a simulated event's intensity parameter is determined, the intensity at each location affected by the event is calculated as discussed below.

4.1 Local intensity calculation data sources

To thoroughly analyze hail, tornado, and convective straight-line wind intensity risk in the conterminous United States, Verisk researchers use information from several agencies, which are listed below.

NOAA's SPC and NCEI Storm Reports	Historical hail, convective straight-line wind, and tornado point data https://www.spc.noaa.gov/wcm/#data Dates: 1979 to 2018
Community Collaborative Rain, Hail, and Snow (CoCoRaHS) Network	Historical hail point data https://www.cocorahs.org/ViewData/ Dates: 1998 to 2018
Severe Hazards Analysis and Verification (SHAVE) Project	Historical severe weather point data https://www.nssl.noaa.gov/projects/shave/ Dates: Mid-spring through late summer, 2006 to 2015
Insurance Institute for Business and Home Safety (IBHS) Severe Hail Field Study	Historical severe hail point data (e.g., maximum and mean hail size, duration, area impacted) in the Central Plains region https://ibhs.org/hail/hailstones/ Dates: Spring Season, 2015 to 2019
NOAA's Next Generation Radar (NEXRAD) Level III Data	Individual radar site reflectivity data, storm cell ID, predicted probability of hail, predicted probability of severe hail, predicted maximum hail size, and hail index overlay products https://www.ncdc.noaa.gov/nexradinv/ Dates: 1996 to 2017 Resolution: 2-km grid spacing; 10-min time intervals
Verisk Weather Solution's RESPOND® Hail Analysis	Near real-time radar-derived hail footprints https://www.verisk.com/insurance/products/respond/hail-analysis-precision/ Dates: 2010 to 2012 (corresponding to the dates of the marquee event set)

4.2 Tornado wind speeds

For tornadoes, wind speed at a specific location is calculated based on wind profiles developed by Verisk researchers. These tornado wind profiles of a given size and maximum wind speed are based on the Enhanced Fujita Scale (EF Scale) and on analyses of damage and claims data from recent events. In general, the wind speed is highest on the centerline of the tornado footprint and decreases as one approaches the edge or endpoint. To account for this change in wind speed with distance, Verisk researchers examined multiple field studies. These studies included Verisk's own damage survey of the Moore, Oklahoma (2013) tornado, which examined the degree of damage that structures endured with respect to their location in the tornado track, and a collaborative study of the 2011 Tuscaloosa, AL and Joplin, MO tornadoes with the National Wind Institute (NWI) of Texas Tech University (TTU).

For the Moore, Oklahoma tornado damage survey, Verisk researchers visited areas along the tornado track where EF-4 and EF-5 intensity winds were reported with the goal of correlating property damage to estimated wind speeds. One specific goal of the survey was to walk perpendicular to the tornado track multiple times and collect quantitative observations.

Verisk researchers also surveyed areas with a high concentration of commercial and residential exposures to gain further insight into the relative vulnerability of various construction and occupancy types.

Verisk's study with the TTU team consisted of collaboratively analyzing archived data from the TTU team's damage survey alongside insurance claims data for the impacted areas of Tuscaloosa, AL and Joplin, MO. Degree of damage ratings were assigned according to the EF Scale "Damage Indicators" for each of the 11,000 buildings surveyed.

A collage of photos from the 2013 Moore, Oklahoma Verisk damage survey along with the degree of damage ratings along the path of an EF-4 tornado that struck Joplin, MO are shown in Figure 60. The photos show complete devastation along the centerline of the tornado track in (A), where the wind speeds are greatest. Progressively less damage is evident as the distance from the centerline increases and the wind speed decreases from (B) to (C) to (D). In (B), unseated roof decking, torn/loose roof covering, and window and wall damage is evident. In (C), moderate damage to roof covering, roof decking, and siding is shown. Finally, in (D), minor damage from flying debris on the upper part of the building is apparent. This observed damage corresponds well with the modeled wind speeds at the respective distances in the wind profile of an EF-4 tornado (also shown in Figure 60).

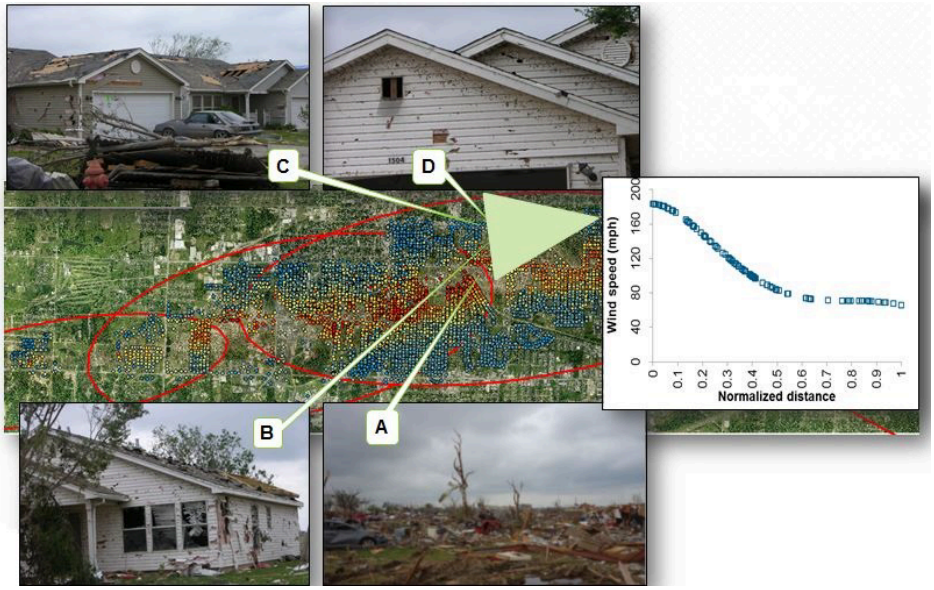

Figure 60. Comparison of damage from the EF-4 Moore, Oklahoma tornado (A-D) versus the modeled wind speed profile for an EF-4 tornado (Source: Verisk)

Wind speed profiles for EF-4 and EF-5 tornadoes are shown in Figure 61.

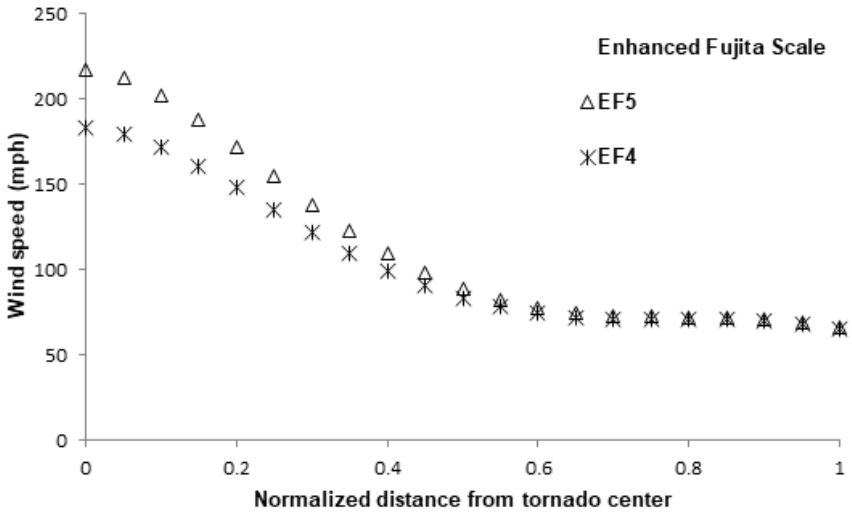

Figure 61. Wind speed profile of EF-4 and EF-5 tornadoes (0 represents the core of the tornado, and 1 represents the outer periphery of the tornado footprint)

The exact tornado wind speed profile calculation uses a normalized parameter as the input, which is approximately described as the normalized distance from the major axis of the tornado's footprint (which is defined by an ellipse) to any point within the ellipse. Using the ellipse properties in Figure 62, the normalized distance, x, is defined as:

$$x = \frac{(PF_1 + PF_2) - 2 \times c}{2 \times a - 2 \times c},$$

where point P is any point within the ellipse, PF_1 and PF_2 represent the distances from point P to each focus, and the variables a and c represent the semi-major axis length and distance from the center to foci, respectively. Points outside of the ellipse will return an x value greater than one, and points along the major axis between the foci will return an x value of zero.

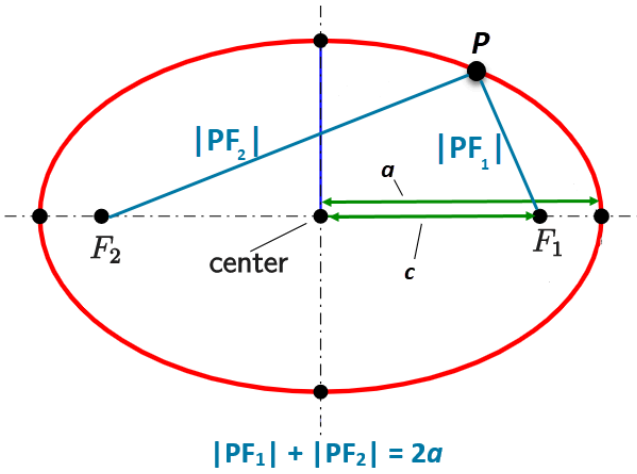

Figure 62. Properties of an ellipse
Source: Ellipse-def0 by Ag2gaeh, CC BY-SA 4.0; labeled by Verisk

Once the normalized distance, x, is calculated, it is used to calculate a scaling factor, which is applied to the tornado's maximum wind speed. The scale factor equation, which is a 5th order polynomial, is defined as:

$$scale\ factor = 1+(-0.0708+(-11.116+(23.624+(-18.012+4.5798x)x)x)x)x$$

Note that while the SPC considers a thunderstorm to be severe any time a tornado is reported, even if it is EF-0 tornado, Verisk does not model EF-0 tornadoes. These weak tornadoes are not modeled because of the large degree of uncertainty with respect to the reporting consistency and accuracy of EF-0 (and F-0) tornadoes in the historical record, as well as their low loss potential as compared to other model components. For example, the SPC classifies a tornado with an unknown rating as an EF-0, yet strong tornadoes can receive an unknown rating when they occur in areas where there is either not enough or no exposures to damage in the first place, which effectively rules out the use of damage indicators. In addition, population density differences are a major contributing factor in the reporting consistency and accuracy of EF-0 and F-0 tornadoes.

See Also
Tornadoes

4.3 Hail impact energy

While hail damage to structures is often limited to roofs, wind-blown hail can pose a significant threat to windows and building cladding. For this reason, Verisk researchers have developed a formulation for hail impact energy that consists of a vertical component, which is the primary source of hail damage, and a horizontal component, which produces damage to the building cladding and windows. Both components are defined in terms of kinetic energy flux density, which is the rate of energy transfer per unit area and is measured

in J/m^{2}s. The vertical component is a result of the momentum of falling hailstones, while the horizontal component is due to the horizontal advection of hailstones by accompanying winds. The total kinetic energy flux density is, therefore, the sum of the horizontal and vertical components.

The general form of the equation used to calculate these components is given by Waldvogel et al. (1978) as follows:

$$KE = \frac{(\pi \times \rho_{hail})}{(12 \times 10^6)} \int_0^{\infty} n(D) \times D^3 \times (v(D))^3 \, dD \quad (1)$$

where $n(D)$ is the concentration of hailstones of diameter, D, per unit volume, $v(D)$ is either the terminal fall speed or the maximum horizontal speed, and ρ_{hail} is the density of hail (900 kg/m^3). The terminal fall speed is given by Mason (1971) as follows:

$$v = v_o D^{1/2} \quad (2)$$

where $v_o = 4.41 \ \ m/(s \cdot mm^{0.5})$. The maximum horizontal speed was obtained by solving for hailstone velocity after being exposed to the wind force for the amount of time it takes a hailstone to travel from the cloud to the ground, or approximately 1,000 meters.

By integrating hailstone number concentrations (hailstones/m^3), terminal fall speeds or maximum horizontal speeds, and hailstone size, the total kinetic energy formulation and its components can account for hail impact energy variability within a single hail swath. This variability is due to the differences in hailstone shapes and sizes (which reach different maximum velocities and result in different hail impact energies) present in a hail swath.

To compare the modeled kinetic energy calculation to those from published studies (e.g., the Tornado and Storm Research Organization (TORRO) Hailstorm Intensity Scale), the results from Equation 1 are multiplied by a time factor such that the resulting values have units of J/m^2. The values for time are obtained by drawing from a log-normal distribution that represents the full range of possible durations a single point within a hail swath could experience from hailstones of various sizes.

For the Verisk Severe Thunderstorm Model for the United States, Verisk researchers developed hailstone number concentration distributions very similar to the Marshall-Palmer distributions, which use inverse exponential relationships to accurately represent various rainfall rates (Marshall and Palmer, 1948). The Marshall-Palmer distribution is represented in general form as follows:

$$n(D) = n_0 e^{-\Lambda D} \quad (3)$$

The distributions are parameterized by the y-intercept, n_0 (number of raindrops with a diameter of 0 mm), and the slope, $-\Lambda$.

According to the Marshall-Palmer distribution equation, as the rainfall rate increases, so does the number of large diameter raindrops. For example, given a rainfall rate of 1 mm/hr, the concentration of 2 mm raindrops is roughly 10^0, or 1 raindrop/m^3, whereas it increases to about 10 drops/m^3 for a rainfall rate of 5 mm/hr. Thus, the distributions are implemented for the simulated hail swaths are based upon the maximum reported hail size for the clustered reports. The choice of maximum hail size as opposed to average hail size is further justified

by previous studies in both the meteorological and engineering communities that have typically focused on maximum hail size in relation to damage estimation due to hailstorms.

The final equation for the vertical kinetic energy that results from substituting Equations 2 and 3 into Equation 1 is as follows:

$$KE = \frac{\left(v_o^3 \times \pi \times \rho\right)}{\left(12 \times 10^6\right)} \times t \int_{0.022}^{\infty} n_o exp(-\Lambda D) \times D^{9/2} \, dD \qquad (4)$$

The integral is bounded on the lower end by a diameter size of 22 mm (0.86 in.). Even though the minimum hailstone size assigned for each microevent in the stochastic catalog is one inch in diameter (i.e., consistent with SPC's definition of a severe hail event), hailstones smaller than this diameter can cause damage, especially in the presence of high wind gusts. The model takes this fact into consideration in its hail energy calculation by integrating over all hailstone sizes (i.e., 0.86 in. or greater) capable of producing damaging energy.

The value of Λ is obtained from a mathematical relationship of the form: $\Lambda = \alpha D_{max}^{b}$. This relationship was obtained by iteratively calculating Λ to match energies from the TORRO Hailstorm Intensity Scale shown in Table 12.

Table 12. TORRO hailstorm intensity scale

Intensity Category	Typical Hail Diameter[12] (mm)	Probable Kinetic Energy (J/m^2)	Typical Damage Impacts
H0 Hard Hail	5	0 - 20	No damage
H1 Potentially Damaging	5-**15**	> 20	Slight general damage to plants, crops
H2 Significant	10-**20**	> 100	Significant damage to fruit, crops, vegetation
H3 Severe	20 - **30**	> 300	Severe damage to fruit and crops, damage to glass and plastic structures, paint and wood scored
H4 Severe	25 - **40**	> 500	Widespread glass damage, vehicle bodywork damage
H5 Destructive	30 - **50**	> 800	Wholesale destruction of glass, damage to tiled roofs, significant risk of injuries
H6 Destructive	40 - **60**		Bodywork of grounded aircraft dented; brick walls pitted
H7 Destructive	50 - **75**		Severe roof damage, risk of serious injuries
H8 Destructive	60 - **90**		(Severest recorded in the British Isles) Severe damage to aircraft bodywork
H9 Super Hailstorms	75 - **100**		Extensive structural damage. Risk of severe or even fatal injuries to persons caught out in the open

[12] **Bold**: Typical maximum reported diameter

Intensity Category	Typical Hail Diameter[12] (mm)	Probable Kinetic Energy (J/m^2)	Typical Damage Impacts
H10 Super Hailstorms	> **100**		Extensive structural damage. Risk of severe or even fatal injuries to persons caught out in the open

Similar to the tornado wind speed profile, Verisk-modeled hail ellipses have an intensity profile, which is generated by applying a scaling factor to the maximum hail impact energy. This intensity profile was developed based on Verisk researchers' analysis of both IBHS Hail Study and Verisk Weather Solution's RESPOND® data as well as results from published studies. The resulting hail energy profile is shown in Figure 63.

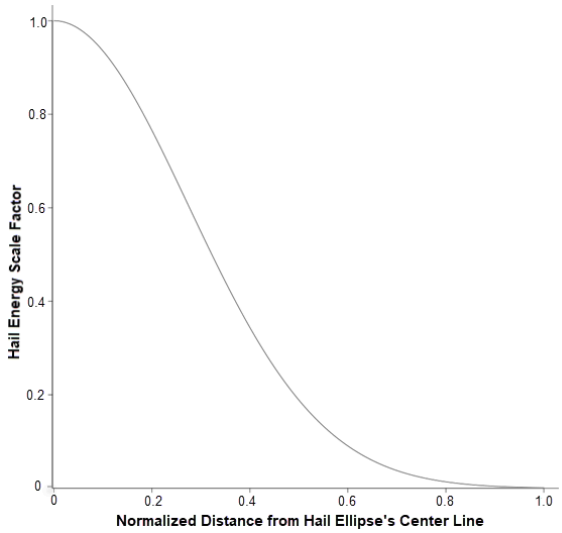

Figure 63. Hail energy swath profile

4.4 Straight-line wind speeds

Wind speeds assigned to stochastic straight-line wind events are drawn from an empirical CDF derived from the clustered SPC reports. These wind reports can either be measured with instrumentation (e.g., anemometer) or estimated by trained storm spotters, emergency management, NWS employees, or the general public. Research has shown that estimated wind gusts are biased high when compared to wind tunnel experiments (Edwards et al., 2018) or actual measured reports. In some cases, these overestimations can be on the order of 20 - 30% higher than actual wind speeds. Moreover, estimated wind speeds comprise the majority (90%) of the SPC severe wind speed database (Edwards et al., 2018). This value closely matches the percentage of wind speed reports that are estimated (approximately 89%) in the Verisk database beginning in 2006.

[12] **Bold**: Typical maximum reported diameter

To account for the high estimated wind speed bias in SPC's clustered wind speed values, Verisk researchers reduce the SPC wind report values that are labeled or assumed to be estimated by 30%. This procedure is completed for wind bin values of 1 mph for each state in the following steps:

1. Compute the percentage of estimated versus total wind speed report values (i.e., estimated plus measured) from post-2006 SPC data, by state and by wind speed (bin values of 1 mph).
2. Use the corresponding calculated percentage to randomly sample that amount of pre-2006 wind reports that are flagged (i.e., assumed) to be estimated for each state and wind speed.
3. Apply a 30% reduction to the wind speed magnitude for reports that are flagged as estimated.

An example of Verisk's wind speed reduction procedure for the state of Illinois is shown in Figure 64 and Figure 65. Figure 64 shows the relative frequency distributions of the original observed SPC estimated and measured wind speed reports from 2006 to 2018. Figure 65 shows the relative frequency distributions of the 1955-2018 original and resulting Verisk-adjusted observed SPC wind speed reports for the state of Illinois. The original and adjusted mean wind speeds are 54 kts and 46 kts, respectively.

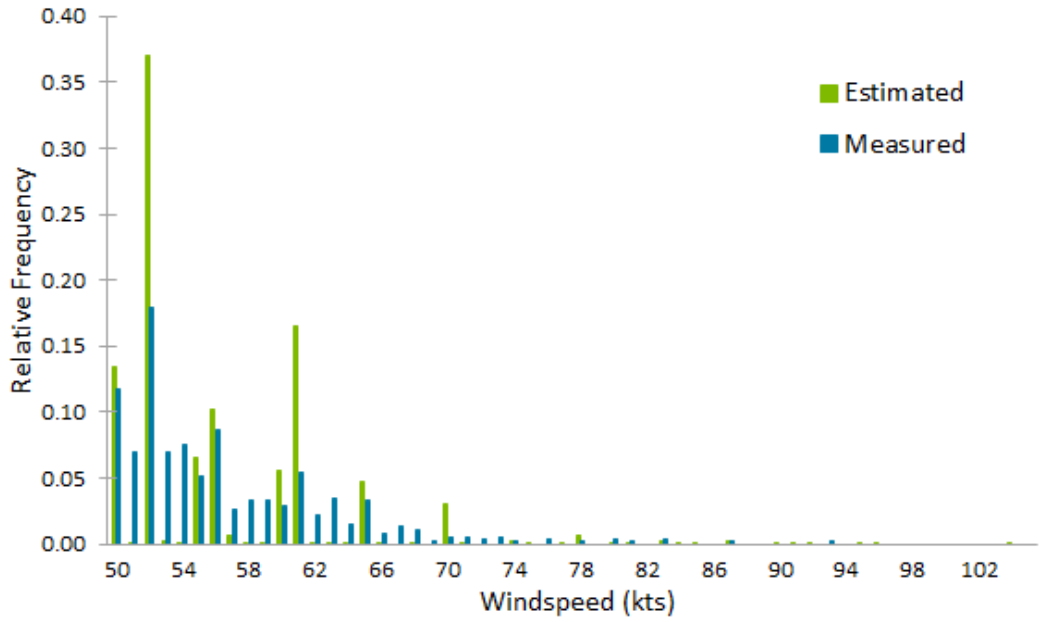

Figure 64. Relative frequency distributions of the 2006-2018 estimated (green) and measured (blue) SPC observed wind speed reports (grouped into 1-kt bins) for the state of Illinois

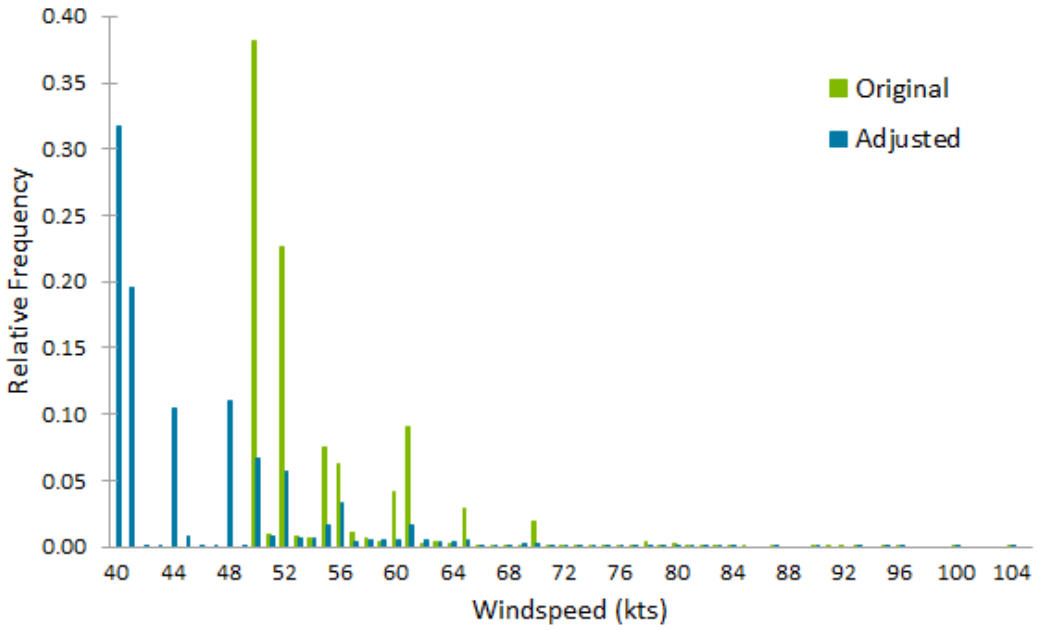

Figure 65. Relative frequency distributions of the 1955-2018 original (green) and adjusted (blue) SPC observed wind speed reports (grouped into 1-kt bins) for the state of Illinois

The following assumptions are made with this wind speed reduction process:

- If a wind bin has less than four reports, the average ratio of the overall estimated to measured wind speed values is used
- If a wind bin has a probability of 0 or 1.0, the calculated rolling mean probability (with a 5-mph window) is used for the wind speed's adjustment probability
- If a wind bin has a rolling mean probability less than 0.02, then the average of the adjacent rolling mean bins is used

To determine the wind speed assigned to a given wind speed swath, the average straight-line wind speed of all reports that fall within a given swath is used. This average wind speed is used because the clustered wind footprints tend to be quite large, but only a small fraction of the area experiences the highest of wind speeds. Using the average reported wind speed allows for the areal coverage of these footprints to be realistically large (as with a derecho, for example) but still produce reasonable loss estimates.

While Verisk considers all SPC wind reports of 58 mph (50 knots) or greater, 58 mph is not, however, the minimum modeled intensity threshold for straight-line winds. The reason being that if the average of the clustered SPC reports is 58 mph (i.e., all the SPC reports within the cluster are 58 mph), it is more than likely, especially given the heterogeneous nature of severe thunderstorm wind fields, that many exposures within the microevent footprint experience wind speeds less than the maximum wind speed. Considering how large the clustered wind footprints can be, particularly in a derecho, for example, the losses would be unrealistically inflated if the modeled intensity threshold was set equal to the SPC minimum intensity threshold. Therefore, when assigning wind speeds to microevents, the intensities can fall below the severe wind speed threshold.

4.5 Validating local intensity

Verisk researchers have extensively validated the local intensity module of the Verisk Severe Thunderstorm Model for the United States against historical observational data. Comparisons of Verisk-modeled hail size, convective straight-line wind speed, and tornado intensity distributions to observational data demonstrate the robustness and reliability of the Verisk model.

Validating hail distribution

Figure 66 compares the Verisk-modeled (green) with 2000-2018 SPC-observed (light blue) and 1996-2017 (minus missing data during 2003-2004) radar-derived (dark blue) 1-in. or greater hail diameter size distribution for the conterminous U.S. The Verisk model was run using the 10K all-events catalog. As evident in the figure, the SPC-observed distribution of hail sizes has notable peaks around common objects (e.g., golf ball), while the Verisk-modeled distribution shows a smoother and more realistic distribution that decreases monotonically from its peak occurrence frequency of one inch. The Verisk-modeled hail distribution more closely matches the observed radar-derived distribution than the SPC-observed distribution.

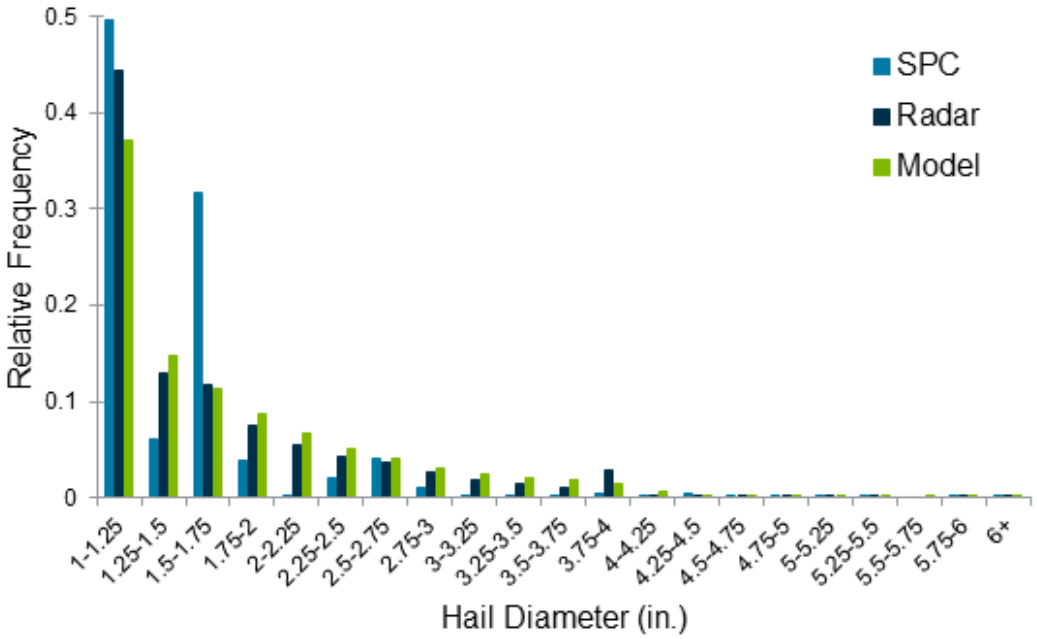

Figure 66. Relative frequency distribution of Verisk-modeled (10K all-events catalog; green), SPC-observed (2000-2018; light blue), and radar-derived (1996-2002 and 2004-2017; dark blue) 1-in. or greater hail diameters across the conterminous U.S.

Validating straight-line wind speed distribution

Figure 67 compares the Verisk-modeled (green) and 2000-2018 SPC-observed (light blue) severe convective straight-line wind speed distributions for the conterminous U.S. The Verisk model was run using the 10K all-events catalog. As evident in the figure, the Verisk-modeled and SPC-observed wind speed intensity distributions closely match.

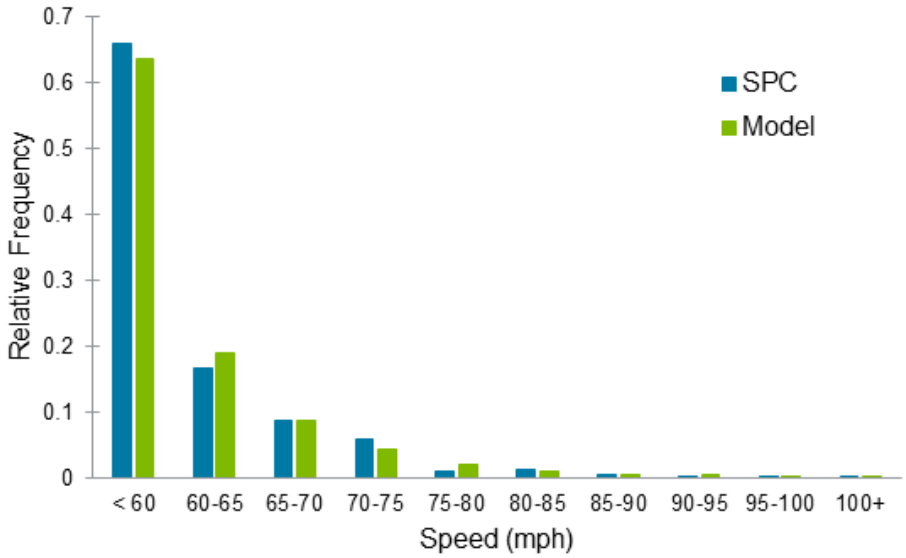

Figure 67. Relative frequency distribution of Verisk-modeled (10K all-events catalog; green) and SPC-observed (2000-2018; light blue) severe convective wind speeds (mph) across the conterminous U.S.

Validating tornado intensity distribution

Figure 68 compares the Verisk-modeled (green) and 2000-2018 SPC-observed (light blue) tornado distributions of EF-1 intensity or greater across the conterminous U.S. The Verisk model was run using the 10K all-events catalog. As evident in the figure, the Verisk-modeled and SPC-observed tornado intensity distributions closely match.

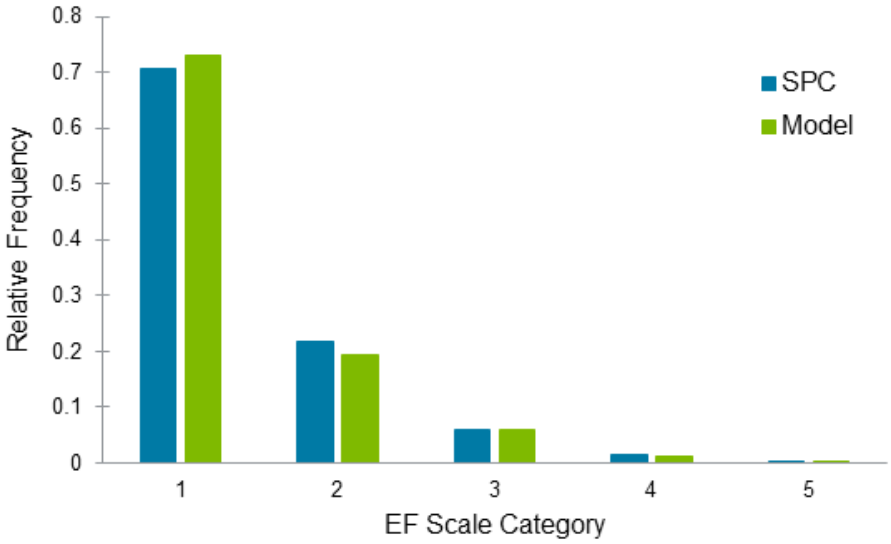

Figure 68. Relative frequency distribution of Verisk-modeled (10K all-events catalog; green) and SPC-observed (2000-2018; light blue) tornadoes of EF-1 strength or greater across the conterminous U.S.

5 Damage Estimation

The vulnerability component of the Verisk Severe Thunderstorm Model for the United States estimates damage caused by severe thunderstorm hail, straight-line winds, and tornadoes to both traditional and specialty lines of business. The local intensity is defined in terms of hail impact energy for the hail sub-peril and wind speed for the straight-line wind and tornado sub-perils. Mathematical relationships, called damage or vulnerability functions, describe the engineering relationship between the local intensity and the physical damage to buildings, including their structural and nonstructural components, in terms of the mean damage ratio (MDR). Separate damage functions relate the losses associated with contents damage and the number of days a building is unusable (i.e., business interruption or loss of use) as a function of building damage.

The MDR is the ratio of the repair cost of the building or contents to its replacement value. The model's damage function component reports the MDR for each intensity level. Probability distributions around the MDR capture uncertainty in the damage level. The model implements separate damage functions for each sub-peril by accounting for the building's primary (i.e., construction type, occupancy class, building height, year built, and gross area) and secondary characteristics. These damage functions not only account for the structure's physical response to a hazard but also encapsulate many other macro-level effects, such as regional variations in building codes and their enforcement, claims adjustment practices, the preparedness and response of individuals and communities to severe thunderstorm risk, and the representation of the hazard in the model.

The losses for buildings, appurtenant structures, and contents are all calculated by applying the appropriate damage function to the respective coverage-specific replacement values. Damage functions that estimate business interruption losses for commercial/industrial properties, loss of use for residential properties, automobiles, and various other asset types are also available. Verisk engineers validate damage functions and damage distributions using location-level claims data, findings from post-event damage surveys, and the latest engineering research.

5.1 Building classifications and resistance to severe thunderstorm damage

The amount of damage a building experiences during a severe thunderstorm depends on a variety of factors, including primary and secondary risk characteristics. For instance, the types of building construction materials used (i.e., construction class) and the building's occupancy class help determine the materials and level of engineering used to construct a building. These factors play an important role in defining the damageability of buildings. As a result, damage functions vary according to construction materials and occupancy class. In the Verisk Severe Thunderstorm Model for the United States, there are 140 distinct construction types, including wood frame, masonry, reinforced concrete, steel frame, and

light metal. Also, there are 112 different occupancy classes, including various subcategories of personal (residential and manufactured home), commercial, industrial, automobile, and utility.

A building's height plays a leading role in determining the level of hail damage to properties. One-story buildings have a relatively higher proportion of their replacement value attributed to the roof, thereby leading to higher damage, in comparison to buildings with two or more stories. Likewise, older properties are more vulnerable to damage than newer properties. Also, a building's square footage or gross area plays a role in determining a structure's damageability. Structure's with larger footprints and higher roof areas may be more prone to damage from some perils, e.g., hail. Subsequent sections in this chapter will characterize the role of various building attributes in determining damage from hail, straight-line winds, and tornadoes.

Residential buildings

Residential buildings include single- and multi-family homes, condominiums, apartment buildings, and manufactured homes. Among single-family residential homes, wood and masonry are the predominant construction classes throughout the United States. Wood frame is the most common construction type overall, although masonry is also common in the Gulf States and along the East Coast. The exterior walls of wood-frame homes can be finished with stucco, wood siding or shingles, vinyl, or aluminum cladding. When masonry is used as the exterior wall material, the walls are normally constructed to full height. Then, wood floors and the roof are framed into masonry, resulting in continuous exterior walls and an overall strong structural frame.

Apartment and condominium buildings tend to have a more diversified construction mix than single-family homes. In addition to wood and masonry, apartments may be comprised of steel and concrete. Concrete and steel buildings can generally withstand high winds better than masonry structures. Unlike single-family or small multi-family houses, large apartment and condominium buildings frequently receive a degree of engineering attention like that given to commercial construction. Nevertheless, apartments and condominiums have exterior features, such as balconies, awnings, and sliding glass doors, that are less engineered at the design and construction stages than the main building structure. These building components make apartments and condominiums quite susceptible to severe thunderstorms. As a result, Verisk engineers have developed separate damage functions for apartments and condominiums.

In the Verisk Severe Thunderstorm Model for the United States, manufactured (mobile) homes have a separate construction classification to distinguish them from the traditional single-family homes. A manufactured home, as defined by the U.S. Department of Housing and Urban Development (HUD), is a structure that is transportable in one or more sections and is at least 8 body feet wide or 40 body feet long during transport. When onsite, it is at least 320 sq. ft., is built on a permanent chassis, and is designed to be used as a dwelling, with or without a permanent foundation, when connected to utilities (24 CFR 3280.2 and 24 CFR 3285.5).

While the design and construction of single-family homes are based on local building codes, or those adopted in a particular state, the design and construction of manufactured homes has been regulated and governed federally by HUD since the National Manufactured Housing and Construction Safety Standards Act was passed in 1974. Therefore, this construction class does **not** include modular homes, which, unlike manufactured homes, are designed and constructed according to the local building codes. Verisk includes modular homes in the classification for single-family homes.

Hail damage to residential structures

Hail damage to structures is a function of the impact kinetic energy of the hail, as determined by the hailstone size and accompanying wind speed. The overall damage expected to a building is generally limited to the building envelope as opposed to structural components. Therefore, envelope integrity and resistance are critical aspects of a building's resistance to hail. In addition to the building's primary features (i.e., occupancy, construction, height, year-built, and gross area), secondary features (such as roof cover, roof slope, roof geometry, and wall siding) dictate a building's resistance to hail.

For conventional buildings (e.g., residential housing or commercial buildings), most of the damage from hail is to roof tiles or shingles, wall claddings, and windows (Figure 69). Buildings built with bitumen layer and gravel roofs are resilient to hail damage, but large hailstones can puncture or damage the surface. Disruption of a gravel surface by large hailstones may leave it more vulnerable to later impacts and shorten its lifespan. Metal roofs appear to only sustain cosmetic damage from dents and dings, but small cracks at the impact points can allow water to enter the building. Damage and scoring of the surface can also make the roof susceptible to rust. While the building envelope is vulnerable to hail damage, damage to structural components (e.g., roof deck/sheathing, beams, or columns) is rare, even in severe hailstorms.

Figure 69. Significant hail damage to a single-family home
Source: NOAA's National Weather Service

Since the building envelope is the most susceptible component of a structure to hail, the expected damage is limited by the ratio of the cost to repair or replace the damaged envelope to the cost of the entire building. As the hail-susceptible components cost increases relative to the overall building, so does the anticipated losses. Alternatively, as the envelope cost decreases relative to the total replacement value, the expected loss ratio decreases. Generally, more value is attributed to the non-susceptible building elements in larger and/or more complex structures than in smaller and/or less complex structures.

Manufactured homes have a high vulnerability to hail damage due to their generally low-cost construction materials. Typically, manufactured homes are constructed with asphalt shingles as roof cover, vinyl wall siding, and annealed glass windows, which are prone to hail damage. Additional building features, such as skirting (i.e., façade around the crawlspace) and attached structures (e.g., screen rooms, carports), are also subject to damage. Hail can dent a manufactured home's roofing and siding, remove paint, and crash through windows (Figure 70) thereby also increasing the potential for damage due to wind driven rain in a severe thunderstorm event.

Figure 70. Significant hail damage to a manufactured home in Lubbock County, Texas
Source: NOAA's National Weather Service

Wind damage to residential structures

Residential structures may see varying levels of wind damage. Wind damage typically initiates at the eaves and ridges of the roof and propagates from there. As the wind flows over sharp corners, the wind flow separates and causes high concentrations of suction pressures in these locations. As a result, most of the damage is limited to the rooftops and chimneys of residences. Uplift of a building's roof edges allows the wind to penetrate underneath the roof deck, resulting in an internal pressure rise beneath the deck. As a result,

at high wind speeds, the integrity of the entire structure can be compromised, particularly in cases where the roof provides lateral stability by supporting the tops of the building's walls. High winds from either tornado or straight-line wind events can also cause objects to become wind-borne. These windborne debris may cause damage to the envelope components of buildings.

When considering residential buildings, masonry structures are generally able to withstand higher wind speeds than those made of wood. As mentioned previously, masonry structures generally have wood floors and roof trusses that are framed into the masonry, resulting in continuous exterior walls and a strong structural frame. This construction is more resistant to wind and the impact of windborne debris than wood-frame buildings.

The square footage of a residential building is also considered when determining the amount of storm damage sustained by the structure. For example, large, high-value homes generally exhibit a high quality of construction, often with sophisticated engineering input and secondary risk characteristics, which have a mitigating effect. They also tend to be well maintained. These homes may feature complex architecture with elaborate roof geometries containing multiple gable ends and corners, which tend to mitigate wind loads.

Structures located near the path of a tornado experience additional high pressures due to the rotation of the wind and high suction forces near the center of the tornado. This additional pressure further exacerbates damage and, in extreme cases, can lead to total destruction of the structure. Therefore, in tornadic events, the proximity of the structure to the core of the tornado has a significant impact on the amount of damage the structure experiences. Figure 71 shows tornado damage inflicted on two single-family homes in Moore, Oklahoma on May 20, 2013. These photos support the theory of different damage levels inflicted by different wind speeds near the center and outer areas of the tornado. Figure 71 (bottom) shows major damage to the roof covering, windows, and walls of a single-family home located just outside the core of the tornado. Figure 71 (top) shows far less serious damage to the siding and roof covering of a single-family home located a block away from the tornado core.

Figure 71. Tornado damage inflicted on May 20, 2013 in Moore Oklahoma.
Images include: (top) A single-family home located a block away from the tornado core experienced minor siding and roof covering damage. (bottom) A single-family home located just outside the core of the tornado experienced substantial roof covering, window, and wall damage. (Source: Verisk)

Another example of destruction inside the core of the Moore, Oklahoma EF-5 tornado (May 20, 2013) is shown in Figure 72.

Figure 72. Catastrophic damage at the core of the EF-5 tornado that struck Moore, Oklahoma on May 20, 2013 (Source: Verisk)

Manufactured homes have a high vulnerability to wind damage due to their light weight, construction materials, and foundation tie downs. Even low to moderate wind speeds can cause significant damage to the exterior components, such as roofs, siding, windows, and doors. As seen in Figure 73, stronger winds can blow manufactured homes over or dislodge them, which is why tie-downs have a significant impact on their vulnerability.

Figure 73. Significant straight-line wind damage to a manufactured home
Source: NOAA's National Severe Storms Laboratory

The wind and hail resistance of all components of manufactured homes vary regionally due to varying tie-down mechanisms and building regulations that govern their design and manufacture. The age of the home affects its vulnerability as well. All components become worn and, therefore, more vulnerable over time.

Commercial buildings

In the United States, the phrase "commercial buildings" is an umbrella term that includes many categories of structures, such as hotels, offices, and restaurants. As with residential buildings, construction materials used for commercial buildings vary regionally. For example, a higher percentage of commercial structures are constructed with steel along the East Coast than in other areas of the United States. Low-rise, non-engineered, commercial structures are generally similar to single-family homes in that they are constructed using wood and masonry. Post-disaster surveys indicate that low-rise commercial wood-frame and masonry buildings have vulnerabilities like those of their residential counterparts because they use similar construction materials and practices.

Hail damage to commercial buildings

As with residential buildings, the envelope of commercial buildings endures most of the hail damage, while damage to the structural components is rare. Most of the variation in vulnerability for commercial buildings is related to the roof type. Small commercial buildings constructed with wood frame or masonry will experience damage similar to residential structures, as described in the previous sections. Bitumen layer and gravel roofs common to

large commercial buildings are resilient to hail damage in general, but large hailstones can puncture or damage the surface. Disruption of a gravel surface by large hailstones may leave it more vulnerable to future impacts and shorten its lifespan. Metal roofs may appear to only sustain cosmetic damage from dents and dings, but small cracks at the impact points can allow water to enter the building. Damage and scoring of the surface can also make the roof susceptible to rust.

For engineered buildings built with reinforced concrete and steel, hail damage is usually evident on nonstructural components, such as mechanical equipment, roofing, cladding, and windows. Large commercial buildings often have a large amount of external glass due to glass windows or cladding, which is quite vulnerable to hail damage.

Wind damage to commercial buildings

Wind damage to commercial structures generally initiates at sharp corners, including the corners of the roof and edges of the roof and walls. The extent of wind damage to commercial buildings largely depends on the construction type. Commercial structures constructed using wood frame and masonry can experience damage similar to what residential structures experience. This damage includes roof and wall siding damage in lower-end wind events; high winds can cause damage to structural components. Steel and concrete commercial buildings are generally well engineered and therefore tend to perform better in wind events. As a result, commercial buildings exhibit a broader damage distribution due to wide variations in construction practices and design.

Extremely strong winds, such as those experienced during significant tornado events, will cause significant damage to well-engineered commercial structures. Roofs, wall covers, and windows are often the first part of a building to be damaged by tornadic winds. The rest of the building is then progressively damaged as the high suction pressure induced by tornadoes, as well as the increasing internal pressure, uplifts roofing systems. Tornado winds can also peel off unsecured slates, roll metal roofs, and damage windward overhangs and eaves. Failure of the roof system weakens the lateral support of walls and compromises the main wind-resisting frames, which contributes to their collapse. Tornado-borne flying debris can break windows allowing further interior damage.

Older commercial buildings with reinforced concrete or brick exteriors sometimes perform better than modern commercial structures, particularly those with a large amount of glass. Figure 74, Figure 75, and Figure 76 demonstrate damage from tornadoes that ripped through Atlanta, Georgia, on March 14, 2008 and Moore, Oklahoma on May 20, 2013, respectively.

Figure 74. Tornado damage to much of the glass in commercial buildings in Atlanta, Georgia, on March 14, 2008
Source: Verisk

Figure 75. Tornado damage to commercial buildings in Moore, Oklahoma, on May 20, 2013
Source: Verisk

Figure 76. Tornado damage to a medical center in Moore, Oklahoma, on May 20, 2013
Source: Verisk

Automobiles

The automobile line of business includes both personal and commercial automobiles. The most common type of automobile in the United States includes four-wheeled vehicles designed for passenger transportation. Automobiles are commonly stored in the open, in covered garages or carports, or underground. Automobiles may also be congregated in outdoor lots, which potentially increases aggregate damage in severe thunderstorm events due to added difficulties in moving the vehicles to safety. Storing automobiles in outdoor lots is common for dealerships and cargo immediately before or after transport.

Hail damage to automobiles

Hail damage to automobiles is the most frequently damaging peril from severe thunderstorms and is also difficult to mitigate. Depending on the size of the hailstones, hail can dent the auto body, remove paint, and crash through windows and windshields (Figure 77). Since severe thunderstorms develop quickly, there is rarely time to move a car to relative safety, especially if the owner is not nearby. Automobiles are also at exceptionally high risk from severe thunderstorms because thunderstorms tend to form late in the afternoon when many commuters are on the road (i.e., at rush hour). As a result, commuters may be caught in traffic and unable to escape the storm.

Figure 77. Baseball-sized hail damage to a vehicle in Lubbock County, Texas
Source: NOAA's National Weather Service

Wind damage to automobiles

Wind damage to automobiles is most typically caused by flying debris and falling trees. In high-wind tornado events, it is possible that the high winds can physically move the automobiles and, in extreme cases, turn them on their sides or upside down. As a result, significant automobile damage occurs in concentrated areas along the tornado's path. Figure 78 is an example of automobile damage in an area hard-hit by the 2013 Moore, Oklahoma tornado.

Figure 78. Automobile damage resulting from the Moore, Oklahoma tornado of May 20, 2013
Source: Verisk

Large industrial facilities

The Verisk Severe Thunderstorm Model for the United States features the capability to assess potential property, content, and business interruption (BI) losses in Touchstone to large industrial facilities (as well as small industrial plants). Large industrial facilities are plants featuring a diverse suite of structures, including stacks, cooling towers, pipes, and tanks located in a widespread open area.

Hail damage to large industrial facilities

Hail damage to large industrial facilities is generally limited. Most of the high-cost components in these facilities, such as cooling towers, tanks, pipelines, etc., typically experience minimal hail damage in severe thunderstorm events. On-site buildings include administrative offices, which have similar vulnerability to those of regular commercial structures. However, the proportional cost of these structures compared to the rest of the facility is generally quite low. As a result, low overall hail damage is expected to these facilities from severe thunderstorms.

Wind damage to large industrial facilities

Large industrial facilities are well designed. Thus, there is generally low wind damage to these industrial facilities from severe thunderstorms. There are, however, a few instances of large industrial damage in the United States due to tornadoes. In May of 1982, a supercell thunderstorm produced at least eight tornadoes near Pampa, Texas. The fourth tornado, rated F-3 on the Fujita Scale, caused extreme damage at the Pampa Industrial Park. Two

teams, The Tornado Intercept Team from the Institute for Disaster Research (IDR) and a damage study team from IDR, documented the storm and performed damage surveys the next day. The damage team found that five of seven newly-erected, pre-engineered, metal buildings (i.e., buildings whose components were prefabricated at a factory and assembled on-site) were completely destroyed by the fourth tornado (Marshall & McDonald, 1983).

Figure 79 is an example of EF-3 tornado damage to a chemical plant near Pampa, Texas on November 17, 2015.

Figure 79. EF-3 tornado damage to a chemical plant near Pampa, Texas
Source: PampaEF3-2015 by NWS Amarillo, Public domain

5.2 Severe thunderstorm building damage functions for traditional risks

Traditional risks include residential and commercial structures constructed using common construction materials, such as wood-frame, masonry, reinforced concrete, and steel. The damage relationships in the Verisk Severe Thunderstorm Model for the United States have been developed based on engineering analyses of construction practices, building code design criteria, design principles of special projects throughout the continental United States, field damage surveys, analyses of location-specific insurance company claims data, and knowledge gained from published literature. The associated damage from each sub-peril is explicitly modeled for each coverage type, such as building, appurtenant structures, content, and time element. The damage functions have been validated based on client claims data pertinent to historical events and analyses of industry losses.

See Also
Validating damage functions
Validating modeled losses

Engineered and non-engineered buildings

The Verisk Severe Thunderstorm Model for the United States further expands the differences between primary construction fields to designate structures as either engineered or non-engineered. Engineered structures are generally constructed with complex building materials, such as reinforced concrete or steel. These buildings can be any height and are often used for commercial risks. Non-engineered structures are typically low-rise residential or commercial structures that have been designed and built with less durable building materials. This class also generally includes structures that may have more prescriptive and less explicit design considerations due to their materials and usage. These materials include wood-frame and masonry, which have strength and size limitations and are traditionally used in lower-occupancy buildings.

The amount of engineering attention, key features, and what building codes were in effect during construction vary according to a building's occupancy and construction classes, height, and year built. For example, the roof-to-wall connection is an important feature in a low-rise building, whereas for a high-rise structure, in which each connection is explicitly designed in detail, the roof-to-wall connection is not as important as other features (e.g., glass type and glass percentage). Table 13 summarizes how engineered and non-engineered structures are defined in the Verisk model, based on occupancy, construction, and building height.

Table 13. Definition of engineered and non-engineered construction

Occupancy Codes	Construction Codes	Height Class	Temporal-Spatial Vulnerability	Engineering Category
300, 301, 303-319, 331-346	101-120	Any Height	Yes	Non-Engineered
	131-140, 151, 153-183	Any Height	Yes	Engineered
	152	Any Height	No	N/A
	191-194	Any Height	Yes[13]	N/A
	100	1 – 3 Stories	Yes	Non-Engineered
		> 3 Stories	Yes	Engineered
		Unknown Height	Yes	Non-Engineered
302	100	Any Height	Yes	Non-Engineered

[13] Although the Verisk model considers spatial and temporal vulnerability changes for manufactured homes, they are classified separately. As a result, engineered and non-engineered classifications are not applicable to these risks.

Occupancy Codes	Construction Codes	Height Class	Temporal-Spatial Vulnerability	Engineering Category
	101-120	Any Height	Yes	Non-Engineered
	131-140, 151, 153-183	Any Height	Yes	Engineered
	152, 191-194	Any Height	Yes[13]	N/A
321-330, 351- 374	Any Construction Class	Any Height	No	N/A
All Occupancies	200 and 2,000 Series	Any Height	No	N/A
400 Series	Any Construction Class	Any Height	No	N/A

This engineered and non-engineered building designation is used to attribute typical building secondary characteristics and features and assign relevant building codes to a given structure. Also, this designation determines how secondary features interact with each other for various sub-perils.

Hail damage framework and vulnerability relationships for traditional risks

Hail damage functions for traditional risks were developed using two main elements, as illustrated in Figure 80. The first component is a base damage function, which relates the mean damage level to the measure of intensity (i.e., the hail kinetic energy) at each location (green line). This base damage function varies based on primary risk characteristics. The second component is a modification function (light blue line), which captures the changes to building vulnerability that result when certain building features are present. This modification function is calculated using a novel, component-based hail vulnerability framework, which accounts for the impact of select primary (height and square footage) and secondary risk characteristics on the hail vulnerability of the structure. The final damage function (black line) is calculated by multiplying the base damage function and modification function.

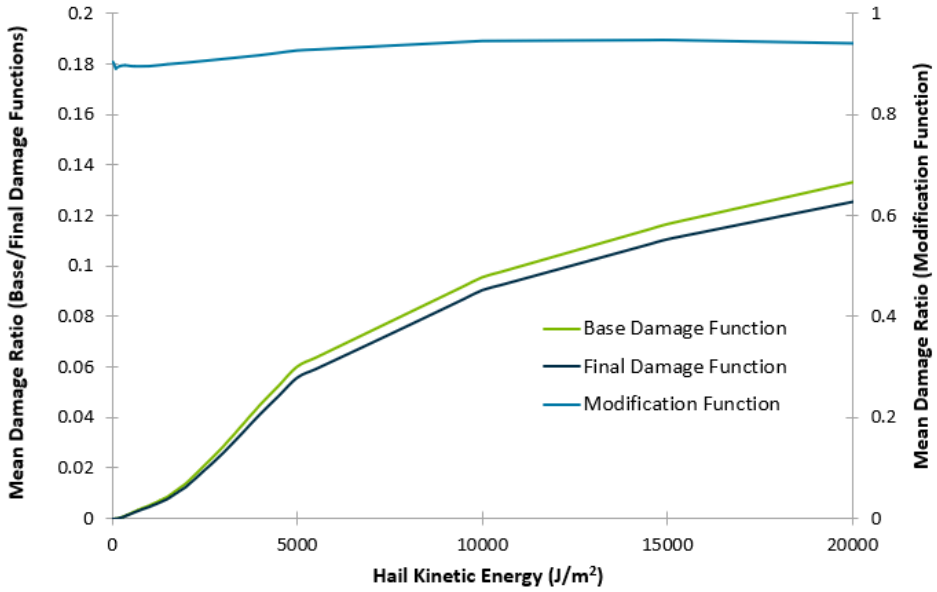

Figure 80. Hail damage function development for traditional risks
A modification function (light blue line; plotted on the secondary y-axis) is applied to the base damage function (green line) to result in the final damage function (dark blue line). This example represents a low-rise (3-story) steel building.

The Verisk Severe Thunderstorm Model for the United States introduces an innovative component-level framework to assess the vulnerability of structures to hail strikes. This framework is based on the physical processes of hail hitting a building at the component level and then determining the relative contribution of each damaged component to the overall building vulnerability. As illustrated in Figure 81, there are three critical elements that must be evaluated to determine each component's vulnerability:

1. Load modification (i.e., hail impact modification): This variable determines a component's susceptibility to being impacted by hail directly, indirectly, or not at all.
2. Component hail resistance: This variable represents a component's inherent resistance to hail impacts based on the material properties and features that could increase or decrease its strength.
3. Component replacement cost ratio: This variable determines the component contribution to the overall building value if the component fails.

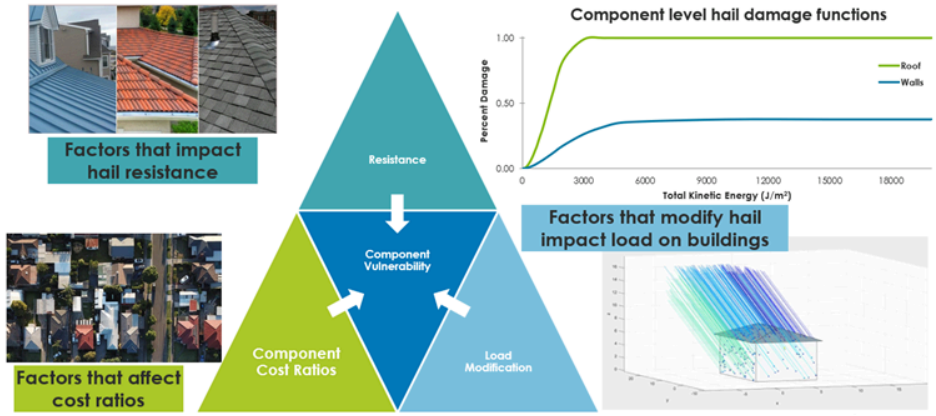

Figure 81. Important building component characteristics that determine hail vulnerability
Source: Verisk

See Also
Hail impact energy

Hail load modification

The Verisk Severe Thunderstorm Model for the United States represents each hail event as a series of elliptical microevents. The measure of hail intensity within the ellipses is defined as the total kinetic energy (KE) over a unit area. This metric is a combination of hail size and hailstone count distributions, event duration, and wind speed. For a given wind speed, the interaction between the hailstones and the building surface can vary significantly and is dependent on several features. Generally, a structure's roof is the most prone to hail damage, and various factors (e.g., roof slope) can deflect or reduce the impact of a direct strike (Petty et al., 2009). In the event of wind-driven hail, wall surfaces may be subject to hail strikes, but not all surfaces will experience the same level of intensity. Therefore, it is highly unlikely that all walls will be damaged, which is evident in post-event storm surveys.

To capture the physical mechanisms of hail strike patterns, the Verisk Severe Thunderstorm Model for the United States incorporates a simulation model that determines the number of hail strikes a typical building will be subject to for a given total KE and calculates the resulting impacts on the structure (Figure 82). This process quantifies the reduction or increase in impact energy on the building surface by varying geometric features (e.g., roof slope and shape). These relationships provide a realistic representation of the physical loads on a structure and how variations in total KE and/or a building's geometric features modify the expected losses.

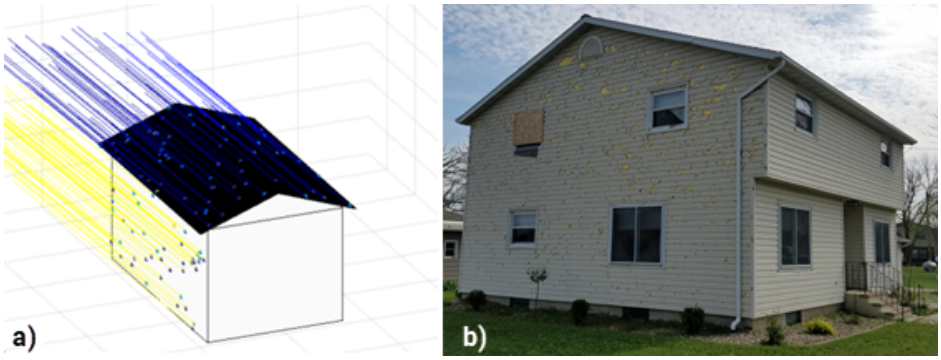

Figure 82. Simulated hail strike patterns (a) are consistent with observations (b)
Source: (a) Verisk and (b) NOAA's National Weather Service, cropped by Verisk

Hail component resistance

Hail damage to a building is dependent on a building's envelope components that are directly impacted by hail strikes. Assessing the damage to each component requires an evaluation of the material resistance of the component as a function of an increasing external load. To derive a load versus response function for various components, Verisk engineers developed a simulation model that produces hailstone distributions (both in size and in number) that are associated with a particular hazard intensity (measured in terms of total KE). This simulation is used to quantify the proportion of a building surface that exceeds a predefined intensity threshold. A simple failed/non-failed criterion is applied to determine the overall component damageability curve as a function of increasing total energy.

To determine the relevant building characteristics and expected performance of components susceptible to hail, Verisk engineers leveraged damage reports and published test standards, reviewed component performance literature, and coupled these findings with Verisk's simulation model. This research, coupled with replacement costs (discussed in subsequent sections), determine how susceptible an individual building is to an increasing hail intensity. This information was validated using physical damage reports from RICOWI's damage surveys following the 2011 Dallas/Fort Worth, Texas hailstorm and the April 11, 2016 event in northern Texas.

While damage surveys present ideal opportunities to observe damage caused by actual events, physical simulations (such as those conducted at IBHS's full-scale testing facility) are also an invaluable resource. The vulnerability component of the Verisk model was informed using results from the IBHS's first-ever indoor hailstorm, a test conducted on February 20, 2013, which was observed by Verisk engineers. These results were used to better quantify the exacerbating effects of hail on the building envelope when hailstones are accompanied by strong winds. In addition, this realistic test demonstrated how key construction features, such as roof covering (non-impact versus impact-resistance asphalt shingles), wall siding (fiber-cement versus vinyl), and windows (vinyl versus aluminum) perform in a hailstorm with varying hailstone sizes. This experiment, various damage surveys, and additional data sources (e.g., Underwriters Laboratory (UL), FM Global standards, Haag Engineering test, and literature) provide Verisk engineers with valuable guidance needed to define the relative importance of the hail secondary risk characteristics.

For a description of the supported hail secondary risk characteristics in the Verisk Severe Thunderstorm Model for the United States, see the *Secondary Risk Characteristics for Verisk Hail Models* document available, with login, on the Client Portal.

Hail component replacement cost ratio

The first two aspects of the hail component module determine the level of damage incurred by a structure due to a particular event. To determine the final vulnerability to hail strikes, the relative contribution of the component damage to the overall building requires detailed cost information. The proportion or contribution of an individual component to the overall building vulnerability is a function of the component's unit cost relative to the overall replacement costs. This ratio, more commonly referred to as the replacement cost ratio, is unitless. Multiplying this replacement cost ratio by a component damageability curve produces component damage functions, which determine the relative contribution of a component to the overall building vulnerability as a function of increasing intensity. The novel hail vulnerability framework uses cost modifiers to modify the relative building component contribution to the overall building value by explicitly accounting for differences in component size and component-to-building proportions. Unit replacement costs for various construction types and occupancy combinations were obtained from Verisk's 360 value as well as other cost-estimating resources (e.g., Gordian's RSMeans[14]).

Accounting for hail Secondary Risk Characteristics

Secondary Risk Characteristics (SRCs), or secondary features, are building features that can increase or decrease the likelihood of damage due to a given sub-peril. Some commonly-used hail SRCs include roof covering, roof deck, wall siding, window protection, and glass type. In addition, since the hail component-level vulnerability framework is developed using the physics of hail strikes on a building's envelope, the relationship between damageability and cost is critical in determining the overall vulnerability. Users can specify property-specific SRCs, which tailor the vulnerability accordingly. In case of a conflict between model assumptions and user-supplied information, the user-supplied information is given priority. Table 14 lists the hail SRCs supported in the Verisk Severe Thunderstorm Model for the United States.

[14] More information about Gordian's RSMeans data is available online at: https://www.rsmeansonline.com/

Table 14. Supported hail Secondary Risk Characteristics

Roof Features	Wall Features	Additional Features
• Roof Attached Structure • Roof Covering • Roof Deck • Roof Geometry • Roof Hail Impact Resistance • Roof Pitch • Roof Year Built	• Glass Percentage • Glass Type • Wall Attached Structure • Wall Siding • Window Protection	• Certified Structures (IBHS)

Some of the more commonly-used hail SRCs are discussed in subsequent sections. For a detailed description of all supported hail secondary risk characteristics in the Verisk Severe Thunderstorm Model for the United States, see the *Secondary Risk Characteristics for Verisk Hail Models* document, which is available, with login, on the Client Portal. In addition, a detailed discussion of the supported wind SRCs will be discussed in subsequent sections.

Roof covering and roof deck

The Verisk Severe Thunderstorm Model for the United States supports various options for roof covering and roof deck in the hail vulnerability framework. Roof covering is the part of the building most susceptible to hail damage and, as a result, is the primary source of insurance claims. The material used for the roof covering has a significant impact on the roof's ability to resist hail damage. If the roof covering is damaged, then the interior of the building and its contents become more vulnerable.

In the United States, a significant portion of the building stock is asphalt shingle roofs (including non-impact and impact-resistant), especially for residential use. Other roofing materials used include ceramic/clay tiles, concrete tiles, wooden shingles, light metal panels, single-ply membrane roofs, and built-up roofs (with and without gravel).

There are a wide variety of roof types that can reasonably be mapped to one class of roof covering. For example, asphalt shingles represent three-tab shingles as well as architectural shingles but may result in a differing amount of damage, all else being equal. In addition, clay and concrete tiles include many types of tiles that have a varied response to severe hailstones. High-profile tiles (e.g., Spanish or barrel tiles) are more prone to breaking than flat concrete tiles, for example. As a result, these various types of roof covering material can be specified using hail secondary features supported in the Verisk model. The failure of roof covering is modeled probabilistically using damageability curves, which indicate the probability of failure for a given hail intensity of loading (measured in terms of total KE).

When a roof covering is substantially damaged, the roof deck may need to be repaired. The roof deck material affects how well the roof deck holds up against hail damage. A damaged roof deck results in a breached building envelope, which causes significant building and contents damage due to wind, hailstone, and wind-driven rain impacts. Since the roof deck is typically not the first line of a roof's defense against hail damage, its damage thresholds are generally higher than those of the roof covering.

For more details on the supported hail roof covering and roof deck secondary risk characteristics in the Verisk Severe Thunderstorm Model for the United States, see the *Secondary Risk Characteristics for Verisk Hail Models* document, which is available, with login, on the Client Portal.

Roof pitch

A building's roof pitch (i.e., roof slope) is important when considering hail damage and associated repair costs, as the resultant impact force on the roof cover is lower if the pitch deflects the hail. Depending on the horizontal component of the hail trajectory and the roof slope, the angle of hail impact can affect the loss experienced.

As the pitch of the roof increases, the size of the roof area and, therefore, the cost relative to the base area (i.e., foundation area) changes, all else being equal (Figure 83). In addition, higher-pitched roofs have greater material and labor costs due to the additional equipment needs and installation difficulty compared to lower-pitched roofs.

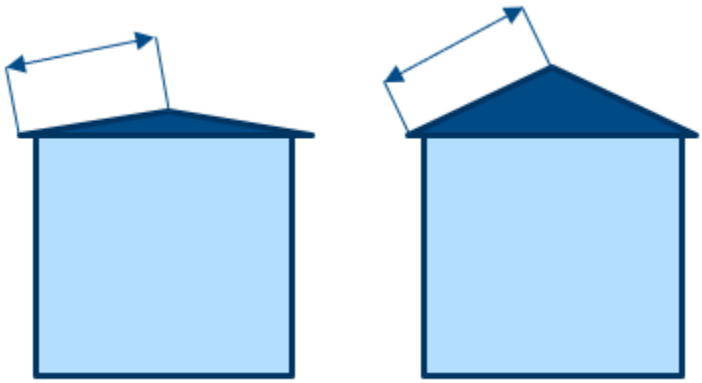

Figure 83. Increasing roof slope results in increased surface area
Source: Verisk

Regionally, areas in the United States that experience high snow loads tend to have steeper roofs to encourage snow to slide off and to prevent ice dam build-up, whereas areas that receive little or no snow have higher proportions of medium-pitched roofs.

For more details on the supported roof slope secondary risk characteristic in the Verisk Severe Thunderstorm Model for the United States, see the *Secondary Risk Characteristics for Verisk Hail Models* document available, with login, on the Client Portal.

Roof age

Roof age bands are used in the Verisk Severe Thunderstorm Model for the United States to indicate the vulnerability of a building's roof to severe hailstones due to its age. Older roofs are more vulnerable to damage than average roofs, which are more vulnerable than new roofs. This vulnerability difference can be attributed to various factors including, but not limited to, aging, material technology, and deterioration.

The following roof age bands are supported in the Verisk model for the hail (and wind) vulnerability frameworks:

- New Roof: Roof built in 2010 or later
- Average Roof: Roof built during the years 2000 to 2009
- Old Roof: Roof built prior to 2000
- Unknown Roof: Roof with unknown year built

For more details on the supported hail roof age secondary risk characteristic in the Verisk Severe Thunderstorm Model for the United States, see the see the *Secondary Risk Characteristics for Verisk Hail Models* document, which is available, with login, on the Client Portal.

Known roof age

When the user enters the roof age (roof year built), two main aspects of the roof age secondary feature are invoked. The first attribute is the roof age band assigned to the structure within the hail (and wind) vulnerability frameworks. These roof age bands include new, average, old, and unknown roof.

The second aspect involves assigning appropriate hail (and wind) secondary features for the roof based on a detailed building code study (described in subsequent sections of this chapter). If the roof age and building age are the same, then these features are those that would be assigned to the default building at that location and point in time based on the year the building was constructed. If the roof age is newer than the building age, then it is assumed that the structure has been re-roofed.

Typically, during a re-roofing, the roof must be updated to follow the current local building code. As a result, the roof-related default building characteristics that are assigned according to the building codes are features associated with the year of re-roofing as opposed to the original year of construction. The building year built would be used to populate all other characteristics, i.e., all characteristics not related to re-roofing. Any user-entered features will still override any assumptions made by the model via Verisk's building code study.

If the user inputs an illogical roof year built (e.g., a roof year built that is older than the building itself), the vulnerability framework will override the roof year built with the building year built. If the user does not enter the roof year built, a roof age credit will be assigned based on unknown roof age assumptions detailed in the following sections. In both cases, secondary features will be attributed to those of the default building based on the building year built or will be overridden with the user-defined features.

Unknown roof age

It is possible that the user does not know the roof age (i.e., roof year built) for a particular risk. In the case of unknown roof age, if the building age (i.e., building year built) is known, the model makes some inferences, which are detailed below.

When a building was constructed in the year 2010 or later, it follows that its roof was also constructed in the year 2010 or later, which falls within Verisk's new roof band. As a result, it is automatically assigned as a "new" roof band. A building constructed during the years

2000-2009 has a roof that falls into an average roof age band or newer. Since an average roof age band is less vulnerable than the country-wide unknown (the unknown, as stated in previous sections, falls between the average and old roof bands), this building is assigned an "average" roof to avoid excessive penalization. If a structure was built in 1999 or prior, no information can be ascertained about the roof age. Therefore, the roof age band is assigned to be "unknown."

There is an exception to the logic detailed above for single-family homes (occupancy code 302), multi-family homes (occupancy code 303), and apartment or condo buildings with wood-frame or masonry construction (occupancy code 306 combined with construction codes 101-104 or 111-119) that uses higher-resolution, county-average roof age data from Verisk when a user does not supply a roof age. Verisk engineers used this detailed roof age dataset to assess county-level unknown roof age averages for residential structures in each roof age band. Thus, for this subset of structures, if a building was constructed in the year 2010 or later and the user does not supply roof year-built information, the new roof age band is assigned. If a building was constructed in 2009 or earlier and the user does not supply roof year-built information, the county-average roof age band is assigned based on the information assessed through the roof age dataset. This dataset provides a more accurate view of roof aging for this subset of risks than using country-wide unknown roof age information. Figure 84 and Figure 85 detail the roof age assumptions for these select buildings built from 2000-2009 and for buildings built prior to 2000, respectively, when the roof age is unknown. Teal indicates a new roof, dark blue indicates an average roof, and black indicates an old roof in both figures.

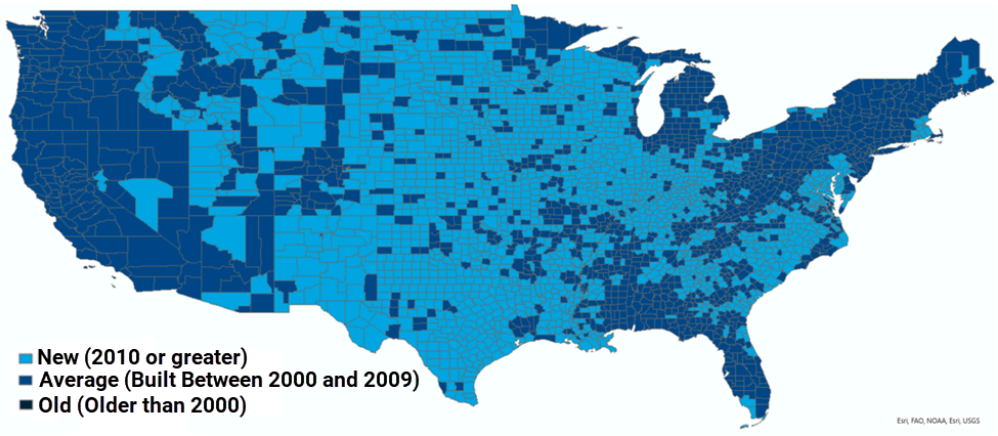

Figure 84. Roof age assumptions for buildings built between 2000 and 2009, when the roof age is unknown, county-averaged
Source: Verisk

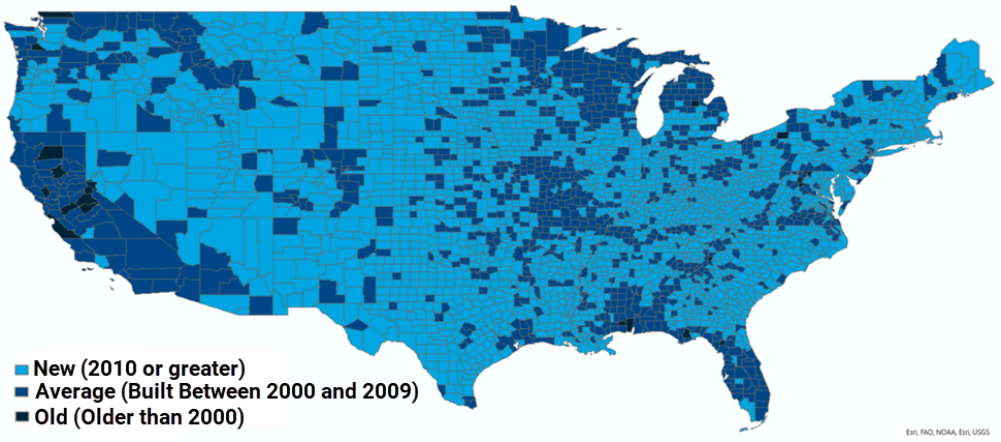

Figure 85. Roof age assumptions for buildings built prior to 2000, when the roof age is unknown, county-averaged
Source: Verisk

In all cases, if the user does not provide the roof year built explicitly, the model does not assume any wind or hail secondary feature overrides for potential re-roofing. Re-roofing assumptions are applied only when the user supplies a valid, known, roof year-built value.

Wall siding

The Verisk Severe Thunderstorm Model for the United States supports various options for wall siding in the hail (and wind) vulnerability frameworks. Wall siding protects the external walls from weathering, and different siding materials have varying degrees of resistance to damage.

Wall siding and openings (e.g., windows) are quite susceptible to hail damage, particularly in the presence of strong winds or along with a roof structure without a significant overhang. A breach in wall siding can expose the wall to high winds and rain, which causes water intrusion. An example of hail damage to a home's vinyl siding and windows is shown in Figure 86.

Figure 86. Hail damage to vinyl siding
Source: NOAA's National Weather Service, cropped by Verisk

The Verisk model uses damageability curves to model the probability of failure of various types of wall siding for a given intensity of loading. These damageability curves are based on various research studies (e.g., Herzog et al., 2012) and engineering expertise.

For more details on the supported hail wall siding secondary risk characteristic in the Verisk Severe Thunderstorm Model for the United States, see the see the *Secondary Risk Characteristics for Verisk Hail Models* document, which is available, with login, on the Client Portal.

IBHS FORTIFIED secondary feature

The "IBHS FORTIFIED" secondary feature activates secondary characteristics in Verisk's hail (and wind) damage framework that are associated with residential and commercial building fortification standards developed by the Insurance Institute for Business and Home Safety (IBHS). The FORTIFIED standards were created by IBHS as minimum suggested strength requirements that address common weaknesses in residential and commercial structures and could result in significant damage to structures in severe weather events. The recommendations given in these standards are based on years of research in studying these severe weather events and the type of damage they cause to both residential and commercial structures. When a structure is officially certified as FORTIFIED Roof, Silver, Gold, or FORTIFIED for Safer Living, the user may activate this secondary characteristic and have appropriate features enabled for each of the respective FORTIFIED levels.

For more details on the supported hail IBHS FORTIFIED secondary risk characteristic in the Verisk Severe Thunderstorm Model for the United States, see the *Secondary Risk Characteristics for Verisk Hail Models* document, which is available, with login, on the Client Portal.

Additional component effects on hail damage costs

In addition to roof slope and building height factors, roof hail impact resistance, roof geometry, building glass percentage, and window protection are important when assessing hail damage and the associated repair costs. The roof hail impact resistance specification is used in the Verisk hail component-level vulnerability framework to modify the strength of the primary roof cover material. For example, if a building's asphalt shingles are impact-rated, the framework will compare the strength of the asphalt shingles to the strength of the applicable hail impact resistance rating, and the strongest of the two will be used. Since there is an added cost associated with higher impact-rated products, a cost modifier will be applied to the base unit costs.

The hail framework also applies cost modifiers to certain roof geometries due to differences in framing costs and/or increases in area for roofs with the same slope. Examples of roof geometries with cost modifiers include gable end with and without bracing, hip, complex, stepped, mansard, pyramid, and gambrel.

As the proportion of glass on a wall facade increases, the proportion of wall siding decreases. Higher glass percentages are associated with higher building costs. Thus, an inverse relationship is used to model the contribution of cost for glass with respect to wall siding. For the same glass percentage, windows that have better opening protection (i.e., non-engineered and engineered shutters) cost more and are associated with an increased cost modifier than windows with no protection.

For more details on the supported secondary risk characteristics in the Verisk Severe Thunderstorm Model for the United States, see the *Secondary Risk Characteristics for Verisk Hail Models* document available, with login, on the Client Portal.

Determining interior damage

A substantial proportion of the building replacement value is attributed to interior elements, such as carpets, interior walls, ceilings, finishings, and fixtures. While these elements are generally protected from hail strikes by the building's exterior envelope, there is the potential for water ingress and subsequent interior damage if the integrity of the envelope is compromised. To account for this dependency, a building's expected interior damage is modeled as a function of its exterior damage.

In some instances, even when there is not any visible hail damage, there may be leaks in the roof cover that lead to damage in the attic. Insulation can then become saturated and cause the ceiling to collapse due to the excessive weight. Alternatively, moisture can build up and lead to mold growth, which may require extensive repair work. Empirical relationships are used to estimate the resultant interior damage given a specific degree of exterior damage to features, such as roof covering, roof deck, and windows. As the height of the structure increases, the contribution of interior damage from the roof diminishes and more emphasis is placed on the window damage. Interior damage is distributed evenly among floors. Similarly, roof-attached structures can increase or decrease the potential for water ingress. Failure of skylights or A/C units can exacerbate the water ingress. Alternatively, secondary water resistance membranes can reduce the risk due to water ingress. Unfortunately, claims data do not distinguish between exterior and interior damage. As a result, these relationships are

based on engineering judgment and calibrated as a part of the claims-based model validation process within Verisk's model development framework.

Total building cost

The unit and size cost factors determine how much the presence of each building sub-component either increases or decreases the building's overall repair cost due to hail damage. To determine the relative change with respect to the overall building, the sum of all modified costs is calculated, and a component cost ratio is derived (i.e., a component's relative contribution to the overall building replacement value). This cost ratio is unitless and is calculated as the modified component cost (dollars per square-foot) divided by the replacement cost (dollars per square foot). Figure 87, Figure 88, Figure 89, and Figure 90 depict sample default cost breakdowns for low-rise (1-story) non-engineered, low-rise engineered, mid-rise engineered, and high-rise engineered buildings, respectively.

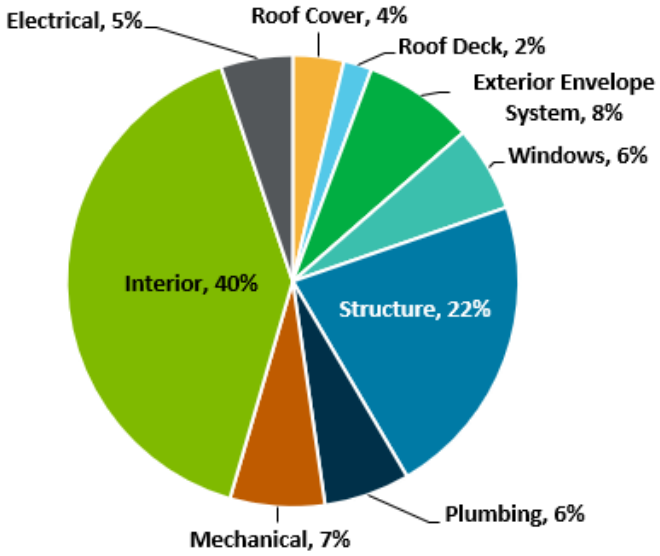

Figure 87. Default cost breakdown for low-rise non-engineered buildings
Source: Verisk

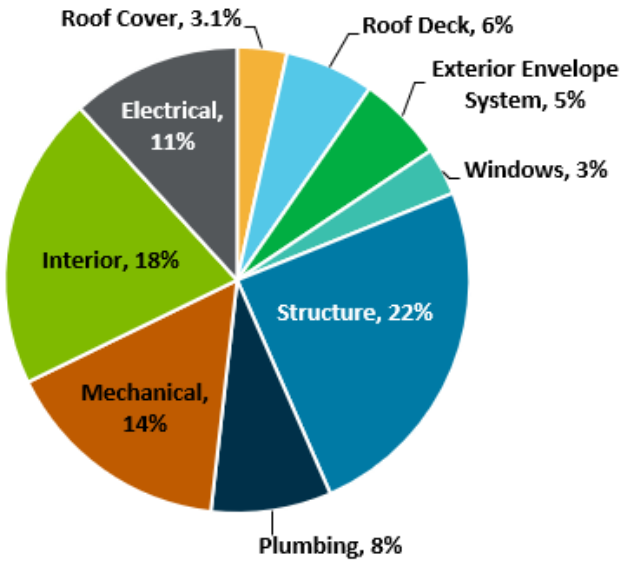

Figure 88. Default cost breakdown for low-rise engineered buildings
Source: Verisk

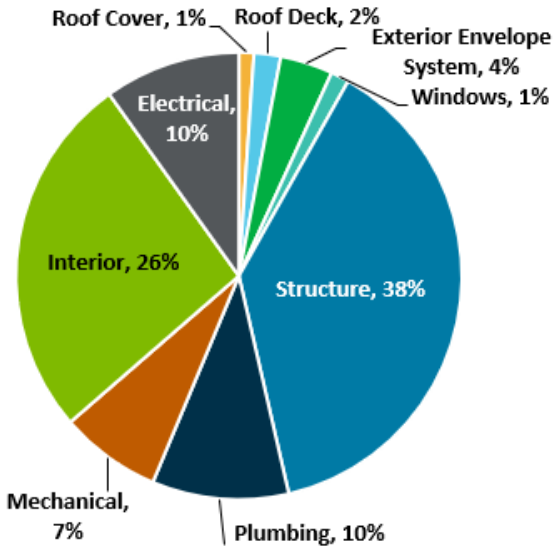

Figure 89. Default cost breakdown for mid-rise engineered buildings
Source: Verisk

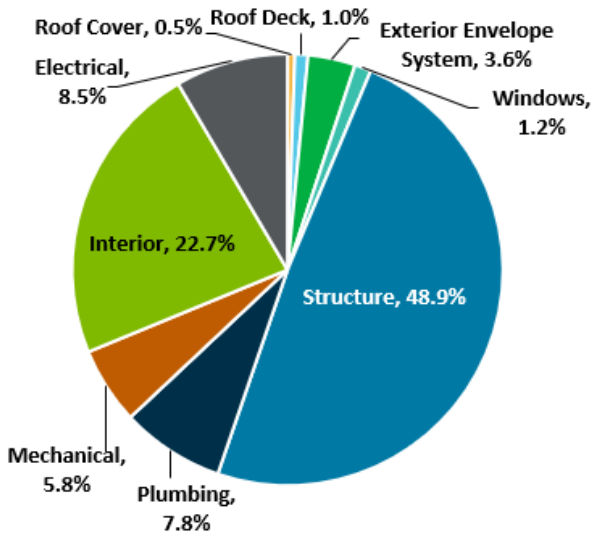

Figure 90. Default cost breakdown for high-rise engineered buildings
Source: Verisk

Final modification function

The final damage functions are created using both a modification function and a base damage function. To develop the final modification function, it is first necessary to develop the component damage curves for the modeled structure using the component load modifications and resistance characteristics. These elements, coupled with the replacement cost ratios, comprise the required elements of the hail component-level vulnerability framework. Costs are recalculated based on user input, and the overall component vulnerability function is generated as a weighted average of the component-level vulnerability functions and the respective cost-based weighting factor.

Figure 91 is an example of the hail component-level vulnerability framework applied to a two-story, wood-frame, single-family home built with the secondary features listed in Table 15. Figure 91 below shows the component-based damage curves using dotted lines, for these specific secondary features. These curves were created for each component option and were weighted using replacement cost ratios shown in Figure 92. These ratios are defined as the percentage of the total building replacement value that is attributed to that specific component. The component-level damage curves are multiplied by these weights and added to obtain the building-level damage curve, which is represented by the solid black line in Figure 91.

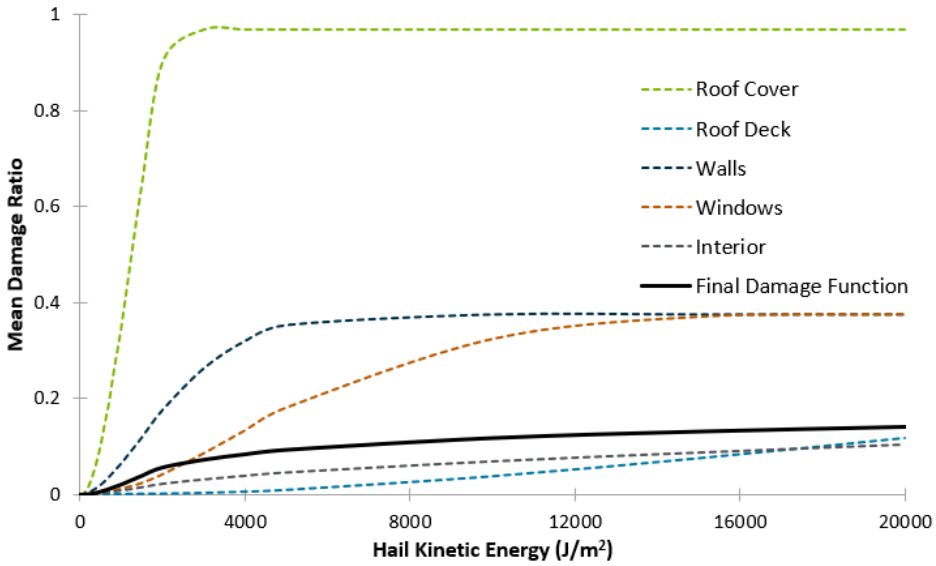

Figure 91. Component-based hail damageability curves and final building damage function for a two-story, wood-frame, single-family home

Table 15. Secondary feature selections

Secondary Feature	Two-Story, Wood-Frame, Single-Family Home	Mid-Rise Steel Commercial Building
Roof Cover	Asphalt Shingles	Single-Ply Membrane
Roof Deck	Plywood	Metal Deck with Insulation Board
Roof Shape	Gable	Flat
Roof Pitch	Unknown	Low
Wall Siding	Vinyl Siding	Unknown

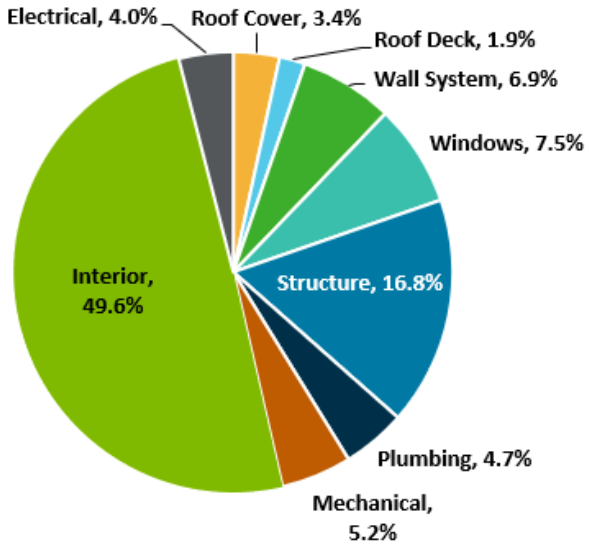

Figure 92. Replacement cost ratios for a two-story, wood-frame, single-family home

Figure 93 is an example of the hail component-level vulnerability framework applied to a mid-rise steel commercial building. The features selected for this structure are given in Table 15. The component-based damage curves for these specific features, illustrated using dotted lines, are shown in Figure 93. These curves were created for each component option. To create the final damage curve, the individual damageability curves were weighted using replacement cost ratios shown in Figure 94 and were aggregated to obtain a system-level damage curve. The weights are determined as the percentage of the total building replacement value that is attributed to that specific component. The final damage curve is shown by the solid black line in Figure 93.

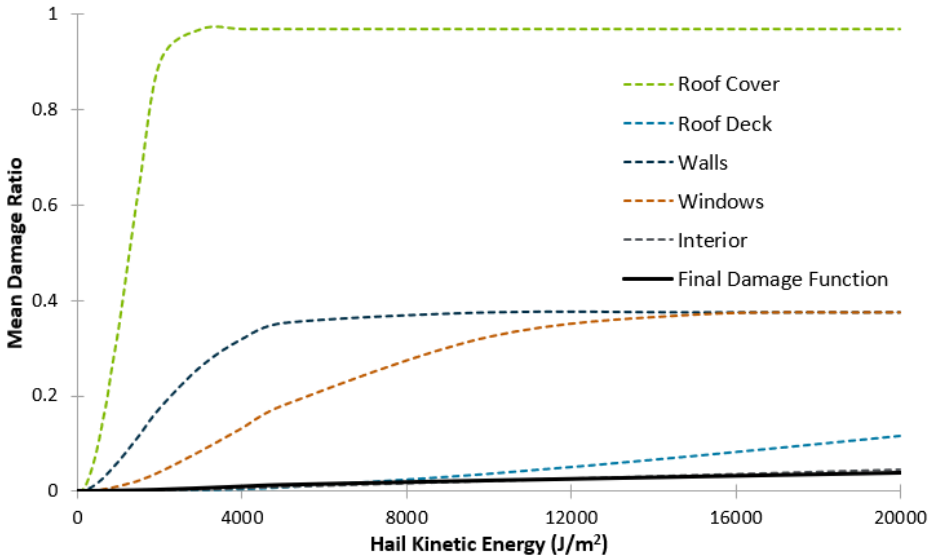

Figure 93. Component-based hail damageability curves and final building damage function for a mid-rise steel commercial building

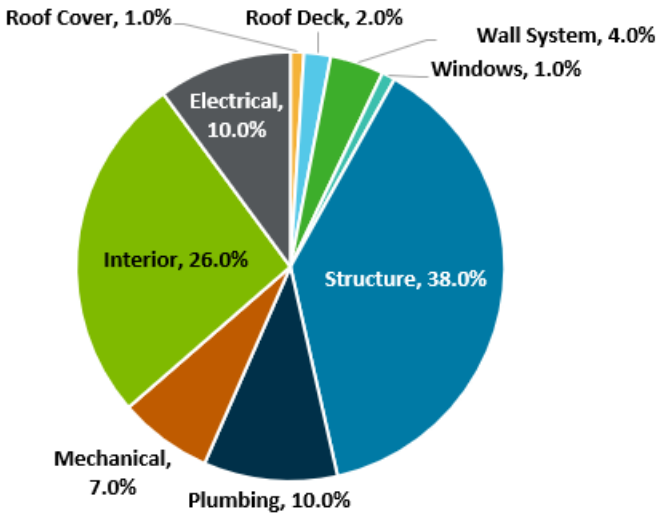

Figure 94. Replacement cost ratios for a mid-rise, steel commercial building

In both cases presented above, component-based damage curves for the structure (i.e., framing), plumbing, mechanical, and electrical systems were not shown on plots. It is assumed that these systems will not be damaged by hail. Therefore, these values will be zero.

The base damage function represents a structure with building characteristics typically found in the U.S. as a whole. Each base damage function is derived using replacement cost distributions and features that are representative of the most common building features, or an average of common building features, in the U.S. for each of the four primary building classes (low-rise non-engineered, low-rise engineered, mid-rise engineered, and high-rise engineered). Once this damage function for a specific building class is created, it must be normalized to create a modification function such that the appropriate cost and size scaling factors are applied to the structure.

See Also

Hail damage framework and vulnerability relationships for traditional risks

Hail base damage function development

Hail base damage functions represent a typical structure in the United States with specific construction and occupancy characteristics. These damage functions are then modified using the modification functions described in the previous sections to account for more specific characteristics. The hail base damage functions for the Verisk Severe Thunderstorm Model for the United States have been calibrated and validated using information from the latest scientific studies and claims analyses of major events in the United States. Key studies include:

- U.S. Insurance Institute for Business and Home Safety's (IBHS) study on the impact of hail on property damage (Brown and Pogorzelski, 2014; IBHS, 2004).
- Roofing Industry Committee on Weather Issues, Inc. (RICOWI) hail damage survey following the 2011 Dallas/Fort Worth, Texas hailstorm (RICOWI, 2012).

- Roofing Industry Committee on Weather Issues, Inc. (RICOWI) hail damage survey following the 2016 North Texas hailstorm (RICOWI, 2016).
- Literature on hail damage to roofing, including the Underwriters Laboratory (UL) roof classes on impact resistance, FM Global standards, and Haag Engineering experiment (Crenshaw and Koontz, 2001; Marshall et al., 2002).
- Hail damage to siding literature (e.g., Petty et al., 2009) and results from the Haag Engineering experiment (Herzog et al., 2012).
- IBHS's first-ever indoor hailstorm, conducted on February 20, 2013. This test, observed by Verisk engineers, has been used to better quantify the exacerbating effects of hail on the building envelope when hailstones are accompanied by strong wind. In addition, this realistic test demonstrated how key construction features, such as roof covers (non-impact vs impact resistance asphalt shingles), wall sidings (fiber-cement vs. vinyl), and windows (vinyl vs. aluminum), perform under a hailstorm with varying hailstone sizes.

Effects of construction and occupancy type on hail damage

Since hail predominantly impacts the roof and façade of a structure, the structure's relative vulnerability will vary based on the cost distributions of roof and façade elements typically associated with that structure's construction type. Wood-frame structures and masonry structures with wood roof systems typically have more cost attributed to the roof relative to the overall structure than concrete or steel structures. Similar to construction type, a structure's occupancy class determines the cost breakdown based on the usage of the structure. For a given construction and occupancy class, the higher the value of non-damageable structural elements, the lower the relative vulnerability. Sample damage functions showing occupancy and construction relationships are shown in Figure 95. Likewise, the height of a building is an important factor in determining cost distributions, as discussed in the next section.

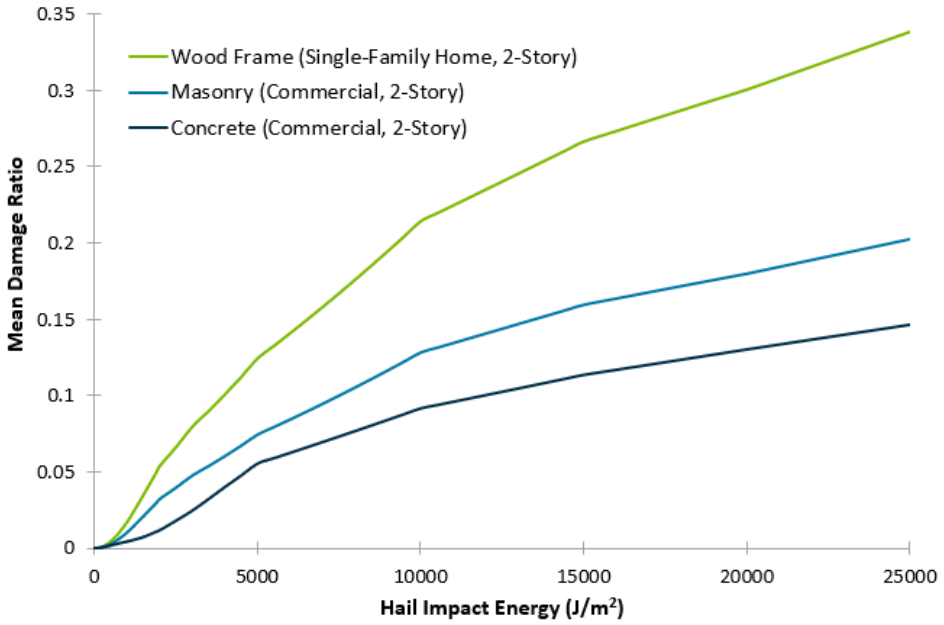

Figure 95. Hail damage functions for select construction and occupancy combinations

Effects of height and square footage on hail damage

Building height and gross area (or square footage) are important when assessing hail damage and associated repair costs. As a building's height increases, the proportion of wall surface area relative to the overall area also increases (Figure 96). Conversely, the proportion of roof surface area with respect to the overall building area decreases with increasing building height. In addition, structures with large floor areas and lower height will have a higher replacement value contribution attributed to the roof than a taller building with the same floor area.

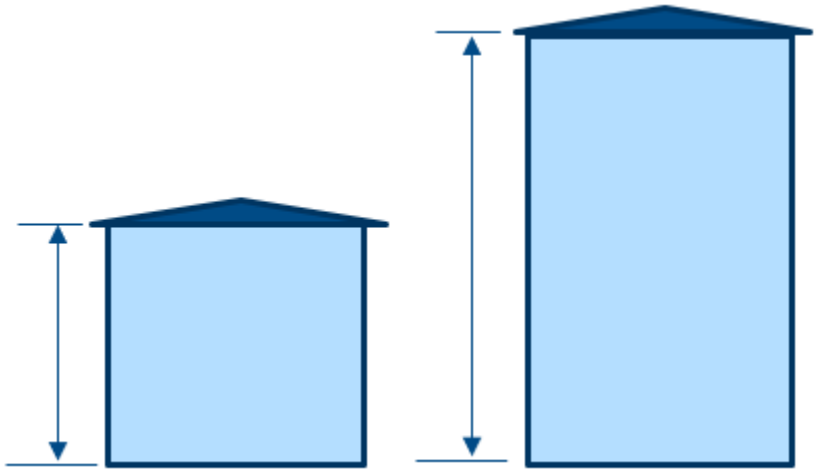

Figure 96. Increasing building height results in increased wall surface area relative to the overall building area
Source: Verisk

The component-level hail vulnerability framework explicitly accounts for variations in vulnerability due to differences in a structure's square footage and height as well as a building's construction and occupancy type (as discussed previously). These features are used to calculate replacement ratios for all subcomponents and systems within a specific group of structures. This process helps assign the appropriate replacement value contribution to the building elements impacted by hail as well as those elements that are not exposed to hail but are still insured. The structural costs for non-damageable elements are scaled according to the size of the building, which reflects the contribution of damageable to non-damageable elements in the damage ratios relative to the total building value. Table 16 provides a summary of supported construction, occupancy, and height variations for hail.

Table 16. Variation in vulnerability by height for the hail sub-peril

<table>
<tr><th rowspan="2">Occupancy Codes</th><th rowspan="2">Construction Class</th><th rowspan="2">Construction Codes</th><th colspan="6">Building Height Category</th></tr>
<tr><th>1-Story</th><th>2-Story</th><th>3-Story</th><th>Mid</th><th>High</th><th>Unknown</th></tr>
<tr><td rowspan="6">300-319, 331-346</td><td>Wood Frame</td><td>101-104</td><td rowspan="4">1</td><td rowspan="4">2</td><td colspan="3">≥ 3</td><td rowspan="4">0</td></tr>
<tr><td>Masonry</td><td>111-119</td><td rowspan="3">3</td><td colspan="2">≥ 4</td></tr>
<tr><td>Concrete</td><td>131-139</td><td rowspan="2">4-7</td><td rowspan="2">> 7</td></tr>
<tr><td>Steel</td><td>151, 153-159</td></tr>
<tr><td>Light Metal</td><td>152</td><td colspan="6">Same vulnerability for all height bands</td></tr>
<tr><td rowspan="2">Wind Resistive</td><td>181, 183</td><td rowspan="2">1</td><td rowspan="2">2</td><td rowspan="2">3</td><td>4-7</td><td>> 7</td><td rowspan="2">0</td></tr>
<tr><td>182</td><td colspan="2">≥ 4</td></tr>
</table>

<table>
<tr><th rowspan="2">Occupancy Codes</th><th rowspan="2">Construction Class</th><th rowspan="2">Construction Codes</th><th colspan="6">Building Height Category</th></tr>
<tr><th>1-Story</th><th>2-Story</th><th>3-Story</th><th>Mid</th><th>High</th><th>Unknown</th></tr>
<tr><td rowspan="2"></td><td>Manufactured Homes</td><td>191-194</td><td colspan="6" rowspan="2">Same vulnerability for all height bands</td></tr>
<tr><td>200, 2000 Series</td><td>≥ 200,
≥ 2000</td></tr>
<tr><td rowspan="9">321-330, 351-374</td><td>Wood Frame</td><td>101-104</td><td colspan="6">Same vulnerability for all height bands</td></tr>
<tr><td>Masonry</td><td>111-119</td><td colspan="3" rowspan="3">1-3</td><td colspan="2">≥ 4</td><td rowspan="3">0</td></tr>
<tr><td>Concrete</td><td>131-139</td><td rowspan="2">4-7</td><td rowspan="2">>7</td></tr>
<tr><td>Steel</td><td>151,
153-159</td></tr>
<tr><td>Light Metal</td><td>152</td><td colspan="6">Same vulnerability for all height bands</td></tr>
<tr><td rowspan="2">Wind Resistive</td><td>181, 183</td><td colspan="3" rowspan="2">1-3</td><td>4-7</td><td>>7</td><td rowspan="2">0</td></tr>
<tr><td>182</td><td colspan="2">≥ 4</td></tr>
<tr><td>Mobile Homes</td><td>191-194</td><td colspan="6" rowspan="2">Same vulnerability for all height bands</td></tr>
<tr><td>200, 2000 Series[15]</td><td>≥ 200,
≥ 2000</td></tr>
<tr><td>300-373</td><td>Unknown</td><td>100</td><td colspan="3">1-3</td><td>4-7</td><td>> 7</td><td>0</td></tr>
<tr><td>374</td><td>Unknown</td><td>100</td><td colspan="6" rowspan="3">Same vulnerability for all height bands</td></tr>
<tr><td>381</td><td>Marine Hull</td><td>260</td></tr>
<tr><td>400-482</td><td>All</td><td>All</td></tr>
</table>

To account for cost differences associated with building height, Verisk's hail vulnerability framework applies cost modification factors based on a building's number of stories in conjunction with a building's gross area (or square footage). These factors increase the repair costs of walls and main fixed system components as well as the relative roof costs as a function of height. Wall cost modifiers are applied to wall cover, windows, and interiors. Roof cost modifiers are applied to roof cover and roof deck. Fixed system cost modifiers are applied to structural, electrical, plumbing, and mechanical systems. Sample damage functions for concrete commercial buildings with different heights are shown in Figure 97.

[15] For a complete list and detailed description of the supported 200- and 2000-series construction classes, please reference the *Touchstone Exposure Data Validation Reference*, which can be accessed from www.unicede.com.

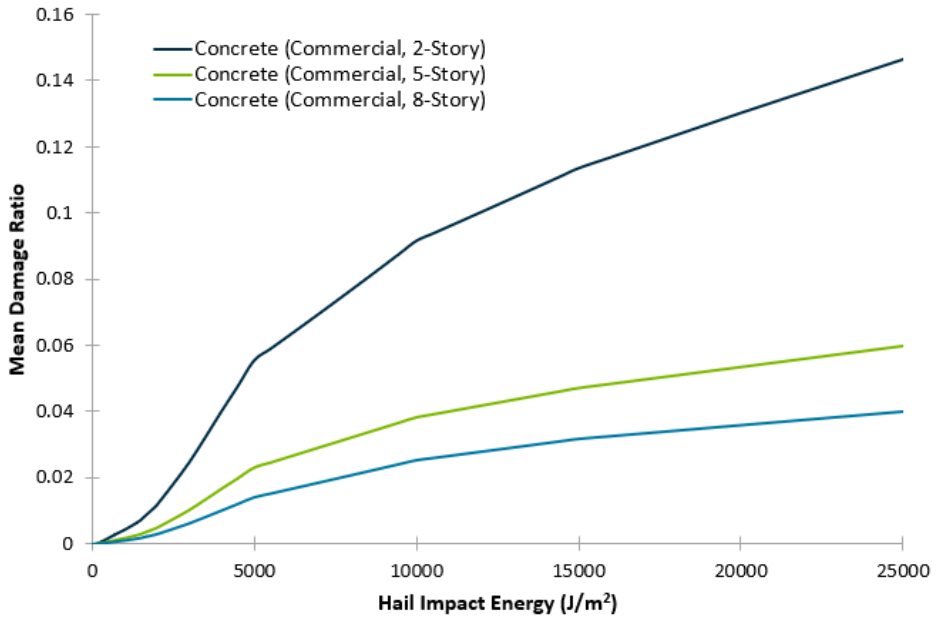

Figure 97. Hail damage functions for concrete commercial buildings with different heights

To determine the impact of building size, Verisk's hail vulnerability framework calculates cost modification factors as a function of a building's base area (i.e., the gross area divided by the number of stories). Specifically, Verisk engineers evaluated the typical system costs for various building subcomponents and evaluated how these costs scale according to size. For both engineered and non-engineered low-rise buildings, component replacement cost per square foot decreases as the building's square footage increases. The rate of decrease is consistent with Gordian's RSMeans construction cost data values for various building types across North America. The effect of size is limited by a lower bound and an upper bound (i.e., buildings generally see no significant variation in cost below or above a certain square footage). Between these two points, the costs generally scale with varying inflection points. For non-engineered structures, the assumed lower bound is 1,500 sq. ft. and the upper bound is 10,000 sq. ft. For engineered structures, the assumed lower bound gross area is 5,000 sq. ft. and the upper bound is 50,000 sq. ft. Buildings with smaller footprints will not see any relative impact due to square footage.

The typical replacement ratios and system cost distributions explicitly account for higher-value homes that may have less value attributed to the roof relative to the overall replacement value. In addition, structures with larger floor areas have larger roofs, but the relative replacement costs will scale the non-damageable portions of the structure accordingly. This scaling generally reduces the overall building vulnerability.

See Also

Engineered and non-engineered buildings

Effects of year built on hail vulnerability

A structure's primary year built determines its age as well as the building codes and standards that were in effect at the time of its construction. While there are generally no building codes or standards that specifically focus on reducing losses due to hail damage, a building's geographic location provides information on the building code requirements in effect when the structure was built to reduce losses due to damage caused by other perils, such as wind, in that area. For example, hurricane-prone regions are required to have more stringent building feature requirements than regions less affected by tropical cyclones. Leveraging detailed building code studies for the United States, Verisk engineers can attribute the typical building code features that were required by code and those that were prevalent for a given year built. As a result, when a user inputs a structure's year built, default building characteristics are automatically assigned for some building features in the Verisk component-level hail vulnerability framework. These standards are consistent with building code requirements for wind design. Any secondary risk characteristics explicitly assigned by users will override any features that would have otherwise been assigned via Verisk's building code study. More information about this study is provided in the "Unknown Roof Age" section of this chapter.

See Also

Unknown roof age

Wind damage framework and vulnerability relationships for traditional risks

In addition to hail, severe thunderstorms can produce gusty straight-line and tornadic winds, which can inflict damage on the built environment. For both straight-line windstorms and tornadoes, damageability is a function of the three-second gust wind speed. Wind damageability depends on many different factors, including occupancy and construction types, height and square footage, year built, secondary characteristics, and construction practices.

When wind comes into contact with buildings, the airflow streamlines separate at the sharp corners of the structure, including wall corners, eaves, roof ridges, and roof corners (Figure 98). The separation at these sharp corners causes additional airflow turbulence and results in highly fluctuating pressures on building surfaces. The magnitude and direction of the wind are significant factors in the magnitude and fluctuation of pressures acting along the surfaces of the building. Generally, the windward wall will experience positive pressure and the side and leeward walls will endure negative, or suction, pressure. The roof may experience either positive or negative pressure; and the pressures endured also depend on the distance from the flow separation points. Wind forces are significantly increased at corners, ridges, and at abrupt changes in the direction of wind flow.

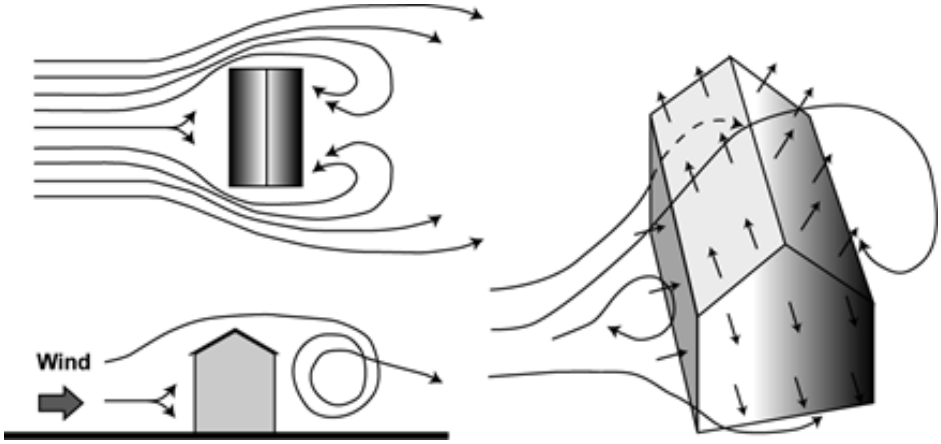

Figure 98. Wind flow around buildings can generate severe suction and pressure forces
Source: Verisk

Damageability relationships within the wind damage framework of the Verisk Severe Thunderstorm Model for the United States are composed of two primary components. The first component is a base damage function, which relates the mean damage level to the measure of intensity (i.e., the three-second gust wind speed) at each location. This base damage function varies based on the occupancy, construction, and height of the risk. The second component is a modification function, which captures the changes to building vulnerability that result when certain building features are present. The modification function varies with wind intensity to reflect the relative effectiveness of a building feature or combination of features when subject to different wind speeds. Figure 99 illustrates the application of modification functions to the base damage functions.

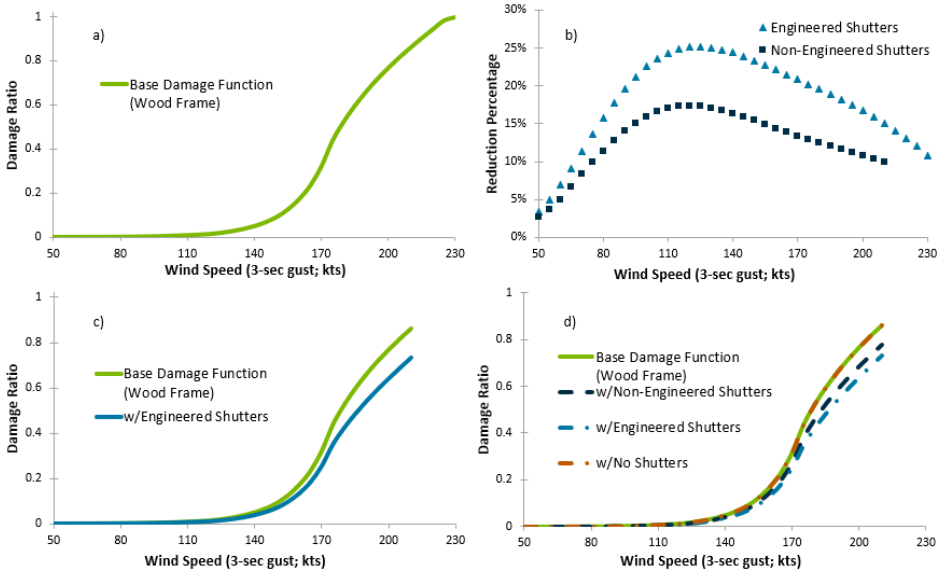

Figure 99. a) Basic damage function for wood-frame construction; b) reduction in damage for engineered versus non-engineered shutters; c) basic damage function and modified function for engineered shutters; and d) envelope of damage functions, all protection options
Source: Verisk

Accounting for wind Secondary Risk Characteristics

Building aerodynamics is a complex phenomenon because the performance of a building depends on the interaction of several building components. Moreover, damage due to wind is progressive: failure at a localized level can eventually grow to a catastrophic level. Thus, it is important to recognize the way in which damage progresses and the role and importance of building components at each stage of failure.

The first step in the development of the modification functions describing these relationships is the identification of building and environmental characteristics that impact the performance of a building in damaging winds. These features (i.e., SRCs) were selected based on research and damage surveys. Some features may be characterized as non-structural (e.g., cladding), while others are structural or parts of structural systems (e.g., roof to wall connection). Finally, others address more general and/or environmental features that affect the building's vulnerability (e.g., building condition, proximity to trees, etc.). The building SRCs that have been identified as important to a structure's wind vulnerability are listed in Table 17.

Table 17. Supported wind Secondary Risk Characteristics

Roof Features	Wall Features	Additional Features
• Roof Anchorage • Roof Attached Structure • Roof Covering • Roof Covering Attachment • Roof Deck • Roof Deck Attachment • Roof Geometry • Roof Pitch • Roof Year Built	• Exterior Doors • Glass Percentage • Glass Type • Wall Attached Structure • Wall Siding • Wall Type • Window Protection	• Appurtenant Structures • Average Adjacent Building Height • Building Condition • Building Foundation Connection • Certified Structures (IBHS) • Floor of Interest • Large Missile • Seal of Approval • Small Debris • Terrain Roughness • Tree Exposure

For more details on the supported wind SRCs in the Verisk Severe Thunderstorm Model for the United States, including definitions and examples, see the see the *Secondary Risk Characteristics for Verisk Wind Models* document, which is available, with login, on the Client Portal.

Verisk's methodology for accounting for SRCs follows a structured and logical approach. When SRCs are provided by the user, these characteristics flow through the component-level vulnerability framework. In the case of a conflict between model assumptions and user-supplied information, the user-supplied information is given priority. Building characteristics are grouped according to their function to reflect the contribution of each characteristic and feature group to the overall building performance. The vulnerability framework creates

an intensity-based modification curve and applies this curve to adjust the base damage functions using the known features and interactions of the features present in a given building.

Verisk's methodology was developed based on structural engineering expertise and building damage observations from historical severe thunderstorm events as well as studies from other wind perils that impact structures. Verisk engineers conducted damage surveys and literature reviews, built simulations, and evaluated numerous reports from multiple events that provide a wealth of data in various scenarios. Severe thunderstorm and hurricane surveys were compared, and similarities were deduced based on structural failure mechanisms caused by wind. When data were scarce, simulations were used to extrapolate the expected building response to extreme winds.

Two distinct metrics are used to develop the relationships behind the modification functions. The first metric is a value assigned to the various *options* for building or environmental features. The value for any given option of any given feature reflects the relative prevalence of use among the options and is independent of other features. Thus, the value is designed such that the most commonly used option is assigned a value close to 1.0. The implication is that a building with this option is expected to perform very similarly to the average, or "typical," building represented by the base damage functions.

The value assigned for an option that is considered to be more vulnerable (i.e., less wind resistive) than the most commonly chosen option is greater than 1.0. That is, a building with this option will be more vulnerable than the average building. Similarly, the value assigned for an option that is considered to be less vulnerable (i.e., more wind resistive) than the most prevalent feature will be less than 1.0. Such a building will be less vulnerable than the average building. If no information is available on the option, the default value is 1.0, which means that there is no modification associated with that particular feature.

The second metric has two types of weighting. One type is used to develop simple weighted averages, which are used to evaluate the loss contribution of several features that, together, constitute a system, such as a roof. They are wind speed dependent; that is, the contribution of each feature varies with wind speed. For example, a roof system may consist of three features: roof covering, roof deck, and roof covering attachment. The loss contribution to the roof system from these three features is expected to be different at different wind speeds. At low wind speeds, the roof covering drives the damage. As wind speeds increase, the roof deck becomes more vulnerable. In this case, roof deck failure will result in loss of roof covering regardless of the type (or option) of roof covering present. Therefore, as wind speed increases, the weight assigned to roof deck increases. In contrast, at higher wind speeds, the weight for roof covering decreases because it is already lost. The weights for the system total 1.0.

The second type of weighting combines the effects of features whose interaction are complex and not necessarily additive. These weights are introduced to evaluate features that modify the performance of the system. If we consider a roof system again, the roof age, roof pitch, and roof geometry modify the performance of the roof. Therefore, the weight should be used as a multiplier. The weights are dependent on wind speed and construction class and are appropriately selected to reflect the importance of a feature at certain levels of building damage. The full impact of aging on a roof is a combination of the roof's age factor and the

building's age factor (i.e., the building's "tech factor," which is applied to an entire building based on the building's year built).

Note that the effects of a building feature on the vulnerability are sensitive to factors, such as wind speed. Thus, it is expected that the relative vulnerability of various features may change based on the event intensity. The relative importance of each modifier will also change based on wind speed. For example, at low wind speeds the roof covering is an important feature, but at very high wind speeds, the roof covering may be damaged and/or no longer attached to the structure. At this point, the roof deck or other features take higher importance. As a result, there is no definitive way to determine which SRCs have the greatest impact on building vulnerability.

The quality and level of detail of exposure and claims data have improved over time. For example, the active U.S. hurricane seasons of 2004 and 2005 increased the data resolution. Prior to these years, most of the available data was aggregated at the ZIP Code level with little to no information about individual building characteristics. Data from more recent events indicate that most companies have started capturing exact addresses and primary building characteristics. Many clients have also started reporting more detailed building characteristics, such as roof covering, roof geometry, and roof-to-wall anchorage. Verisk has analyzed these data to validate the impact of characteristics both individually and in various combinations.

Although much of the data that is available is related to hurricane events, it is possible to leverage this information for straight-line wind and tornadic severe thunderstorm events. A significant amount of research has been performed in the last few decades to understand the difference between straight-line wind events and tornadoes, both in academic institutions and at Verisk. This information has helped Verisk engineers better translate findings from one sub-peril to another.

Straight-line wind and tornado base damage function development

The model's base damage functions for straight-line winds and tornadoes are based on claims and damage survey data as well as published engineering research. Verisk engineers conducted their own studies in computational fluid dynamics (CFD), to better understand the difference in the wind fields of tornadoes, straight-line winds, and hurricanes. CFD numerically simulates fluid flows around buildings using numerical solutions.[16] CFD analyses provide valuable insights into the damage mechanisms and relative vulnerability of various building types and their features by evaluating the distribution of wind pressures on the envelope of low- and high-rise buildings.

Research shows that straight-line winds have a similar vertical wind profile as hurricanes. Thus, Verisk engineers leveraged their extensive research on building vulnerability to hurricane winds to inform vulnerability relationships for straight-line winds. Like hurricanes, the intensity of straight-line winds gradually increases with height as opposed to tornadoes, where the wind speed is very high near the surface and then begins to decrease at higher elevations (Figure 100). The negative vertical wind speed profile of tornadoes introduces

[16] http://www.air-worldwide.com/Publications/AIR-Currents/2013/Where-the-Wild-Winds-Blow%2C-Part-I/

more suction and uplift pressure on low-rise buildings as compared to straight-line winds and causes overloading on the structures. These increased forces affect both the components and cladding and the main wind force resisting system. In extreme winds, these forces can lead to the structure's collapse. Experimental studies at Iowa's tornado simulator (Sarkar and Haan, 2010) and a CFD study (Selvam and Millett, 2005) support this finding.

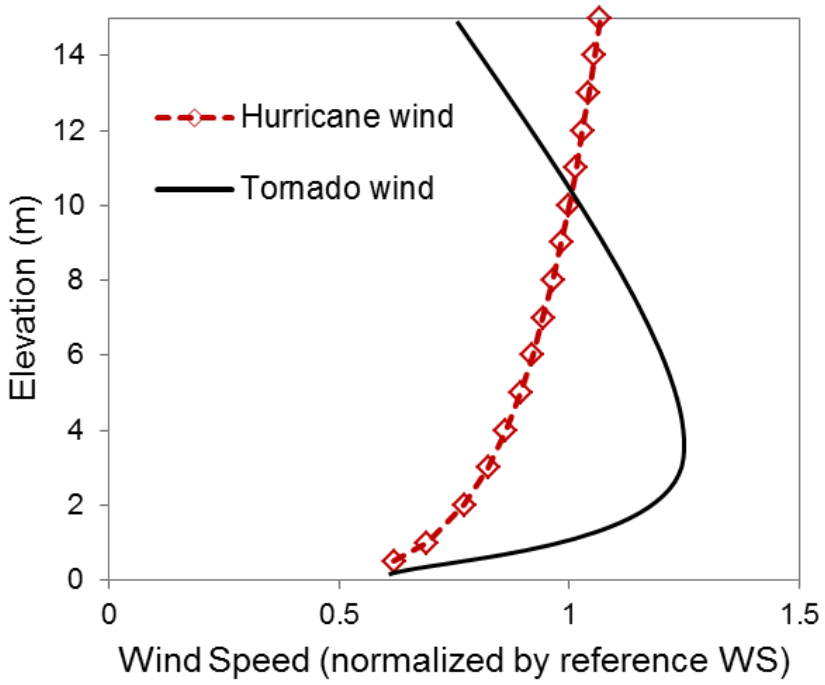

Figure 100. Vertical tornado wind profile as compared to a hurricane profile
Source: Verisk

Following the Joplin, Missouri tornado on May 22, 2011, the American Society for Civil Engineers/Structural Engineering Institute (ASCE/SEI) committee conducted a building damage survey and issued guidelines to mitigate building damages caused by tornadoes (Prevatt, D.O. et al., 2012; van de Lindt, J.W. et al., 2013). This committee recommended a similar methodology for estimating tornado design loads as has been done for straight-line winds and hurricanes. Specifically, they recommended that the standard ASCE 7 wind pressures be computed first and then modified to account for tornado wind field characteristics. As a result, Verisk's engineers leveraged the knowledge gained from modeling hurricanes, with appropriate modifications that consider the unique nature of tornado winds, in developing the tornado damage functions. To complete this work, Verisk researchers addressed the two distinct ways in which tornado wind loads differ from hurricane wind loads:

1. Tornadoes are characterized by a central vortex (i.e., a rapidly-rotating column of air around a region of low pressure). This central vortex leads to greater upwards vertical forces on structural components and higher suction pressures than hurricane winds.
2. The width of a tornado wind field is significantly smaller than that of a hurricane. Tornadoes have diameters on the scale of hundreds of meters and are produced from a

single convective storm (i.e., a thunderstorm or cumulonimbus cloud). A tropical cyclone, however, has a diameter on the scale of hundreds of kilometers and is comprised of several to dozens of convective storms.

The seminal work in understanding the effects of tornado-induced wind loads was conducted at Iowa State University using a tornado simulator (Haan Jr., F. L. et al., 2010). The simulator was used to determine how building wind pressures in tornadoes differ from that of hurricane winds for identical peak three-second gust wind speeds. The results of this study include:

1. No increase in wind pressure in the lateral direction.
2. Up to a 50% increase in wind pressure in the transverse direction.
3. Uplift suction pressure increases by 1.5 to 3.2 times in the vertical direction.

To calculate tornado damage, Verisk engineers converted the one-minute sustained wind speeds of a hurricane to three-second gust tornado wind speeds and incorporated the effect of wind-borne debris. Statistical variation in the increase in suction pressures due to component geometry, orientation, anchoring, and roofing area is accounted for in these damage ratio calculations. Figure 101 shows two typical damage functions for single-family homes, one for straight-line wind events, and the other for tornadoes. It is evident that straight-line wind damageability is less than that of tornadoes for a given three-second gust wind speed in the Verisk model.

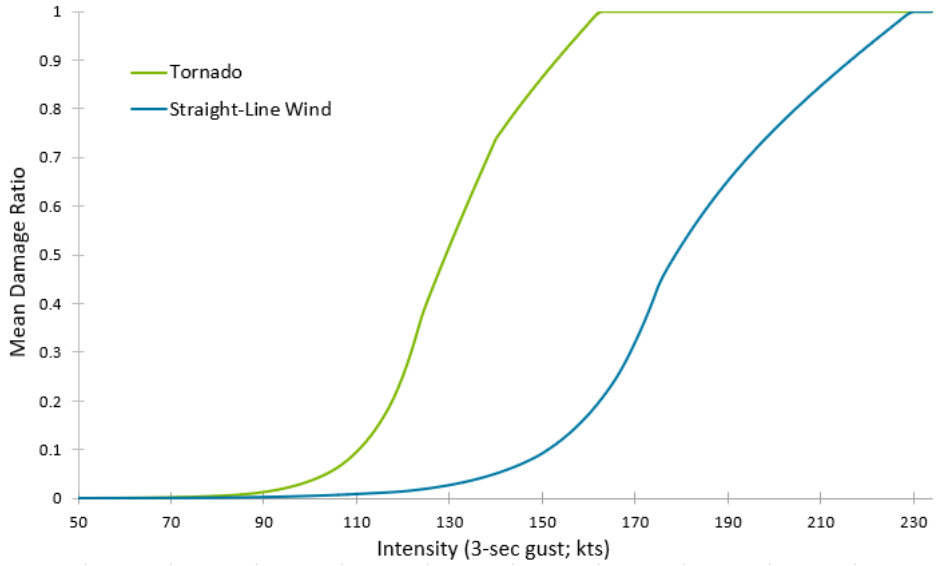

Figure 101. Sample damage functions for straight-line wind and for tornado for a single-family home

Effects of construction type on straight-line wind and tornado damage

Construction type is a primary feature that affects a building's wind vulnerability. Masonry buildings perform better than wood-frame structures when exposed to heavy wind loads and wind-borne debris, especially when they are designed and constructed with adequate reinforcement and connecting elements. Reinforced concrete buildings, however, generally perform better than residential masonry buildings when exposed to wind loads. Reinforced

concrete also performs better than steel when used for commercial structures, while light metal is the least resistant. Figure 102 shows select Verisk straight-line wind damage functions for various construction classes in the U.S.

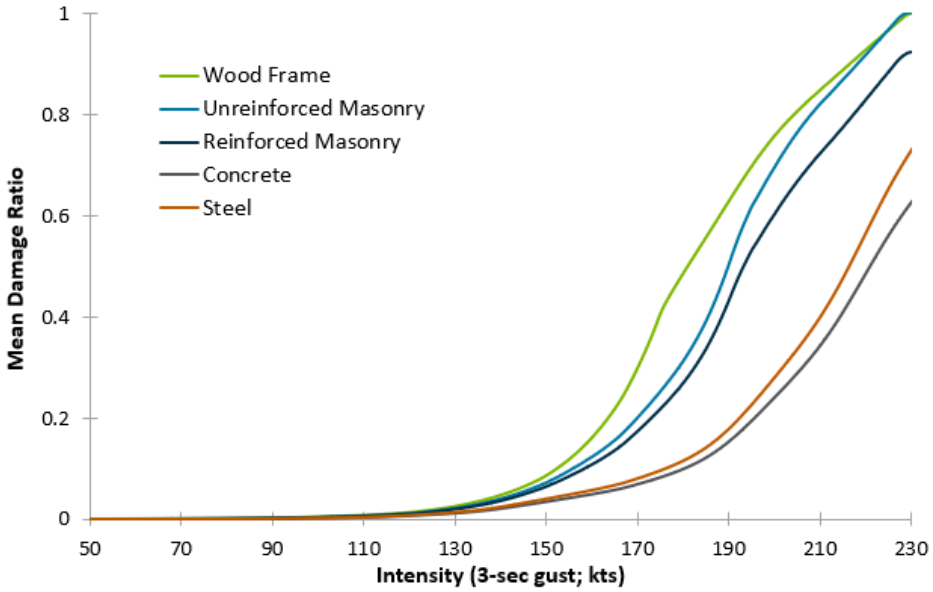

Figure 102. Straight-line wind damage functions for select construction classes
Source: Verisk

Table 18 shows the most common construction types used in the United States. A full list of supported construction classes is included in the *Verisk Severe Thunderstorm Model for the United States Supplement* available, with login, on the Client Portal.

Table 18. Common construction classes

Class	Description
Wood Frame	Mostly one-story to three-story structures. Stud walls are constructed of 2" x 4" or 2" x 6" wood members vertically set 16" or 24" apart. Walls are braced by plywood or by wood or steel diagonals.
Masonry Veneer	Wood-frame structures with one width of non-load-bearing concrete, stone, or clay brick attached to the stud wall.
Unreinforced Masonry	No steel reinforcing within a load-bearing masonry wall. Floors, roofs, and internal partitions are in a load-bearing wall. Usually wood buildings.
Reinforced Masonry	Consists of load-bearing walls of reinforced brick or concrete-block masonry. Floor and roof joists constructed with wood framing are common.
Reinforced Concrete	Consists of reinforced concrete columns and beams.
Steel	Consists of steel columns and beams.
Light Metal	Made of light-gauge steel frame and usually clad with lightweight metal or asbestos siding and roof, which is often corrugated. Typically, these are 1-, 2-, or 3-story structures.

Class	Description
Unknown	Represents a weighted average of all the above construction types.

See Also

Tornado wind speeds

Effects of occupancy type on straight-line wind and tornado damage

Occupancy type is another key factor that affects a building's ability to resist hail and wind damage. Different occupancy classes require different building practices and are subject to different codes and code enforcement, which vary by state. Common occupancy classes include, but are not limited to, residential, commercial, industrial, and agricultural. In addition, there are several sub-classifications within each class.

Residential buildings are usually designed using prescriptive design methods, which mean that they tend to be designed using design tables and each component is not necessarily individually engineered. While plan review and inspection processes should be in place for these types of structures, code enforcement does vary based on the governing code jurisdiction. As a result, some residential buildings are not strictly built to code. In general, damage to residential buildings tends to be low when wind speeds are less than about 110 mph (177 km/hr); in such cases, damage tends to be limited to roof covering and cladding. At higher wind speeds, damage may propagate to roof sheathing, connections, and openings. Catastrophic damage may occur when wind speeds are greater than 160 mph (257 km/hr). In such cases, the roof framing may be severely damaged, resulting in lateral instability of walls, possibly causing their collapse and, ultimately, complete building destruction.

Commercial structures are generally well-engineered and are subject to stricter building code standards than residential buildings. As a result, they are generally less vulnerable to wind damage than residential properties. Structures associated with some businesses (e.g., auto repair shops) tend to have large openings, such as roll up doors and open bays, which contribute to increased vulnerability.

Apartments and condominiums frequently receive a degree of engineering attention similar to that given to commercial construction. From a structural viewpoint, therefore, commercial and apartment/condominium construction is similar. Nevertheless, apartments and condominiums have some building components that make them more susceptible to hailstorms and windstorms than commercial construction. These components include balconies, awnings, and double-sliding glass doors, which are more vulnerable to hail and wind because they are less engineered at the design and construction stages. As a result, Verisk engineers have developed separate damage functions for apartments and condominiums.

Effects of height on straight-line wind and tornado damage

The Verisk model's damage functions explicitly account for building height. Separate damage functions have been developed for three height ranges, which include: low-rise, mid-rise, and high-rise. Although the wind hazard increases with height due to increased wind speeds, wind vulnerability typically decreases for high-rise buildings. High-rise buildings tend to be built

under more stringent engineering standards and adhere to stricter code guidelines than low-rise structures. In addition, while roofs are particularly vulnerable to hail and wind damage, replacement costs are significantly affected by the share of the roof as a fraction of the total building replacement cost. As building height increases, the share of the roof decreases, thereby reducing vulnerability for both wind and hail perils. The percentage of replacement cost represented by cladding, which is also highly vulnerable to hail, wind, and debris impact, also decreases as the total building size increases.

The definitions of low-, mid-, and high-rise buildings are different for different construction types and sub-perils because vulnerability varies by construction type and sub-peril. The model's height bands for the wind and tornado sub-perils are shown in Table 19.

Table 19. Variation in vulnerability by height for the straight-line wind and tornado sub-perils

Occupancy Codes	Construction Class	Construction Codes	Building stories			
			Low	Mid	High	Unknown
302	All	All	Same vulnerability for all height bands (low-rise)			
300, 301, and 303-374	Wood Frame	101-104	1	> 1	-	0
	Masonry	111-119	1	2-3	> 3	0
	Concrete	131-139	1-3	4-7	> 7	0
	Steel	151, 153-159	1-3	4-7	> 7	0
	Light Metal	152	Same vulnerability for all height bands (low-rise)			
	Manufactured Homes	191-194	Same vulnerability for all height bands (low-rise)			
	Wind Resistive	181, 183	1-3	4-7	> 7	0
		182	1	2-3	> 3	
	200, 2000 Series	≥ 200	Same vulnerability for all height bands (low-rise)			
300, 301, and 303-373	Unknown	100	1-3	4-7	> 7	0
374	Unknown	100	Same vulnerability for all height bands (low-rise)			
381	Marine Hull	260	Same vulnerability for all height bands (low-rise)			
400-482	All	All	Same vulnerability for all height bands (low-rise)			

Figure 103 illustrates the relative vulnerability for reinforced concrete commercial buildings by height for the straight-line wind and tornado sub-perils. Notice that low-rise buildings demonstrate the highest vulnerability, while high-rise buildings demonstrate the lowest.

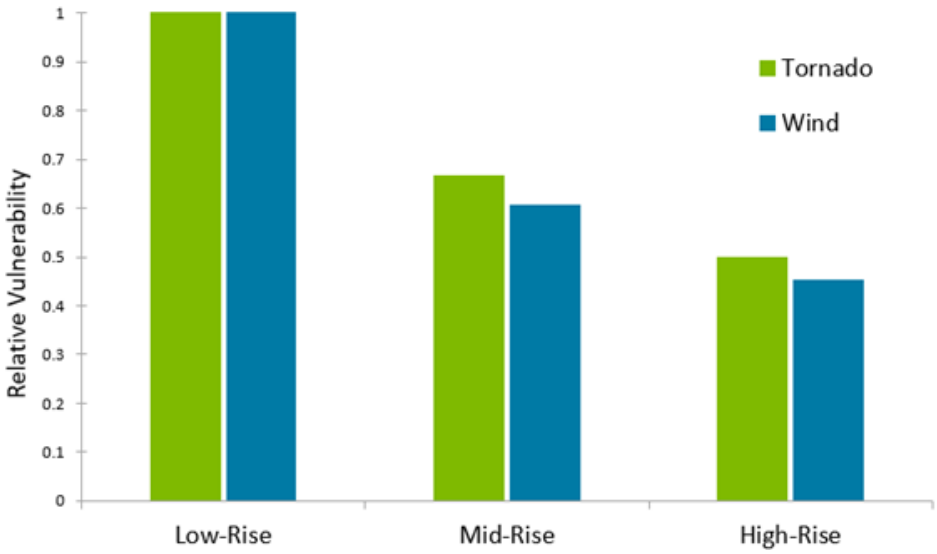

Figure 103. Relative vulnerability of reinforced concrete commercial buildings by height and sub-peril

Assessing the vulnerability of large, high-value homes to wind perils

Large, high-value homes generally exhibit a high quality of construction, often with sophisticated engineering input and often with SRCs. They also tend to be well maintained. They may feature complex architecture with elaborate roof geometries containing multiple gable ends and corners. Verisk classifies large homes as those with livable square footage over 3,000 ft^2. The square footage is based on livable space rather than the home's footprint, thereby accommodating multi-storied homes. Note, however, that even very large single-family homes are generally low-rise (i.e., 3 stories or less). In the Verisk model, the square footage-based vulnerability distinction for large homes applies only to the general residential occupancy class, single-family homes, and multi-family homes (occupancy classes 301, 302, and 303, respectively).

Verisk engineers performed an extensive analysis of the wind vulnerability of larger homes. The first step in the analysis involved a study of claims data from recent historical events from which abundant claims data were available. The study included claims from the 2004 and 2005 hurricane seasons, including Hurricane Katrina (2005), as well as Hurricane Ike (2008), Hurricane Irene (2011), and Hurricane Sandy (2012). Although these are hurricane events, the results can be reasonably extended to other wind perils.

Analysis of detailed company claims data for high-value homes from recent hurricane events show that the mean damage ratio for a single- or multi-family home decreases with increasing gross area, or its square footage. Plausible explanations for this inverse relationship include:

- An increase in building resistance of larger homes through the presence of better SRCs and maintenance.
- A change in the relative replacement value of different building components.

- A change in wind loads due to different building and roof geometries used for larger buildings.

However, Verisk engineers also found a relative reduction in this inverse correlation at higher wind speeds, indicating that under very strong winds, the size of the home had a diminishing impact on the damage ratio.

When determining the vulnerability of buildings to wind loads, it is important to consider building resistance and wind loads separately. The reduction in vulnerability of large homes due to building resistance capabilities can be captured with the appropriate SRCs. To accurately assess the vulnerability difference based on building size alone, it was necessary to decouple the effects of those SRCs, as well as some primary ones. Therefore, to fully understand these effects, Verisk engineers conducted a second step in the analysis, which used computational fluid dynamics (CFD) to understand the reduction in wind loads with increasing gross area when coupled with increased complexity in roof geometry.

The focus on roofs is a natural one. Post-event damage surveys suggest that a significant driver of insurance claims is damage to roofs. This damage may be caused by overloading due to pressure, fatigue loading due to turbulence, or debris impact. To thoroughly isolate the effects of home size, and subsequent changes in roof design, on wind vulnerability, Verisk first developed simulated structures that would effectively represent the impact of building size alone. Idealized "virtual" buildings representing each type of home (average and high-value) were modeled. As shown in Figure 104, the added complexity of the larger, high-value homes was captured by changing the number of walls, corners, and the roof type (i.e., number of hip and gable ends). Studies show that as the structural square footage and complexity of the roof increases, the fraction of the total roof area that is subjected to damaging critical pressure coefficients decreases. This decrease is due to flow modification from the structural complexity of the home.

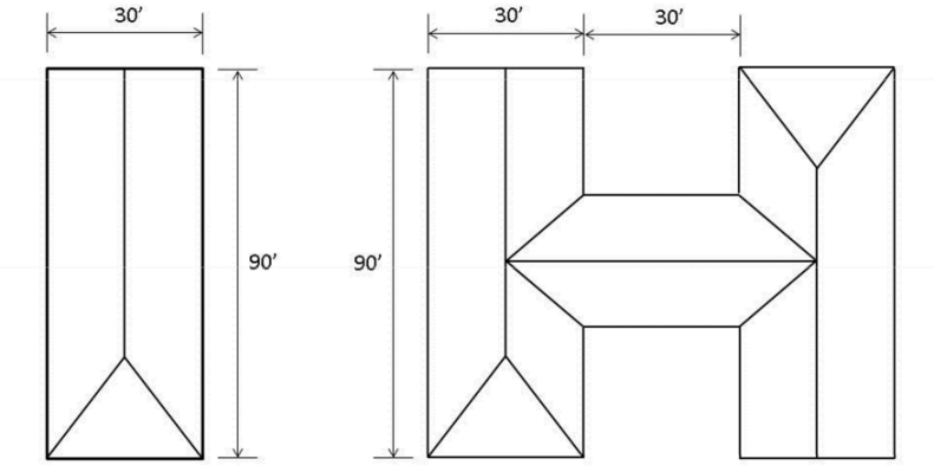

Figure 104. Layout of simulated buildings with increasing levels of complexity
Source: Verisk

For the CFD output, the mean pressure coefficient (C_p) values on the roof surfaces were obtained. The measurement of the roof surface pressures was based upon the assumption that for many high-value homes, most of the loss from wind damage is due to roof damage,

which can result from pressure overloading, fatigue due to turbulence, or from flying debris. In this experiment, "failure" occurred through pressure overloading. In other words, mean pressure coefficients greater than a threshold value indicated areas where failure could possibly occur.

To compare the impact between buildings, the percentage of the roof area beyond a specific negative pressure coefficient threshold was derived from the CFD output. The ratio of this area to the total area of the roof was calculated to define the percentage of roof area beyond the threshold. The percentage change in area was compared between structures, and for various threshold levels. Different negative pressure thresholds were established, but not with the implication that these thresholds produce damage. Rather, they indicate that the portions of a particular roof prototype where the mean pressure coefficients exceed these thresholds are likely to be areas where the failure of roof components may occur (Figure 105).

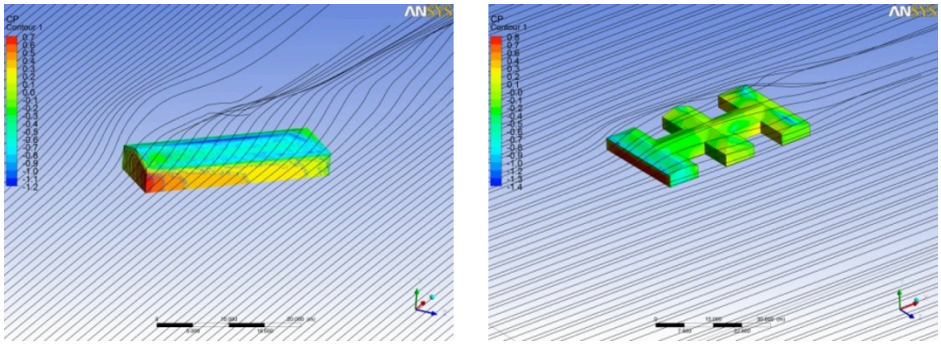

Figure 105. Prototypes of homes show different areas of critical pressure thresholds
Typical average-sized home (left) and typical larger-sized home (right). Source: Verisk

The results indicated a clear trend of a significant decrease in the roof area impacted by negative pressures beyond a threshold with increasing home size. This decrease in the roof area impacted appears to be asymptotic; once the square footage is beyond a certain size, there does not appear to be any further reduction in the relative area of roof that is impacted.

Based on these findings, Verisk researchers developed damage functions that account for square footage based on homes that are less than 3,000 ft^2 with a reduction factor applied to accommodate increases in size beyond 3,000 ft^2. The result is illustrated in Figure 106 as a damage surface that reflects the vulnerability reduction as a continuous function of square footage, with increasing size resulting in lower vulnerability. Note that this methodology captures the reduction in the vulnerability of high-value homes purely from the standpoint of external wind pressures or loads. The reduction in vulnerability due to the presence of superior features can be captured using SRCs.

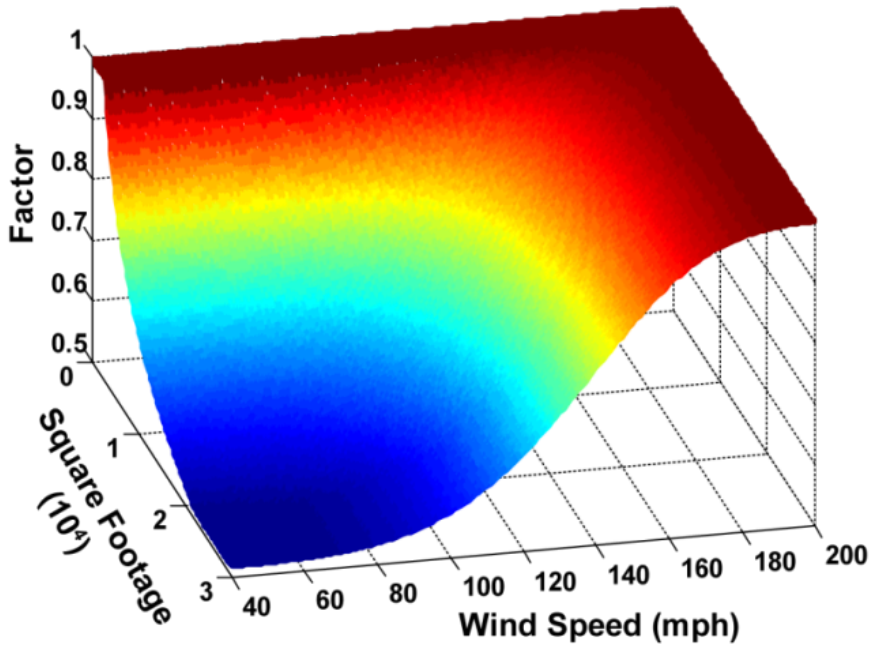

Figure 106. Damage surface of the vulnerability reduction factors applied homes of 3,000 ft^2 and larger
Source: Verisk

Effects of year built on wind and tornado vulnerability

The year built of the structure has a significant impact on the structure's damageability when subject to wind and tornado events. The Verisk model considers the effect of year built in several different ways, depending on whether the year built and additional SRCs are populated. Several cases are considered, as outlined below:

- Case 1: Year built and all SRCs known
- Case 2: Year built known and SRCs unknown
- Case 3: Year built unknown

This section will focus on the first case presented above, i.e., when the year built and all secondary features are populated by the user.

Wind vulnerability continually changes over time due to continual changes in building construction materials and practices as well as structural aging and building maintenance. In the Verisk model, the effects of macro-level changes, such as structural aging and changing materials, and the incorporation of newer materials are accounted for using year-built adjustments. Buildings built prior to 1995 are perceived as old from these perspectives, and buildings built within the last six years (2015-2020) are considered new from an aging perspective. Between 1995 and 2015, there is a continuous change in the year-built adjustment to account for structural aging and similar factors.

Accounting for spatial and temporal variation in vulnerability

Engineering studies, claims data, and damage surveys indicate that there can be significant variation in building vulnerability by region and time period. This variation is due to changes in building codes, construction practices, structural aging, and upgrading. Since reliable loss estimation depends on accurately capturing significant differences in vulnerability between time periods and regions, Verisk undertook a comprehensive, peer-reviewed study to enhance the understanding of the evolution of wind load standards, building codes, construction, and enforcement throughout the United States. Detailed findings of this study have been incorporated in the model to capture regional and temporal variations in wind and tornado vulnerability. Although building codes do not specify hail design requirements, wind design has implications for envelope features and materials that are additionally relevant to hail vulnerability, and therefore regional and temporal variations are also incorporated to differentiate hail vulnerability when applicable. Since construction and code enforcement practices of individual jurisdictions may be difficult to ascertain in detail, claims data from recent storms were used to calibrate and validate Verisk's damage estimation module.

When the user provides the structure's location and year built, the results of this study are used to supplement unknown SRC information based on the building codes in effect and the degree of code enforcement for that region and time period. As indicated in the previous section, the model uses the year built in a number of ways:

- Case 1: Year built and all SRCs known
- Case 2: Year built known and SRCs unknown
- Case 3: Year built unknown

The next section will focus on Case 2.

Spatial and temporal variations in building codes

The Verisk model takes a comprehensive approach to developing damage functions for each region and year built in the United States, while drawing on many years of experience and research conducted at Verisk. The model utilizes a detailed methodology based on engineering analysis and the vulnerability of individual building features. Detailed claims data from recent storms are used to calibrate and validate the damage estimation module and model performance.

There are many sets of building codes released in the United States, with varying levels of adoption and enforcement. Building codes are adopted by a jurisdiction at the state, county, or local level to specify the minimum requirements, by law, under which structures must be designed and constructed. These building codes reference building standards, which provide suggested guidance by professional organizations, such as the American Society of Civil Engineers. These codes and standards reflect the current state of engineering and scientific knowledge at that point in time. Verisk engineers thoroughly studied these building codes and their referenced standards by region and time period to capture regional and temporal variations in vulnerability across the model domain. The vulnerability implications of this study are incorporated into the Verisk Severe Thunderstorm Model for the United States.

A complete list of vulnerability changes by region and construction type are available in an appendix to this document.

To incorporate building code information at a local level for all regions, Verisk engineers take a top-down approach, illustrated in Figure 107. First, engineers study the wind standards, followed by the building codes, the state codes, and, finally, any local code amendments, enforcement practice changes, and building construction practices. These factors indicate building vulnerability at a local level.

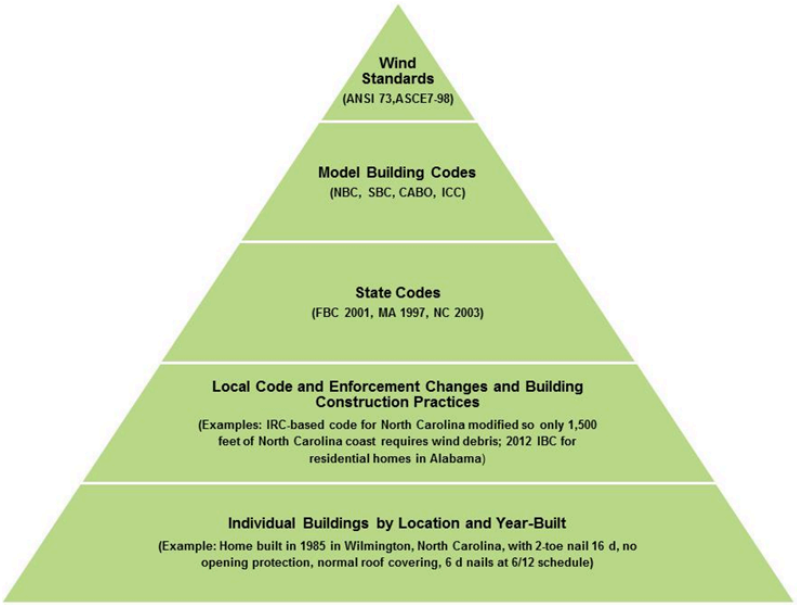

Figure 107. Verisk's comprehensive methodology for estimating relative vulnerability by region and year built
Source: Verisk

The following aspects of the codes and referenced standards are critical for assessing a building's vulnerability to wind:

- **Design wind speed**—In the United States, building codes rely on building standards, such as those provided by the American Society of Civil Engineers (ASCE) Load Standards (ASCE-7), to provide guidance on the wind hazard at a particular location using design wind speed maps.
- **Local terrain**—Design wind speed maps, along with the local terrain, are used to determine the loads that a structure must be designed to resist.
- **Minimum building design requirements**—These requirements include, but are not limited to, member sizing and/or spacing, connection strength, and the wind speed rating of roof covering.

By rigorously studying these code-related aspects and how they evolve over time in jurisdictions across the model domain, Verisk engineers have gained an in-depth understanding of expected spatial and temporal changes in structures' vulnerability across the modeled states. Thus, when the user provides the structure's location and year built, the

results of this study are used to supplement unknown SRC information based on the building codes in effect and the degree of code enforcement for that region and time period.

See Also

Temporal Vulnerability Changes

History of building code adoption

To understand how a structure's year-built information is incorporated into the model, it is important to first have a more detailed understanding of the history of building code adoption in the United States. Prior to 2000, the following three model building codes were used in the United States:

- Building Officials and Code Administrators (BOCA) code—used primarily in the Northeast and Midwest
- International Conference of Building Officials' Uniform Building Code (UBC)—used primarily in the West
- Southern Building Code Congress International, Inc.'s Standard Building Code (SBC)—used primarily in the South

Prior to Hurricanes Hugo (1989) and Andrew (1992), codes mainly focused on the wind design of the Main Wind Force Resisting System (MWFRS) of a structure and were loosely adopted and enforced. Significant damage from these events called attention to the importance of the building's envelope, including the roof covering, which led to a stronger focus on building envelope and component and cladding design. In the mid-1990s, changes, such as roof shingle testing and roof sheathing connection testing, were introduced. Glazing standards were also updated, but these standards were used in only the South Florida Building Codes until around the year 2000.

Prior to 1995, building codes were mandatory in only a few states. In the mid-1990s, building code administrators combined to form the International Code Council (ICC) to create code uniformity across the United States. These codes incorporated more stringent building envelope design, similar to that of the South Florida Building Codes, which led to a decrease in structural vulnerability in the jurisdictions adopting these codes. The ICC codes were first published in 2000 and have been updated regularly, generally every three years. The ICC codes were also more widely adopted than earlier codes, especially in coastal states. Most states have enacted statewide, mandated building codes. However, there is still significant state-to-state variation in building code adoption over time.

Comprehending changes to building vulnerability as the building codes evolved requires an understanding of both changes in building codes and in the standards referenced in these building codes. The wind design chapter of the building codes references, by name, the wind loads chapter of the American Society for Civil Engineers 7 (ASCE 7) standard. This standard provides guidance regarding the design wind speeds that must be used to develop the design wind loading conditions for structures built using the codes and, as a result, the minimum structural requirements.

ASCE 7 has undergone several significant changes throughout the years. Figure 108 illustrates the changes in the ASCE 7 Design Wind Speed Maps in Florida resulting from changes to this Standard:

- ASCE 7-88: The design wind speed map (Figure 108.a) used in the 1988 version of this standard (ASCE 7-88) was developed using a distribution of hurricane wind speeds that was determined using simulation techniques. The basis for the map was in terms of the one-minute fastest-mile wind speed.
- ASCE 7-98: The 1998 version of the standard (ASCE 7-98) updated the design wind speed maps (Figure 108.b), where the hazard defined in the maps was defined in terms of the three-second gust wind speed. These new maps were determined using a stochastic simulation capturing the frequency and intensity of simulated hurricane tracks, and new data and research were used to define the parameters of the stochastic simulation. The design wind speed maps in ASCE 7-02 and ASCE 7-05 are similar to those in ASCE 7-98.
- ASCE 7-10: In the 2010 version of the standard (ASCE 7-10), the wind speed maps (Figure 108.c) were again updated due to new research, which resulted in a re-simulation of the hurricane winds. Additionally, there was a shift in design methodology from Allowable Strength Design (ASD) to Load and Resistance Factor Design (LRFD) to make the wind and earthquake methodologies consistent. Finally, one design aspect, the structure's risk category, that was considered in previous versions of the standard using a separate factor, was absorbed into the design wind speed maps in ASCE 7-10.
- ASCE 7-16: The 2016 version of the standard (ASCE 7-16) updated the design wind speed maps according to new research. The updated wind speed maps are very similar to the ASCE 7-10 wind speed maps in coastal locations, except for the northeast portion of the United States, which had updates to contour locations. Across inland locations, additional wind speed contours have been added in ASCE 7-16 as compared to ASCE 7-10, leading to a general decrease in design wind speeds, most notably in the middle and western portions of the country. An additional map was added for Risk Category IV buildings. These buildings had been addressed on the same design wind speed map as Risk Category III buildings in ASCE 7-10. Changes were also made to some sections of the standard that have implications for design wind loads. These changes include a separate section detailing wind loads of rooftop solar panels (which were grouped with "Components and Cladding" loads in previous versions of the standard), and modifications to component and cladding pressure coefficients on the roof.

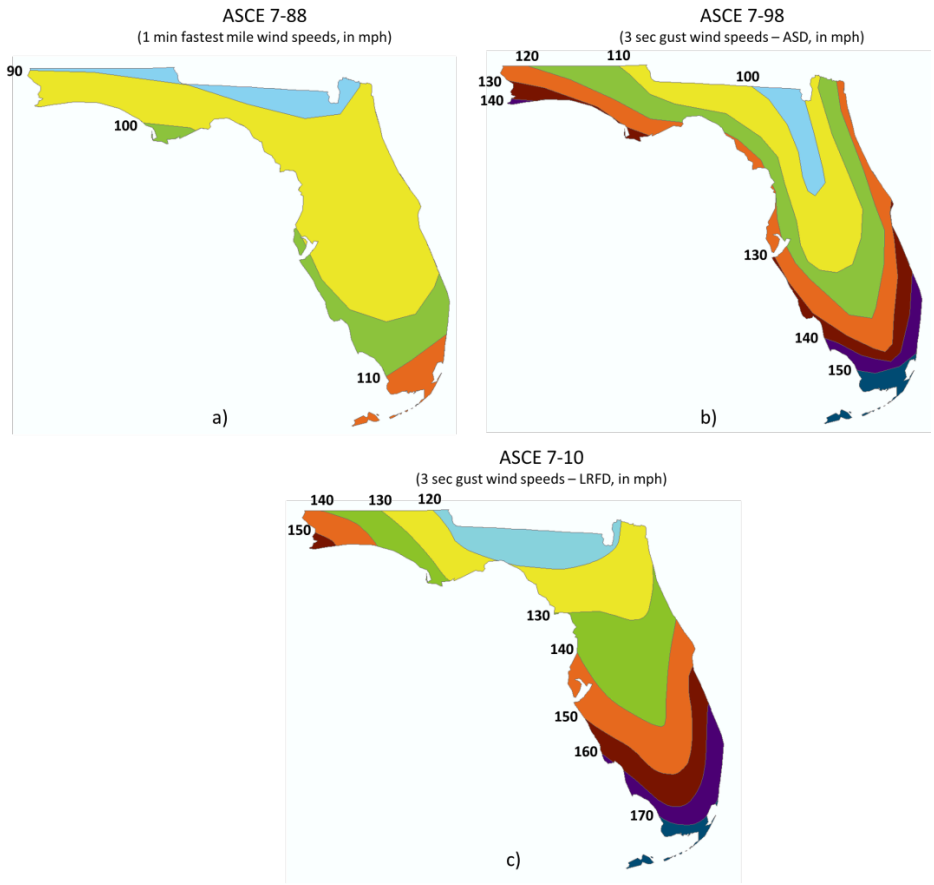

Figure 108. ASCE 7 Design Wind Speed maps with evolving standards
Evolving versions of the ASCE 7 Standard for Risk Category II Structures include: a) ASCE 7-88; b) ASCE 7-98; and c) ASCE 7-10. Note that ASCE 7-16 is not shown because the map did not change significantly between ASCE 7-10 and ASCE 7-16 in Florida.

Building location and local terrain

Two important aspects in building design are the building's location and the local terrain around it. Building vulnerability can vary within a given state due to a building's proximity to the coast or a mountainous area. Thus, building codes include location-varying design wind speed specifications. For example, buildings located in coastal regions are less vulnerable than their inland counterparts because they are designed for higher wind speeds using stronger building components, connections, and mitigation features. States with mountainous areas like Colorado, for example, have different minimum code requirements depending on the building's location. These differing requirements account for terrain effects on the design wind speed. To account for this spatial variability, vulnerability can vary by latitude and longitude in the Verisk model.

Depending on the local terrain around a building, the wind field may be exposed to different turbulent or surface drag effects. The following four broad "Exposure" categories are defined in ASCE 7 to account for these local terrain effects:

- Exposure A: terrain in large city centers

- Exposure B: terrain in urban and suburban areas
- Exposure C: open country and grassland
- Exposure D: areas exposed to wind flowing over open water

Wind speeds are higher where the local terrain is smoother; therefore, structures in Exposure C areas are designed to withstand higher wind speeds than structures in Exposure B areas, for example.

When the Exposure definitions change, the design wind loads change accordingly. These changes impact the vulnerability of structures that were designed using different versions of the building codes and standards. While these Exposure category descriptions themselves have largely remained the same, their applicability has changed with different versions of the code. For example, in the Florida Building Code (FBC), Exposure A was used only in early versions of the code and was removed from the later versions. Exposure D was removed from ASCE 7 in the mid-2000s, and was reintroduced in ASCE 7-10 and in the referencing building codes, i.e., the 2012 ICC codes and the 2010 FBC. State and local building codes may also amend these definitions. The exposure category is rarely delegated by the building codes. Instead, it is typically the responsibility of the design engineer to choose the appropriate exposure category. An exception is in select areas in Florida. In these cases, the Verisk model makes appropriate assumptions consistent with these explicit requirements. In other cases, users may use the "Terrain Roughness" secondary feature to select the appropriate exposure category for the asset being modeled, if this information is available to them.

ICC code adoption

Prior to the adoption of the ICC codes, most building codes referenced ASCE 7-88. The 2000-2009 versions of the ICC building and residential codes reference ASCE 7-98, -02, and -05; these standards all use the same design wind speed map. The 2012 and 2015 ICC building and residential codes reference ASCE 7-10, and the 2018 ICC building codes reference ASCE 7-16.

Significant changes in structural vulnerability are expected when the ICC codes are first adopted by a jurisdiction and again when the 2012 or later versions of the ICC codes are adopted. These significant changes are due to:

- Design wind speed map updates
- Modifications to the minimum structural requirements associated with the changes in the design wind loads. These requirements include changes to nailing schedules, roof anchorage requirements, and material ratings, among other components.

In some areas of South Carolina, for example, the adoption of the 2012 ICC codes resulted in a design wind speed transition from 110 mph to 100 mph. This transition resulted in changes to connections, nailing schedules, and component attachment requirements. For example, the building code may previously have called for a roof covering attachment of screws; after the update to the 2012 ICC codes, nails would be required (Bobby et al. 2017, Kordi et al. 2017).

Year-built bands

In the Verisk Severe Thunderstorm Model for the United States, year-built bands are defined as "bins" that are used to infer the building code that was in effect at a particular time and location and subsequently the minimum code requirements. The years delineating these bands are as follows:

1. **1995**: Stricter building codes came into effect around 1995 as a result of the devastation caused by Hurricanes Hugo (1989) and Andrew (1992), among others.
2. **ICC1**: Denotes the year that the ICC codes were first adopted in a jurisdiction. Specifically, this year refers to the first year that any of the 2000-2009 versions of the code were adopted and is jurisdiction dependent. For example, South Carolina implemented the 2000 version of the ICC codes in 2003, and, therefore, year 2003 is the ICC1 year in South Carolina.
3. **ICC2**: Denotes the year that the 2012 or later version of the ICC codes were first adopted in a jurisdiction. For example, South Carolina implemented the 2012 version of the ICC codes in 2013, and, therefore, the year 2013 is the ICC2 year in South Carolina. New Jersey did not adopt the 2012 version of the ICC codes, but the state adopted the 2015 version in 2015. Therefore, the year 2015 is the ICC2 year for New Jersey.

Using the above delineation logic, the following four year-built bands are implemented in the model to delineate vulnerability due to building code updates:

1. **Pre-1995**: The time period before Hurricane Andrew-era codes were adopted
2. **1995-ICC1**: The time period after the adoption of Hurricane Andrew-era codes but before the ICC codes were adopted
3. **ICC1-ICC2**: The years that any of the 2000-2009 versions of the ICC codes were in effect
4. **Post-ICC2**: The years that the 2012-2018 versions of the ICC codes were in effect

During the development phase of the current U.S. Severe Thunderstorm Model, few areas of the country had adopted the 2018 ICC codes. Specific analyses were performed for those areas to analyze the impact of moving to the 2018 ICC codes. It was determined that for those specific areas, moving to the 2018 ICC codes would not require the addition of a separate year-built band to capture vulnerability differences due to the new code adoption. Therefore, it was reasonable to include the 2018 version of the ICC codes in the "post-ICC2" era. It is also important to note that not all jurisdictions have four distinct bands, depending on whether the ICC codes were adopted. For example, some jurisdictions in Mississippi do not adopt any version of the ICC codes; therefore, these jurisdictions do not have an ICC1 or ICC2 year. Jurisdiction-specific ICC1 and ICC2 years are available in an appendix to this document.

For each jurisdiction and for each of the relevant year-built bands, a "model" building is determined using the building code minimum requirements. It is defined in terms of individual risk features, such as roof covering, roof sheathing, roof-to-wall connection, and opening protection.

The relative vulnerability of different model buildings is assessed based on the impact secondary building features have on the overall building vulnerability. By repeating this

process for all regions in the United States, model buildings are defined for all locations and time periods.

For example, Table 20 and Table 21 show the key structural characteristics of a typical single-family wood-frame home and a typical commercial reinforced-concrete building, respectively, in Wilmington, North Carolina. These structures were built according to the code requirements in place in Wilmington in 1998 and in 2005.

Table 20. Key structural characteristics of non-engineered buildings built according to building codes in Wilmington, North Carolina in 1998 and 2005

Location	Year Built	Roof Covering	Roof Sheathing Nailing	Roof to Wall Connection	Window Protection Required	Gable-end Bracing Requirement
Wilmington, NC	1998	Asphalt Shingles or Equivalent	8d @ 6/12	Clips	None	Yes
	2005	Hurricane wind rated covering	8d @ 6/6	Hurricane Ties	None	Yes

Table 21. Key structural characteristics of engineered buildings built according to code requirements in Wilmington, North Carolina in 1998 and 2005

Location	Year Built	Roof Covering	Wall Siding	Secondary Water Protection	Window Protection Required
Wilmington, NC	1998	Single Ply or Equivalent	Siding with poor resistance to wind	No	None
	2005	Hurricane wind rated covering	Siding with strong resistance to wind	Yes	None

Another example is given in Table 22, which shows the key structural characteristics of a typical single-family wood-frame home in Pensacola, FL. Two year-built values for the structures are shown. The first indicates the code requirements for a structure built in 2002 under the 2001 FBC; the second is for a structure built in 2013 under the 2010 FBC.

Table 22. Key structural characteristics of non-engineered buildings built according to building codes in Pensacola, FL in 2002 and 2013

Location	Year Built	Roof Geometry	Roof Pitch	Roof Covering	Roof Deck	Roof Covering Attach.	Roof Deck Attach.	Roof Anchorage	Window Protection Required
Pensacola, FL	2002	Gable End with Bracing	Medium	Hurricane wind rated covering	Plywood	Nails/ Staples	8d @ 6/6	Structurally Connected	None

Location	Year Built	Roof Geometry	Roof Pitch	Roof Covering	Roof Deck	Roof Covering Attach.	Roof Deck Attach.	Roof Anchorage	Window Protection Required
	2013	Gable End with Bracing	Medium	Hurricane wind rated covering	Plywood	Screws	8d @ 6/12	Anchor Bolts	Engineered Shutters

Likewise, Table 23 shows the key structural characteristics of a typical commercial reinforced-concrete building in Pensacola.

Table 23. Key structural characteristics of engineered buildings built according to code requirements in Pensacola, FL in 2002 and 2013

Location	Year Built	Roof Geometry	Roof Pitch	Roof Covering	Roof Deck	Roof Covering Attach.	Roof Deck Attach.	Roof Anchorage	Window Protection Required
Pensacola, FL	2002	Flat	Low	Hurricane wind rated covering	Reinforced concrete slabs	Screws	Structurally Connected	Structurally Connected	None
	2013	Flat	Low	Hurricane wind rated covering	Reinforced concrete slabs	Screws	Structurally Connected	Structurally Connected	Engineered Shutters

When the year built of the structure is provided, its vulnerability is assessed based on the characteristics of the model buildings. However, if a structure has a particular secondary characteristic that is input into the model, this input will override the default secondary characteristic present in the model. For example, if a structure is built in 2005 in Wilmington, NC, the default window protection assumption is "No Window Protection." However, if the structure has non-engineered shutters, which is input by the user for that exposure, then the "No Window Protection" assumption indicated in Table 20 is overwritten with the "Non-Engineered Shutters" specification input into the model, and the structure's vulnerability is modified accordingly.

The vulnerability of structures is highly dependent on code adoption practices. Also important are code enforcement practices, which may vary considerably across and within states. Generally, code enforcement is more stringent in coastal counties, which have a higher hazard risk. Important, too, are the enforcing department's training resources for inspectors and code officials. Verisk engineers have studied the enforcement practices across the United States through direct conversations with code enforcement officers. This information is supplemented by results of independent studies, including the IBHS code adoption and enforcement survey.[17] Verisk engineers have also worked with teams at Verisk's Insurance Services Office (ISO) to create a more granular view of enforcement than has been previously possible through these internal and external studies. This partnership resulted in the evaluation of jurisdiction-specific code adoption and enforcement data that are collected

[17] Insurance Institute for Business and Home Safety (IBHS), *Rating the States 2015: An Assessment of Residential Building Code and Enforcement Systems for Life Safety and Property Protection in Hurricane-Prone Regions.* IBHS, Tampa, FL, 2015.

across the country through ISO's Building Code Effectiveness Grading Schedule (BCEGS) program. Ultimately, the enforcement-related information behind this dataset was extracted and used to fine-tune Verisk's understanding of enforcement at a county level. Figure 109 is an example of the resulting BCEGS-based relative code enforcement factors for Georgia.

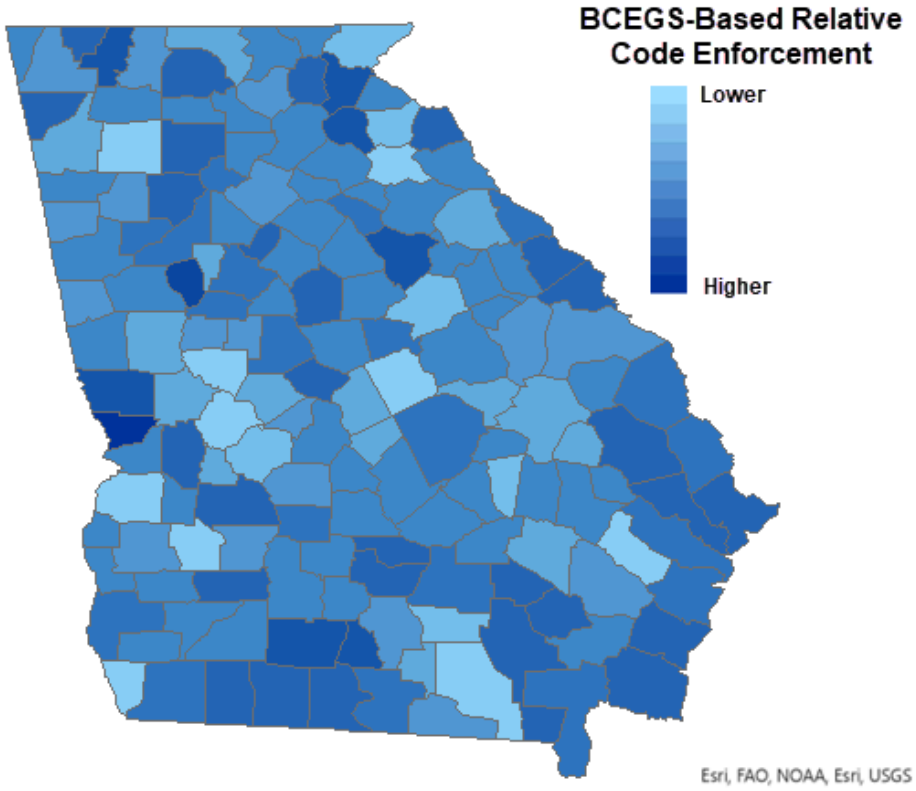

Figure 109. BCEGS-based relative code enforcement factors

See Also
ICC Year Bands

Spatial variability differences for structures with unknown year built

Although generally year built is a well-populated field within exposure books in the United States, it may be the case that users do not know the year built of a structure. When considering the cases presented previously and summarized below, this situation is described by Case 3.

- Case 1: Year built and all SRCs known
- Case 2: Year built known and SRCs unknown
- Case 3: Year built unknown

In this case, the Verisk model develops an age-based weighted average of the vulnerability of applicable model buildings associated with that location using the same vulnerability framework indicated in the previous sections. For each year-built value starting with 1994, a damage function is defined that is consistent with the results of the building code study

at that particular location. Age-based weights are determined for each damage function, where the weight represents the proportion of the buildings built in that year at that location, according to data from the U.S. Census Bureau's American Community Survey. An age-weighted damage function is then developed for that particular risk. Structures built prior to 1994 have similar vulnerability to those constructed in 1994 in Verisk's vulnerability framework. Thus, the weighting factor associated with the 1994 damage function also includes structures built in prior years. The unknown year-built functions are calculated on a 10-km grid resolution.

Damage functions for buildings with unknown primary characteristics

Buildings with unknown characteristics include the 300 and 301 occupancy codes, the 100 and 111 construction codes, the 0-story height code, and all their valid combinations. To model risk vulnerabilities for buildings with these unknown primary characteristics, the Verisk model uses an exposure-weighted average of building damage functions for which these characteristics are known. The weights are computed by considering the relative share of the total insurable value of each class, as reflected in Verisk's 2019 Industry Exposure Database for the contiguous United States. Different damage functions are used depending on how many variables, and which ones, are unknown.

For example, the damage function for a particular exposure of known construction and occupancy but unknown height would be a weighted average of the damage functions, for the same construction and occupancy classes, corresponding to all the different height classes. The damage function for a particular exposure of known occupancy but unknown construction and height, would be a weighted average of the damage functions for the same occupancy class corresponding to all combinations of construction and height classes.

The figures below give several examples of unknown damage functions and how they relate to damage functions describing risks with known primary features. Figure 110 shows a one-story unknown residential damage function for wood-frame buildings and how this relates to one-story wood-frame damage functions for single-family homes, multi-family dwellings, and condos. The unknown residential damage function is very close to the single-family home damage function because the majority of one-story residential risks in the Verisk Industry Exposure Database are single-family homes.

Figure 111 shows a series of damage functions for commercial one-story buildings. These damage functions vary based on construction type. Here, we see that the unknown lies between the known damage functions based on relative Industry Exposure Database weights. Figure 112 illustrates various height damage functions for concrete commercial buildings. Here, we also see that the unknown falls within the known values and lies between a low-rise and a mid-rise structure based on Industry Exposure Database weights.

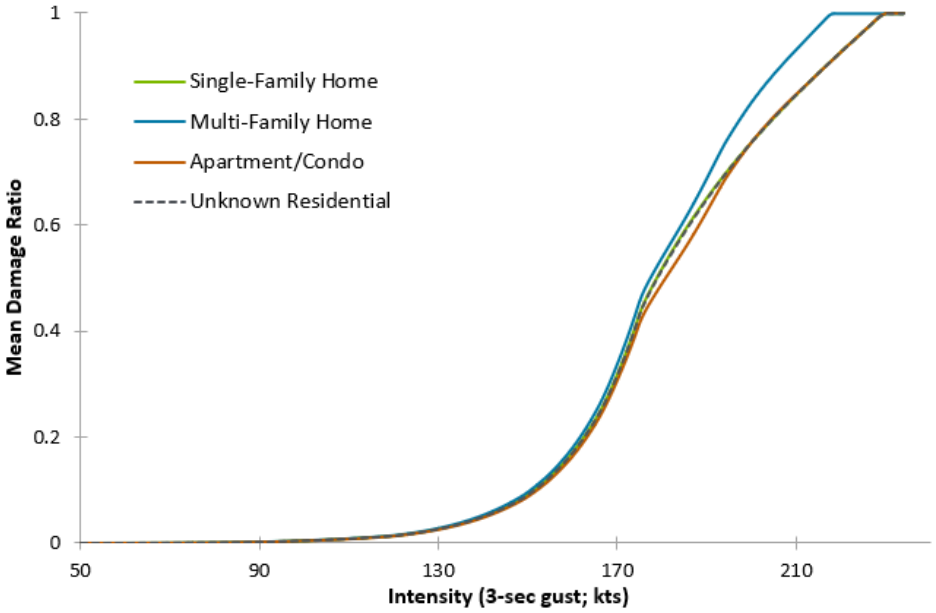

Figure 110. Unknown residential wind damage function shown alongside other residential occupancy wind damage functions, for a one-story wood-frame building

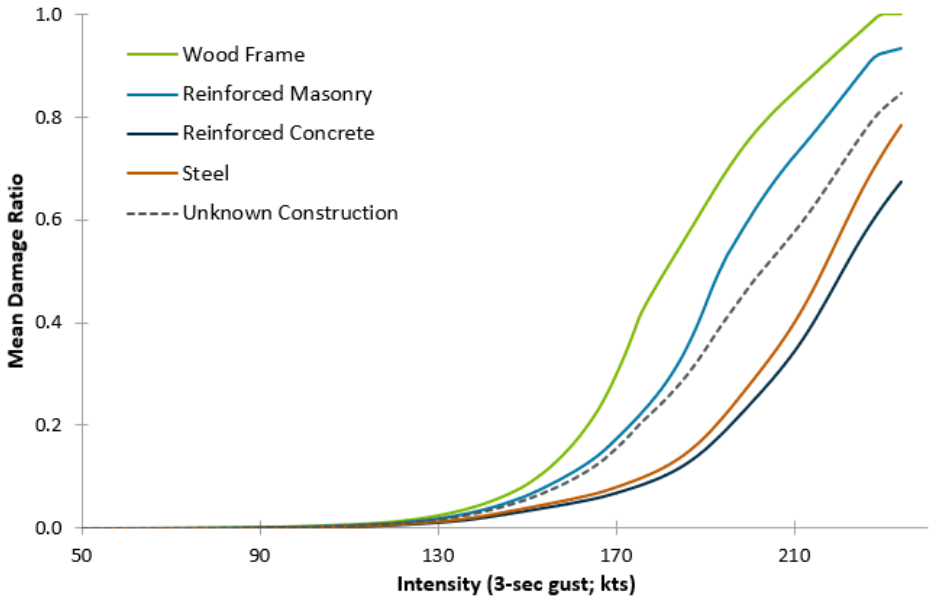

Figure 111. Unknown construction wind damage function shown alongside various other construction wind damage functions, for a one-story general commercial building

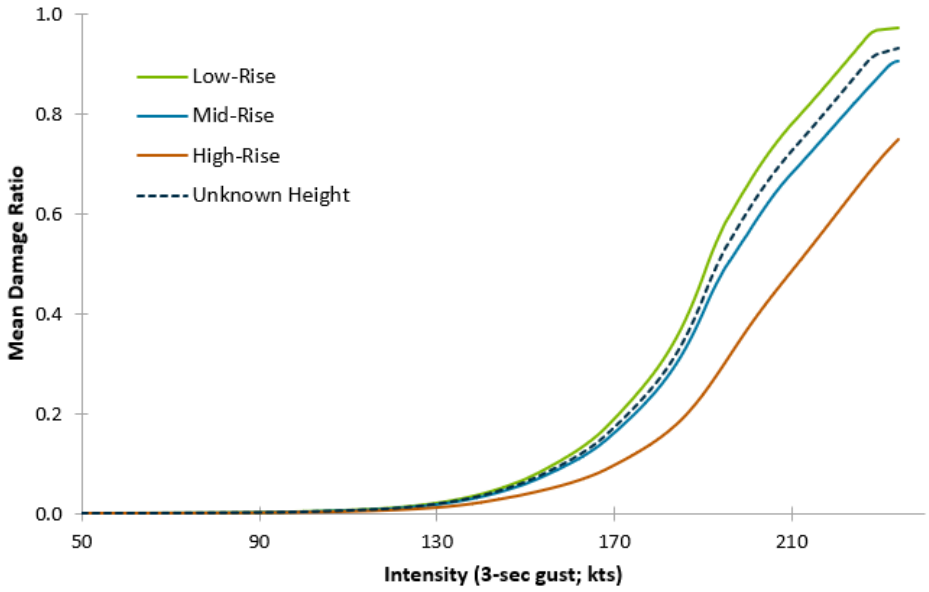

Figure 112. Unknown height wind damage function shown alongside various other height class wind damage functions, for a concrete general commercial building

See Also

Damage functions for unknown characteristics

5.3 Damage functions for manufactured homes

A proper understanding of damage mechanisms and damage progression is key to developing realistic and reliable vulnerability estimates for all buildings, including manufactured homes. The strength of the superstructure, roof, and the envelope of a manufactured home play a critical role in its vulnerability to severe thunderstorms. Damage to manufactured homes can be grouped into two categories: direct damage to the superstructure or to the home itself, and damage due to the failure of the anchorage system.

The high vulnerability of manufactured homes to severe thunderstorms is due not only to their foundation types and installation procedures, but also to their lower design/construction standards making the superstructures weak with respect to hail and, especially, straight-line wind and tornado resistance. When an improperly installed manufactured home experiences strong winds, it is prone to uplift. Uplift can cause the supporting piers to collapse, followed by the superstructure sliding and/or overturning, which results in substantial damage or complete collapse.

The characteristics of manufactured homes differ from other homes in that construction type and height are not considered. For manufactured homes, wind damage functions are determined by the age band, type of tie-downs (full, partial, none, or unknown), and the region. The age band indicates which codes were in effect when the manufactured home was built, which, in turn, dictates the standards set in place for construction and tie-down requirements.

These standards vary regionally based on the HUD-defined wind zones. Tie-downs deteriorate over time due to various environmental factors, which impact their effectiveness.

Regulations governing the design, construction, and installation of manufactured homes have evolved considerably since the passage of HUD's National Manufactured Housing and Construction Safety Standards Act in 1974. The Verisk model explicitly considers the evolution of manufactured home standards in its manufactured home wind vulnerability framework. Specifically, the Verisk model uses age bands that were designed exclusively for manufactured homes: pre-1976, 1976-1994, and post 1994. These age bands were selected based on the evolution of HUD standards. There are two key dates with respect to manufactured home construction regulations: 1976, when HUD code was first enforced; and 1994, when the HUD code was reinforced in the wake of Hurricane Andrew (1992). Prior to 1994, there was no real wind zone delineation regionally, but manufactured homes built after 1994 are required to be designed to one of three specified wind zone standards depending on where the home will be located. Most recently, the HUD installation regulation, 24 CFR 3285 Model Manufactured Home Installation Standards, was issued in October 2007. Today, it serves as a minimum standard for manufactured home design, construction, and installation. States that do not comply with these standards must have substitute regulations that provide protection equal to, or exceeding, those from the aforementioned regulation.

To model the wind vulnerability for manufactured homes with unknown tie-down type and/or year-built, the Verisk model uses a weighted average of manufactured home damage functions for which these characteristics are known. For example, if the type of tie-downs used is unknown, then the model uses a weighted average of the damage functions for each tie-down type, based on the year built. If the year built is unknown, then the model uses a weighted average of damage functions, for the region of interest, for each of the manufactured home age bands, and for each tie-down type. If the type of tie-down is known but the year built is unknown, then the model uses a weighted average of damage functions for different age bands, with the weights determined by the region.

As with traditional building codes, HUD codes for manufactured homes do not specify hail provisions. Although the wind codes do vary based on region, HUD wind codes have little impact on the hail vulnerability of these structures; while tie-down configuration is quite important for wind, it is not relevant for hail resistance. Instead, hail vulnerability of manufactured homes depends on the resistance of envelope components to hail damage. There are no specifications that higher-quality envelope materials be used in hail-prone areas. Therefore, hail vulnerability functions are similar for all types of supported manufactured homes in all regions.

Manufactured homes have some similarities in envelope and roofing materials with traditional building structures. Most manufactured homes have vinyl wall siding, low-sloped roofs, and asphalt shingles. The hail resistance of these materials is similar regardless of whether the material is used for a manufactured home or a single-family home; however, the cost breakdown of building components does differ between the two risk types. Thus, material-related vulnerability information gleaned from the component-based hail vulnerability framework was used in developing damage functions for manufactured homes. The damage functions were then calibrated using industry claims data.

5.4 Damage functions for automobiles

In the Verisk Severe Thunderstorm Model for the United States, automobile damage functions represent the vulnerability of four-wheeled automotive vehicles for passenger and commercial transport. To create and validate separate damage functions for strong winds and hail, Verisk researchers used post-event damage surveys as well as actual loss data. The loss data for both wind and hail implicitly includes different types of damage associated with severe thunderstorm events, such as flying debris, falling trees, and water damage.

Automobile damage from strong winds, including tornadoes, can be caused by flying debris and falling trees. In very severe tornadic winds, the vehicles themselves can be pushed or sometimes even carried aloft a short distance. Tornado damage increases more quickly with increasing wind speed than straight-line winds, due to the greater uplift pressures exerted by tornado winds.

The Verisk automobile damage functions are a composite of two components. The first considers the number of vehicles exposed, including those on the road or in uncovered parking lots, which is a function of time of day. The second component addresses how much damage an exposed vehicle incurs, which is a function of the sub-peril intensity (e.g., maximum wind speed or hail kinetic energy). The automobile damage functions were additionally calibrated using industry loss data. The automobile damage functions implicitly reflect the fact that severe thunderstorm occurrence varies by time of day and tends to peak in the late afternoon during commute hours, when the number of vehicles exposed is relatively high. Figure 113 below is an example of the distribution of hail reports by hour.

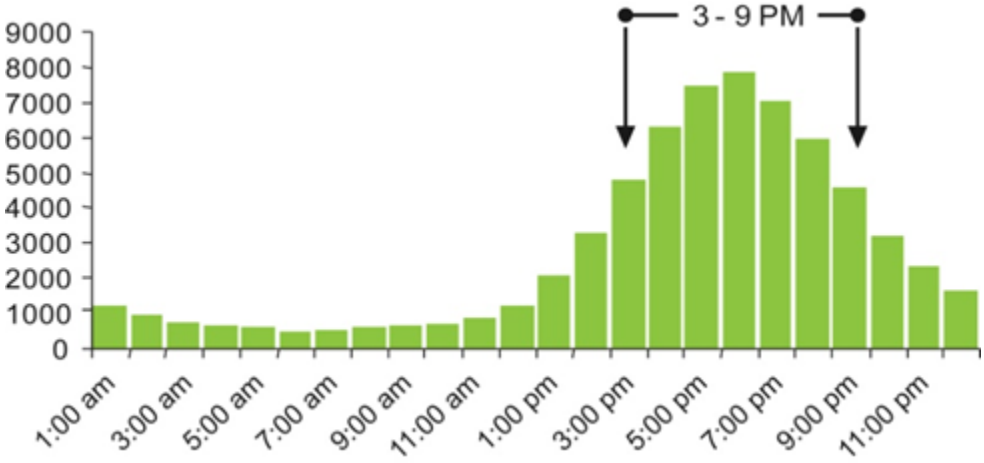

Figure 113. Hailstorm reports by time of day

The model also incorporates two distinct hail damage functions: one for personal automobiles, and one for commercial car dealerships or large open lots that encompass a significant number of vehicles, such as rental car and taxi lots. The car dealership hail damage function specifically recognizes the correlation of damage associated with large numbers of automobiles directly exposed to potential hail damage in a limited area. Figure

114 shows a comparison of hail damage functions for automobiles that are personally owned versus those in car dealerships.

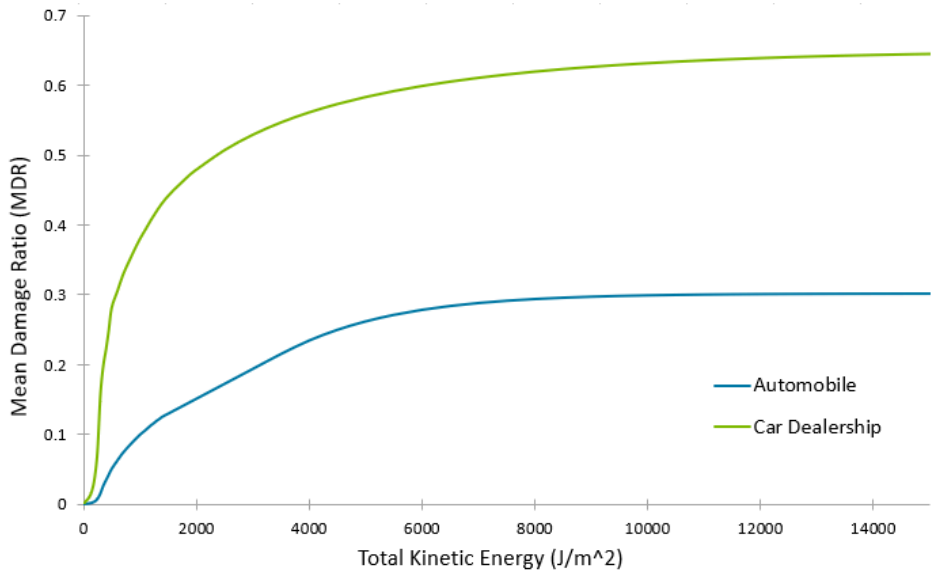

Figure 114. Hail damage functions for automobiles and car dealerships

5.5 Damage functions for specialty risks

Specialty risks are defined as risks that require unique coverage or policies. Although the types of risks that fall within specialty lines will vary based on the (re)insurer, risk types other than the traditional building risks described in previous sections will be detailed in the subsequent sections. These risks include industrial facilities, infrastructure, marine, and agricultural risks.

Estimating damage to large industrial facilities

Verisk employs a component-based approach to evaluate damage and loss to an entire industrial facility. This method accounts for the primary components of an industrial facility as well as their interconnectivity. Primary components have been categorized into classes and sub-classes to account for variations in vulnerability within each component class. Verisk has developed more than 400 damage functions for approximately 550 distinct industrial components and subcomponents.

Figure 115 and Figure 116 provide examples of types of large industrial facilities and industrial facility components.

Figure 115. Examples of large industrial facilities
Top left to lower right: steel mill,[39] wastewater treatment plant,[40] paper mill,[41] hydroelectric power plant,[42] aluminum plant,[43] electric substation,[44] chemical plant,[45] petroleum refinery,[46] and cement plant.[47]

[39] Source: Kobe Steel, Ltd-Kakogawa Works 1172657 by Matsuoka Akiyoshi, CC BY-SA 3.0
[40] Source: Marlborough East Wastewater Treatment Plant Aerial by Nick Allen, CC BY-SA 4.0
[41] Source: Rumford paper mill 2 by Alexius Horatius, CC BY-SA 3.0
[42] Source: Ožbalt Hydroelectric power plant by Josef Moser, CC BY-SA 3.0
[43] Source: Bogoslovsky aluminum plant by Kostya Wiki, CC BY-SA 2.5
[44] Source: MLGW electric substation Person Ave Memphis TN 01 by Thomas Machnitzki, CC BY-SA 3.0
[45] Source: Polymer plant along the Ohio River near the settlement of Apple Grove in Mason County, West Virginia by Carol M. Highsmith, Library of Congress Prints and Photographs Online Catalog
[46] Source: Anacortes Refinery 31911 by Walter Siegmund, CC BY-SA 3.0
[47] Source: Lafarge, ZI Horizon Sud, Frontignan, Hérault 01 by Christian Ferrer, CC BY-SA 3.0

Figure 116. Examples of large industrial facility components
Top left to lower right: buildings,[48] open frame structures,[49] cooling towers,[50] processing towers,[51] distillation towers,[52] flare towers,[53] tanks,[54] conveyors,[55] pipe racks,[56] transformers,[57] high voltage circuit breakers,[58] and transmission towers.[59]

To develop damage functions for an industrial facility, Verisk made assumptions regarding the characteristics of individual components. Aggregated functions based on component and subcomponent damage functions were developed for each industrial facility type. Each component and subcomponent damage function was assigned a weighting factor, based on

[48] Source: Volkswagen factory in Wolfsburg, Germany by Andreas Praefcke, CC BY 3.0
[49] Source: Modular, portable GTL plant outside Houston Texas by Serge Zolotukhin, CC BY-SA 4.0
[50] Source: Industrial cooling towers for a power plant by Cenk Endustri, CC BY-SA 3.0
[51] Source: Petroleum refinery in Anacortes, Washington, United States by Walter Siegmund, CC BY 2.5
[52] Source: A double effect distillation plant by Luigi Chiesa, CC BY 3.0
[53] Source: Gas flare, PetroChina Jabung field, Jambi, Indonesia by Darmawan Kwok, CC BY-SA 4.0
[54] Source: Spherical gas tank farm in the petroleum refinery in Karlsruhe MiRO by Michael Kauffmann, CC BY 2.0
[55] Source: Large sulfur pile at North Vancouver, B.C., Canada, by Leonard G., CC SA 1.0
[56] Source: Pipe rack constructing by Pbujair, CC BY-SA 4.0
[57] Source: Trafostation Alter Hellweg by Rainer Knäpper, CC BY-SA 2.0
[58] Source: Circuit Breaker 115 kV by Wtshymanski, Public Domain
[59] Source: High voltage switchgear at a transmission substation by Dingy, CC BY-SA 3.0

its replacement value relative to the replacement value of the industrial facility, to determine the damage function for the industrial facility as a whole.

This approach provides damage estimates that are transparent, realistic, and consistent for a variety of facilities. Further, the component-based approach is essential for a reliable assessment of business interruption (BI) losses, which depend on numerous interactions between a facility's various components and lifelines.

Hail damage functions

Evaluating hail damage to large industrial facilities is a challenging task due to a lack of historical data and damage studies that specifically address this topic. Therefore, it is not possible to develop hail damage functions based directly on damage data at this time. However, Verisk engineers investigated the vulnerability of large industrial facilities to hail damage on a broad engineering scale by evaluating what types of components are typically present in these facilities and the hail vulnerability of these components.

Large industrial facilities are typically comprised of non-building type structures that have a small percentage of their value in building envelope materials. Most industrial facility components are built from structural steel or metal members and robust materials that are meant to serve a functional purpose. For example, open-frame structures do not have any windows or wall cladding and are primarily comprised of steel beams and columns. Other common components include, but are not limited to, tanks, pipelines, and towers.

Experimental studies provide details on the effect of hailstone impact on structural components like wind turbine blades and aircraft composites for cladding. Although the applicability of these studies is restricted to thin-walled structures operating at high impact speeds, their findings can be used to infer some general behavior of extreme hail loading to similar materials. For example, one study determined that hailstone impact at velocities much higher than those observed in extreme hailstorms cause minimal structural damage, if any, to thin-walled composite materials (Roach and Duvall, 2011). Since most industrial facility components are made from materials that are typically stronger and more robust than thin-walled metal materials and hailstones rarely travel at the velocities simulated in this experimental study, it is likely that industrial facilities as a whole will experience very minor damage, if any, due to hail impact. At most, denting of cladding material may be observed for specific components, such as process towers.

Nevertheless, there are components in an industrial facility that may be susceptible to hail damage. For instance, certain types of industrial plants have electrical and mechanical equipment directly exposed to weather, which may be impacted by hailstones. These exposed light metal components can suffer permanent inelastic deformations that affect their serviceability. The replacement cost of these light metal components in an industrial facility, however, is generally small compared to overall cost of the plant. Some typical buildings may also exist for on-site offices and administrative functions. Although these buildings are more vulnerable than other facility components, they generally contain few aesthetic features. Furthermore, these buildings do not comprise a significant amount of the replacement cost of the facility.

Based on these analyses, it is reasonable to infer that most of the components located in these large industrial facilities have low susceptibility to hail damage. As a result, most industrial facility components, and the facility as a whole, will have low hail vulnerability. Figure 117 shows a comparison of hail damage functions for a commercial steel building (higher relative hail vulnerability) versus a heavy fabrication facility (lower relative hail vulnerability).

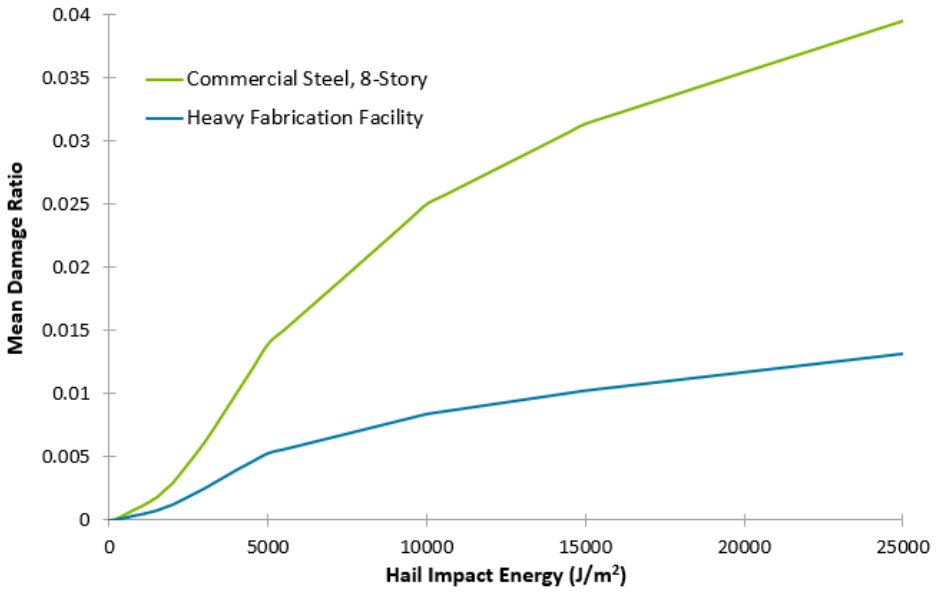

Figure 117. Hail damage function comparison between a commercial steel building (green line) and a heavy fabrication facility (blue line)

See Also

Hail impact energy

Straight-line wind damage functions

Unlike hail, the industrial facilities straight-line wind damage function module incorporates findings from the latest published engineering research and analyses and leverages Verisk's more than 20 years of experience in developing wind damage functions for its commercially-successful Verisk Hurricane Model for the United States. Since multiple damage surveys conducted in the aftermath of severe thunderstorm events showed ample similarities between hurricane and straight-line wind damage,[60] Verisk researchers concluded that the same manner of structural response and damage modes is observed for both sources of wind. Consequently, Verisk engineers estimated wind pressures due to straight-line winds in the same manner that wind pressures are estimated during hurricane events. As a result, damage from straight-line winds is assumed to be similar to that of a hurricane for the same peak wind speed.

[60] http://www.stormtrack.org/library/damage/lessons1.htm

Developing damage functions for an industrial facility

For each industrial facility, aggregated damage functions based on the component and subcomponent damage functions were developed. These component and subcomponent damage functions were then assigned a weighting factor, based on its replacement value relative to the replacement value of the industrial facility, to determine the damage function for the industrial facility as a whole. The weights for different industrial facilities are based on scientific research, the Applied Technology Council report ATC-13,[61] and HAZUS® data.[62]

This approach provides damage estimates that are transparent, realistic, and consistent across a variety of facilities. Furthermore, the component-based approach is also essential for a reliable assessment of BI losses, which depend on the numerous interactions between the various components and lifelines at an industrial facility.

Figure 118 shows straight-line wind damage functions for a sample industrial facility and its components. The facility-level damage function represents a weighted average of the damage functions of the individual components. Weighting factors for each of the components in this example are given in parentheses on the right.

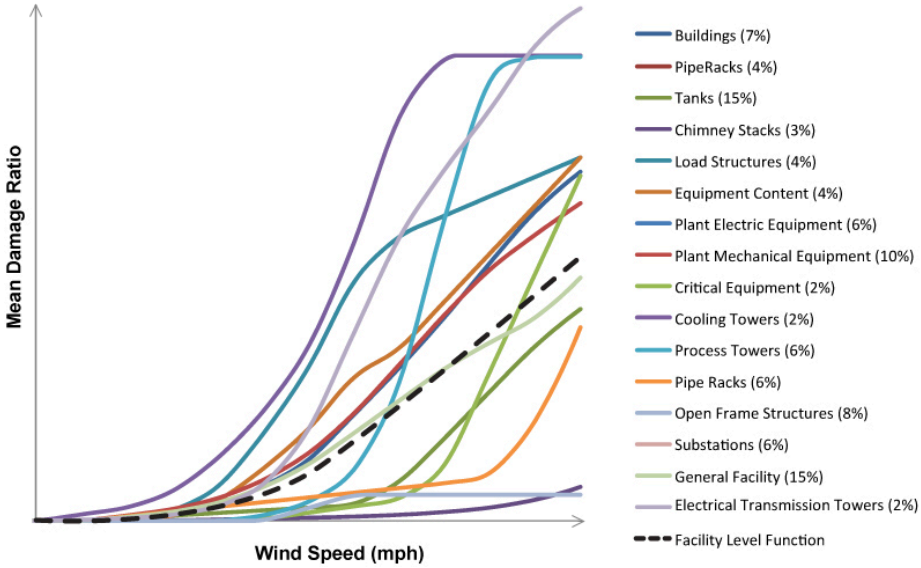

Figure 118. Straight-line wind damage functions for a sample industrial facility

Damage functions for industrial facility components

The Verisk model can be used to estimate damage to over 550 different industrial components and their many associated subcomponents. To develop these damage functions, Verisk researchers conducted thorough analyses of the components commonly found in industrial facilities, such as storage tanks and process towers. They represent actual industrial facilities and were selected from structural drawings, design specifications, and other sources.

[61] https://www.atcouncil.org/pdfs/atc13.pdf
[62] http://www.fema.gov/hazus

The remaining components and subcomponents are implicitly included in the damage estimate based on whether they are generally part of a typical type of industrial facility in a certain area and their relative contribution to the total facility's damage. Major industrial facility components are listed in Table 24.

Table 24. Industrial facility components in the Verisk Severe Thunderstorm Model for the United States

Components of Industrial Facilities		
Air Handling Units	Distribution Panels	Motor-Driven Pumps
Baffles	Electric Power Backup	Open-Frame Structures
Basins	Electric Transmission Towers	Paddles
Battery Chargers	Elevated Pipes	Pipe Racks
Battery Racks	Engine Generators	Pipes and Pipelines
Boiler/Pressure Vessels	Equipment	Potential Transformers
Boilers	Fans	Pressurized Reactors
Buildings	Filter Gallery	Process Towers
Chillers	Flares	Pumps
Chlorination Equipment	Generators	Scrapers
Circuit Breakers	Equipment	Sediment Flocculation Equipment
Commercial Backup Power	Highways/Runways/ Railroads	Silos
Compressors	Large Horizontal Vessels	Stacks/Chimneys
Control Panels	Large Motor-Operated Valves	Switch Gears
Cooling Towers	Large Vertical Vessels with Formed Head	Tanks
Coupling Capacitors	Lightning Arrestors	Transformers
Current Transformers	Loading Structures (Cranes/ Cargo Handling/Conveyor Systems)	Tunnels
Dams	Motor Control Centers	Wells
Disconnect Switches	Large Motor-Operated Valves	Valves

For many industrial facility components, there is insufficient damage data or available research to derive accurate damage functions. In such cases, information from many sources, including historical damage data, scientific literature, site-specific measurements, and structural analyses, was incorporated to assign mean damage ratios over a range of hazard intensities. The resulting damage functions for select industrial facility components are shown in Figure 119.

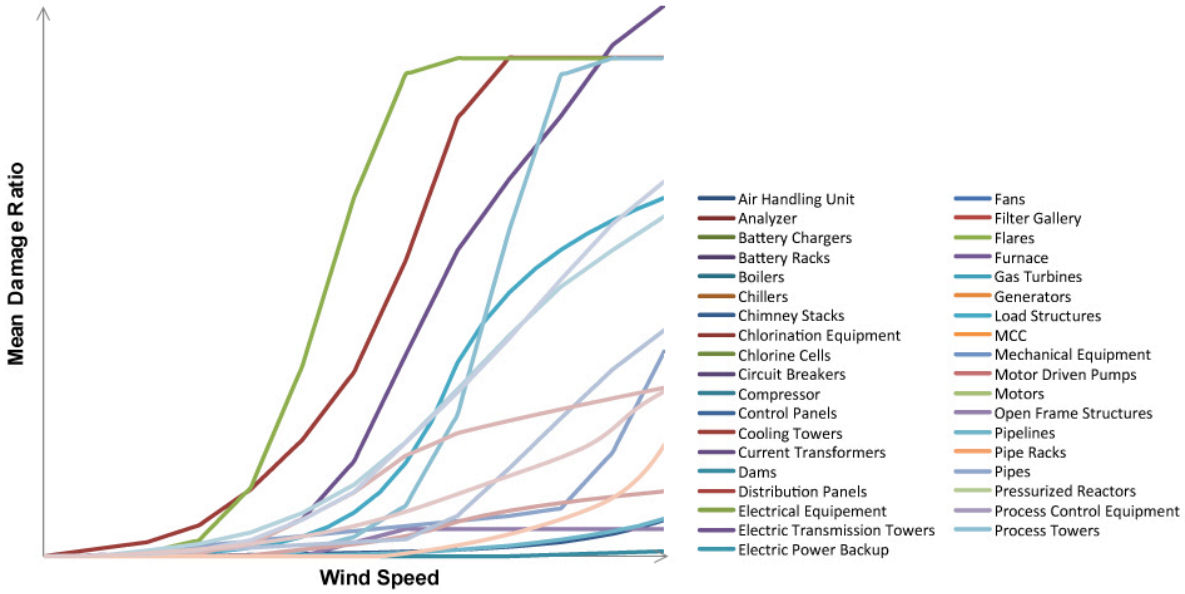

Figure 119. Straight-line wind damage functions for industrial facility components

Note that damage functions for industrial facility components are not applicable to any individual asset at a particular location (e.g., a specific pump or cooling tower). The damage functions have been developed considering a range of characteristics and behaviors within any specific component class or subclass and are intended to represent the average damage ratio for a group of many individual components. Thus, for a given wind speed, the actual damage sustained by some components within a class may be higher or lower than the mean damage ratio specified by the corresponding damage function. This range is due to differences in material properties, wind field patterns, construction quality, building maintenance, and the presence or absence of flying debris.

Storage tanks

Storage tanks are probably the most common components found in industrial facilities. Their vulnerability to wind varies widely depending on the tank's aspect ratio (the ratio of height to diameter), its fill level, and the anchorage at its foundation. Large diameter storage tanks (which have a relatively low aspect ratio), for example, tend to buckle at lower wind speeds than tanks with higher aspect ratios. Tanks with very high aspect ratios, however, can fail by being overturned or moved before their walls begin to buckle. Such tanks, however, are typically anchored at their foundation. Short, squat tanks (those with a lower aspect ratio) are usually not moved by the wind and are usually not anchored.

Verisk engineers undertook a variety of engineering studies in developing damage functions for storage tanks. In one set of tests, structural analytical models of storage tanks were developed using the computer engineering software SAP. Wind pressure distributions (based on the published results of wind tunnel studies) were applied to the models incrementally, thus simulating increasing wind loads. Figure 120 illustrates the distribution of wind pressure

around a tank. The red area indicates the area exposed directly to the wind, where the pressure is highest.

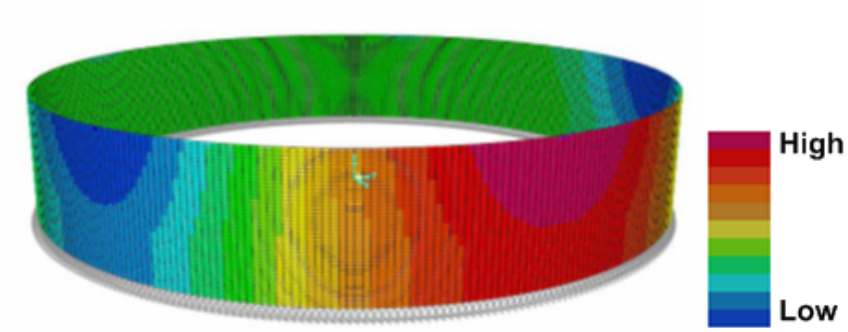

Figure 120. Distribution of wind pressure around a tank wall
Source: Verisk

The loading-factor was raised until elastic buckling developed, indicating a local failure of the tank wall. Figure 121 illustrates the deflection of a tank wall due to elastic buckling, showing a greater amount of buckling where the wall is thinner. Buckling is the primary form of damage seen on shorter tanks because a larger portion of the tank wall becomes damaged as compared to a tall tank. These tests were repeated with the storage tanks modeled to hold three different liquid levels (empty, half-full, and full).

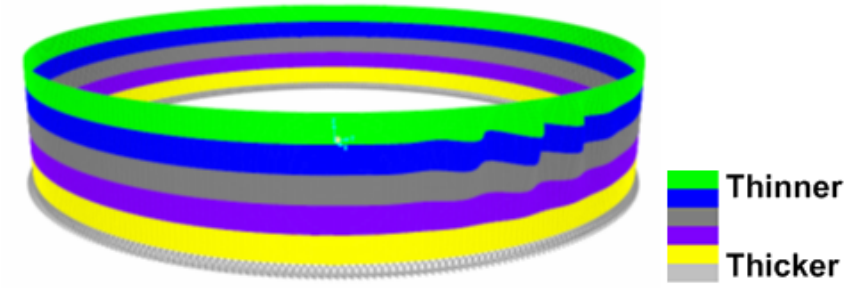

Figure 121. Deflection of tank wall due to elastic buckling at onset of buckling
Source: Verisk

Buoyancy calculations were performed for a range of tank dimensions, assuming an equal probability of liquid level within the tank. This analysis was performed for tanks with and without foundation anchorage. A damage ratio of 50% was assigned to unanchored tanks because it is likely that most floating tanks would experience minimal displacement during a severe thunderstorm and can be reused with minimal repair costs. Anchored tanks were assigned a damage ratio of 75% because anchor failure would likely result in additional repair costs for both the anchor and the tank.

Open-frame structures

Open-frame structures support plant equipment and product-loading mechanisms for both rail and marine transport. They vary in height, size, and bracing, and generally consist of a

combination of welded and bolted steel connections forming open-steel frames, with little or no exterior cladding. An example of an open-frame structure is shown in Figure 122.

Figure 122. Open-frame petrochemical plant
Source: TASNEE 001 by Secl, CC BY 3.0

The wind vulnerability of open-frame structures was evaluated using an analytical model. Wind pressure distributions, based on ASCE 7 guidelines, were used to apply incrementally-increasing wind loads to the structure. Loading was increased until the onset of elastic buckling at a brace member, at which point the structure's lateral load resistance decreased and partial or complete collapse of the structure occurred. The results of the analysis indicate that open-frame structures perform well when subjected to severe thunderstorm winds.

Cooling towers

Cooling towers are designed to release heat produced by industrial processes into the atmosphere. Damage usually starts with the loss of exterior cladding and fan cylinders. Collapse of the tower frame is possible. Unless the damage progresses toward the interior of the tower, the interior cells may remain operational even after an extreme wind event. Smaller portable cooling towers typically sustain less damage than larger ones because they contain less equipment. An example of a cooling tower is provided in Figure 123.

Figure 123. West Ford Flat power plant geothermal cooling tower
Source: West Ford Flat Geothermal Cooling Tower by Rtracey, Public domain

Observations indicate that fan shroud damage is possible at wind speeds between 55 and 100 mph. As wind speeds approach 100 mph, minor to moderate damage to louvers can occur as well as to sidewall cladding, fans and fan cylinders, and shrouds. There may be limited instances of partial or complete collapse of cell frame structures, which would result in the loss of tower functionality. The damage ratio for events with wind speeds between 73 mph and 124 mph is approximately 10-20%. This ratio increases to 20-50% for events with wind speeds exceeding 124 mph, during which louvers, sidewall cladding, fans and fan cylinders, and shrouds will experience moderate to major damage, and additional equipment, such as motors and gearboxes, will also be damaged. Given the lower intensity of straight-line winds produced in severe thunderstorms, fan shroud damage is generally not expected.

Process towers

Process towers are walled steel cylinders bolted to a concrete foundation and insulated for temperature control (Figure 124). Piping and access decks are often attached at various levels of the process tower, which imparts additional wind loading to the structure. Damage at wind speeds of 100 mph or greater is typically limited to the insulation. There are, however, isolated observational accounts of strong winds that cause towers to lean at an angle due to their elongated anchor bolts.

Figure 124. Example of a process tower
Source: Colonne distillazione by Luigi Chiesa, CC BY 3.0

Historical wind damage reports indicate structural damage to process towers is usually associated with anchor-bolt yielding or rupture. Wind pressure, as defined by ASCE 7, was computed for three typical process towers with heights ranging between 80 and 140 ft. In the study, wind pressure was increased incrementally until the first anchor bolt yielded, leading to anchor-bolt elongation and subsequent leaning of the process tower. The wind pressure was further increased until the first anchor bolt ruptured, causing the loss of lateral capacity and ultimate collapse of the process tower.

The damage functions for process towers assume no damage until the first anchor bolt yields and complete damage at the point where the first anchor bolt ruptures. A low-vulnerability damage function, which increases with wind speed, was used to represent damage to insulation and other minor damage associated with flying debris.

Flare towers

Flare towers are tall structures that burn off industrial waste gas. To develop damage functions for flare towers, Verisk engineers analyzed three different types: freestanding, guyed flare, and derrick-supported, as shown in Figure 125.

Figure 125. Examples of flare tower types: freestanding (left), guyed flare (middle), and derrick-supported (right)
Source: Left image: Gas flare, PetroChina Jabung field, Jambi, Indonesia by Darmawan kwok, CC BY-SA 4.0; middle image: Flare, Bayport Industrial District, Harris County, Texas by Jim Evans, CC BY-SA 4.0; and right image: Shell haven flare, by Terryjoyce, CC BY-SA 3.0

Structure failure occurs at wind speeds upwards of 125 mph. The wind damage functions for flare towers incorporate a steep increase in the damage potential beginning with wind speeds at around 55 mph and approaching almost complete damage at wind speeds of 100 mph.

Damage functions for industrial facility types

Figure 126 show wind damage functions for selected industrial facility types in the United States. Damage functions for the unknown (general) facility type are based on the weighted average of the damage functions for different industrial facility types.

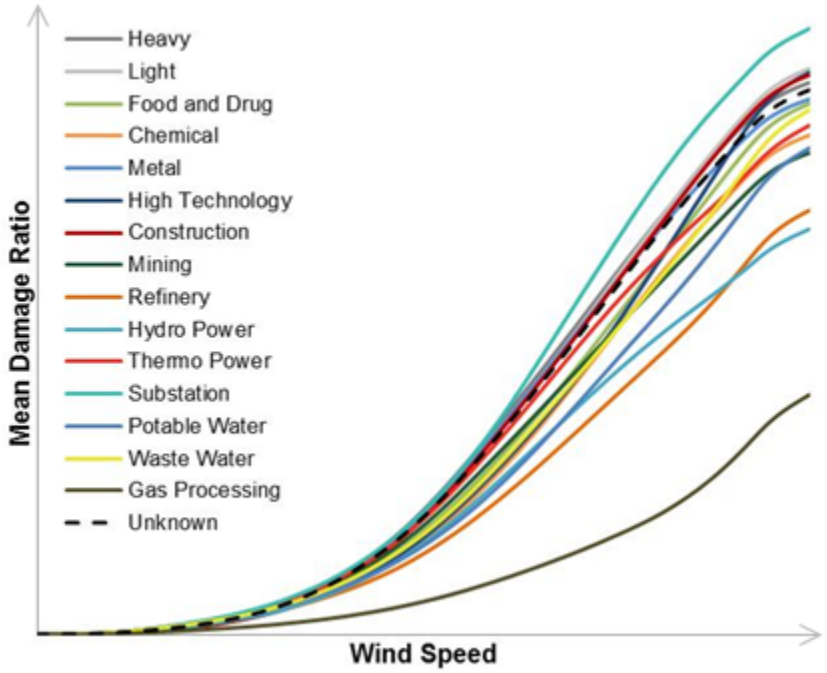

Figure 126. Wind damage functions for different types of industrial facilities

Tornado damage functions

The industrial facility tornado damage functions follow the same component-based approach as the straight-line wind damage functions and leverage Verisk's extensive experience in developing hurricane wind damage functions. Verisk researchers used the hurricane damage functions as a starting point and then developed the damage estimates by accounting for the specific differences in structural response to tornado winds versus hurricane winds.

Based on a review of publicly-available literature, Verisk researchers concluded that there is very little damage data or specific research pertaining to tornado damage to industrial facilities. However, tornado damage can be estimated by extending some of the principles that have been developed for analyzing conventional buildings under tornado wind loading. Thus, Verisk researchers followed a similar methodology as was done for conventional buildings in adapting the component-based wind damage functions from the Verisk Hurricane Model for the United States to develop tornado component-based damage functions.

As is true for conventional buildings, the resultant force on an industrial facility component is always higher in a tornado event as compared to a hurricane event for the same 3-second gust wind speed. Thus, the tornado damage functions are always higher than the hurricane damage functions for any given component. Figure 127 illustrates this difference by comparing the component damage functions of an anchored gas turbine.

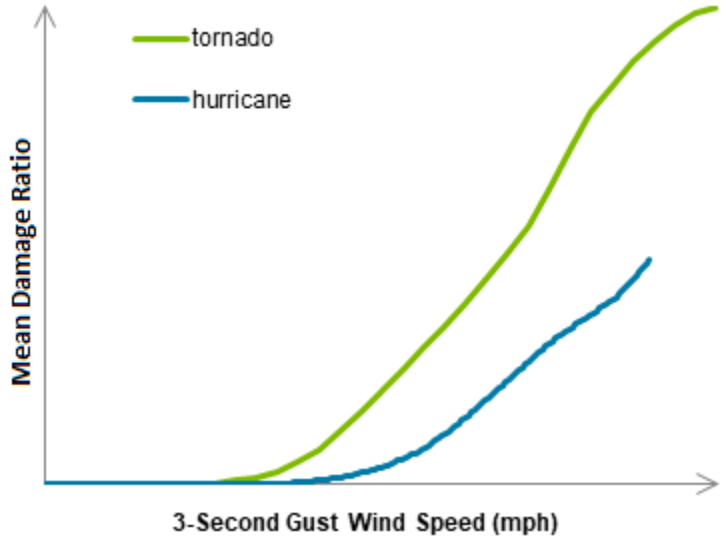

Figure 127. Comparison of tornado and hurricane component damage functions of an anchored gas turbine

See Also

Effects of construction type on straight-line wind and tornado damage

Industrial facility size effect for tornadoes

For large industrial facilities, the width of the tornado may be smaller than the size of the plant. Furthermore, the extent of damage across the entire area of the plant is not uniform. As a result, ignoring the effect of size and applying a uniform damage ratio for all the components in the industrial facility may lead to overestimation of damage due to the tornado.

The size effect can be addressed by applying a reduction factor to the facility-level damage functions. The estimation of the size-effect reduction factors is a 4-step process:

1. Generate a large set of stochastic scenarios representing likely tornado paths.
2. For each track, model the wind field along its path.
3. For each track, obtain the damage to the plant by convolving the damage function with the tornado wind field along the entire path.
4. Estimate the reduction factor by averaging the reduction factor for each of the possible tornado scenarios generated.

This methodology is illustrated in Figure 128.

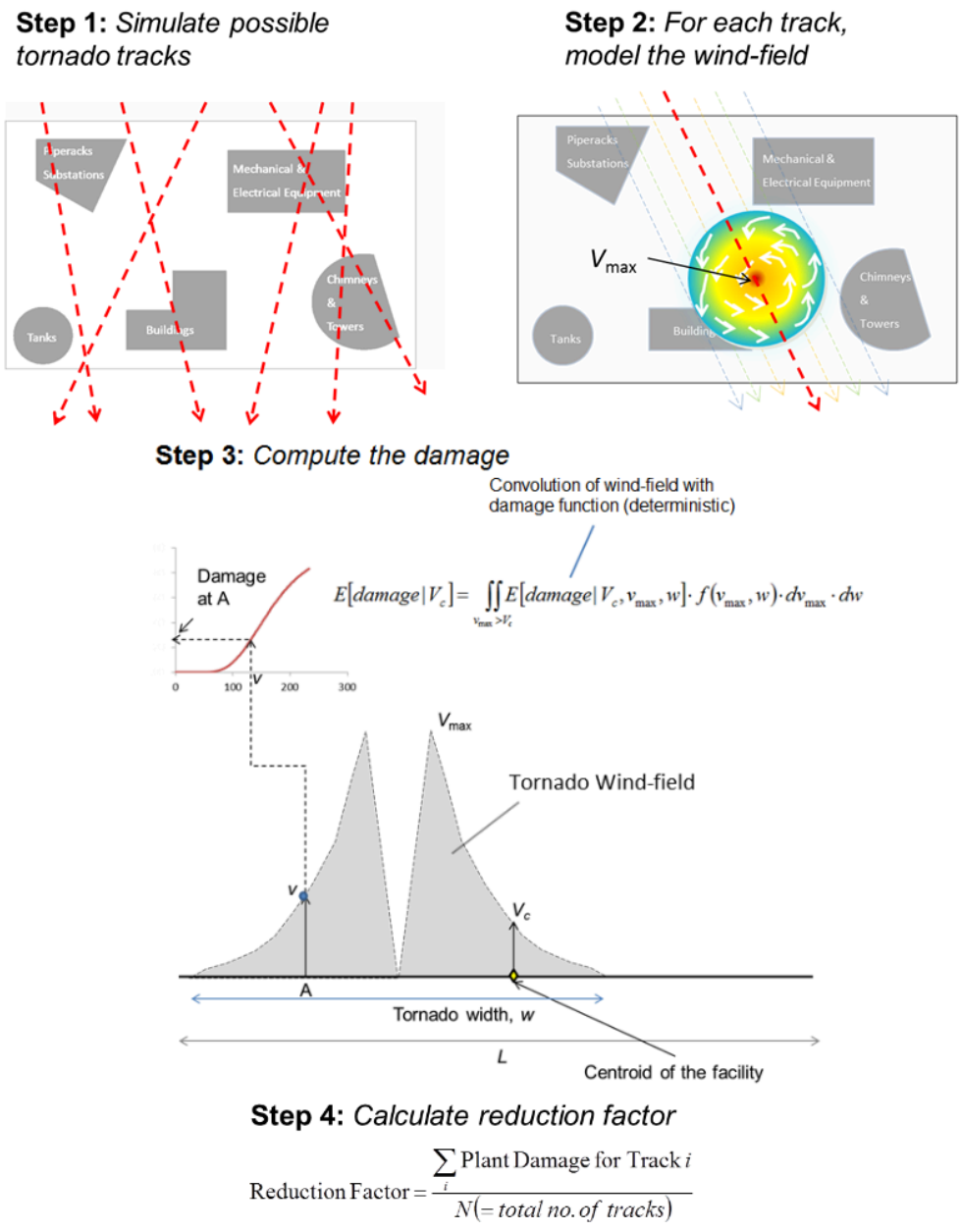

Figure 128. Methodology for calculating the size-effect for large industrial plants
Source: Verisk

Table 25 gives the values of the reduction factor for select industrial facility lengths, L. Figure 129 shows the damage functions of a food processing facility both with and without size effects.

Table 25. Size-effect reduction factors for facility-level tornado damage functions

L (ft)	Size-effect Reduction Factor
0	1

L (ft)	Size-effect Reduction Factor
250	0.7
500	0.6
2,000	0.25

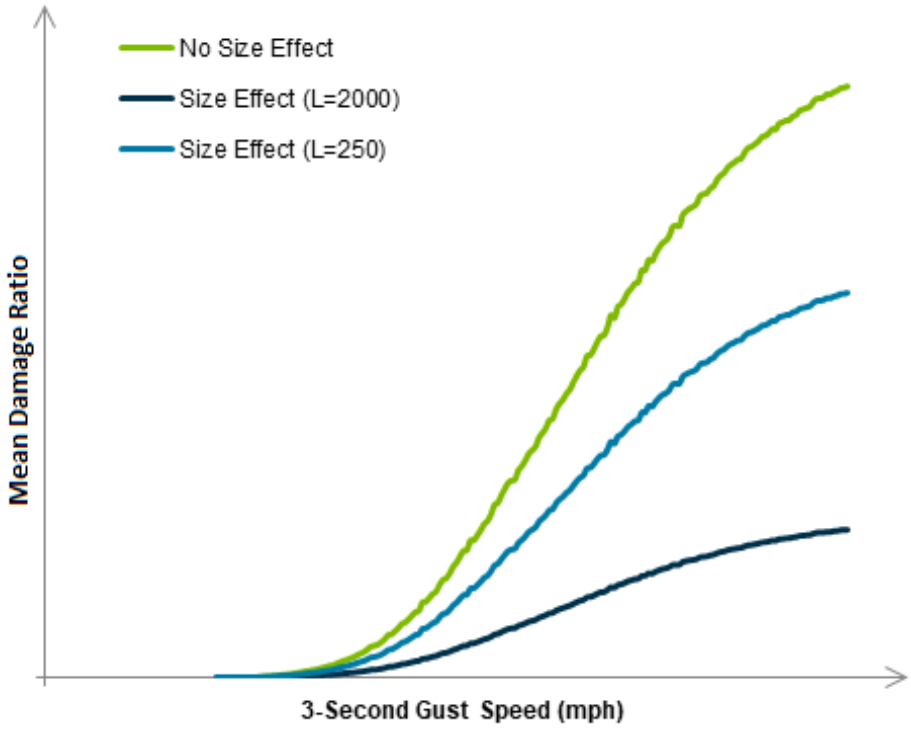

Figure 129. Tornado damage functions of a food processing plant with and without consideration of size-effect

Infrastructure and mechanical/equipment risks

The Verisk Severe Thunderstorm Model for the United States supports damage functions for a wide variety of infrastructure, including, but not limited to, bridges, railroads, dams, chimneys, towers, tunnels, storage tanks, pipelines, and pavement. Several equipment risks are also supported, including cranes, pumping stations, compression stations, and mechanical/electrical/residential equipment. The damage assessments for these risks are challenging because the response to severe thunderstorm hail, straight-line winds, and tornadoes is not universal across all risks. A full list of infrastructure and equipment risks supported by the US Severe Thunderstorm Model is listed in Table 26. Some examples of typical infrastructure risks supported in the model are shown in Figure 130.

Table 26. Infrastructure and equipment risks supported by the Verisk Severe Thunderstorm Model for the United States

• Bridges • Canals • Chimneys • Conveyor Systems • Cranes • Dams • Earth Retaining Structures • Equipment • Pavement	• Pipelines • Pumping and Compression Stations • Railway Property • Storage Tanks • Trains, Trucks, and Airplanes • Towers • Tunnels • Waterfront Structures

Figure 130. Examples of typical types of infrastructure
Top left to lower right: Golden Gate bridge,[72] trees down on roadway,[73] Glen Canyon concrete dam on the Colorado River in Arizona,[74] fuel storage tank,[75] industrial pipeline,[76] industrial chimneys - Big Bend Power Station near Apollo Beach, Florida,[77] tornado-damaged transmission lines,[78] tornado-damaged cell phone tower,[79] and computer servers.[80] Images cropped by Verisk.

Infrastructure and equipment risks generally experience low damage due to hail. Hail damage to infrastructure risks is particularly minimal because infrastructure are composed primarily of structural components made of robust materials. For example, bridge decks, bridge

[72] Source: GoldenGateBridge-001 by Rich Niewiroski, Jr., CC BY 2.5
[73] Source: Birmingham tornado 2005 damage by User Oosoom on en.wikipedia, CC BY-SA 3.0
[74] Source: Glen canyon dam by Agunther, CC BY 3.0
[75] Source: Fuel tank gnangarra by Gnangarra, CC BY 2.5 AU
[76] Source: Ammiakoprovod NS by Антон Оболенский (Azh7), CC BY-SA 2.5
[77] Source: Big Bend Power Station by Wknight94, CC BY-SA 3.0
[78] Source: Crumpled transmission towers after 2011-04-27 tornado IMG 0952 by Samt2565393, CC0 1.0
[79] Source: PlainviewTXEF2 by NWS Lubbock, TX, Public domain
[80] Source: IBM Blue Gene P supercomputer by Argonne National Laboratory's Flickr page, CC BY-SA 2.0

piers, and dams are not expected to sustain hail damage. However, damage can occur to nonstructural components, including lighting and signage. These nonstructural components generally comprise a small portion of the replacement value for these risks; therefore, damage is expected to be low. Historically, there have been few reports of hail damage to storage tanks and towers. However, it is possible for hail to damage equipment attached to towers. In addition, the uncovered mechanical elements of conveyor systems and pumping and compression stations may experience some damage from hail.

While straight-line wind can cause damage to infrastructure and mechanical risks, it will primarily cause damage to non-structural components (e.g., signage and lighting) of well-engineered risks (e.g., bridges, roadways, and dams). Tornadoes are generally more destructive than straight-line wind. Storage tanks, pipelines, and towers may experience moderate to significant damage from wind and tornadoes, especially for higher-speed winds. Severe winds may cause elevated tanks and elevated pipelines to fail. Towers, such as electrical transmission and broadcast towers, are quite vulnerable to both tornadoes and straight-line winds. In extreme cases, high winds may cause towers to collapse.

Marine risks

The marine line of business comprises a heterogeneous mix of products and assets. It includes assets transported over water (also known as "ocean-going cargo") and land (via truck or train) as well as warehoused assets (typically referred to as "inland transit"). Marine hull and pleasure boats are also included in the marine line of business. Marine assets are typically mobile and/or change in value over time.

The Verisk Severe Thunderstorm Model for the United States explicitly models damage estimation due to wind and hail for marine assets, including:

- Pleasure boats and yachts (construction codes 365-367)
- Marine cargo (construction codes 270-276)
- Inland transit/transit warehouse cargo (construction code 259)
- Marine hull (construction code 260)

There is no spatial variation in vulnerability for marine assets. There is temporal variation in vulnerability for pleasure boats and yachts (for straight-line wind and tornado only) but not for marine cargo, inland transit, or marine hull.

Pleasure boats and yachts

Damage to pleasure boats and yachts is a function of wind speed and hailstone intensity. Damage from high winds can affect components on a boat or force the boat to break loose from its moorings. Airborne debris and hailstones can also damage boats. Boats that become undocked and are blown by the wind can collide with anything in their erratic path, including other marine craft, docks, pilings, or the ground. These collisions can damage many components of the boat, including the hull, which increases the possibility of sinking.

The pleasure boats and yachts marine risk classification is divided into two main categories: motorboats and sailboats. The type, size, and age of a boat all affect its vulnerability. In terms of boat type, the Verisk model includes damage functions for sail- and motor-powered

pleasure boats and yachts, as well as for those whose source of power is unknown. Different style boats contain distinct components that are vulnerable to damage. For example, sailboats (Figure 131) have additional components (i.e., sails, masts, and riggings) as compared to power boats. The addition of these extra components means not only do sailboats have more components at risk of severe thunderstorm damage, but also these components increase the force of intense winds on the overall boat structure, further increasing the boat's vulnerability compared to power boats. While smaller boats are easier to trailer and remove from the water before a storm strikes, they tend to suffer more damage than larger boats when left in place. Larger boats are more likely to be under the care of a dedicated crew with a reliable procedure for securing the craft. Boat owners also tend to invest more time and effort towards protecting newer boats. The amount of wear and tear on a boat increases with age due to exposure to the elements as well as prolonged use.

Figure 131. Sailboat
Source: A Nash 26 sailboat named *Namaste* by Ahunt, CC0 BY-SA 1.0

Boat damage can be mitigated by transporting these vehicles out of the water and into dry stack storage, or by moving them to inland water areas, such as canals. Another mitigation technique is to moor boats to a floating dock. Floating docks change height along with the boat in high waves, decreasing the likelihood of boats being torn from their moorings. The effects of mitigation are implicitly captured in the model to the extent that such practices are represented in the actual reported losses used for validation purposes.

Marine cargo assets

Marine cargo assets are classified using occupancy code 354 (Sea and Inland Waterways), which is the supported code for ocean-going cargo assets. Two supported marine cargo assets are shipping containers and dry bulk material and are shown in Figure 132. The complete list of supported construction codes is described in Table 27.

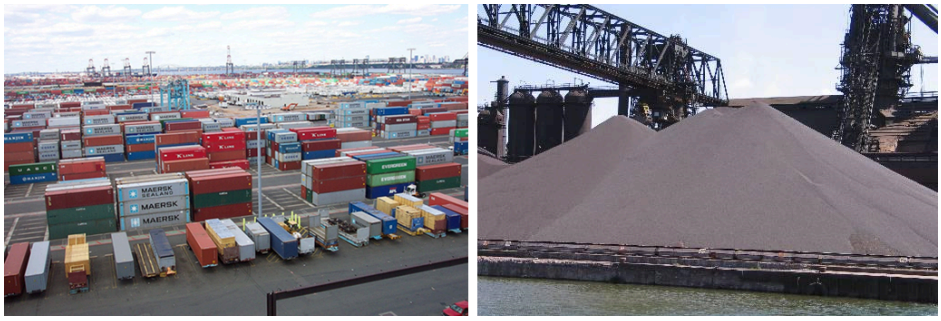

Figure 132. Shipping containers (left) and dry bulk (right) marine cargo
Source: Left image: Shipping Containers at the terminal at Port Elizabeth, New Jersey - NOAA by Captain Albert E. Theberge, NOAA Corps (ret.), Public domain; and right image: Iron ore pellets by Lars lentz, CC0 BY-SA 1.0

Table 27. Construction codes for supported marine cargo assets

Construction Code	Category and Description
270	Carpool: Cars parked in open areas near harbors before shipment in car containers.
271	Cargo Containers (General and Refrigerated): Used to transport freight (including electronic equipment) on ships. The containers are approximately 20-40 ft long by 8 ft wide by 8 ft high.
272	Heavy Cargo: Oversized items and machinery that are too large to fit into general cargo containers (e.g., construction machinery, harbor equipment, luxury yachts). Heavy-lift ships, barge tows, and dock ships typically transport heavy cargo.
273	Refrigerated Cargo: Cargo shipped in containers that have additional electrical equipment to keep the cargo cool.
274	Dry Bulk Cargo: Grains and solid materials, such as coal, metal ore, and lumber, that are stored on the ground in an open yard.
275	Liquid Bulk Cargo: Oil, liquid natural gas, and liquid chemicals that are stored in onshore tanks.
276	General/Unknown

Damage functions for marine cargo assets include physical damage to cargo and related liabilities while the cargo is in transit by sea and for up to 60 days while the cargo is in storage. The asset location is typically the location at the port, the territory in which the insured resides, or where its business establishment is located. The replacement value of the ocean-going cargo is classified as Coverage A. Enter the asset location as the location at the port (preferred) or the business location of the insured. Enter the exposure value into the software as the daily exposure.

Damage to marine cargo risks largely depends on the type of cargo that is being represented as well as the sub-peril damaging the risk. For example, containerized cargo is largely protected from hail; therefore, it is expected that hail damage is minimal to containerized risks. However, carpool is particularly susceptible to hail damage. Large hailstones may dent the vehicles and break glass, resulting in unsellable vehicles.

Wind and tornado damage to marine cargo risks also depends largely on the risk type. High winds may cause stacked containers to fall, which would damage the cargo inside. Refrigerated containers may also lose power, resulting in the spoilage of contents. Finally, wind-borne debris may cause damage to risks that are not stored in containers, including heavy cargo and carpool among others.

Inland transit assets

Inland transit cargo assets are assets that are in transport or in transit warehouses waiting to be distributed (Figure 133). Inland transit cargo are generally stored in warehouses or other facilities that are further from the ocean than ports. Warehouses are generally very susceptible to wind damage due to their long spans and large doors, which can easily be damaged by large uplift and suction forces. Once the building envelope is breached, hailstones and heavy precipitation can cause significant damage to the cargo in the warehouse.

Figure 133. Cargo inside a warehouse
Source: Allentown Project 042, CC BY-SA 3.0

The Verisk model includes damage functions for marine cargo stored in warehouses as well as the warehouses themselves. Cargo in transport on vehicles outside of the warehouse are not included. The supported occupancy codes for these inland transit warehouse assets (construction code = 259) are listed in Table 28.

Table 28. Occupancy codes for supported inland transit assets

Occupancy Code	Category
300	Unknown
313	Wholesale
322	Heavy Fabrication

Occupancy Code	Category
323	Light Fabrication
324	Food and Drug
325	Chemical Processing
327	High Technology

The inland transit asset that is being modeled is the cargo stored inside the warehouse. When in a warehouse, the damage to the cargo is dependent on the level of protection the warehouse provides. Thus, the inland transit assets are modeled as content and should be entered under Coverage C. The vulnerability of the contents further varies based on the content itself. For example, food and drug or chemical inland transit assets are modeled as more vulnerable than heavy fabrication assets due to the vulnerability difference of the asset. While hail damage is generally to the envelope of the warehouse structure, breaches in the envelope can cause water intrusion during the event, which can damage the contents in the warehouse. Warehouses are also susceptible to wind damage due to their long spans and large doors, which can easily be damaged by large uplift and suction forces. If the structure is heavily damaged, precipitation may be able to enter the building, and if there is significant roof damage, portions of the roof may become unstable and cause damage to the contents below. Therefore, the model appropriately considers the protection that is provided by the warehouse at lower hazard intensities, as well as the potential increased damage that could occur to the inland transit warehouse at higher hazard intensities due to damage of the housing structure. The replacement value for the warehouse itself is Coverage A and need not be entered for the contents damage to be calculated.

Marine hull assets

The marine hull line of business includes the hull of a ship, which is the structure of the vessel, and the vessel machinery. It does not include the cargo that the vessel is carrying. Vessel machinery is equipment that generates the power to move the vessel and control the vessel's lighting and temperature system, including the boiler, engine, cooler, and electricity generator. In the Verisk Severe Thunderstorm Model for the United States, this asset can be modeled whether the vessel is at port, at a shipyard undergoing regular maintenance and/or repair, or at a shipyard under construction (Figure 134, Figure 135, and Figure 136, respectively).

Figure 134. Marine hull at port, New Orleans, Louisiana
Source: MSC Marina docked at Port of New Orleans by Gnovick at English Wikipedia, CC BY 3.0

Marine hull assets are generally constructed with robust materials. Therefore, it is expected that hail damage is generally low, though larger hailstones may cause some damage to the vessel. Wind damage to marine hull assets at port is primarily caused by collision with other ships, a barge, a dock, or a pier. The marine hull at port asset generally has a higher hail and wind vulnerability compared to marine hull at a shipyard, due to the unprotected nature of exposure.

Figure 135. Marine hull at a shipyard, under repair
Source: USS Tripoli (LPH-10) drydocked, 1991 by JO2 Hatzakos, Public domain

Damage to the marine hull asset under repair at a shipyard is typically caused by collision with the dock or pier. The marine hull at shipyard while under repair asset has a generally

lower vulnerability due to the protected nature of exposure (in drydock) as compared to marine hull on a berth.

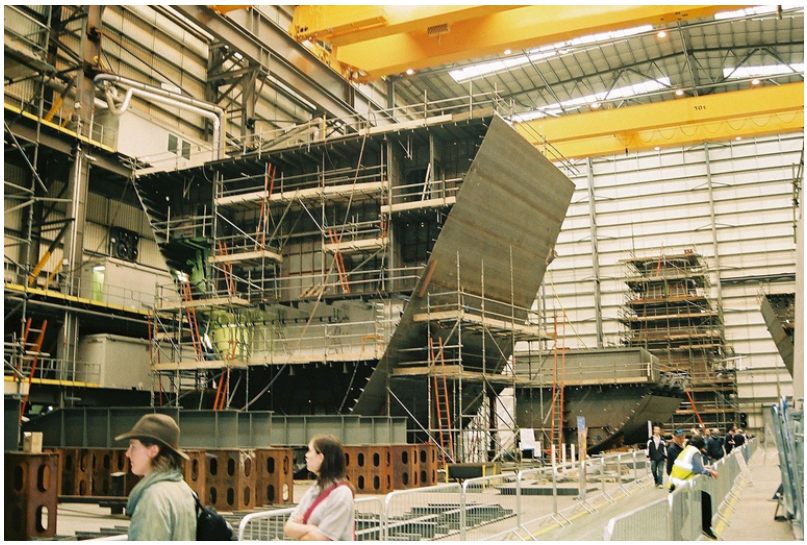

Figure 136. Marine hull at a shipyard, under construction
Source: HMS Dauntless D33 by Steel city ady at English Wikipedia, Public domain

The marine hull at a shipyard while under construction has a similar damage mechanism to the marine hull under repair. The value and vulnerability of the marine hull under construction risk changes throughout the construction process. On an annual basis, the vulnerability of the marine hull under construction asset is lower than marine hull under repair asset because the value of the marine hull is much lower during construction. The insured value is the contract price, or the estimated completed value of the vessel, if there is no contract price. The period of insurance is from the time of the start of construction to the time of vessel delivery.

The supported occupancy codes for these marine hull assets (construction code = 260) are listed in Table 29.

Table 29. Occupancy codes for supported transit marine hull assets

Occupancy Code	Category
300	Unknown
314	Marine Hull at Repair
354	Marine Hull at Port
381	Marine Hull Under Construction

The replacement value of the vessel and its machinery is classified as Coverage A. Enter the exposure value at the time of the event into the software in terms of the average daily exposure. For marine hull under construction (occupancy code 381), use the total replacement value.

Greenhouses

The greenhouse occupancy class includes buildings on farms, orchards, and nurseries that are primarily used in the production of crops, plants, vines, and trees (excluding forestry operations).

There are three main types of covering for greenhouses:

- Glass
- Rigid plastic sheets
- Plastic films

Glass has been the typical standard cladding for greenhouses. Annealed glass is brittle and relatively vulnerable, while tempered glass is 3 to 5 times stronger and costs approximately twice as much. Figure 137 is an example of glass greenhouses, and Figure 138 shows the inside of a typical glass greenhouse.

Figure 137. Glass greenhouses
Source: Westland kassen.jpg by Quistnix, CC BY 1.0

Figure 138. Inside of a glass greenhouse
Source: Botanischer Garten BS.Seerosen.jpg by Mattes, Public domain

Rigid plastic sheets can be durable, depending on the material used. Most are constructed as double walls using common materials like polyvinylchloride (PVC), glass reinforced polyester (GRP), polymethylmethacrylate (PMMA), and polycarbonate (PC).

Plastic films are much more vulnerable than the other two types of greenhouse coverings. Plastic films are commonly made of low-density polyethylene (PE; e.g., PE with UV-stabilization and PE-infrared films), ethylene-vinyl acetate (EVA), and PVC films. Figure 139 is an example of a plastic film greenhouse.

Figure 139. Plastic film greenhouse
Source: Greenhouse New Zealand by Eric T. Gunther, cropped by Verisk, CC BY-SA 3.0

Due to their large glass or plastic content, greenhouses are generally quite vulnerable to fierce winds and impact from flying debris and hailstones. Greenhouse covering failure is

the most prevalent type of damage from severe thunderstorms. These buildings have a large roof area, but their high glass content leaves the entire building more vulnerable to damage, unlike other buildings where roof damage is the most prevalent. Greenhouses can collapse completely, particularly those that have wood frames; and therefore, the contents are particularly vulnerable and are also supported in the Verisk model. Non-crop contents may include heating systems, lighting fixtures, watering systems and supplies, furniture, and other items.

Wind turbines

Wind turbines convert wind kinetic energy into electrical energy, providing a renewable energy resource. Wind turbines are installed individually and in groups, called wind farms, and can be located either onshore or offshore. Most currently operating turbines are installed onshore. Offshore wind farms, however, are becoming more popular for several reasons. Wind speeds are higher offshore due to lower surface roughness, which means increased energy-producing potential. Additionally, offshore wind farms have lower visual impact, making it possible to install larger and more effective wind turbines with greater acceptance from the local community.

Wind turbine systems include a tower, hub, and blades (which together comprise the rotor), and a nacelle (which houses the generator), as shown in Figure 140. They are typically attached to a reinforced concrete foundation. Based on the wind characteristics of the site (e.g., average annual wind speed and turbulence intensity), these structures are generally designed to conform to the International Electrotechnical Commission (IEC) 61400-1 wind turbine design class.

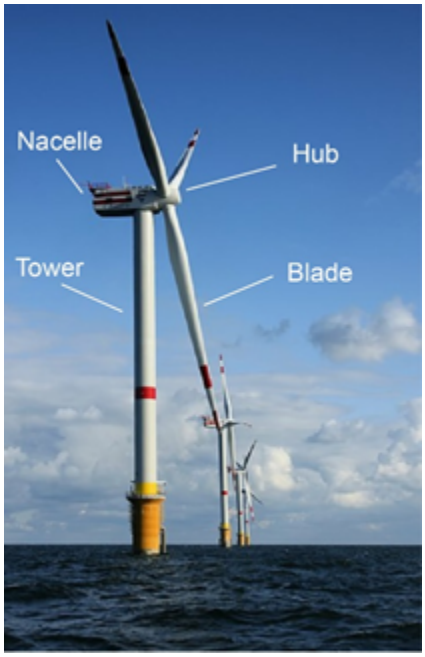

Figure 140. Wind turbine components
Source: Windmills D1-D4 (Thornton Bank) by Hans Hillewaert, labeled by Verisk, CC BY-SA 4.0

There are very few wind turbine damage reports and almost no claims data available in either the United States or in other parts of the world. This lack of data presented Verisk researchers with a serious modeling challenge. For a variety of reasons, including much uncertainty about control systems and damage criteria, Verisk researchers chose to use a statistical analysis approach and collected damage data from historical events and calculated damage ratios based on cost analysis.

Figure 141 and Figure 142 show the wind turbine component cost distribution and the cost breakdown of both onshore and offshore wind turbines, respectively. Careful searches of news, reports, and papers resulted in over 30 onshore wind farm damage records across the world, including wind speed, damage type, and turbine type. Damage functions were derived based on statistical analysis of these data while accounting for uncertainty in hazard and site distribution.

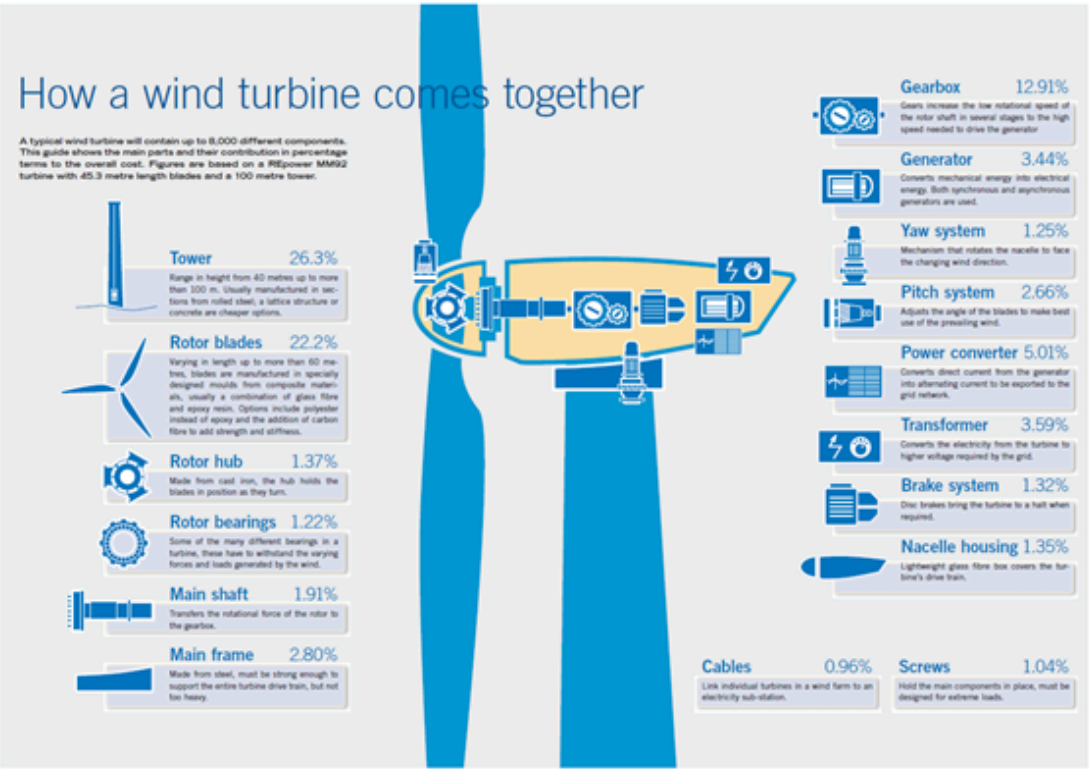

Figure 141. Main components of a 5-MW wind turbine and their share to the total overall turbine cost
Source: EWEA, 2007 in IRENA, 2012 - Economics of Wind Energy Report

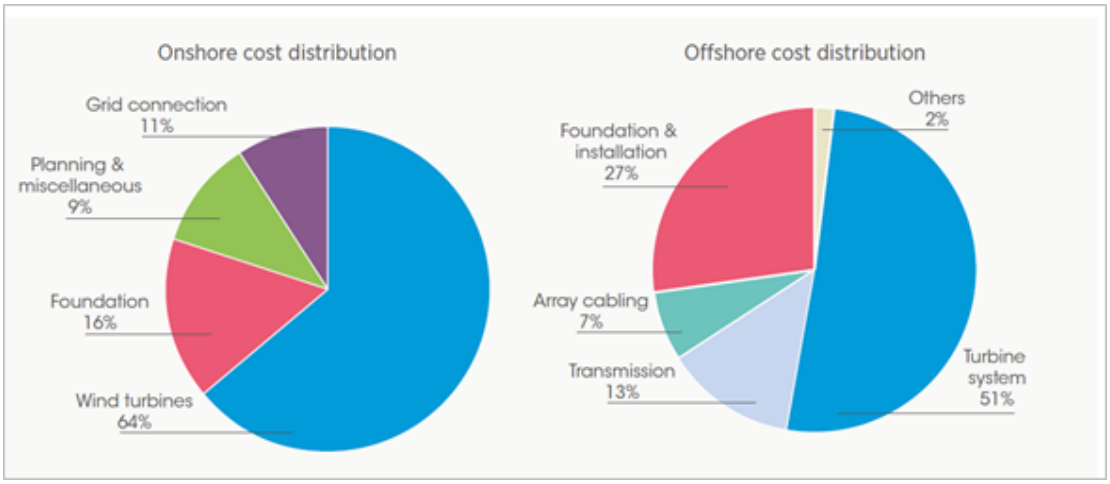

Figure 142. Capital cost breakdowns for typical onshore and offshore wind systems
Source: Blanco, 2009 in IRENA, 2012

While both onshore and offshore wind turbines are designed according to International Electrotechnical Commission (IEC) 61400-1 wind turbine design requirements, there are a few differences between the two. Offshore turbines are subjected to less turbulence from wind, primarily due to their open water exposure. Wave load, which depends on wind speed and the ocean bathymetry, is a more important consideration in the design of offshore turbines than for onshore turbines. In addition, the cost contribution of the turbines and tower to the total cost of offshore turbines is higher than for its onshore counterpart. In accordance with these differences, damage functions for offshore wind turbines have been created that account for the lower turbulence and higher wave loads that these turbines endure.

Primary hail damage to wind turbines involves turbine blade and nacelle damage and includes:

- Surface erosion
- Failure in the substrate for high impact hits
- Delamination between plies
- Cracking through matrix material
- Crushing of reinforcing fiber

This damage is typically relatively minor and often goes undetected after an event. Hail, however, is recognized as one of the key causes of erosion of wind turbine blade composite materials. When an active turbine is in a hailstorm, damage can occur to the blade material during hail impact due to high impact velocity. Typically, the first signs of damage are pits in the paint that, with repeated impact, can form gouges. Continued damage can lead to delamination and damaged interior material layers. Normally, damage starts at the tip and leading edges and later propagates outwards towards the base of the blade and to other surfaces of the airfoil (MacDonald et al., 2016; Keegan et al., 2013). In addition to the turbine blade, hail can damage the nacelle covering (DNV/Risø, 2002).

Lightning contributes to a much higher percentage of blade damage than hail, and damage is much more catastrophic, including:

- Broken and disintegrated blades
- Electrical and control system failure
- Generator burn-out

Wind turbine damage functions were created for both onshore and offshore turbines.

5.6 Damage functions for building contents

The Verisk model represents damage to contents by each sub-peril separately. In addition, the model supports explicit content damage functions for residential, commercial, industrial, and greenhouse building occupancy types, among others. Content damageability is a function of building type and occupancy class; that is, for each category of occupancy class, there exists a contents damage function that is a function of the building damage ratio.

The type of occupancy can be used to determine what contents are most likely to be present and their potential vulnerability. Office buildings usually have a large amount of electronic equipment and can incur heavy losses if windows break or, in the case of hail, a punctured roof allows rain to enter the interior. Hospitals can incur large losses if equipment is damaged. Greenhouses can have climate control equipment damaged.

The contents damage ratio is the loss to the contents divided by the replacement value of the contents. Just as for building damage functions, the content damage function for unknown occupancy (occupancy code 300) and general residential (construction code 301) uses the weighted average of all known occupancies and all known residential construction. Unknown contents damage functions are calculated for each sub-peril separately.

Figure 143 depicts the relationship between mean building damage and mean contents damage for single-family homes in the Verisk model. In general, the contents damage functions are less than the building damage functions at low wind speeds and low hail impact energies. Significant damage to contents is not likely to occur unless there is significant damage to the roof covering, loss of roof decking panels, or window failure. Thereafter, both building and contents damage functions will escalate with increasing wind speed and increasing hail impact energies. The contents damage functions will increase at a faster rate than building damage as wind speeds and hail impact energies increase, which, in turn, are more likely to penetrate the exterior and damage the contents within. Water infiltration, common in the case of a hailstorm, will also cause substantial damages to building contents. The contents damage functions in the model reflect these relationships, which are also observed in claims data.

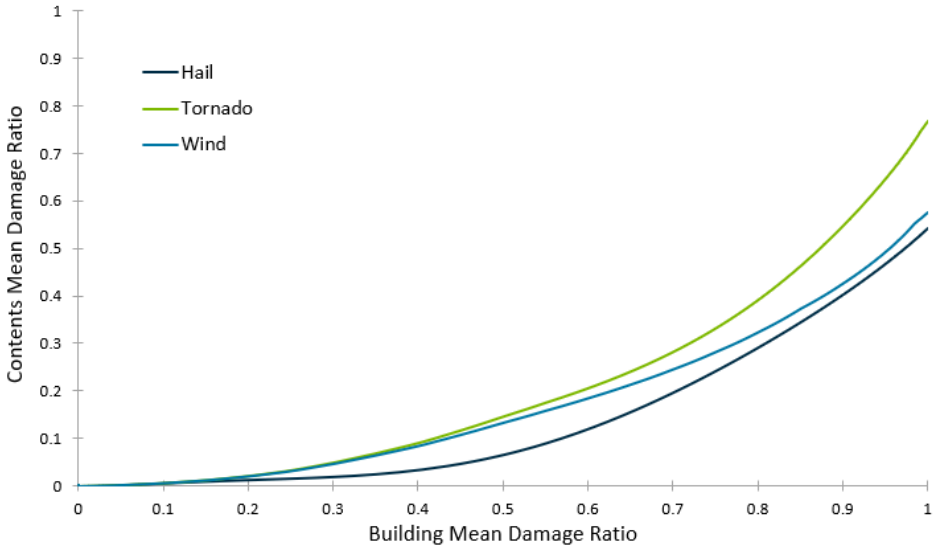

Figure 143. Relationship between mean building damage and mean contents damage

5.7 Time element (business interruption) damage functions

For time element coverage, the damage ratio represents the per-diem expenses or business interruption (BI) losses associated with the expected number of days that the building is uninhabitable (residential structures) or unusable (commercial structures). Time element damageability is a function of the mean building damage ratio, the time required for repair or reconstruction, and occupancy.

The time element damage function combines the effect of all the three sub-perils (i.e., tornado, hail, and straight-line wind) together and estimates the BI losses for the duration of the storm system. Figure 144 illustrates a sample additional living expense relationship between repair/reconstruction time and the mean building damage for a residential structure.

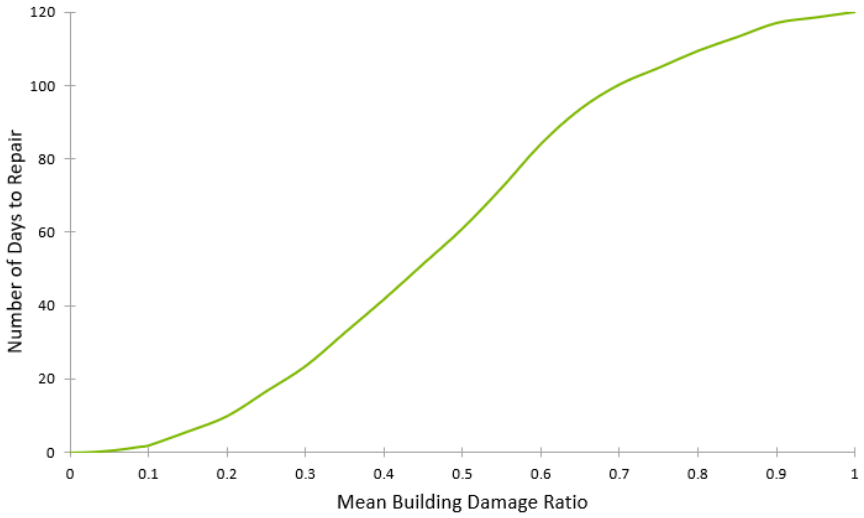

Figure 144. Time element vulnerability relationship for a residential structure

Building damage alone cannot explain total BI losses. Therefore, the model also accounts for building characteristics, such as size, contents, and complexity of the building system; business characteristics, such as the potential for relocation or for continued operations during repairs; and building damage (Figure 145). In addition, the Verisk model captures complex business income policy features, including extra expenses, civil authority issues, dependent building damage, and extended period coverage.

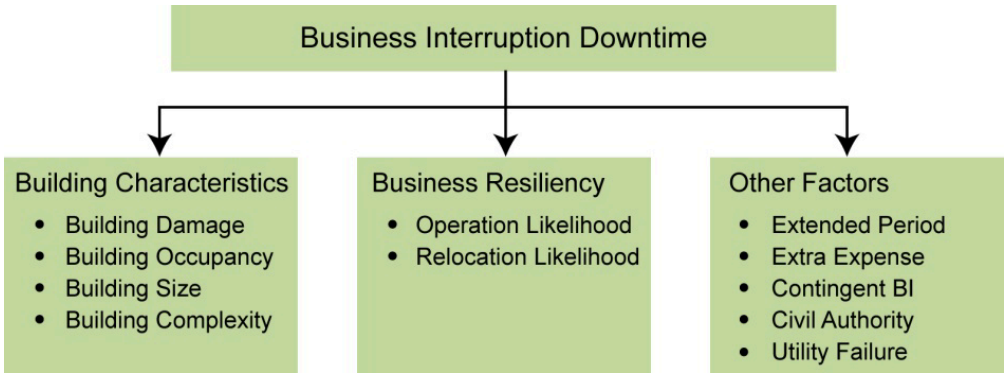

Figure 145. Factors influencing business interruption downtime
Source: Verisk

The methodology does not require any additional input from the user, but instead uses existing input variables, such as occupancy and characteristics of typical BI policies, to model total BI losses for any given occupancy and the variation in BI losses across different occupancies.

Understanding business interruption coverage and inputs

Business income has two primary components: (a) net income that a business will lose due to disruption and (b) normal expenses that must be paid even if the business is not operating.

Business interruption at a location can occur for a variety of reasons, and how much is recoverable from insurance depends upon the policy conditions. Direct BI occurs if there is physical damage to the insured building for the covered peril. In fact, these policies require that physical damage must cause the suspension of the business and there must be a loss due to the suspension.

Business interruption can occur even when there is no physical damage to the insured building. For example, the building may be inaccessible due to utility failure, the directives of civil authorities, or damage and disruption at a dependent building. Indirect BI (which for purposes of the discussion herein includes BI due to damage to dependent buildings, civil authority, and utility failure) is not automatically covered under all BI polices; these optional coverages are available by endorsement for an extra premium.

The complex nature of BI losses and their governing insurance policies make them difficult to accurately model. The Verisk model is based upon extensive internal and external research, including Applied Technology Council papers, U.S. Census construction reports, U.S. Department of Energy building-size data, insurance literature, damage reports, and actual claims data.

Estimating business interruption downtime

Downtime, or the number of days before the business can return to full operation, is the primary parameter in estimating business interruption losses.[81] Figure 146 illustrates the "event tree" approach the model uses to estimate mean business interruption downtime. For comparison purposes, it also highlights hypothetical event paths for an office and a hotel. The event tree shows the sequence of events that can occur in a system. For example, an office building is likely to take a different path to recovery than a hotel and, hence, it will have a different downtime in the event of interruption.

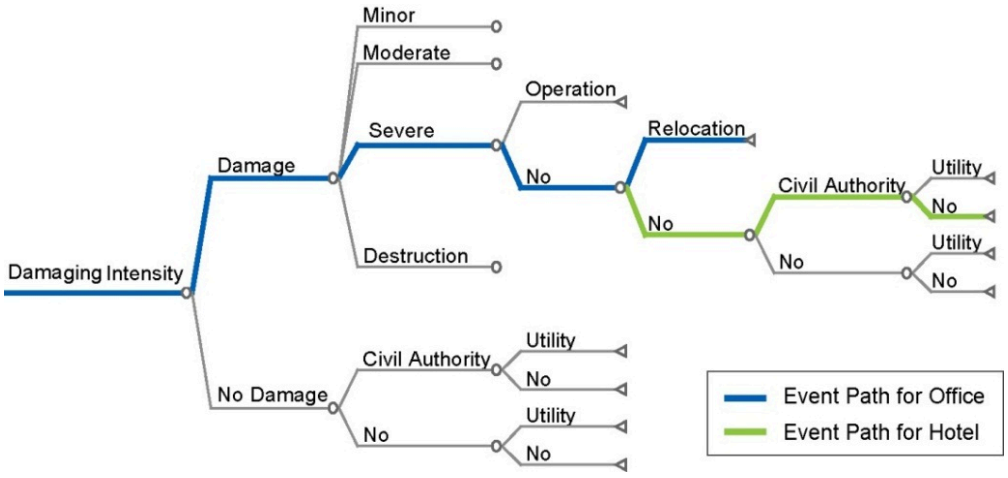

Figure 146. Hypothetical event tree for office building and hotel
Source: Verisk

[81] See the Verisk publication, Jain and Guin (2009) "Modeling Business Interruption Losses for Insurance Portfolios," *Proceedings of the 11th Americas Conference on Wind Engineering, San Juan, Puerto Rico, June 22-26, 2009*. Available at: http://www.iawe.org/Proceedings/11ACWE/11ACWE-Jain.Vineet1.pdf

The Verisk model calculates downtime for each stage of the damage assessment and recovery process. The first stage, also known as "pre-repair," is the time before repairs begin. Before the repairs begin, the damage must be assessed, the repair cost must be negotiated with the contractors, and the building permit must be obtained. The next stage is the "repair period." Some businesses choose to relocate rather than wait for repairs, but relocation takes time as well. Once repairs are completed, revenues may not immediately resume at the pre-disaster level; it may take some time to regain market share and/or rebuild a labor force that may have found employment elsewhere.

The estimated number of days needed to restore the business to full operation depends on many key factors, including the level of damage sustained, the size of the building (square footage), and its architectural complexity. For a given damage ratio, a 25,000 square-foot hotel will take significantly longer to repair than a 5,000 square-foot professional office. For a given square footage, buildings with significant architectural complexity will also take more time to repair. Warehouses can be quite large, but repairs are likely to take place quickly because of their architectural simplicity. Interior finishes must also be considered. Hotels are not only typically larger than office buildings but can take more time to repair due to the higher quality of interior finishing.

Some types of businesses, such as hospitals, are more resilient than others and may be able to restart operations before repairs are complete, or they may have had disaster management plans in place that allow them to relocate quickly. For other businesses, such as hotels, location is critical, and relocation is not an option. Since many parameters (e.g., building size, complexity, and business resiliency) that play an important role in determining business interruption are generally not available for input into the model, occupancy class is used as a proxy to determine these parameters.

Occupancy is also used to estimate the probability that there may be business interruption at a dependent building within the storm footprint, such as at the building of the supplier of a necessary manufacturing input, that will exacerbate BI losses at the principal building. Estimation of the impact of the dependent building's damage on the principal building requires the knowledge of the location and the degree of interdependence between the dependent and principal buildings. Since this level of detailed information is generally not available, logical assumptions are made to estimate the impact of the dependent building on the principal building's downtime.

Once the damage state of the dependent building is estimated as a function of the principal building's damage state, BI losses are calculated based on the maximum of BI downtime associated with the damage states of the principal and dependent buildings. This assumption implies that the impact of the dependent building damage is more significant at lower principal building damage states than at higher damage levels of the principal building. A similar logic-based approach is used to estimate the impact of civil authority and utility failure on the downtime of the principal building. Downtime is also adjusted to account for BI policy conditions, such as limited ordinary payroll, extra expense, and the extended business income coverages.

Figure 147 shows sample mean BI curves for three occupancies: hotels, offices, and hospitals. Not only is the mean BI downtime different for different occupancies for a given mean building damage ratio, but also the relativity between occupancies varies as a

function of building damage ratio. That is, repair time, which is a function of building size and complexity, determines the shape of the BI curve for all levels of building damage.

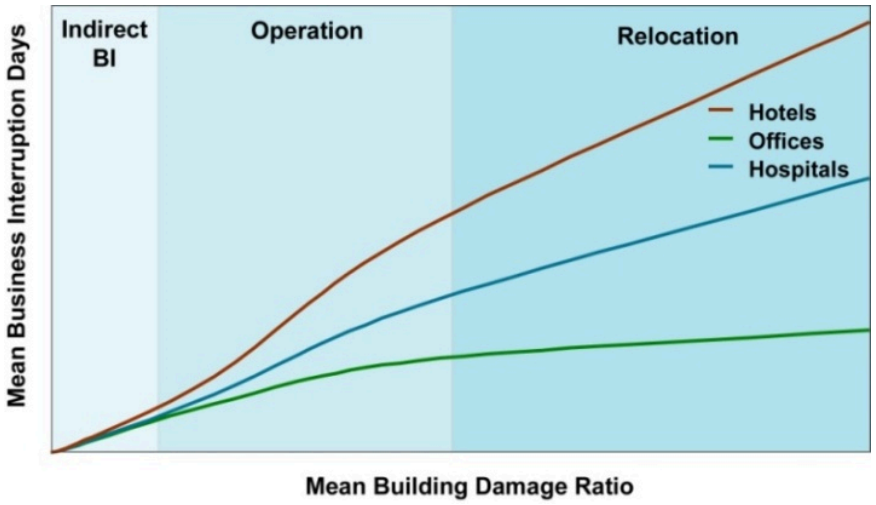

Figure 147. Impact of factors determining business interruption downtime varies with occupancy and severity of building damage

The impact of the many determining factors varies with the degree of building damage. For example, the impact of indirect BI and other factors, such as extra expense, on the shape of the BI curve is particularly important at low levels of damage. At moderate levels of building damage, the likelihood of continued operation while repairs are underway determines the shape of the BI curve. As building damage increases and continued operation becomes less likely, the impact of relocation on the BI curve increases. Office buildings are likely to be relocated at a certain level of building damage, so the BI curve does not change with increasing damage beyond that point. However, since it is unlikely that a hotel or hospital will be relocated, the BI curve increases with increasing levels of building damage for these occupancies. Thus, at higher levels of building damage, relocation becomes the determining factor in estimation of the BI curve.

Figure 148 shows, for different mean damage ratios, the modeled BI damageability of selected occupancies relative to the general commercial occupancy.

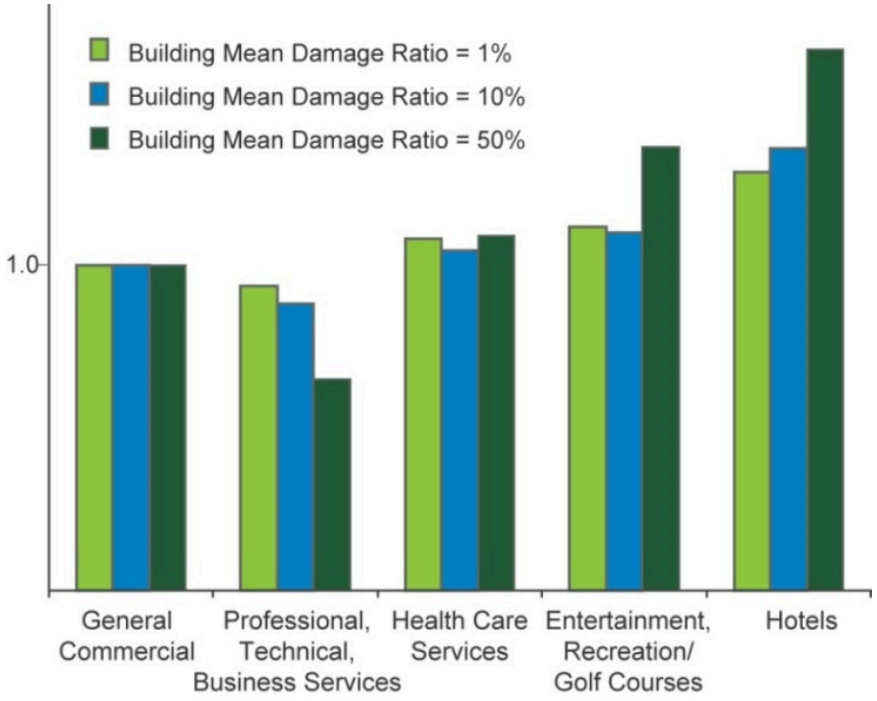

Figure 148. Relativity of business interruption damageability across commercial occupancies
Source: Verisk

The methodology for calculating BI losses relies, in part, on expert judgment in the face of limited available exposure data, but it has been rigorously calibrated using detailed claims data from recent severe thunderstorm experience.

Business interruption losses for industrial facilities

Assessing business interruption (BI) losses for industrial facilities is complex, particularly in the case of highly-integrated facilities. The major contribution to BI losses is the loss of revenues incurred when product chains are rendered completely or partially non-functional. Loss of functionality can occur due to physical damage to the components, the interconnectivity between components, or lifelines, such as electricity and water systems. The Verisk model's BI damage functions at the facility level are derived from component distribution information and the individual component and subcomponent downtime functions.

Downtime is the primary parameter for assessing BI losses. To assess these losses for an entire industrial facility, time element BI damage functions are determined for each component for each stage of the damage assessment and repair process. As in any other BI assessment, the time before repairs can get underway, or pre-repair, is determined and combined with the time required for the actual repair. Once the time element functions are determined for all components, the model aggregates the functions by determining a weighted average of the component functions. Figure 149 illustrates time element damage functions for select industrial facilities components.

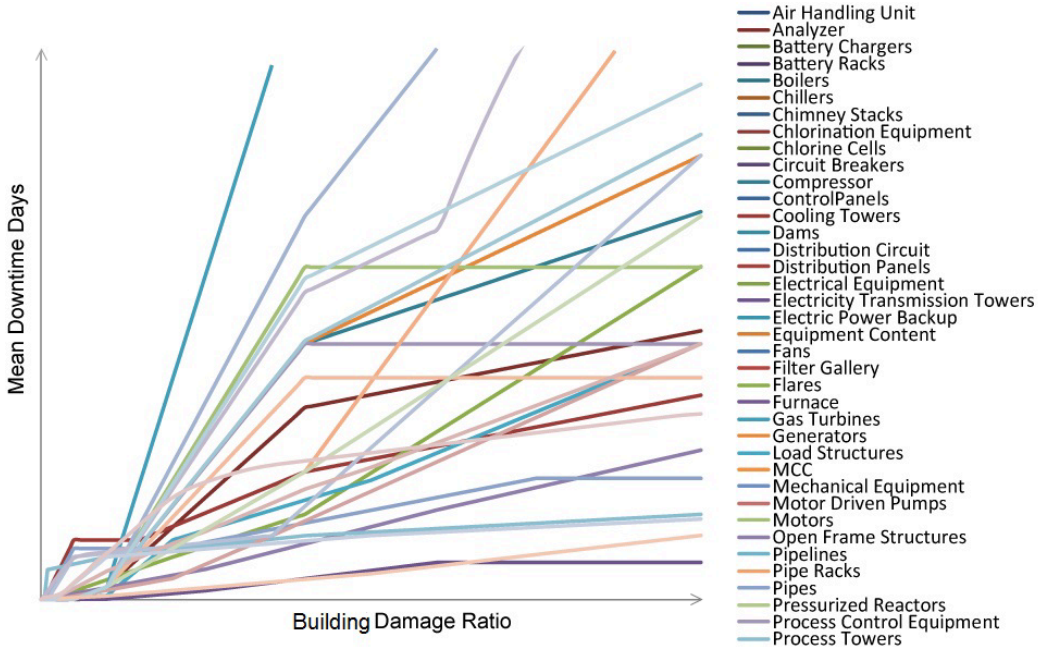

Figure 149. Time element functions for industrial facility components

As described above, time element functions at the facility level are derived from component distribution information and the individual component and subcomponent downtime functions. Figure 150 shows the time element functions for select industrial facilities in the United States for the straight-line wind sub-peril.

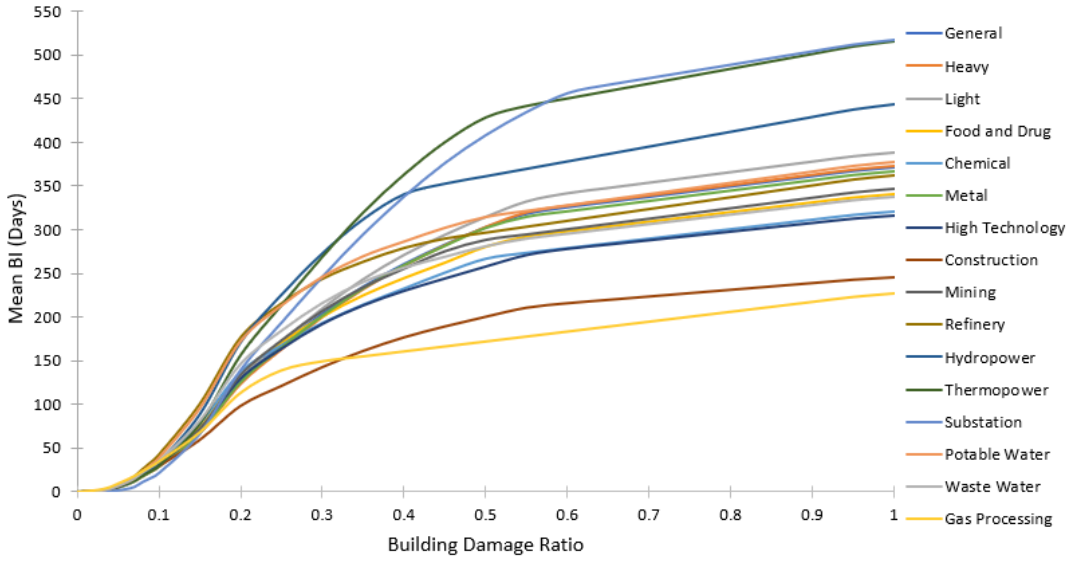

Figure 150. Time element functions for straight-line wind damage to industrial facilities

A partial correlation between components is used to assess modeled BI losses to industrial facilities. The analysis implicitly incorporates the numerous connections between

components, lifelines, and product chains. The high degree of site-specific connectivity and the complexity of the product chains that exist at most plants make the estimation of downtime for industrial facilities a challenge. It is a many-faceted calculation involving numerous operations, including evaluations of onsite process interactions, bottlenecks and redundancies, offsite interdependencies, and revenue generators. Downtime estimation is accomplished by building a "network model" that constructs a simulation of the many interconnections between components, processes, lifelines, and product chains. It accounts for components to be idle even if undamaged or already fixed if other components or lifelines remain down.

Note on the importance of business interruption exposure data quality

Since business income exposure is generally defined in terms of dollars per unit of time, two key user inputs are needed to model direct BI losses: BI exposure value and the number of days associated with the exposure. For example, a business may generate USD 1 million in business income exposure per year, or 1/365 million USD per day. If USD 1 million is entered as the business income exposure, 365 must be entered for the number of days. If a user enters 1/365 million for business income exposure, 1 day must be entered as the number of days. The per diem exposure, together with the modeled estimated number of days of downtime, provides an estimate of BI loss.

The model estimates the number of days of downtime as a function of building and contents damage, occupancy, size and complexity, business resiliency, and other factors discussed above. Ground-up losses are calculated by multiplying BI exposure per day by the number of downtime days. Note that when calculating BI losses, the occupancy field, and not the gross area, is used as a proxy for building size.

As is the case with building replacement values, high-quality BI exposure data are essential for generating reliable loss estimates. During Verisk 's continuing audits of client exposure data, it has become apparent that large numbers of locations have very low BI/day values. In most cases, business interruption limits have been entered as annual BI exposure. Exacerbating the problem, Verisk also found evidence of the use of loose "rules of thumb" to determine the BI limit, rather than the use of BI worksheets for each location in multi-location policies. Finally, Verisk found evidence of a general underestimation of the number of locations that may sustain damage in a catastrophe. Verisk cautions that these problems with BI exposure data quality will result in significant underestimation of BI losses.

5.8 Combined damage from multiple sub-perils

With the explicit modeling of three individual sub-perils (hail, straight-line winds, and tornado), damage due to each sub-peril is calculated separately. This methodology provides accuracy in the effects of each individual sub-peril. However, the estimates still need to correctly account for the combined effect of all three modeled sub-perils impacting an exposure at about the same time. For example, severe weather may begin with straight-line winds from a

downdraft followed by a hailstorm. Many structures sustain damage from a combination of sub-perils, particularly if the damage is severe. This section describes the methodology that the Verisk Severe Thunderstorm Model for the United States follows to accurately account for damage due to multiple sub-perils.

In the Verisk model, the first step to estimating damage to an exposure is determining which microevents contained within a given macroevent inflict damage at the exposure's location. For those microevents affecting the location, the model takes the maximum straight-line wind speed, tornado wind speed, and hail impact energy at the exposure's location. These intensity measures are then used to calculate building damage caused by each sub-peril independently. This calculation results in mean damage ratios (MDRs) for each peril for Coverage A (Building).

A crucial component of calculating damage due to multiple sub-perils is ensuring that a given damage is not attributed to more than one sub-peril. This type of "double counting" would increase the damage and loss estimation, potentially resulting in a total MDR that exceeds 100%. To avoid this problem, the Verisk model does not allow both tornado and straight-line wind damage at the same location due to the same macroevent. Thus, the model computes the straight-line wind and tornado MDRs for Coverage A and uses the larger of these two MDR values. The smaller MDR value is set to zero. In addition, the model computes the hail MDR for Coverage A, if applicable.

Next, the total building MDR is calculated as the combination of the hail MDR and the larger of the straight-line wind and tornado MDRs. If this total building MDR value exceeds 100%, the hail MDR is reduced. Verisk researchers chose to reduce the hail MDR rather than the straight-line wind or tornado MDRs because properties are most likely to be damaged first by either straight-line winds or a tornado. Then, after the wind-based sub-perils, hail would damage whatever remained. An example is featured in Table 30. Note that if the sub-peril specific MDRs for Coverage A are very small (i.e., less than 10^{-5}), the loss calculation ceases on the assumption that it is unlikely that a claim would be filed for such a small MDR.

Table 30. Sample calculation of sub-peril specific MDRs

Calculation Steps	Wind	Hail	Tornado
1. Original Coverage A sub-peril MDRs exceed 1.0	0.5	0.6	0.4
2. Sub-peril MDRs after eliminating the tornado MDR because straight-line wind is the dominant sub-peril	0.5	0.6	0
3. Reduce hail MDR such that the total MDR for Coverage A is 1.0	0.5	0.5	0

The next step in the damage calculation is to combine the MDRs for the sub-perils and coverages. The Coverage C MDRs are calculated as a function of building damage for each sub-peril. The normalized MDR values for Coverage A are used in this calculation. Normalization is applied to Coverage C in the same way as it was applied to Coverage A to ensure that the total MDR value does not exceed 100%. Once the combined MDRs for Coverages A and C are determined, the model distributes the Coverage D MDR (combined for all three sub-perils) amongst the sub-peril MDRs for Coverage A. The amount distributed per sub-peril is proportional to each sub-peril's normalized MDR for Coverage A.

5.9 Uncertainty around the mean damage ratio

In creating the secondary uncertainty wind and hail damage ratio distributions, Verisk's primary goal is to define the uncertainty around a given mean damage ratio (MDR), represented by the blue line, using claims data, represented by the red dots, as shown in Figure 151. These distributions are constructed using the inflated transformed beta family of distributions (Extreme Optimization, 2004-2016; Ospina and Ferrari, 2010; Venter, 1983; Venter, 2003). They have two discrete spikes at zero damage ratio and a maximum possible damage ratio, given a mean damage ratio that represents the probability of no damage or maximum damage, respectively, as well as the main part of the distribution for the damage ratios between these two extremes.

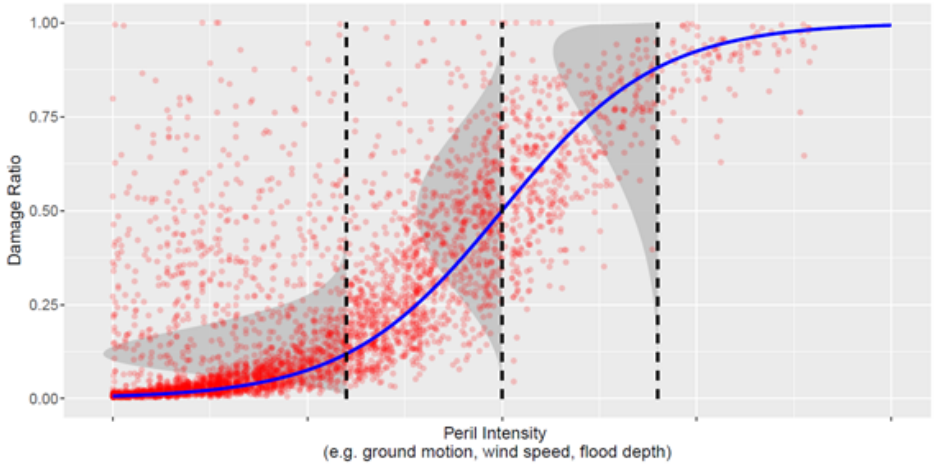

Figure 151. Representation of secondary uncertainty distributions around a given MDR (blue line)
Source: Verisk

In the Verisk model, secondary uncertainty wind damage ratio distributions are based on approximately 1.6 million claims, and the hail distributions are based on approximately 17.5 thousand claims. The data are from multiple events and several major companies, and are mainly from the United States, where detailed information on claims and exposure characteristics is available to derive distributions. Secondary distributions were created for residential and commercial lines of businesses for all four coverages.

A key feature is the smoothly transitioning shapes of the spikes and the main body of the distribution as the MDR increases. Figure 152 shows that the distributions transition in a natural manner from monotonically-decreasing to bell-shaped, with the main part of the distribution moving towards the spike at maximum damage. Furthermore, the support of each distribution is a single connected interval. Thus, there are no large gaps with zero probability in the main part of the distribution as shown in Figure 152.

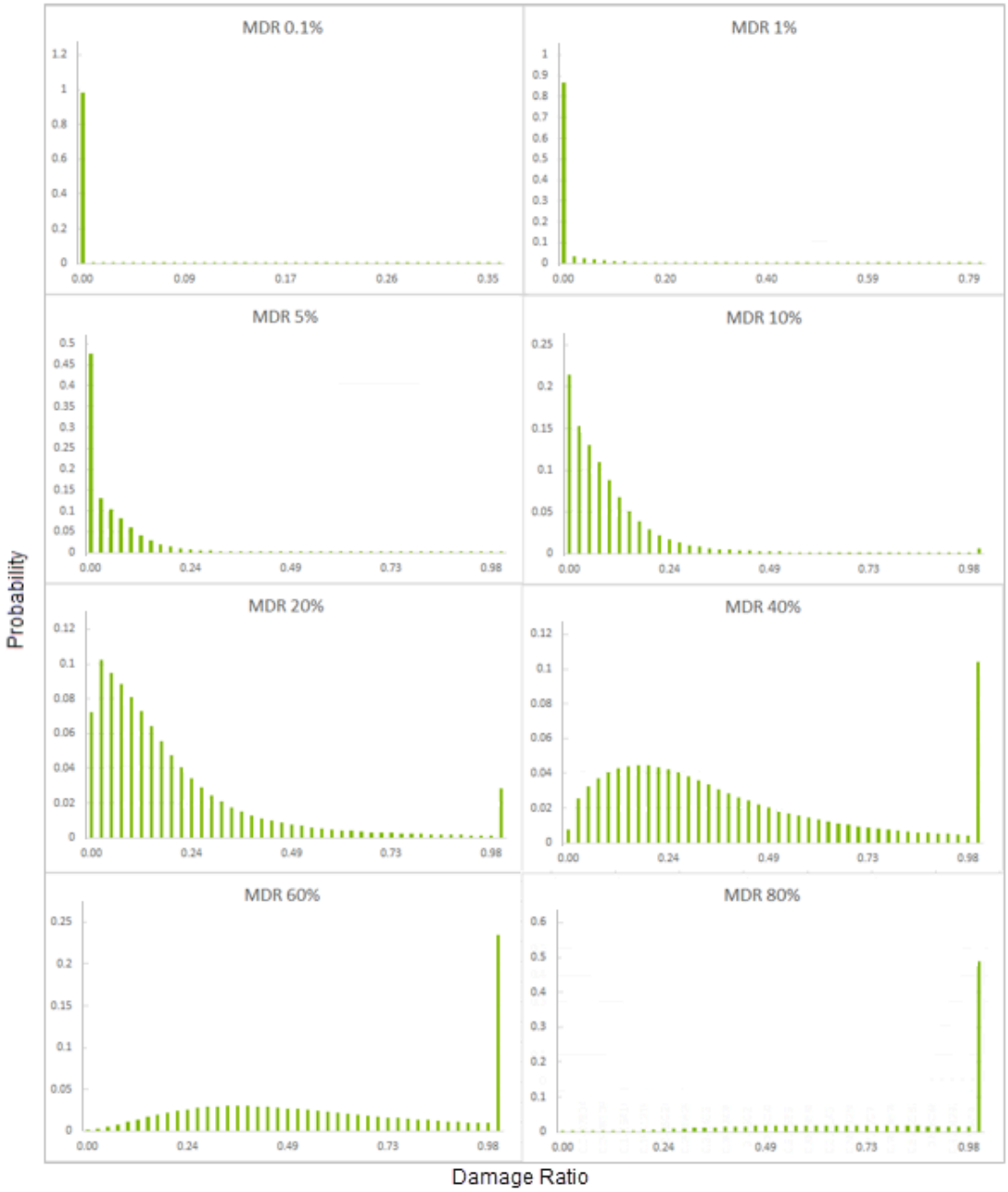

Figure 152. Smoothly-transitioning shapes of the new residential coverage A distributions
Source: Verisk

Another key feature of these distributions is the use of inflated transformed beta distributions for fitting of the claims data. This five-parameter family of distributions affords great flexibility in producing a variety of shapes represented by the claims data at different MDRs, and particularly in reproducing the heavy tails exhibited by the data. To ensure smooth transitioning of shapes, a functional relationship for the parameters of the inflated transformed beta distribution is imposed.

Since most of the claims have low or moderate MDR (Coverage A MDR is less than 8% for 99% of straight-line wind claims and less than 2% for hail claims), the robust amount of data available enables direct fitting of distributions to data in this MDR range. In other MDR ranges, extrapolation of the distribution parameters was used to fit basic summary statistics of these data, such as the standard deviation and coefficient of variation. Although ground-up losses have been reconstructed by adding back the effective deductible to the claim amount, censored claims do not exist in the dataset, and their ground-up losses cannot be reconstructed. Therefore, special attention was paid to censored claims[82] using advanced statistical estimation techniques based on the Kaplan-Meier method (Kaplan and Meier, 1958). The fitted distributions are shown in Figure 153 for various MDRs. Note that the tails of the fitted distribution match the heavy tails of the claims at higher damage ratios, whereas the small differences at low damage ratios can be attributed to the correction for the censored claims and smoothly-transitioning distributions.

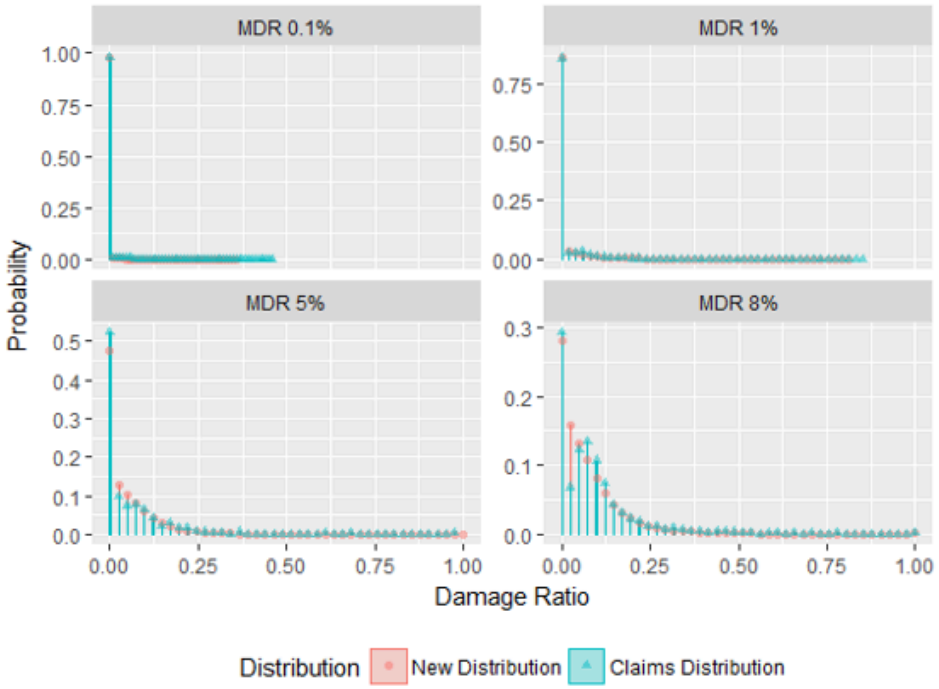

Figure 153. Smoothed parametric fit of residential Coverage A distributions to claims data
Source: Verisk

This procedure for fitting the distributions is followed for residential Coverages A, C, and D. Additionally, intuitive relationships between different coverages' distributions are enforced. For example, during the fitting procedure, the probability of zero loss for Coverage C is modeled to be greater than that for Coverage A. For wind perils, it is generally accepted that building damage is prerequisite to contents damage, and even significant building

[82] Exposures omitted from the dataset because losses fell below the deductible

damage can result in relatively low contents damage. For example, a window may break and allow rain to enter a room, but if the room is empty, there may be zero contents loss. The remainder of the distributions are derived from one of the fitted distributions by applying Verisk's knowledge of the behavior of various occupancies and construction types. Coverage B distributions should reflect greater uncertainty in their structure types, vulnerability, and replacement value. Therefore, Coverage B distributions should have higher standard deviation with thicker tails and have higher probabilities of zero and maximum loss.

Commercial distributions for Coverages A and B are derived from their respective residential distributions, first noting that commercial exposures tend to be better engineered buildings with the following properties:

- Engineered buildings have lower vulnerability than non-engineered buildings, and vulnerability is generally limited to specific components of the structure (e.g., windows). Therefore, commercial distributions have a higher probability of zero loss and a lower probability of maximum loss than residential distributions.
- Smaller variations in components of engineered buildings, less variability in their construction practices, and more streamlined claim adjustment practices indicate less uncertainty for distributions for engineered buildings. Therefore, given that loss is incurred, commercial distributions have a smaller standard deviation than residential distributions.

Wind speed and hail differ in two key ways as indicated by the claims data. Hail damage distributions have a smaller variance and significantly lower probabilities of total loss than wind speed damage distributions. As a result, wind speed distributions have higher variance and higher probability of zero loss than hail distributions. These differences can be seen in Figure 154.

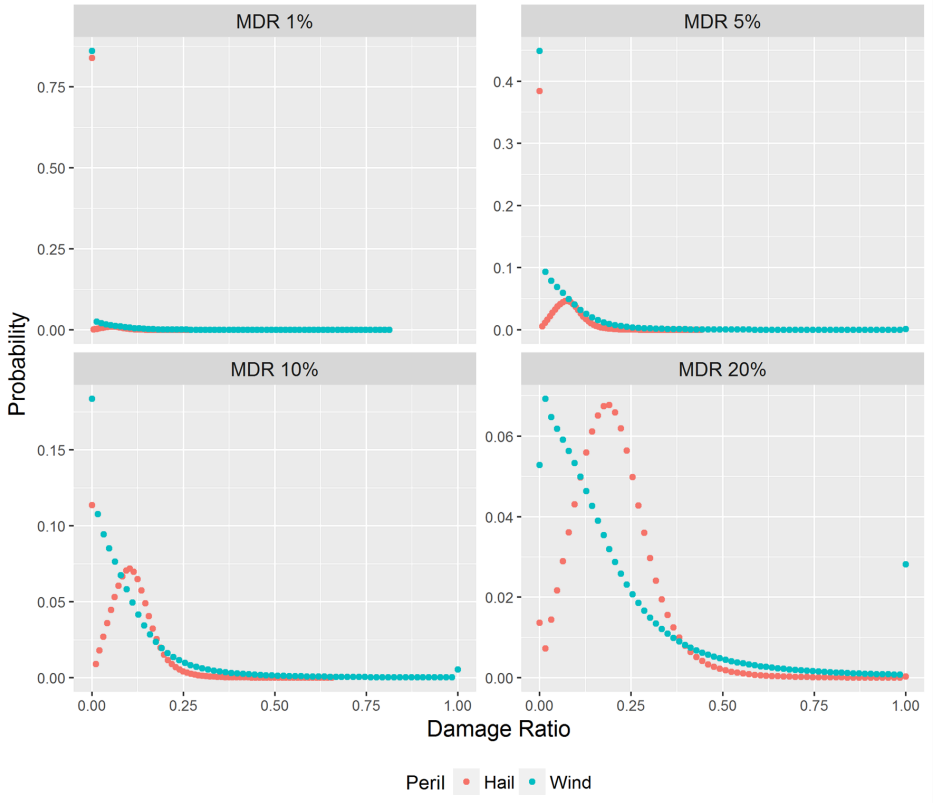

Figure 154. Comparison between hail and wind secondary distributions for several MDRs
Source: Verisk

As part of the fitting procedure, the distributions were validated against claims data for agreement on basic statistics (e.g., standard deviation). Another important statistic to validate is the behavior of gross-to-ground-up losses. At a given location, the gross-to-ground-up loss ratio (LR) can be calculated by the following equation:

$$LR = \frac{Mean\ Gross\ Loss}{Mean\ Ground\text{-}Up\ Loss}$$

This loss ratio can be computed for any coverage, for either residential or commercial occupancy types. Figure 155 shows good agreement between the loss ratios produced by the Verisk distributions and the claims data. Note that the loss ratio varies with the deductible given as a proportion of the replacement value.

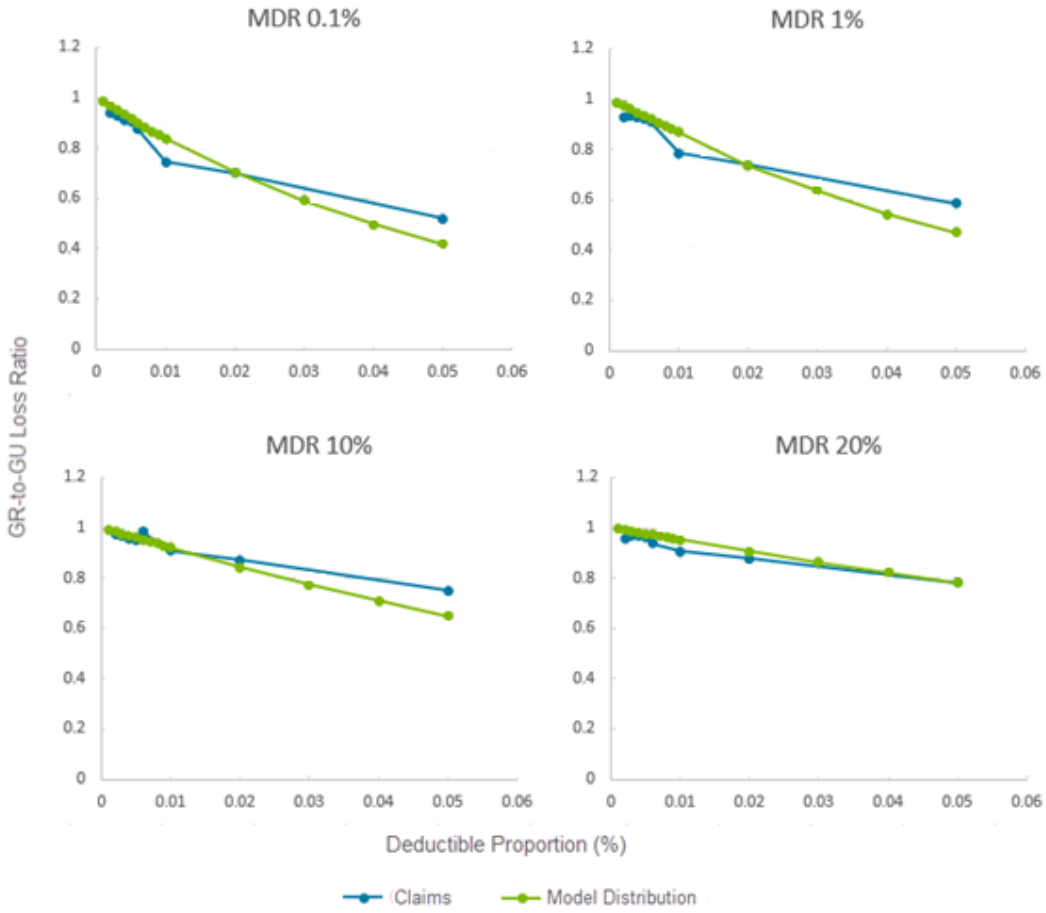

Figure 155. Validating the gross-to-ground-up loss ratio for residential Coverage A, at varying MDRs and deductibles
Source: Verisk

The impact of the distributions on gross losses can be summarized as follows:

- The loss ratios for both commercial and residential distributions are monotonically increasing with MDR and monotonically decreasing with deductible proportion.
- For a given MDR and deductible proportion, the loss ratio for the commercial distribution is greater than that for residential distribution.
- For any fixed deductible proportion, the difference between the loss ratios of the commercial and residential distributions decreases as MDR increases (Table 31).

Table 31. Gross-to-ground-up loss ratios for commercial and residential Coverage A distributions, at varying MDRs and deductible proportions

	0.5% Deductible		1% Deductible		2% Deductible		5% Deductible	
MDR	Com	Res	Com	Res	Com	Res	Com	Res
0.001	0.931	0.917	0.864	0.837	0.754	0.704	0.508	0.418
0.010	0.947	0.934	0.895	0.868	0.796	0.737	0.572	0.469

	0.5% Deductible		1% Deductible		2% Deductible		5% Deductible	
MDR	Com	Res	Com	Res	Com	Res	Com	Res
0.100	0.969	0.961	0.937	0.921	0.875	0.843	0.716	0.648
0.500	0.990	0.990	0.980	0.980	0.961	0.960	0.903	0.901

5.10 Validating damage functions

The Verisk Severe Thunderstorm Model for the United States leverages Verisk's over 20 years of experience in developing hail, straight-line wind, and tornado damage functions. In addition, the model's damage functions incorporate claims data analyses, engineering research and analyses, and damage surveys that consider the effects of both wind loads and hail impact on components and cladding. These damage functions are extensively validated and calibrated.

Validating the relative vulnerability of different construction and occupancy classes is a critical component of damage function development. For example, Figure 156 compares the relative vulnerabilities of single-family homes for different construction types for the hail sub-peril. Both observed (i.e., claims) and modeled relativities for a certain intensity level are shown in the figure. The observed relative vulnerabilities are obtained from claims data analyses from major insurers after significant loss events. As seen, the actual and observed data compare well.

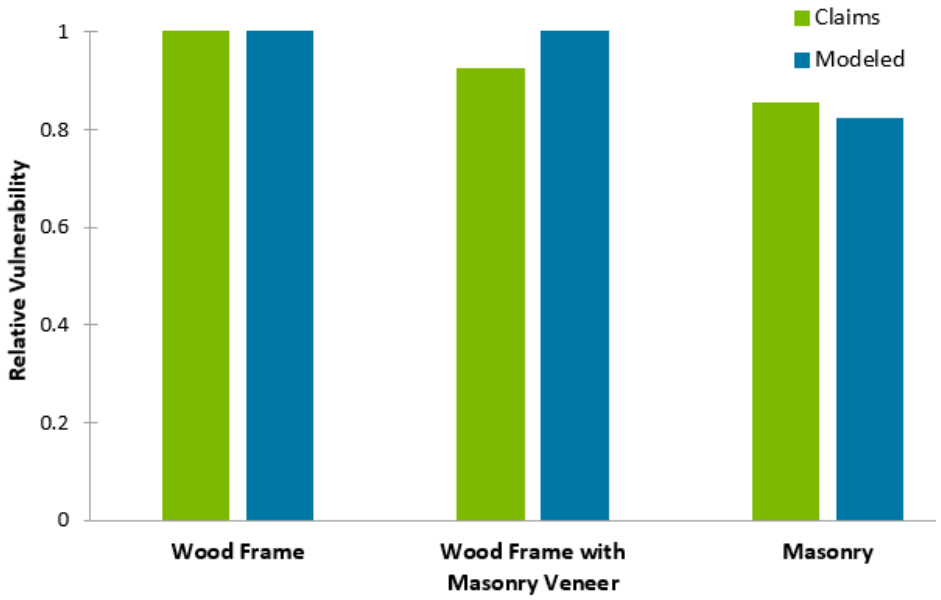

Figure 156. Relative vulnerability of single-family home construction classes at a certain hail intensity level

Verisk researchers also validated the mitigating impacts of key individual building characteristics that are included in the model's secondary risk module. Figure 157 compares

the percent change in vulnerability that occurs in the model versus in client data when certain mitigating features are included (i.e., shingles that meet FBC hurricane wind standards, engineered shutters, hip roof, tie downs, and 8d nails) versus when they are excluded. Verisk researchers also compared the combined effect of all these individual features in a single mitigated building versus an unmitigated building. Note that these characteristics are available as options for their corresponding secondary risk features in Touchstone.

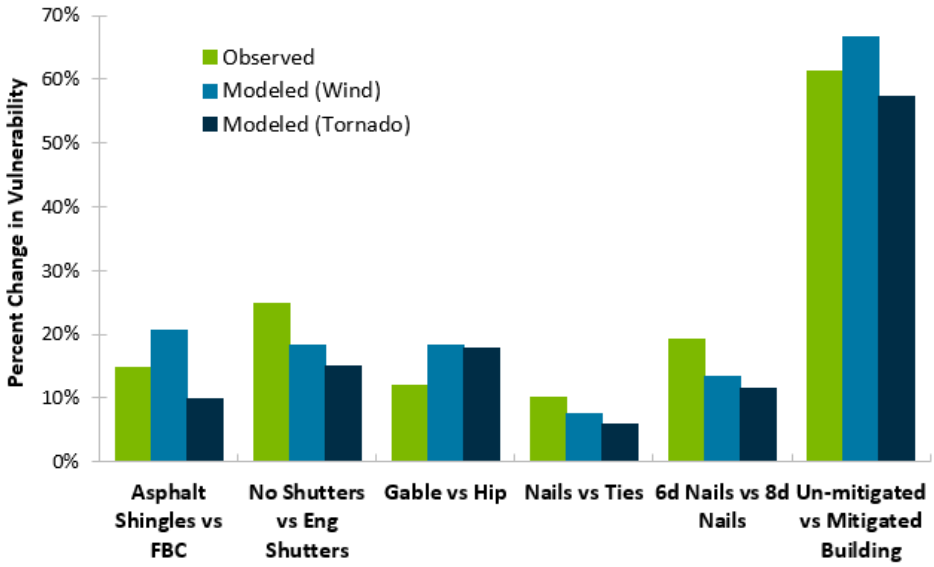

Figure 157. Validation of the impact of secondary risk characteristics alone and in combination

Location-specific insurance company claims and engineering expertise were used to develop the model's sub-peril-specific damage distributions to account for uncertainty associated with the localized hazard and mean damage ratio (MDR). Figure 158 shows the model's uncertainty distributions for both hail and straight-line wind for a low MDR. Note that the distinct difference at the lower damage levels is supported by the claims data.

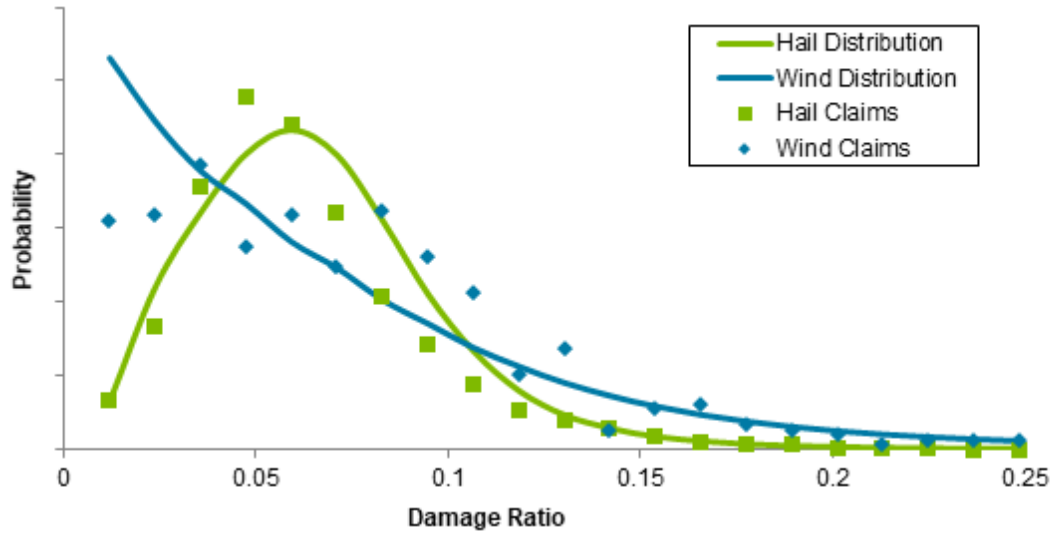

Figure 158. Comparison between claims data and hail and wind uncertainty distribution for a low MDR

The contents damage functions were developed based on Verisk's analysis of location-specific claims in combination with engineering expertise. Figure 159 shows the breakdown in the claims data by sub-peril type. Note that the claims data support wind (including tornado) having a higher content damageability than hail for a given building damage ratio.

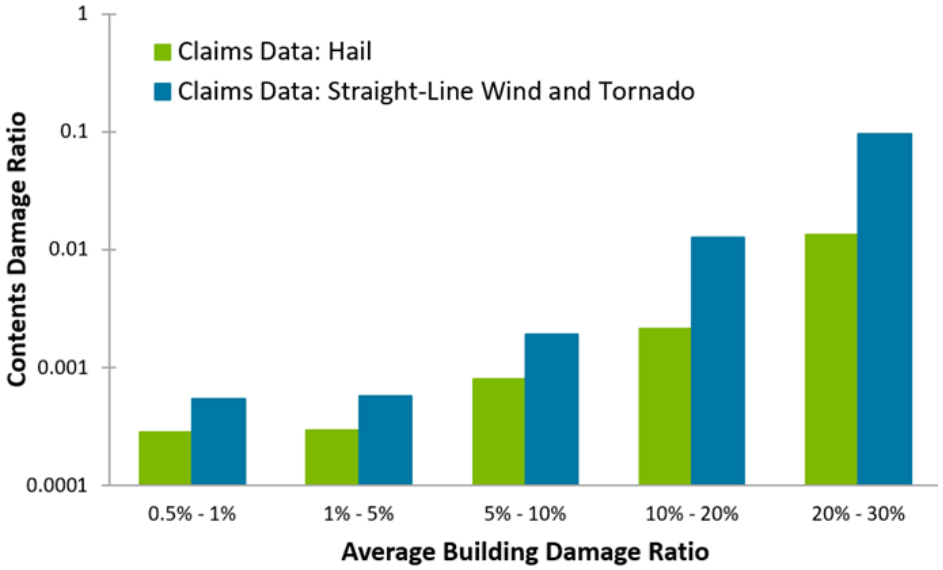

Figure 159. Validation of content vulnerability by sub-perils and building damage ratio

As part of damage function validation, Verisk engineers also compared claims data to Verisk's damage functions for contents and time element coverages. Figure 160 shows how the Verisk model's content straight-line wind and tornado damage functions for residential

risks compare to the wind claims data. The damage function is unbiased within the spread of claims. Note that the y-axis in the graph is on a logarithmic scale.

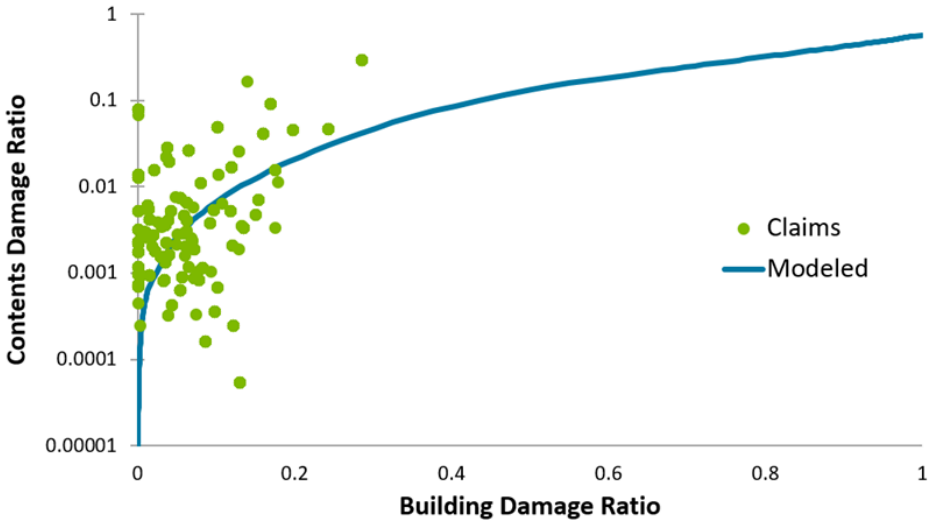

Figure 160. Straight-line wind and tornado contents damage function versus company claims data

As evident in the figure, there is a lack of large claims for severe thunderstorm straight-line wind events. As a result, engineers relied on sound engineering judgment in estimating the contents damage at those higher building damage ratio levels. When appropriate, research results from other wind perils within similar regions were used in developing these portions of the damage function curve.

After damage function calibration was performed based on individual claim comparisons, assessments were also performed to ensure that the coverage contribution to total losses was reasonable. The percent of total loss that was attributed to buildings, contents, and time element (BI/ALE) was compared using claims data for marquee events when appropriate breakdowns were available in the claims data. These claims data came from several large insurers within the United States. Figure 161 and Figure 162 show these comparisons for building, and contents and time element, respectively. Two separate plots are used to show these comparisons due to the large magnitude of difference between the contribution of loss due to building (Coverage A) and the remaining coverages (Coverages C and D). As seen in these plots, the model is unbiased for all coverages for wind (including both straight-line wind and tornado) and hail.

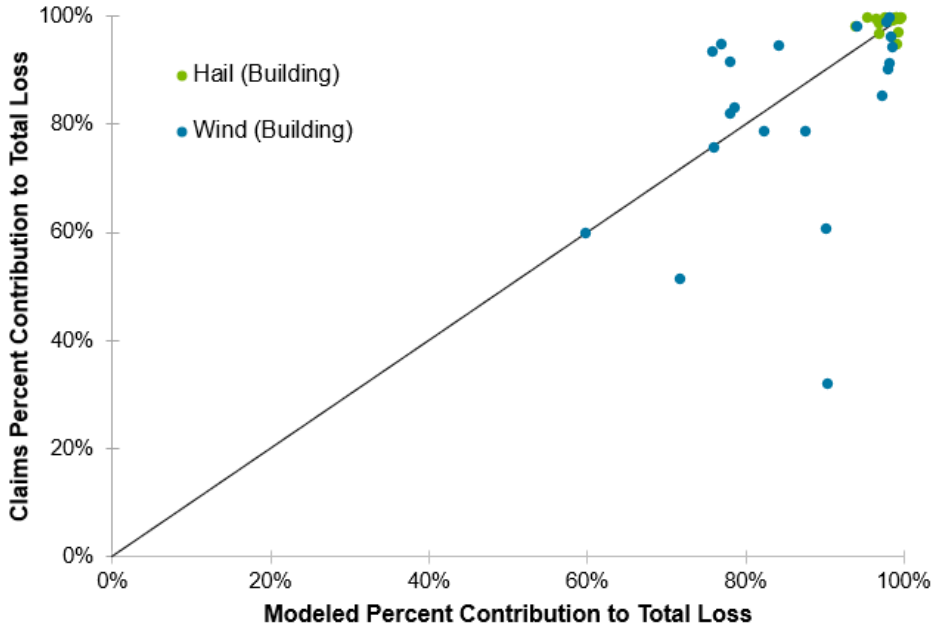

Figure 161. Verisk-modeled and company claims data percent contribution to total building (Coverage A) losses in the U.S. for hail (green dots) and for straight-line winds and tornadoes combined (blue dots)

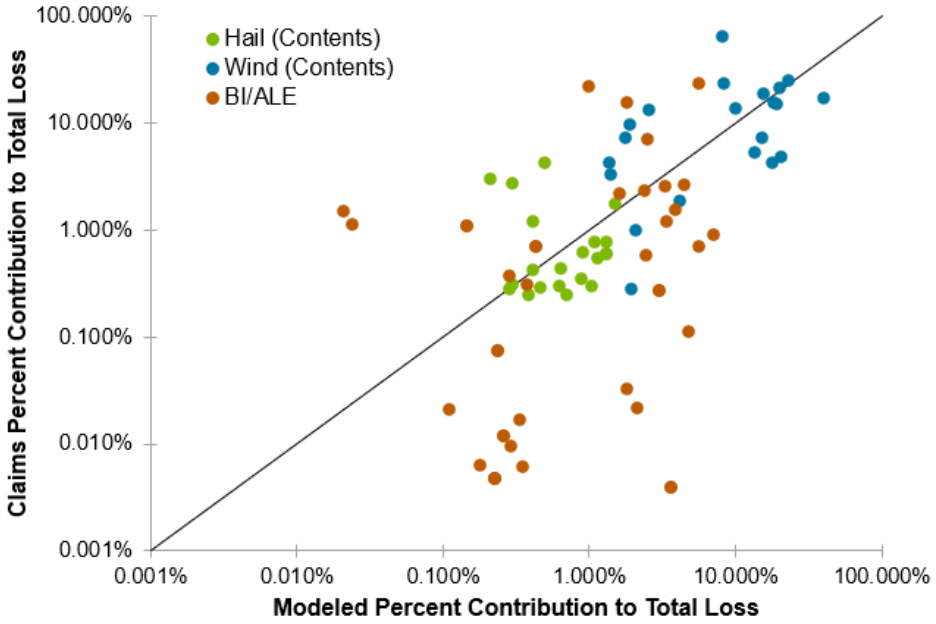

Figure 162. Verisk-modeled and company claims data percent contribution to total contents (Coverage C) and time element (BI/ALE; Coverage D) losses in the U.S. for hail and for straight-line winds and tornadoes combined

The availability of loss data for non-traditional risks is, unfortunately, quite lacking. In the absence of claims data, literature reviews, research, and engineering judgment were required

to determine the reasonability of damage functions. For example, the availability of data regarding tornado damageability of industrial facility components is very limited in existing literature. As a result, validation of component-level vulnerability functions was carried out by comparing modeled damage ratios with NOAA, HAZUS®, and historical damage data.

NOAA's team of meteorologists and wind engineers compiled a set of EF-Scale Damage Indicators for 28 types of structural and non-structural systems.[83] For each system, the indicators list damage states and the corresponding range of tornado wind speeds. These data were used to plot a range of indicative tornado damage ratios for select modeled industrial facility components. Figure 163 compares Verisk's tornado damage functions for industrial facility buildings with those computed using NOAA's EF-Scale Damage Indicators.

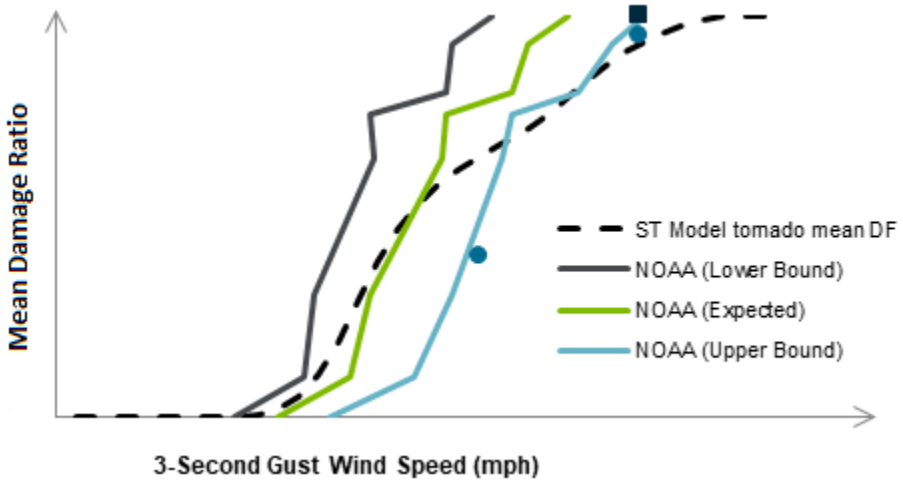

Figure 163. Validation of tornado damage function for industrial facility buildings

Similarly, FEMA's multi-hazard risk analysis platform's HAZUS® MH MR1 technical manual[84] contains replacement/repair costs and damage ratios corresponding to various damage states for numerous lifeline and industrial facility components, which can also be used as validation points for tornado damage functions. Figure 164 illustrates validation of the electrical substation damage functions with HAZUS® data as well as damage data for this component type from the EF-5 Memphis tornado in 2009, the EF-5 Joplin tornado in 2011, and the EF-2 Fox Valley tornadoes in 2008. The Verisk damage functions agree well with the observed data and existing damage studies.

[83] http://www.spc.noaa.gov/faq/tornado/ef-scale.html
[84] http://www.fema.gov/hazus

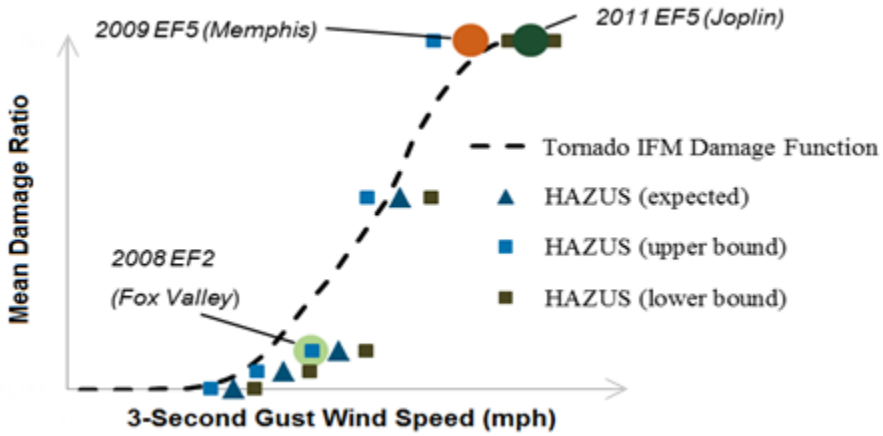

Figure 164. Validation of tornado damage functions for electrical substations

See Also

Tornado damage functions

Damage functions for building contents

6 Insured Loss Calculation

In this component of the Verisk Severe Thunderstorm Model for the United States, ground-up damage is translated into financial loss. Insured losses are calculated by applying policy conditions to the total damage estimates resulting from the damage estimation module. Policy conditions may include deductibles, coverage limits, loss triggers, and risk-specific reinsurance terms.

6.1 Aggregating losses probabilistically

Post-disaster surveys and actual claims data reveal an inherent variability in the damage that results from a given wind speed or hail impact energy. Loss estimates generated by the Verisk Severe Thunderstorm Model for the United States capture this variability by accounting for both primary and secondary uncertainty. Primary uncertainty derives from the uncertainty associated with the stochastic event generation process, while secondary uncertainty describes the uncertainty in damage resulting from a given event. This secondary uncertainty captures the uncertainty in damage and in the local intensity estimation. The uncertainty in building damage arises due to a degree of inherent randomness in the response of buildings of similar construction to a given intensity, as well as from variability in building characteristics, construction materials, and workmanship. The uncertainty in local intensity of the hazard can be attributed to unmodeled phenomena and local site factors.

Damage is calculated using damage functions that provide, for a given event intensity, a mean damage ratio (MDR) and a probability distribution around the mean that captures the variability in damage. The damage functions are used to produce, for each event, a distribution of ground-up loss by location and coverage. Limits, deductibles, and reinsurance terms are applied in the financial module to the ground-up loss distribution to produce gross and net loss estimates. Note that insured losses can accumulate even if the mean damage ratio is below the deductible, because some structures are damaged above the mean damage ratio and the deductible. The distributions are applicable to the analysis of a single exposure and, in this case, usually have a high degree of uncertainty. The individual distributions are combined to obtain the portfolio distribution, where the uncertainty relative to the mean is lower than that for a single exposure.

The financial module aggregates losses probabilistically at various levels. Specifically, computational techniques have been developed for statistically aggregating nonparametric distributions. That is, even though the ground-up, coverage-level damage distributions typically use parametric distributions, after the application of location and policy terms, the distributions cannot be represented in a parametric way. Further aggregations of such loss distributions are achieved using numerical algorithms.

Convolution is a method used to statistically derive the probability distribution of the sum of losses. The convolution of two independent random variables X and Y with discrete probability density functions p_X and p_Y, respectively, can be computed as:

$$p_S(s) = p_X \oplus p_Y = \sum_x p_X(x) p_Y(s-x)$$

where $S = X + Y$.

The Verisk models employ an efficient and accurate numerical algorithm for "convolving" any number of nonparametric loss distributions. Extreme care must be taken when combining distributions with differing loss sizes. This technique allows the shape of the loss distributions to be correctly represented throughout the financial loss estimation process. Preserving the right shape is particularly important when insurance terms apply to the tails of the distributions.

The financial module within Verisk's software applications allows for application of a wide variety of location, policy, and reinsurance conditions. Location terms may be specified to include limits and deductibles by site or by coverage. Supported policy terms include blanket and excess layers, minimum and maximum deductibles, and sublimits. Reinsurance terms include facultative certificates and various types of risk-specific and aggregate treaties with occurrence and aggregate limits. Please see product-specific documentation available, with login, on the Client Portal as well as details on the industry standard UNICEDE data format (www.unicede.com) for additional information.

See Also

Damage Estimation

6.2 Demand surge

Market forces generally ensure that the availability of materials and labor in any specific geographical area is sufficient to accommodate a normal level of demand without affecting price. However, demand can increase sharply and unexpectedly after a catastrophe. Sudden, widespread property damage can create extremely high demand for building materials and labor, which, in turn, causes prices to inflate temporarily. Demand for related services and resources, such as transportation, equipment, and storage, can also escalate in the affected area.

Scarce resources can also increase the time required to repair and rebuild damaged property, which may cause greater business interruption losses and additional living expenses. Infrastructure damage, delayed building-permit processes, and a shortage of available building inspectors also increase time element loss. These factors can lead to insured losses exceeding expectations for a specific event and portfolio, a phenomenon known as demand surge. The greater and more widespread the damage from an event, the greater the resulting demand surge and insured losses.

Verisk engineers and statisticians have developed a mathematical function that relates the amount of demand surge to the amount of modeled industry insurable losses from a specific event. This function was developed based on historical data, statistical analysis, economic time-series reviews, and analysis of construction-material and labor-cost data.

The demand surge function currently implemented in the Verisk software systems is the result of over 15 years of research and refinement. Verisk will continue to make

improvements as new data become available. For details on the methodology used to develop the Verisk demand surge function and its validation, please see the client-confidential technical document *Verisk U.S. Demand Surge Function*, which is available with login on the Client Portal.

6.3 Validating modeled losses

The losses produced by the Verisk Severe Thunderstorm Model for the United States are extensively validated against loss estimates issued by ISO's Property Claim Services (PCS), actual claims data consisting of company claims as well as ISO residential (2009-2018) data, and Xactware residential and commercial (1990-2018) data. Policy level claims data used for model development and validation includes over a decade of daily data, which is crucial for quantifying and validating both the cat and the non-cat components of the risk.

Industry loss validation by event

Validating industry event losses ensures a model's overall performance, and comparing historical and modeled losses is a critical component of model validation. Both industry losses (PCS) and policy level claims data are used to validate marquee events. When industry losses are used, PCS losses are trended to modern day values (2019) before comparing them to Verisk-modeled industry losses. Verisk's trending methodology accounts for inventory growth, labor and material costs, and inflation, among other factors. The modeled losses are obtained by running the Industry Exposure Database for the United States through the Verisk Severe Thunderstorm model for the United States. For a given event, the loss estimate issued by PCS represents the total losses from all event sub-perils; the Verisk model similarly reports losses using Verisk's own industry exposure for all sub-perils combined. When client losses are validated, client losses based on claims data are compared to client modeled losses calculated by running client exposure, as of the time of the event, through the Verisk Severe Thunderstorm model for the United States.

Figure 165 compares the Verisk-modeled and PCS-reported (trended to 2019 values) gross industry insured losses for selected historical severe thunderstorm outbreak events, where modeled losses from all states are included (Figure 165(a)) and where only modeled losses from states where PCS losses were reported (Figure 165(b)). Where losses from all states are included in the event totals, the model appears to be biased high (Figure 165(a)); however, there is reasonable agreement between the Verisk-modeled and PCS-reported industry insured losses when the Verisk modeled loss event totals include only the states for which PCS losses were reported (Figure 165(b)).

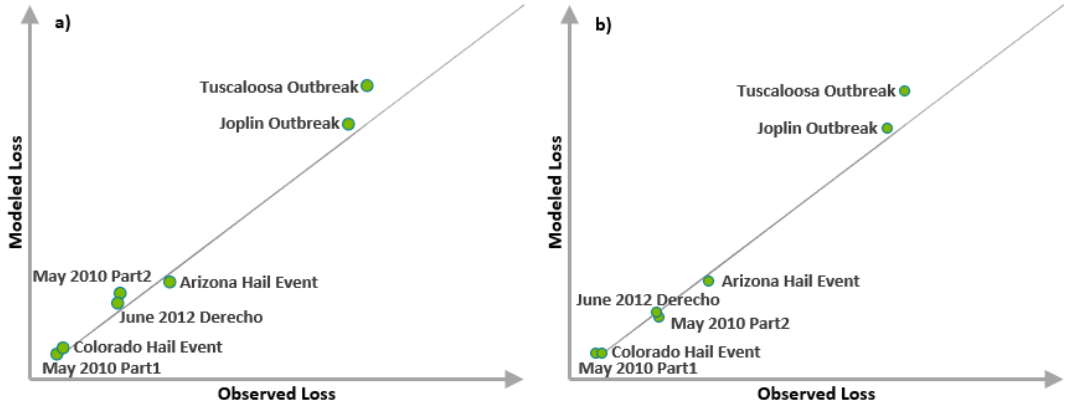

Figure 165. Comparison of Verisk-modeled and PCS (1988-2019; trended to 2019) industry gross insured losses for selected historical severe thunderstorm outbreak events in the United States
a) Comparison using modeled losses from all states, and b) Comparison using only modeled losses from states where PCS losses were reported

Figure 166 shows modeled losses compared to trended PCS-reported industry losses for all seven events in the marquee catalog. The modeled losses in this exhibit represent all modeled losses for all states included in the event as determined using historical data. While the marquee catalog contains five realizations of each marquee event, the losses presented in Figure 166 are for the median event. Additionally, the first two marquee events have been validated together because they occurred in rapid succession and in close proximity to one another, which made the claims difficult to separate. While the modeled and industry losses show good agreement, the modeled losses are notably higher than the industry losses for nearly all events. As evidenced by historical meteorological data, some modeled severe thunderstorm activity occurred outside of states where PCS industry-reported losses exist. When comparing trended industry losses to modeled losses using only states corresponding to those with PCS losses, the modeled and historical losses are in better agreement (Figure 167).

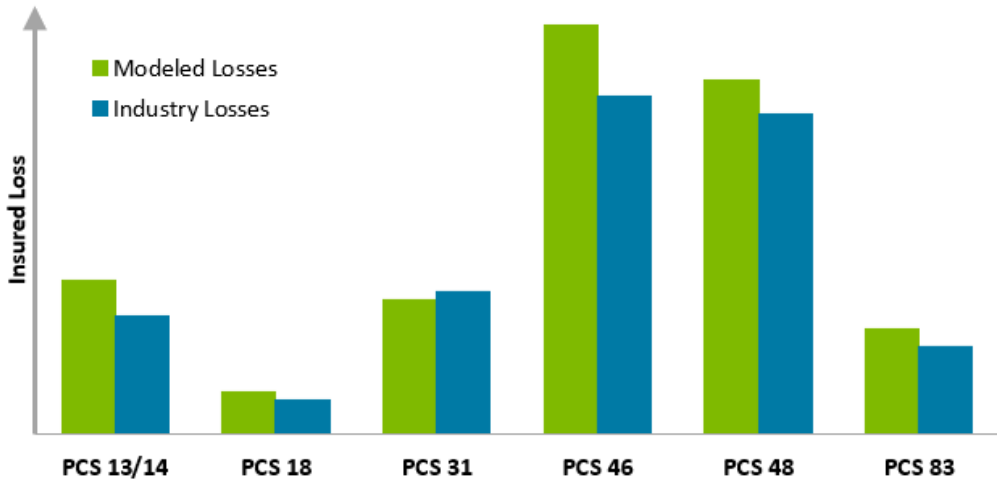

Figure 166. Modeled loss validation for all seven events in the marquee catalog

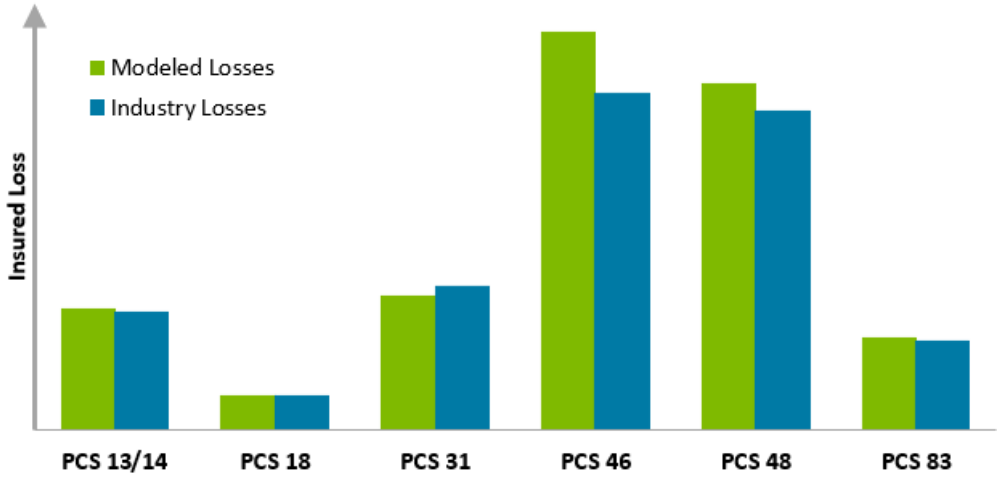

Figure 167. Modeled loss validation for states where PCS losses exist, for all seven events in the marquee catalog

Figure 168 shows the Verisk-modeled losses by sub-peril for the median of the five perturbations of each marquee event. Note that PCS does not subset losses by sub-peril; however, Touchstone users can calculate losses by sub-peril.

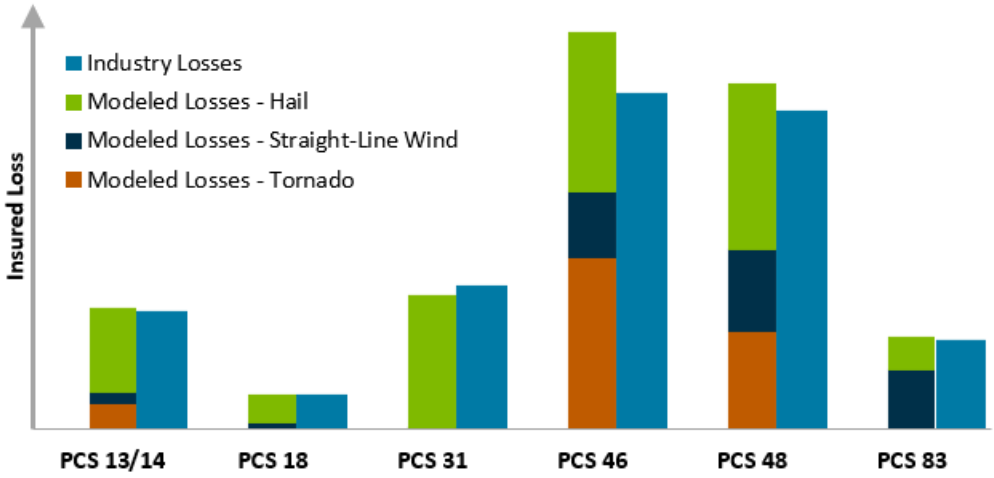

Figure 168. Verisk-Modeled loss validation for all seven events in the marquee catalog, by sub-peril

May 10 - 16, 2010 Outbreak

Validation for the May 10 - 16, 2010 Outbreak event was performed for all seven days combined, even though this "event" is a combination of two separate events in the marquee catalog. These two events were combined because they occurred in such rapid succession that it is extremely difficult to separate them, as evidenced by claims data.

Figure 169 compares Verisk-modeled to PCS-estimated (trended to 2019 values) industry losses, by line of business. As seen in these pie charts, the Verisk-modeled and PCS-

estimated loss breakdowns exhibit good agreement for this event. While the model may not show exact agreement with PCS losses, the breakdowns are similar and, hence, are well represented by the model for this event.

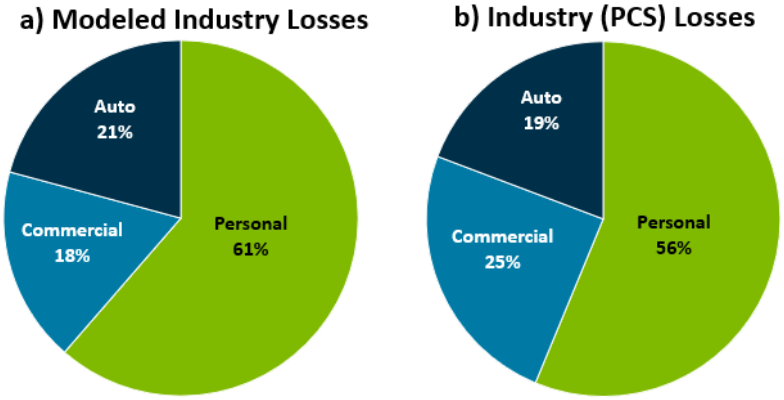

Figure 169. Modeled loss validation for the May 10 - 16, 2010 Outbreak, by line of business

Verisk-modeled and PCS-estimated industry losses for states most impacted by the May 10 - 16, 2010 outbreak are shown in Figure 170. The states with highest modeled losses are shown on the plot; states with lower losses are included as "All Other" states on the right-most bars. Overall, losses show reasonable agreement at the state level. Again, it is evident in this figure that not all states with severe thunderstorm activity had losses reported by PCS. In these cases, the modeled losses are shown on the figure without a PCS comparison.

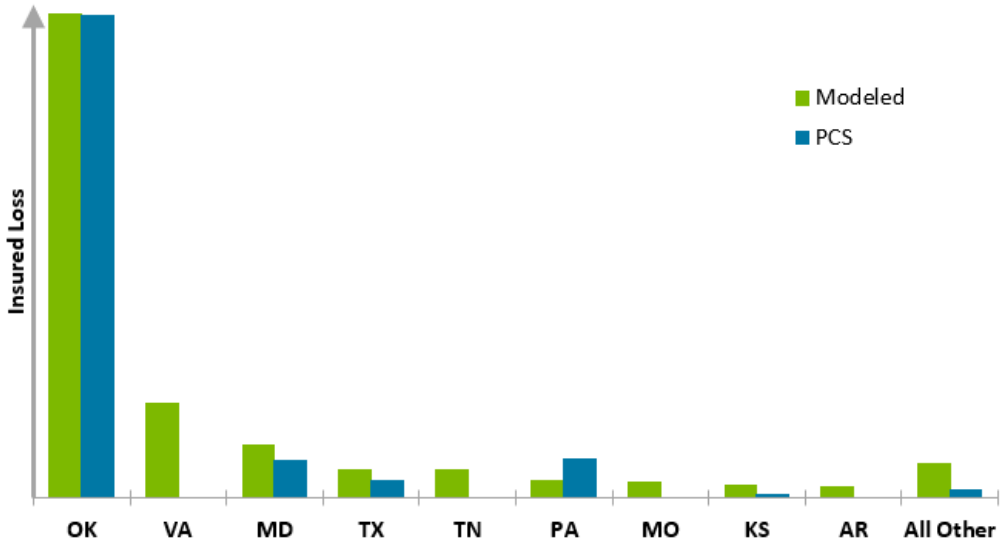

Figure 170. State-level modeled loss validation for the May 10 - 16, 2010 Outbreak

June 10 - 16, 2010 Outbreak

Industry loss validation for the June 10 - 16, 2010 Outbreak, also known as the Colorado Hail Event, is presented in this section. Figure 171 compares Verisk-modeled to PCS-reported

(trended to 2019 values) event-level industry losses, by line of business. As seen in these pie charts, the Verisk-modeled and PCS-estimated loss breakdowns exhibit good agreement for this event. While the model may not show exact agreement with PCS losses, the breakdowns are expected to be similar for individual events.

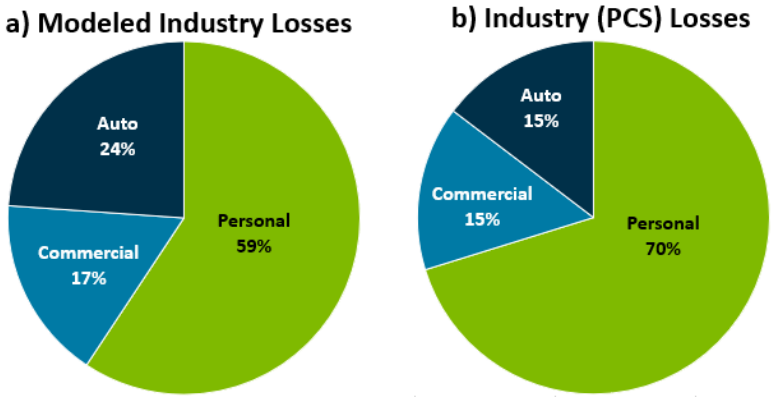

Figure 171. Modeled loss validation for the June 10 - 16, 2010 Outbreak, by line of business

Verisk-modeled losses and industry loss estimates for states most impacted by the June 10 - 16, 2010 Outbreak are shown in Figure 172. The states explicitly shown in this figure are those with the highest modeled losses. Losses from all other states are aggregated into the last set of bars on the right-hand side of the plot (i.e., "All Other"). It is evident that modeled and reported industry losses compare well at the state level and are relatively unbiased. Again, it is evident in this figure that not all states with severe thunderstorm activity had losses reported by PCS.

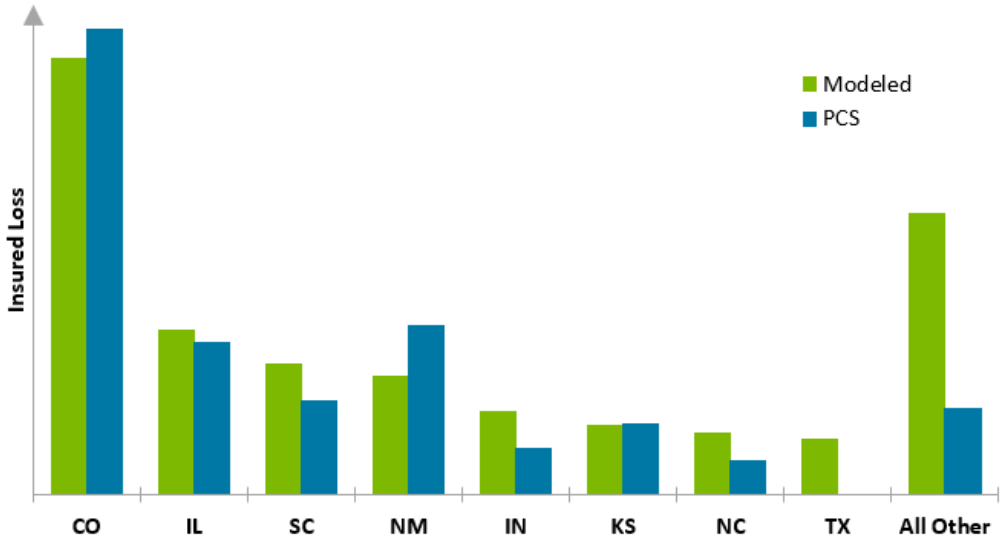

Figure 172. State-level modeled loss validation for the June 10 - 16, 2010 Outbreak

October 4 - 6, 2010 Outbreak

The October 4 - 6, 2010 Outbreak was a unique event in that it caused large losses, mainly due to hail, in primarily one state: Arizona. Since losses in other states were negligible, state-specific validation exhibits are not shown in this section. Figure 173 compares the Verisk-modeled to the 2019-trended PCS estimated event-level industry losses, by line of business. It is evident from these pie charts that the modeled and estimated loss breakdowns show relatively good agreement for this event.

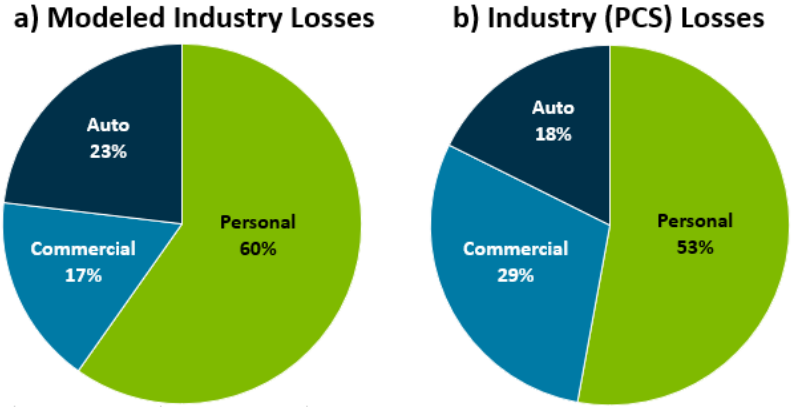

Figure 173. Modeled loss validation for the October 4 - 6, 2010 Outbreak, by line of business

April 22 - 28, 2011 Outbreak

Validation for the April 22 - 28, 2011 Outbreak, also referred to as the Tuscaloosa Tornado Event, was performed for industry losses. Figure 174 compares Verisk-modeled to PCS-reported (trended to 2019 values) event-level industry losses, by line of business, for all states. As seen in these pie charts, the Verisk-modeled and PCS-estimated loss breakdowns exhibit good agreement for this event. While the model may not show exact agreement with PCS losses, the breakdowns are similar and, hence, are well represented by the model for this event.

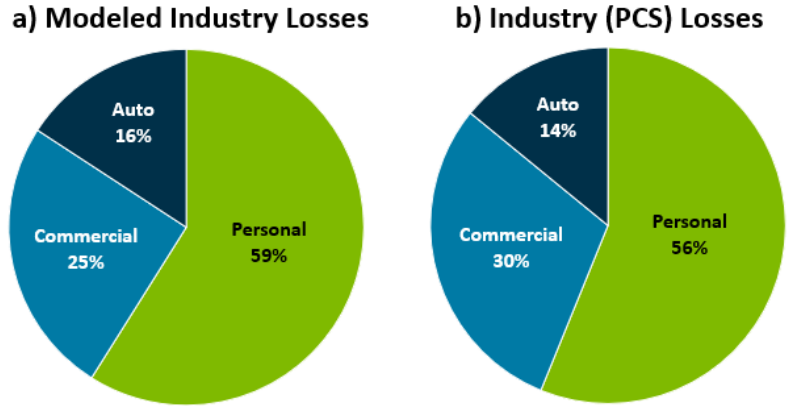

Figure 174. Modeled loss validation for the April 22 - 28, 2011 Outbreak, by line of business

Figure 175 shows the modeled and industry loss comparison, by state, for states with the highest modeled losses. States with lower losses are aggregated into the "All Other" bars on the right-hand side of the figure. Verisk-modeled and industry PCS-reported event losses match well.

Figure 175. State-level modeled loss validation for the April 22 - 28, 2011 Outbreak

May 20 - 27, 2011 Outbreak

Validation for the May 20 - 27, 2011 Outbreak, also referred to as the Joplin Tornado Event, was performed for industry losses. Figure 176 compares Verisk-modeled to PCS-reported (trended to 2019 values) event-level industry losses, by line of business. As seen in these pie charts, the Verisk-modeled and PCS-estimated loss breakdowns exhibit reasonable agreement for this outbreak event. While the model may not show exact agreement with PCS losses, the breakdowns are expected to be similar for individual events.

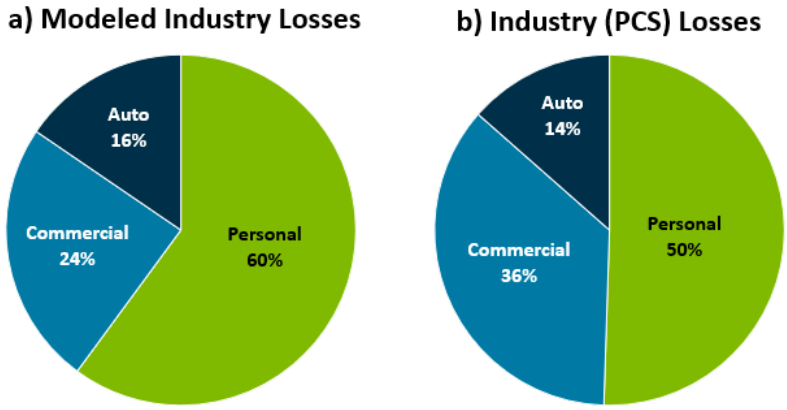

Figure 176. Modeled loss validation for the May 20 - 27, 2011 Outbreak, by line of business

When viewing the data by state (Figure 177), the Verisk model is unbiased. The states with the highest modeled losses are shown in Figure 177. Losses from additional states are aggregated and displayed in the rightmost bars labeled "All Other" states.

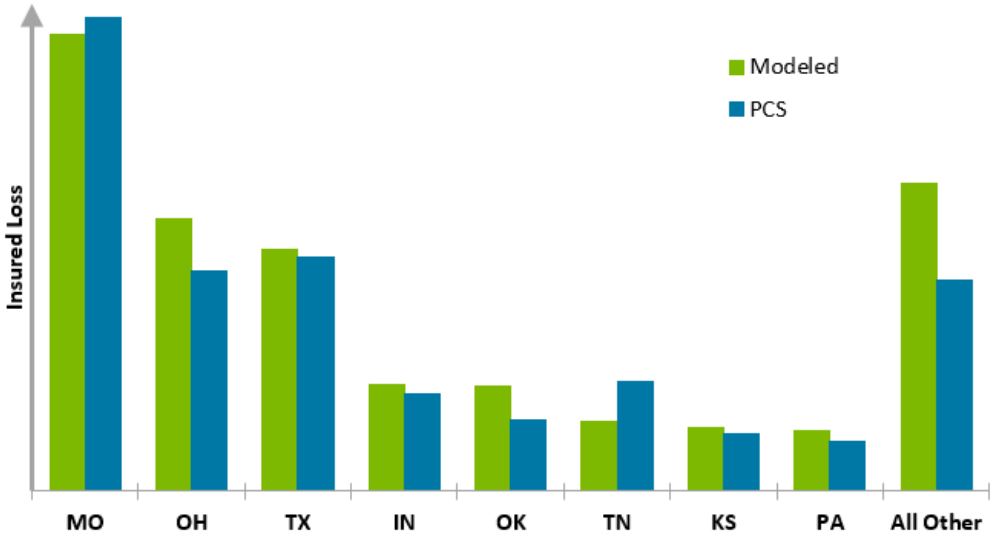

Figure 177. State-level modeled loss validation for the May 20 - 27, 2011 Outbreak

June 28 - July 2, 2012 Outbreak

Validation for the June 28 - July 2, 2012 Outbreak, also referred to as the "Super Derecho" event, was performed for industry losses. These Midwest and Mid-Atlantic region losses were primarily a result of straight-line wind damage, although severe hail also impacted these areas.

Figure 178 compares Verisk-modeled to PCS-reported (trended to 2019 values) event-level industry losses, by line of business. As seen in these pie charts, there is good agreement in coverage breakdowns between the modeled and PCS losses for this event.

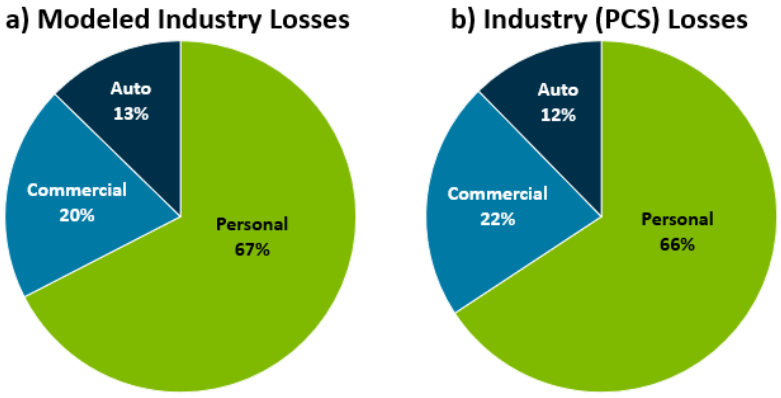

Figure 178. Modeled loss validation for the June 28 - July 2, 2012 Outbreak, by line of business

When examining the Verisk-modeled and PCS-reported industry losses by state (Figure 179), the Verisk model is relatively unbiased. The states with the highest modeled losses are shown in Figure 179. Losses from additional states are aggregated and displayed in the rightmost bars labeled "All Other" states.

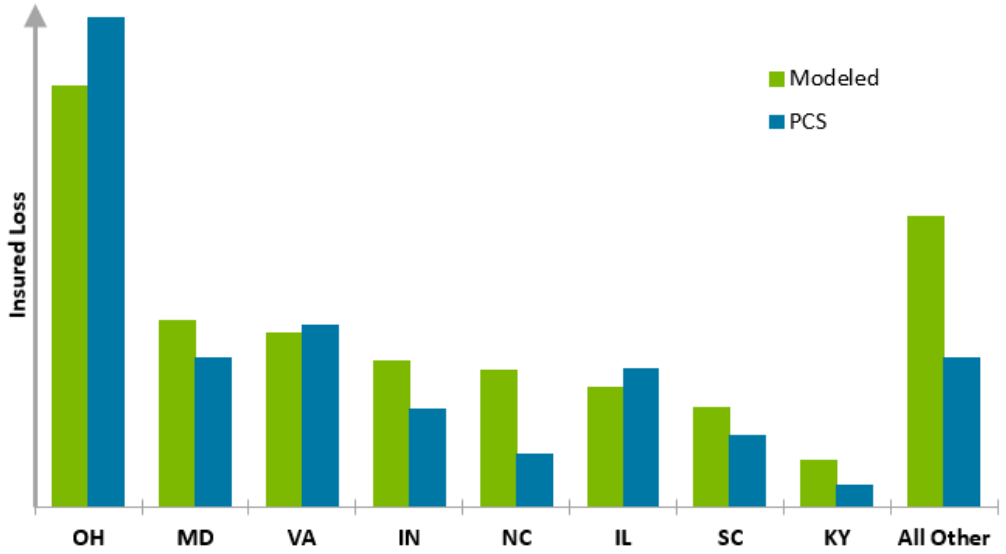

Figure 179. State-level modeled loss validation for the June 28 - July 2, 2012 Outbreak

Event loss validation using claims data

Validation was performed between Verisk-modeled and client gross losses based on claims data. Note that the modeled losses are based on exposure data provided by the client at the time of the event. Figure 180 shows modeled compared to claims losses for all client data, at the marquee event level. Good agreement is generally seen, and the model is relatively unbiased. When comparing modeled losses to claims by company and event (Figure 181), good agreement is still evident. Thus, the model is unbiased when evaluating across all companies and all marquee events.

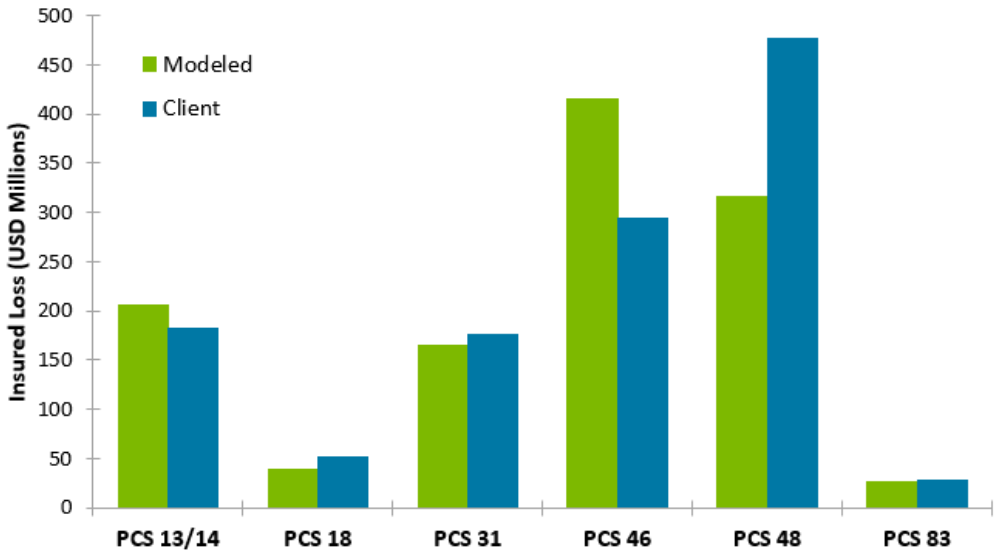

Figure 180. Modeled loss validation for all seven events in the marquee catalog using claims data

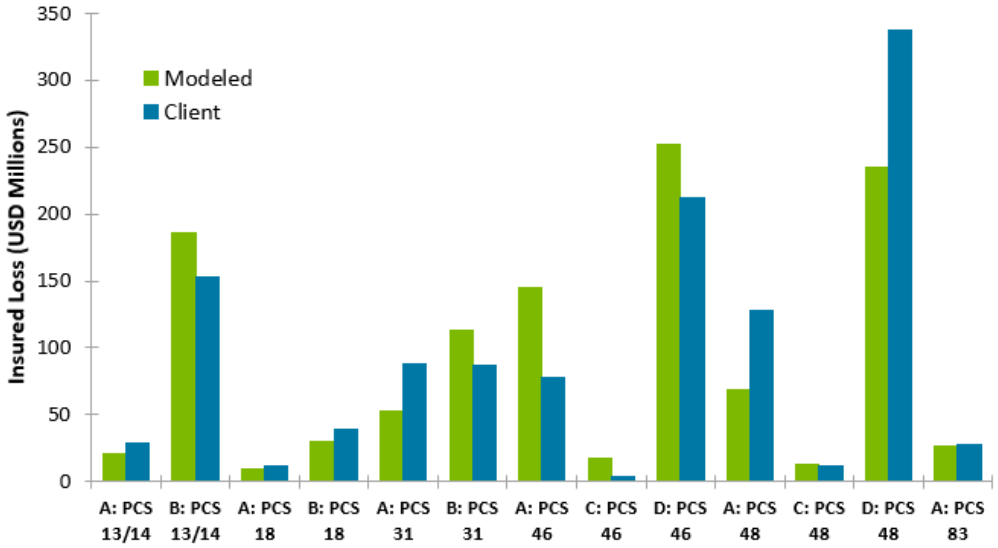

Figure 181. Modeled loss validation for all seven events in the marquee catalog using claims data, by client

Loss validation using exceedance probabilities

Verisk-modeled losses due to severe thunderstorm hail, straight-line winds, and tornadoes are validated using 1988 - 2019 PCS industry and 1998 - 2019 PCS line-of-business insured loss data trended to 2019 USD. Due to differences in survey procedures, loss thresholds, and underreporting, PCS data prior to 1988 were not used. Due to great uncertainty in the historical loss data at higher return periods, Verisk researchers concentrated their validation efforts within the 2-year to 10-year return periods using 32 years of PCS insured loss

estimates. Annual occurrence losses are well-captured by PCS data because these losses represent the maximum event loss in a given year. However, annual aggregate losses may be significantly underestimated by PCS events due to the limited PCS dataset and the changing industry-defined catastrophic loss threshold over time.

Verisk-modeled losses due to severe thunderstorm hail, straight-line winds, and tornadoes are also validated using 2009 - 2019 ISO and Xactware claims data trended to 2019. These data are used to estimate the non-PCS industry insured loss. ISO residential claims data (excluding tenants/condos) are available for all states except Texas at the ZIP Code level, and Xactware residential and commercial claims data are available for all states at the ZIP Code level. These claims are tagged to a PCS event, if possible, based on the date and cause of loss. Claims not associated with a PCS event are tagged as non-PCS. These data are used to create an aggregate view of industry losses that captures losses from both events reported by PCS and lower-loss events.

The ISO and Xactware data were also used to create scaling factors to further adjust the PCS-based AALs and aggregate EP curves, to account for non-PCS losses, and create "industry" EP curves. To perform this adjustment, Verisk researchers first calculated two AALs for each state: one AAL from PCS events, and one AAL from non-PCS events. Then, for each state, Verisk researchers determined the average ratio of AAL from non-PCS events to the AAL from PCS events. Next, for each state, for each line of business, the PCS AAL was multiplied by this ratio to yield a scaled AAL that accounts for non-PCS loss. Next, for each state and line of business, the difference between the scaled AAL and the PCS AAL was calculated. This difference, which represents aggregate loss captured by non-PCS events, was added to the PCS aggregate exceedance probability losses at each return period, to yield industry aggregate exceedance probability curves.

Figure 182 compares the Verisk-modeled and industry gross insured aggregate losses for the United States by AAL for all lines of business combined, as well as for the personal, commercial, and automobile lines of business. There is reasonable agreement between the Verisk-modeled and industry AALs across all lines of business.

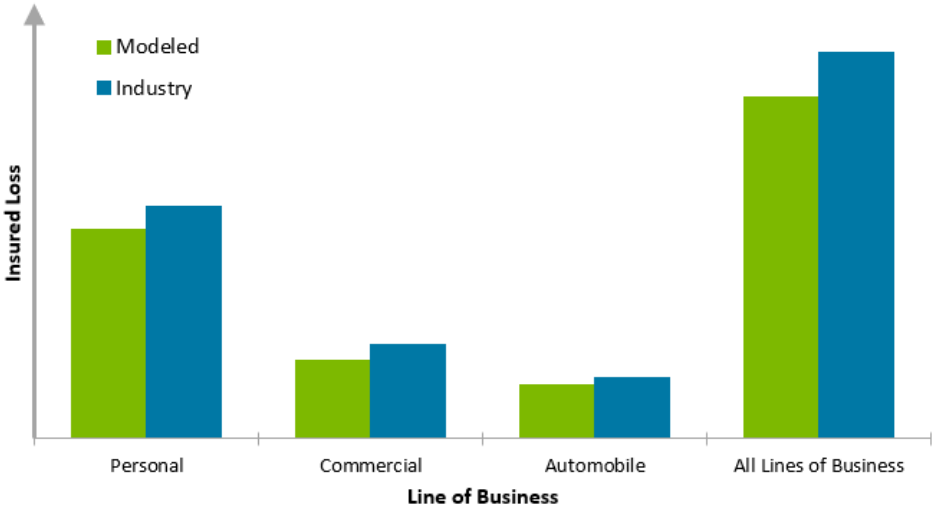

Figure 182. Comparison of Verisk-modeled and industry (1988-2019; trended to 2019) gross insured aggregate average annual losses (AAL) for the United States, for various lines of business

Figure 183, Figure 184, Figure 185, and Figure 186 compare the Verisk-modeled industry gross insured occurrence losses for the United States by return period and average annual occurrence losses (AOL) to that of PCS for all lines of business combined as well as for the personal, commercial, and automobile lines of business, respectively. There is reasonable agreement between the Verisk-modeled and PCS-reported industry occurrence return period losses across all lines of business.

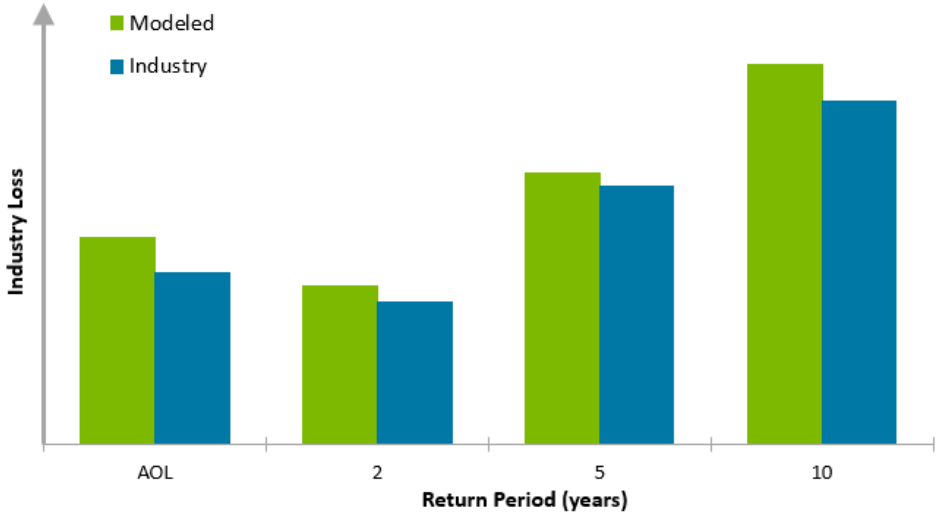

Figure 183. Comparison of Verisk-modeled and PCS (1988-2019; trended to 2019) industry gross insured average annual occurrence losses (AOL) and occurrence return periods (years) for the United States, for all lines of business

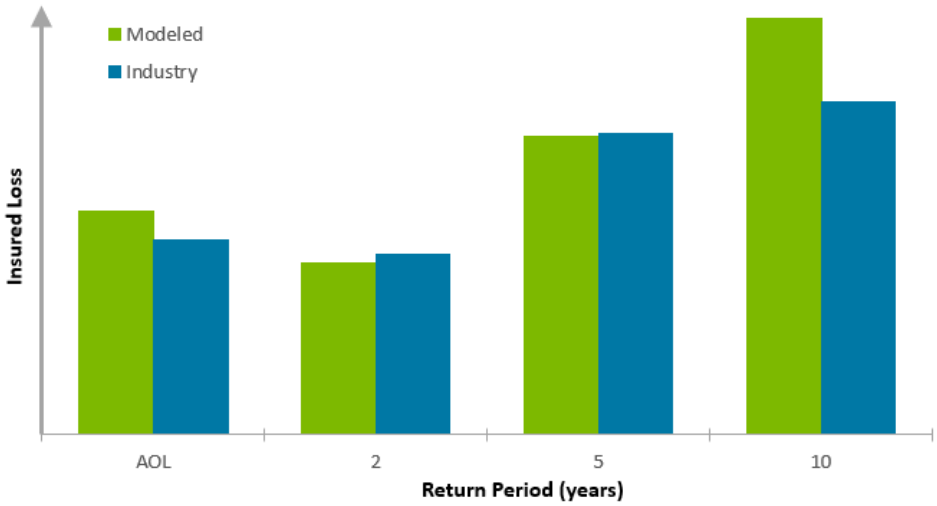

Figure 184. Comparison of Verisk-modeled and PCS (1988-2019; trended to 2019) industry gross insured average annual occurrence losses (AOL) and occurrence return periods (years) for the United States, for the personal line of business

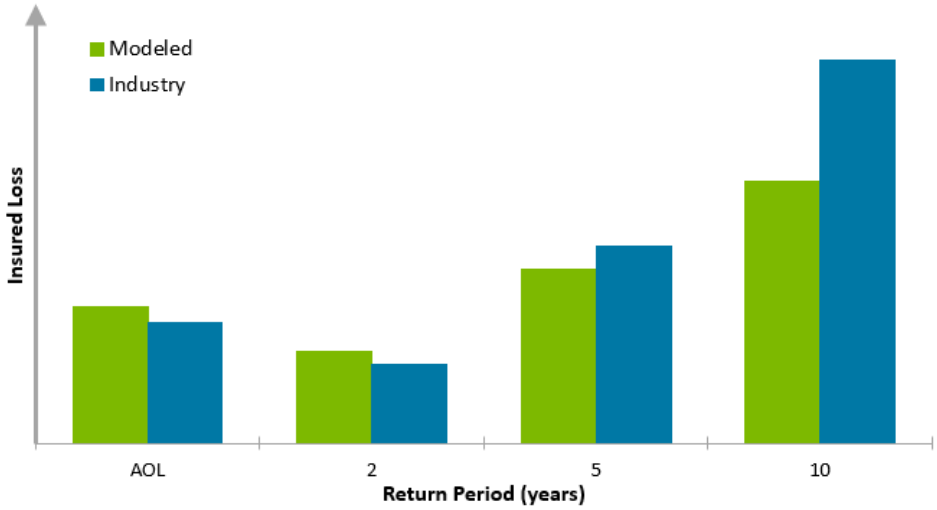

Figure 185. Comparison of Verisk-modeled and PCS (1988-2019; trended to 2019) industry gross insured average annual occurrence losses (AOL) and occurrence return periods (years) for the United States, for the commercial line of business

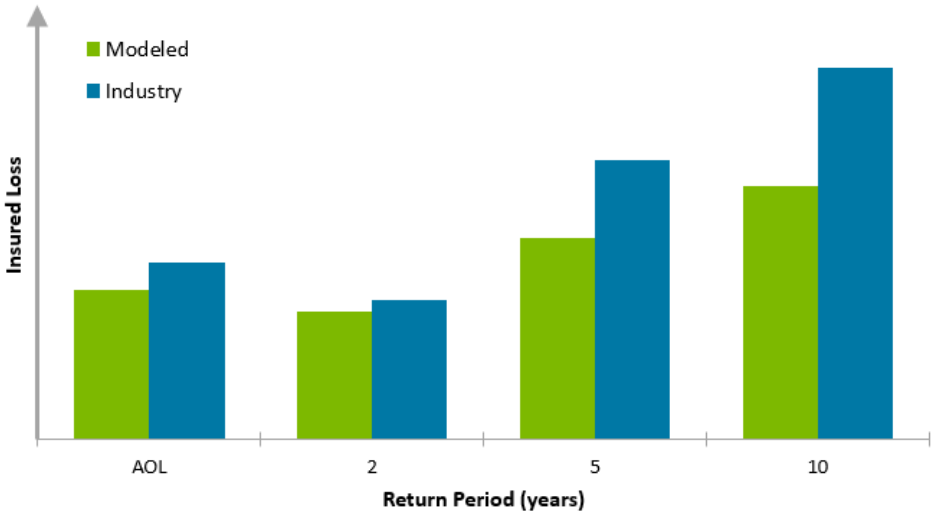

Figure 186. Comparison of Verisk-modeled and PCS (1988-2019; trended to 2019) industry gross insured average annual occurrence losses (AOL) and occurrence return periods (years) for the United States, for the automobile line of business

Verisk researchers benchmarked the predicted frequency of losses that result from simulated storms as captured in the stochastic catalog. While Verisk's stochastic catalogs tend to reflect the long-term view of severe thunderstorm risk in the United States, the reasonability of the modeled loss frequencies can be evaluated using available data for recent historical events. For example, Figure 187 compares the Verisk-modeled industry gross insured average AOL and occurrence return periods to observed industry gross insured return period losses for selected historical severe thunderstorms in the United States. These losses include all perils combined and all lines of business combined.

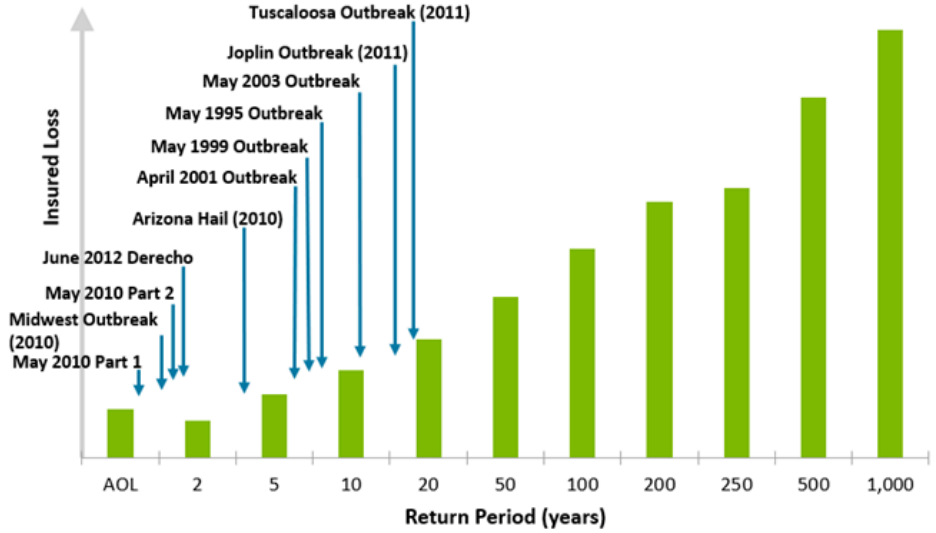

Figure 187. Comparison of Verisk-modeled industry gross insured average annual occurrence losses (AOL) and occurrence return periods (years) to observed industry gross insured return period losses for selected historical storms in the United States (all perils combined, all lines of business)

7 Accounting for Climate Change

Climate change affects extreme weather events (Stott, 2016). To account for these effects, Verisk incorporates the current and near-current climate (the last 30 years) into its catastrophe models. For the Verisk Severe Thunderstorm Model for the United States, Verisk researched how severe thunderstorm hail, straight-line wind, and tornado events have changed and will change to incorporate how the Verisk model captures these trends.

Detecting and attributing climate change impacts on various weather phenomena is a relatively new branch of climate science that is growing in demand and sophistication. Attribution confidence depends on many factors, including:

- how robustly climate models simulate impacts;
- whether the climate models agree with one another;
- whether there is a detectable trend in the historical data that agrees qualitatively with the modeled future result; and
- how well we can physically connect and understand the modeled or observed effect on climate.

Figure 188 shows the relative degree of confidence scientists have in ascribing climate change impacts to individual weather events. Temperature phenomena are most confidently assessed because of the direct physical connection between increasing carbon dioxide (and other greenhouse gases) and a warming atmosphere.

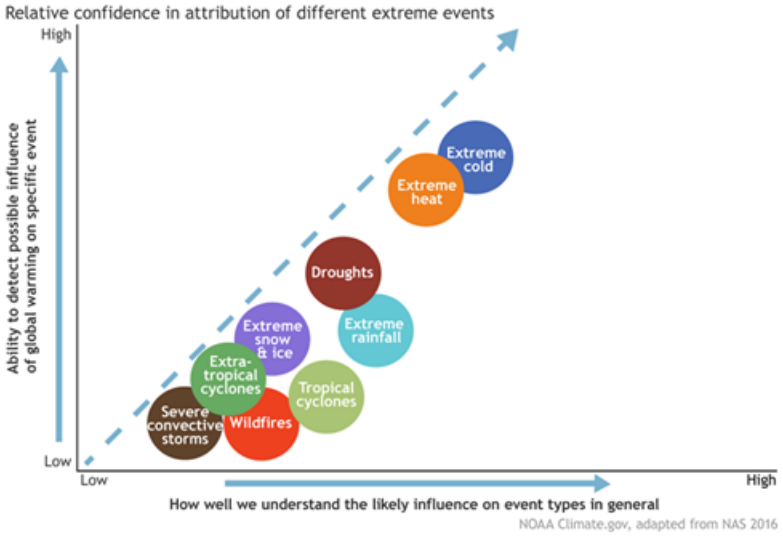

Figure 188. Relative degree of confidence that climate change is impacting various weather phenomena. (Source: NOAA climate.gov)

There is less confidence that climate change is impacting severe thunderstorms (i.e., severe convective storms) relative to other types of weather phenomena (such as extreme heat/ cold). Reasons for this low confidence include:

- their relatively small spatial scale (i.e., typically less than 1,000 km), which climate models cannot explicitly resolve;
- their dependence on subtle changes in the environment in which they grow (e.g., planetary boundary layer inversions);
- a historical record with changes in observational uncertainty over time, particularly associated with population biases in reports; and
- the inherently nonlinear physics driving these events.

7.1 Global climate models and reanalysis datasets

Even though severe thunderstorms and their sub-peril components cannot be explicitly resolved, global climate models (GCMs) can resolve the larger-scale environmental conditions favorable for their development over a reasonably long time period. These environmental factors can be used as proxies for severe thunderstorm development and include temperature and moisture vertical profiles (i.e., lapse rates), the change in wind speed and direction with height (i.e., vertical wind shear), and convective triggering mechanisms (e.g., cold fronts). These favorable environments can be quantified using various parameters, including convective available potential energy (CAPE), vertical wind shear, moisture advection, and freezing level. By analyzing changes in these quantities over time, the extent to which climate change and/or natural variability may be playing a role in these trends can be examined. However, it is important to keep in mind that even with increasingly favorable environmental conditions, these conditions are only proxies for severe thunderstorm development. Thus, changes in these parameters do not necessarily imply the same changes in severe thunderstorm characteristics over time. In addition, reanalysis datasets have their own uncertainties due to their numerical modeling component as well as the temporal evolution of the data used to produce these datasets (e.g., satellite-derived data used in reanalyses began in 1979). Nonetheless, many studies use GCMs to examine the potential impact climate change may have on U.S. severe thunderstorm frequency and intensity.

Using GCMs and a high-resolution regional climate model to compute CAPE and 0-6 km vertical wind shear, Trapp et al. (2007) examined the potential change in U.S. severe thunderstorm frequency due to climate change. They concluded that the number of days with severe thunderstorm environments (NDSEV) throughout the continental U.S. by the late 21st century is projected to increase. Large increases in CAPE, which are favorable for severe thunderstorm development, are found across much of the eastern two-thirds of the country, with the greatest increases (by as much as 500 J/kg) occurring across the Southeast during the summer months. Decreases in vertical wind shear, which are unfavorable for organized severe thunderstorms, are greatest across the central latitudes of the U.S., with increases seen over the northern Great Plains and along the U.S.-Mexico border. While this reduction in vertical wind shear is evident, the authors conclude that the large increase in CAPE far outweighs the amount of decreased shear in this study. The net result is a predicted increase

in the NDSEV across much of the continental U.S., with the greatest increase evident across the southern and eastern U.S. during the summer months.

More recently, Diffenbaugh et al. (2013) used daily CAPE and both low-level (0-1 km) and deep-layer (0-6 km) vertical wind shear output from the Coupled Model Intercomparison Project, Phase 5 (CMIP5) General Circulation Model ensemble to analyze NDSEV across the continental U.S. Their results (Figure 189) show appreciable increases in the NDSEV across the eastern half of the U.S. and significant increases in CAPE across the continental U.S. during all seasons by the late 21st century under a Representative Concentration Pathway 8.5 (RCP8.5) greenhouse gas concentration trajectory scenario. A large percentage of the NDSEV in their study is associated with high CAPE coupled with strong low-level vertical wind shear and low convective inhibition. In contrast, weak vertical wind shear days are often coupled with low CAPE days. These findings support the theory that increased CAPE likely results in increased NDSEV, despite decreased vertical wind shear, due to surface heating and increased moisture having a significant impact on increasing the thermal instability of air parcels near the ground.

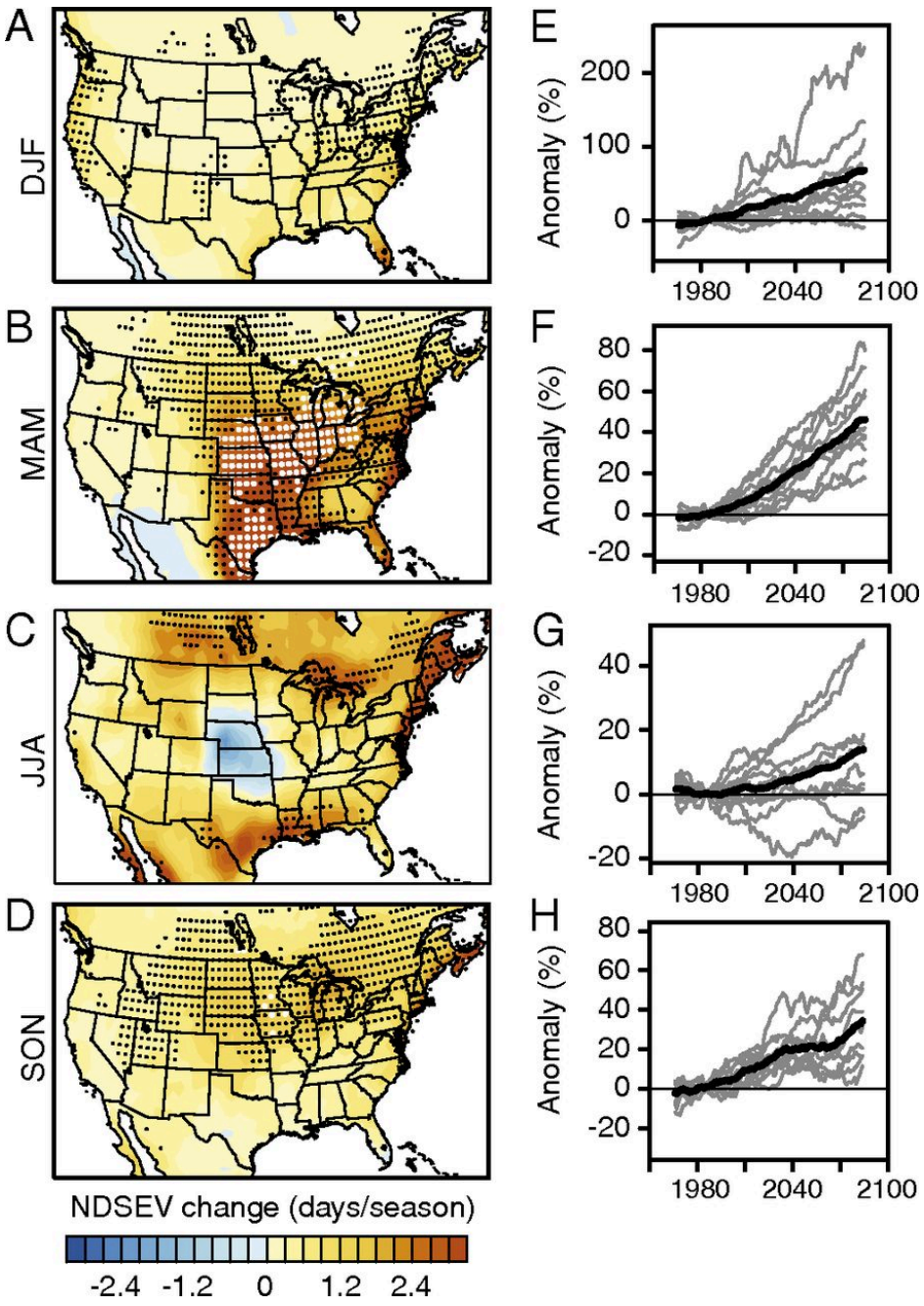

Figure 189. Projected change in NDSEV by the late 21st century using an RCP8.5 scenario during A) winter (December - February; "DJF"), B) spring (March - May; "MAM"), C) summer (June - August; "JJA"), and D) fall (September - November; "SON").
The warm (cool) colored areas for the panels on the left (A-D) represent an ensemble model mean positive (negative) NDSEV change between RCP8.5 period 2070-2099 and the baseline period 1970-1999. Robust (highly robust) changes (i.e., areas where the ensemble signal is >1 (>2) standard deviation(s) above the ensemble noise) are indicated by the black (white) dots. The anomaly (as a percent of the 1970-1999 baseline mean value) in the eastern regional (i.e., land area within a 105–67.5°W, 25–50°N box) average NDSEV value is plotted for each

individual model run as gray lines in the panels on the right (E-H). The black line in these plots represents the mean value of the individual model runs (Source: Diffenbaugh et al., 2013).

In addition to using GCMs to predict future changes, other studies use reanalysis datasets to assess changes in severe thunderstorm activity that have occurred to date using relevant environmental parameters. For example, Koch et al. (2021) used the North American Regional Reanalysis (NARR) dataset to examine changes in CAPE, 0-3-km storm relative helicity (SRH), and PROD (i.e., a parameter based on CAPE and SRH, where PROD = $(CAPE)^{1/2}$ x SRH (in m^3/sec^3)) maxima from 1979 to 2015 within an area spanning from -110° to -80° longitude and from 30° to 50° latitude. Since large/extreme values of CAPE, SRH, and PROD represent environments favorable for severe thunderstorm development, the authors examined extreme CAPE, SRH, and PROD values to see if any temporal trends in these data exist. Their results show that severe thunderstorm risk is increasing across portions of the central U.S., an area already particularly prone to severe thunderstorms, during April and May. They found non-negligible increases in PROD maxima in April, May, and August, in CAPE maxima in April, May, and June, and in SRH maxima in April and May. The April PROD spatial and temporal maxima trends are shown in Figure 190. (Note that a subsetted geographical area encompassing northeast Texas, northern Louisiana, southern Nebraska, southern Iowa, and much of Kansas, Oklahoma, Missouri, and Arkansas was used to calculate the region-averaged April PROD maxima time series plot in the figure).

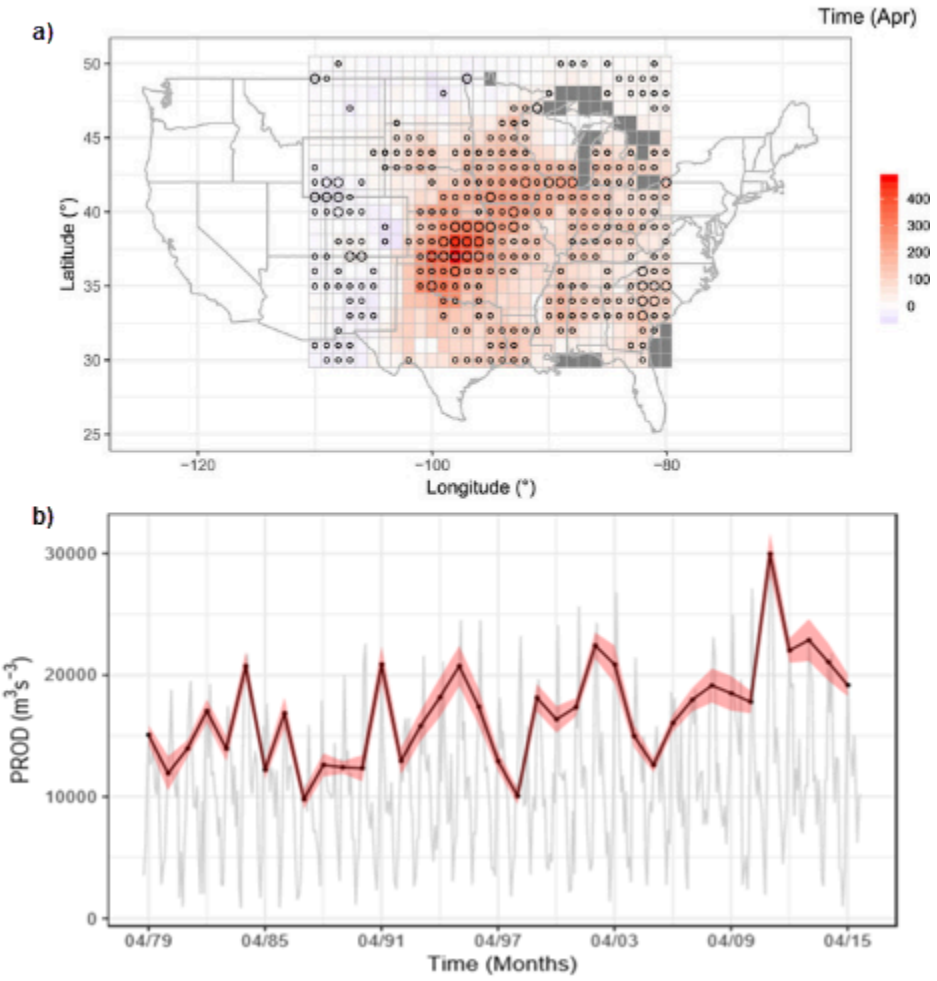

Figure 190. April PROD a) spatial and b) area-averaged temporal maxima trends from 1979 to 2015 using the NARR dataset.
The shading in the top figure indicates the magnitude of the slope over the analysis period, and the large (small) circles indicate statistical significance at a p=0.05 (p=0.20). The black line in the bottom figure represents the area-averaged April maxima time series, the red shaded region indicates its 95% confidence interval bounds, and the gray lines represent the area-averaged monthly maxima time series for all 444 months (Adapted from: Koch et al., 2021; CC BY-SA 4.0).

While regional reanalysis datasets provide insight into past environments favorable for severe thunderstorm development, and global climate modeling studies provide the best estimates of future impacts on severe thunderstorm activity, the more relevant challenge for catastrophe risk modeling is quantifying the effects of climate change that has occurred already on current severe thunderstorm risk. Given the magnitude of the GCM-simulated changes expected by late this century, one may expect that non-negligible changes are already occurring. As a result, many studies have analyzed trends in severe thunderstorms thus far. The noted limitations in observational records, including regional variations in observational quality and quantity, make it difficult to determine whether any observed trends

are robust or meaningful. As a result, trends in both environmental and observational sources are discussed in this chapter to provide a comprehensive analysis of the extent to which climate change may be impacting U.S. severe thunderstorm activity.

See Also

Atmospheric indices

7.2 Historical trends

Historical trends in hail activity

The effect of climate change on hail frequency has received much attention, not just in the U.S. but also globally, due to hail's high frequency of occurrence and the resulting amount of hail damage sustained worldwide. Unfortunately, observed hail report data are adversely affected by significant population biases and suffer from a relatively short observational record. Thus, the extent to which climate change plays a role in any temporal trends seen in the observed data is difficult to determine. To minimize these population biases and isolate temporal trends due to climate change and/or natural variabilities, many studies analyze temporal trends in hail days (i.e., days containing at least one report of hail) instead of the raw hail reports themselves. Results from these studies have generally found no overall trend in U.S. hail frequency over time but, on a regional level, some statistically-significant increases in hail frequency may exist.

As seen in Figure 191 and Figure 192, Verisk researchers analyzed time series of annual 1-inch or greater and 2-inch or greater hail days, respectively, across the contiguous U.S. along with U.S. population from 1955 to 2018. It is evident from both plots that there is an upward (i.e., increasing) trend in hail days until around 1990, after which the total hail days are relatively stable. Plotting a ratio of the two (not shown) indicates that the proportion of 2-inch or greater hail days to 1-inch or greater hail days has increased slightly since 1990. The stability of the hail day frequency record since 1990 is consistent with other studies (e.g., Allen and Tippett, 2015) and suggests there is no observed temporal trend in the overall U.S. hail frequency.

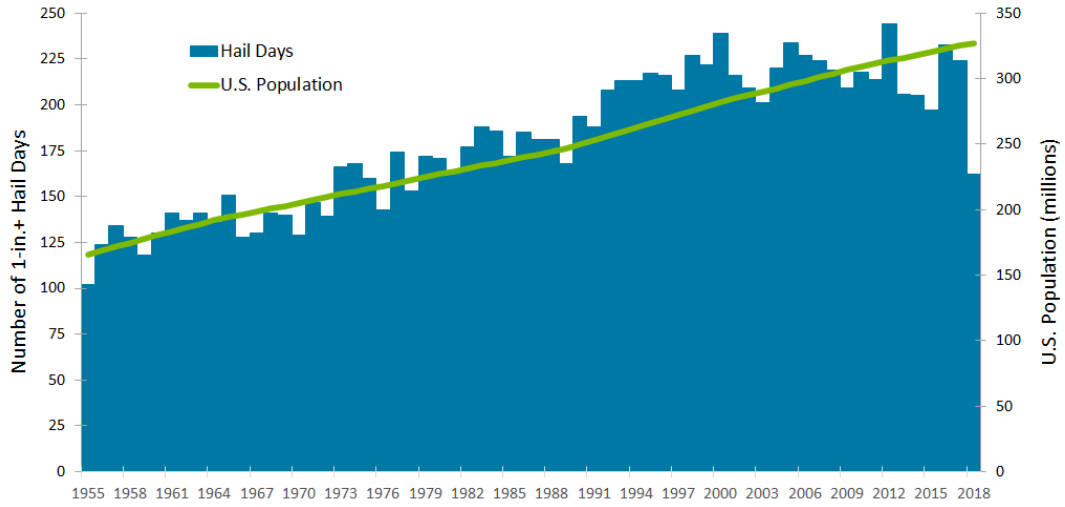

Figure 191. Number of 1-inch or greater hail days (blue bars) and population (green line) across the contiguous U.S. from 1955 to 2018 based on SPC's Storm Reports database

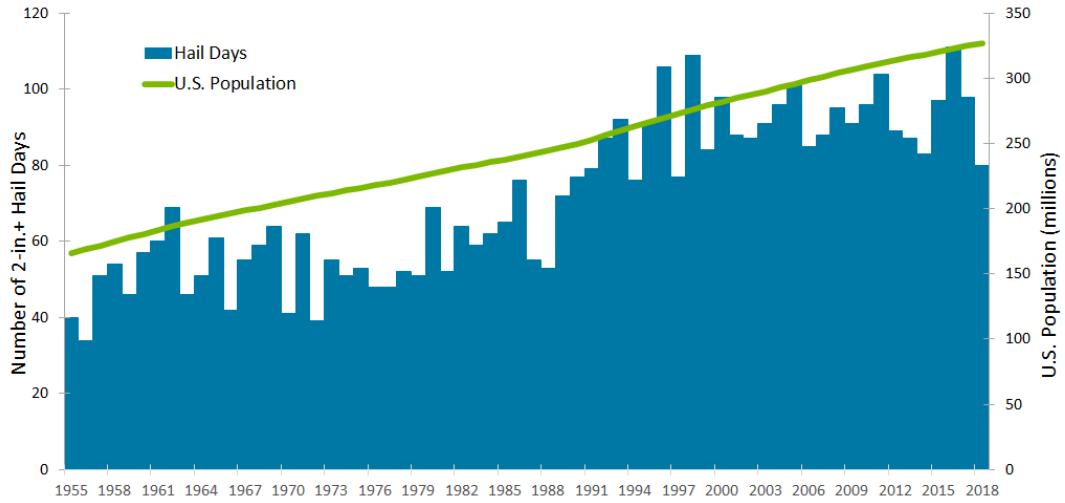

Figure 192. Number of 2-inch or greater hail days (blue bars) and population (green line) across the contiguous U.S. from 1955 to 2018 based on SPC's Storm Reports database

On a regional level, Verisk researchers have found hail frequency trends unrelated to population biases, which is consistent with other studies (e.g., Tang et al. 2019). For example, Verisk researchers compared the mean annual number of 1-inch or greater hail days in 1990 to the mean annual number of hail days in 2018, by state, (Figure 193 and Figure 194, respectively), which were calculated using a best-fit curve through the 1990-2018 time series of SPC reports in each state. Hail days were once again used instead of hail reports to reduce population biases in the observed data. The numbers in red in Figure 194 represent statistically-significant changes from 1990 to 2018, as determined by a two-sided t-test with a confidence of 95%. As seen in Figure 193 and Figure 194, relative changes are largest in states along the west and east coasts; some of these changes are primarily a result of the

low overall numbers in these states. Four southern states (Texas, Oklahoma, Louisiana, and Florida) show a decrease in hail days from 1990 to 2018 but, apart from Louisiana, these changes are statistically insignificant. Due to the relatively short observational record, it is difficult to draw any conclusions in longer-term regional severe hailstorm trends based on these results alone.

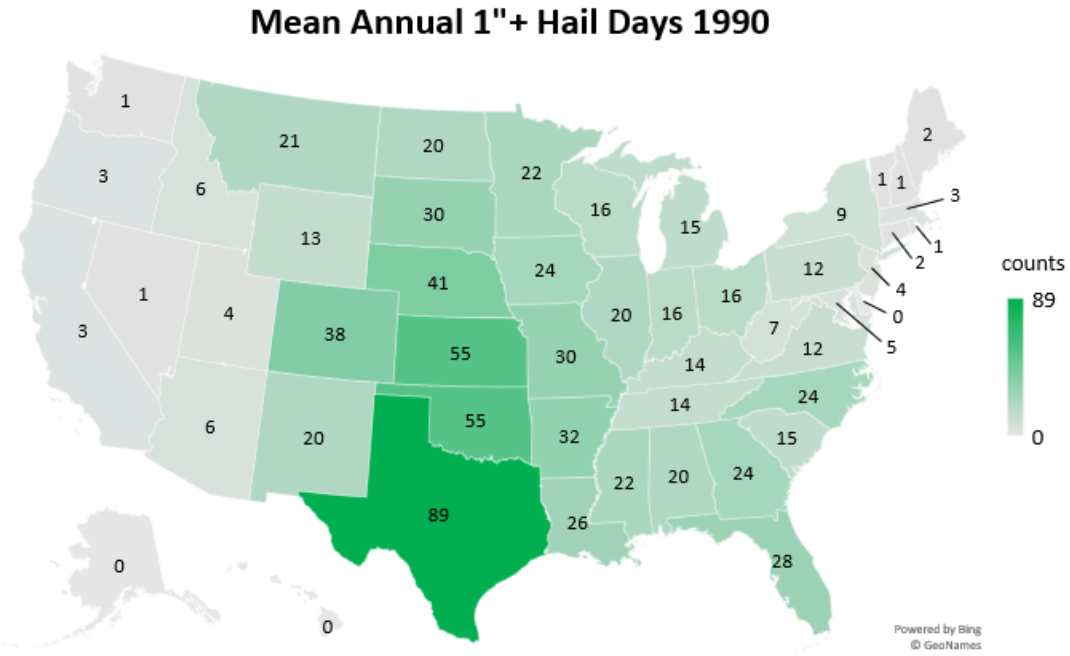

Figure 193. Mean annual number of 1-inch or greater hail days in 1990 based on values along a best-fit line through the 1990-2018 times series of SPC reports in each state.

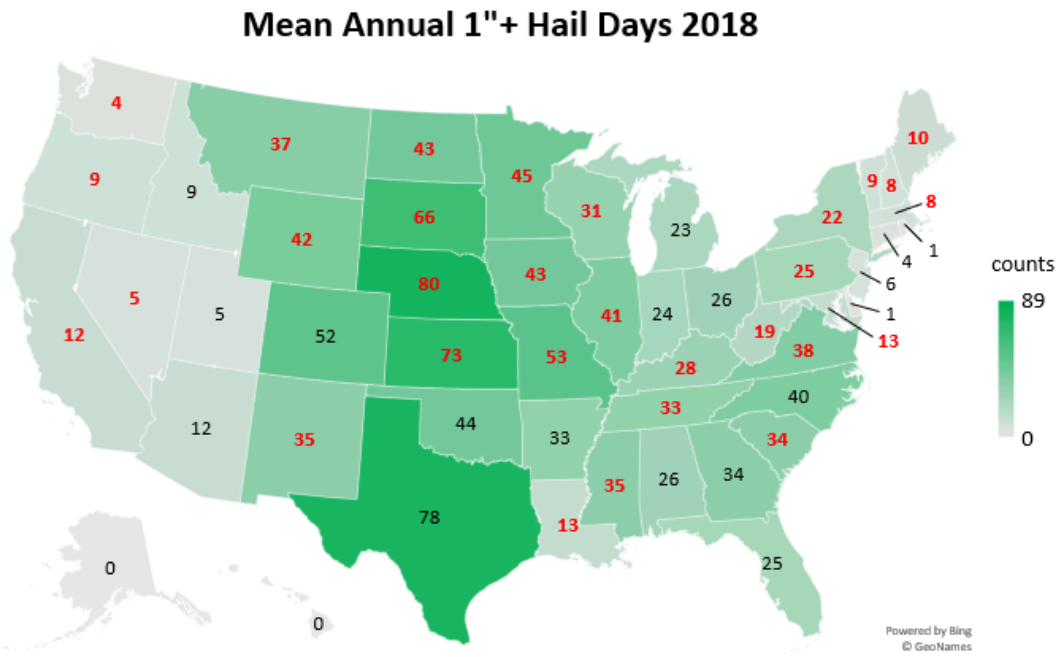

Figure 194. Mean annual number of 1-inch or greater hail days in 2018 based on values along a best-fit line through the 1990-2018 times series of SPC reports in each state. The red numbers represent statistically-significant changes from 1990 to 2018, as determined by a two-sided t-test with a confidence of 95%.

Many studies have attempted to circumvent the relatively short stable hail report record by analyzing environmental conditions favorable for hail development over longer historical periods. For instance, Allen et al. (2015a) evaluated various environmental parameters within the NARR dataset to develop a four-parameter model that correlates best with observed hail activity from 1979 to 2012. These four parameters include: convective precipitation, CAPE, storm relative helicity, and 0-1 km specific humidity. In comparing the model-simulated mean monthly values across the continental U.S. to observed interannual activity, they found that while the model captured the year-to-year changes in sign, it did not reveal an increasing frequency trend over the entire period like seen in the observations. Allen et al. (2015a) hypothesized this lack of a nationwide trend may be a result of the NARR data not capturing the individual component trends of the environmental factors used in the model, and/or not capturing regional behavior well, as evidenced by the model underestimating warm season events in the eastern U.S. in their study.

Tang et al. (2019) examined environmental conditions conducive for hail activity using a combination of NARR data, SPC reports, and radar data and found significant increasing trends in large hail (≥2 in.) parameter (LHP) days[85] in the eastern two-thirds of the U.S. since 1979. These LHP days were identified in the NARR by evaluating environmental conditions that correlate strongly with large hail production. Specifically, they found LHP-day and SHiP-day time series strongly correlate with large hail reports and radar-derived maximum

[85] The LHP is defined similarly to SHiP, as a nonlinear combination of six variables: MUCAPE, hail growth zone (−10 °C to −30 °C) thickness, the 700–500 hPa lapse rate, bulk wind difference between the surface and parcel equilibrium level, wind direction difference between the equilibrium level and the 3–6 km layer, and the storm-relative wind difference between the 3–6 km and the 0–1 km layers.

estimated size of hail (MESH) signatures in the Midwest and in the Northeast, and good correlations are also seen in portions of the Southeast. As seen in Figure 195 and Figure 196, significant correlations between NARR parameters and SPC reports are evident everywhere except for the Rocky Mountain Region, where slight decreasing trends in LHP days and SHiP days are noted. Of particular interest are the statistically-significant correlations between the Midwest and Northeast annual large hail environmental areas and the radar-derived MESH areas, as well as weak (i.e., not statistically significant) correlations in other regions. While radar-indicated hail is still another proxy for severe thunderstorm development, it is more closely related to the occurrence of actual severe hail than other environmental proxies. However, due to the limited radar dataset available (1995-2016), it is difficult to draw any conclusions in longer-term severe hailstorm trends based on these MESH signatures alone.

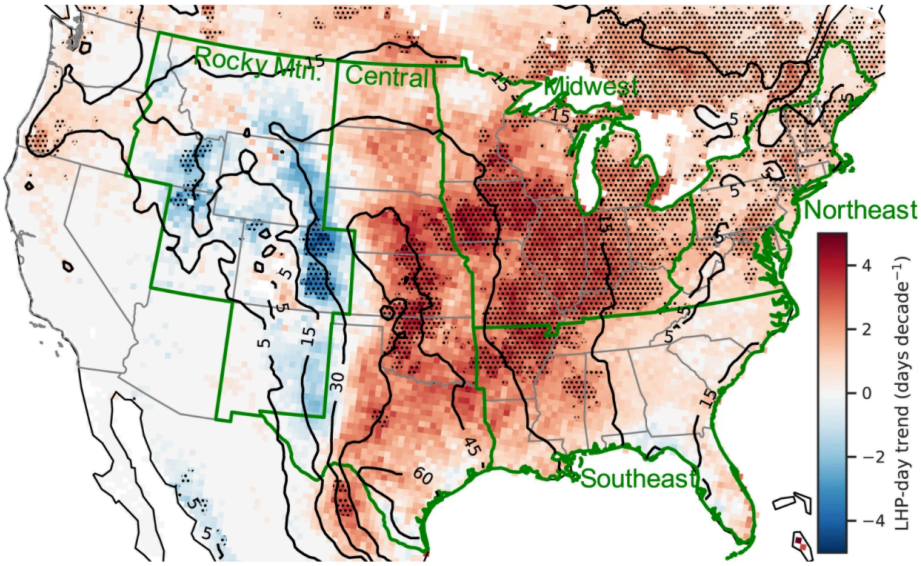

Figure 195. 1979-2017 LHP days trend (shaded) and annual mean number of LHP days (contoured) using NARR data.
The 95% confidence level statistically-significant trends are indicated by the green dotted regions. The green outlines define the regions used in the study (Adapted from: Tang et al., 2019; CC BY-SA 4.0).

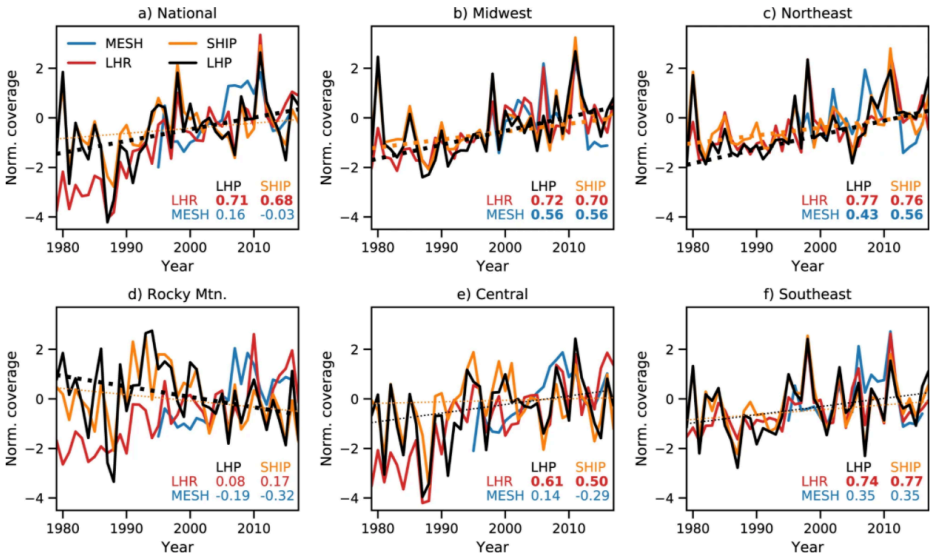

Figure 196. National (a) and regional (b-f) normalized annual trends in 1979-2017 LHP-day area (solid black line), SHiP-day area (solid orange line), large hail report-day area (LHR-day area; solid red line), maximum radar-estimated size of hail-day area (MESH-day area; limited to 1995-2016; solid blue line), and annual mean number of LHP days (contoured). Annual LHP-day area and annual SHiP-day area linear trends are represented by the black and orange dotted lines, respectively. Bold/thick dotted lines indicate these trends are statistically significant. The linear correlation values are presented in the lower right portion of each graph, with the 95% confidence level statistically-significant correlation trends emphasized using bold text (Source: Tang et al., 2019; CC BY-SA 4.0).

Historical trends in tornado activity

Similar to hail, time series of tornado reports suffer from population biases and a relatively short observational record. There has been large growth in the annual number of reported tornadoes since records began, but this trend is largely due to the increase in reporting of the weakest tornadoes. When considering only EF-1 tornadoes and greater, there is no discernible trend in their annual frequency. Since tornadoes are rated based on observed damage, classifying intense tornadoes is highly dependent on both observing them and the exposure(s) they impact. Despite these limitations with the historical dataset, studies have found no nationwide long-term temporal trend in EF-1 or greater tornado frequency overall. However, studies have found an increase in annual tornado occurrence variability, including a longer and earlier start to the tornado season, decreased number of tornado days, and a growing number of tornado days with numerous tornadoes. In addition, regional trends in tornado frequency are more evident than with hail. Still, the extent to which climate change plays a role in any temporal trends in tornado frequency and/or intensity seen in the observed data is difficult to determine.

Verisk researchers analyzed the temporal trend in SPC tornado reports of EF-1 strength or greater over approximately the last 40 years (i.e., from 1979 - 2018) across the continental U.S. Results from this study show that tornado reports have been fairly stable during this time

period, even when examining individual reports rather than tornado days, as seen in Figure 197.

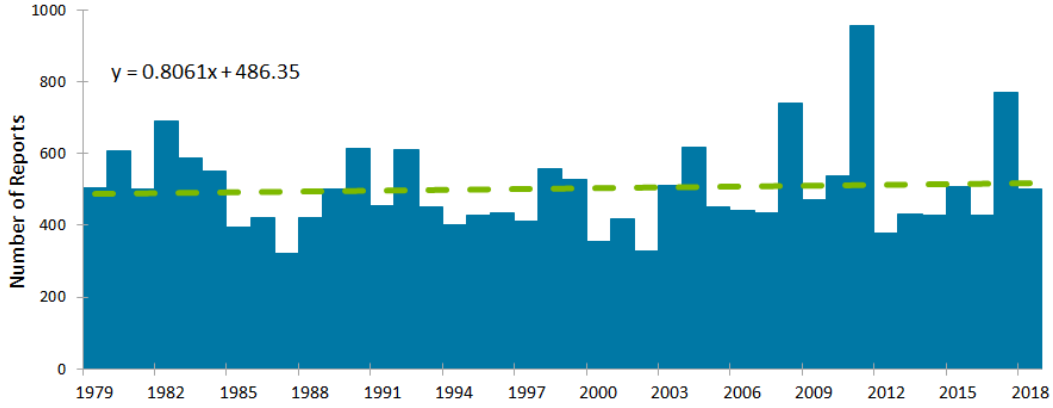

Figure 197. Number of annual tornado reports of EF-1 or greater strength (blue bars) and the corresponding linear trend line fit to the data (green dashed line) across the contiguous U.S. from 1979 to 2018 based on SPC's Storm Reports database.
The linear trend line equation is included in the chart.

Various studies have found notable changes in tornado occurrence variability over time. For example, Brooks et al. (2014) noted that while the frequency of EF-1 or greater intensity tornadoes has not increased, their occurrence variability across the U.S. has increased since the 1970s. This increased variability results from a decreased annual number of tornado days but an increased number of days with numerous tornadoes, which is supported by various other studies (e.g., Tippett and Cohen, 2016; Tippett et al., 2016). Long and Stoy (2014) found that peak tornado occurrence in the central and southern U.S. Great Plains has shifted seven days earlier in the year over the last six decades, or about 1.55 days per decade. Lu et al. (2015) studied tornado activity along with environmental variables favorable for tornado development (e.g., CAPE and SRH) in the U.S. and found significant semiannual and annual variability in their occurrence. Their results show that the seasonal variability in CAPE greatly contributes to the earlier start and peak of the tornado season, while SRH is more instrumental in the enhanced peak tornado activity. This earlier start is consistent with expectations based on an increasingly unstable early spring evident in climate change studies (Diffenbaugh et al., 2013; Hoogewind et al., 2017). However, Tippett et al. (2016) noted that while both tornado outbreak and, especially, super outbreak frequency (i.e., days with at least six and twelve, respectively, tornadoes of at least EF-1 intensity) have increased across the U.S. since 1965, it is difficult to know if these trends are a result of climate change and/or will continue in the future.

Verisk researchers analyzed the temporal trend in annual U.S. super outbreak tornado days from 1979 to 2018 using SPC's Storm Reports dataset. To significantly reduce biases in the data, only tornado reports of EF-1 intensity or greater were included. As seen in Figure 198, Verisk's results show an increase in super outbreak tornado days over time. This increase, with a p-value of 0.0261, calculated using a two-sided t-test with a confidence of 95%, is statistically significant and supports other studies' results.

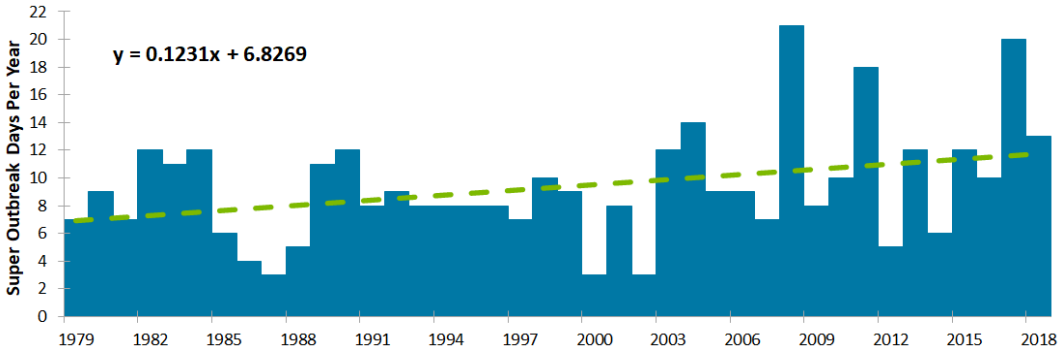

Figure 198. Number of super outbreak EF-1 or greater tornado days per year are reported in SPC's Storm Reports dataset (blue bars) and the corresponding linear trend line fit to the data (green dashed line) across the contiguous U.S. from 1979 to 2018.
The linear trend line equation is included in the chart.

Numerous studies have examined and found regional changes in tornado activity over time (e.g., Agee et al., 2016; Gensini and Brooks, 2018). For example, Gensini and Brooks (2018) examined regional trends using tornado reports from SPC's Storm Reports database from 1979 to 2017 and calculated the significant tornado parameter (STP) based on NARR data. This STP is used as a representative measure of favorable tornado environments, and the annual sum of daily max STP is a measure of a year's total favorability for atmospheric conditions conducive to tornadoes. Their results show that both favorable tornado environments and tornado frequency (Figure 199 and Figure 200, respectively) have increased in parts of the Midwest and Southeast U.S. and have decreased in sections of the central and southern Great Plains since 1979. As seen in Figure 201, these regional trends vary by season, with Texas experiencing the largest decrease in favorable tornado environment frequency from March to May, and much of the Great Plains seeing the largest drop from June to August, for example. In addition, the increase in favorable tornado environments travels northward throughout the year.

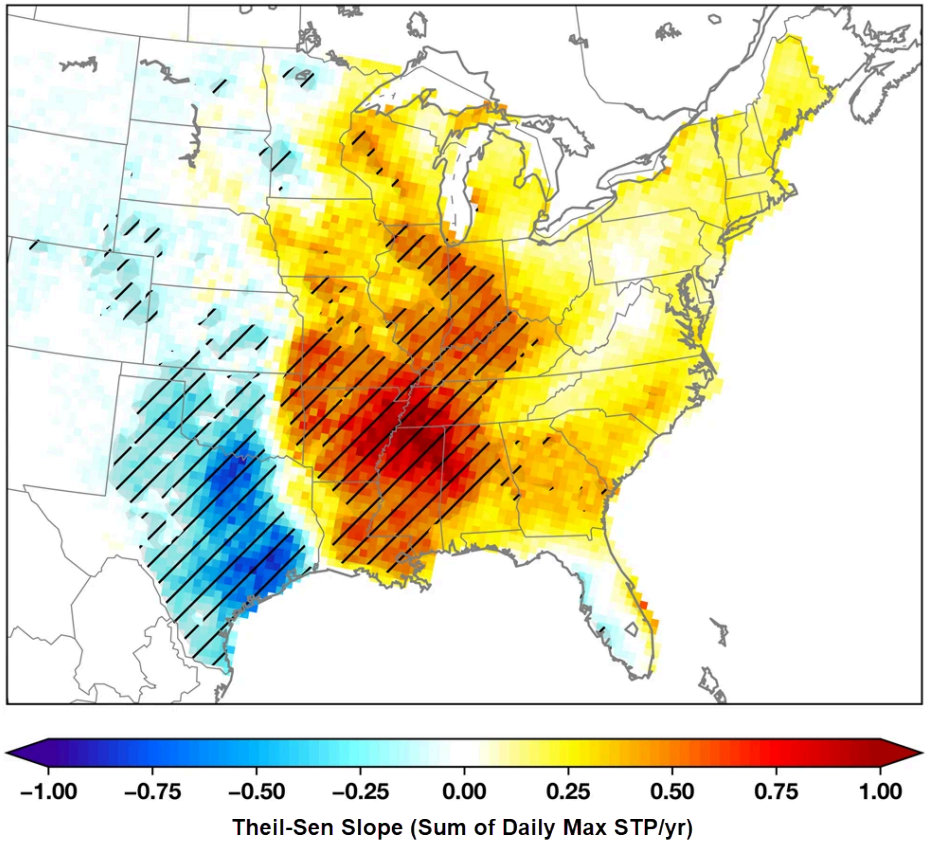

Figure 199. Theil-Sen slope analysis (a linear trend estimator not sensitive to outliers) of the annual gridpoint daily max STP sum (contours) from 1979 to 2017.
Hatched lines represent p values of ≤0.05 significance using Kendall's τ statistic. (Source: Gensini and Brooks, 2018; CC BY-SA 4.0).

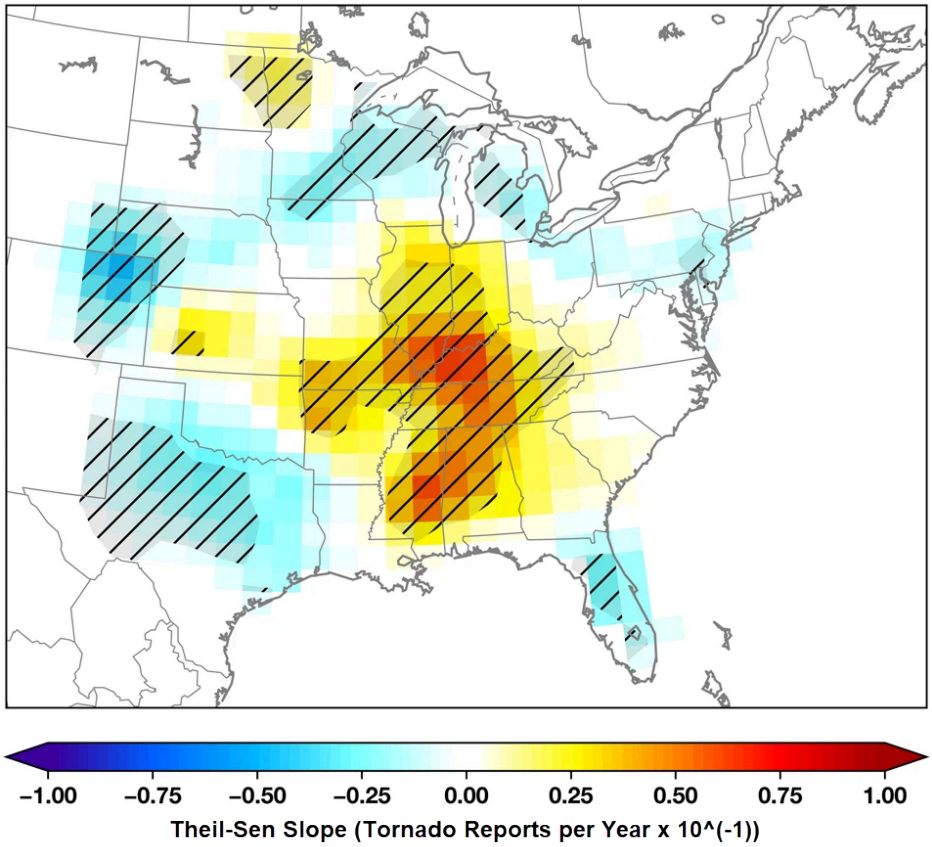

Figure 200. Theil-Sen slope analysis (a linear trend estimator not sensitive to outliers) of annual gridded tornado reports (contours) from 1979 to 2017.
Hatched lines represent p values of ≤0.05 significance using Kendall's τ statistic. (Source: Gensini and Brooks, 2018; CC BY-SA 4.0).

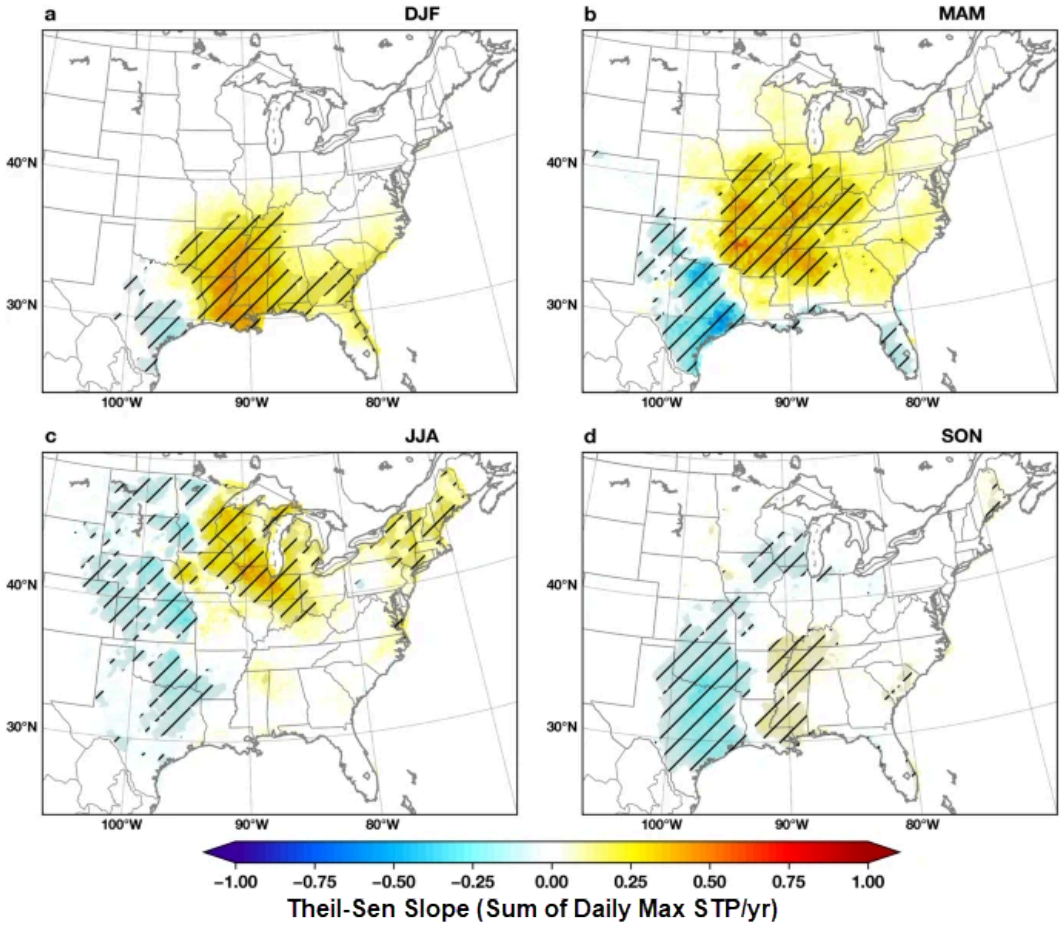

Figure 201. Theil-Sen slope analysis (a linear trend estimator not sensitive to outliers) of the annual gridpoint daily max STP sum (contours) from 1979 to 2017 for a) December, January, and February; b) March - May; c) June - August; and d) September - November. Hatched lines represent p values of ≤0.05 significance using Kendall's τ statistic. (Source: Gensini and Brooks, 2018; CC BY-SA 4.0).

Verisk researchers examined regional trends in tornado frequency by analyzing the mean annual number of EF-1 or greater tornadoes by state during 1979 and during 2018, normalized with respect to state size to reflect activity per 5° latitude x 5° longitude unit area. This normalization eliminates large jumps in tornado counts where smaller-sized states share a border with larger-sized states and results in a spatially-coherent picture of change in activity over time. As seen in Figure 202, Figure 203, and Figure 204, tornado frequency has decreased across the western half of the U.S. but has greatly increased over Illinois, Indiana, Kentucky, Tennessee, Mississippi, Alabama, and Georgia over time. Varying changes in tornado frequency are evident over much of the rest of the eastern half of the U.S.

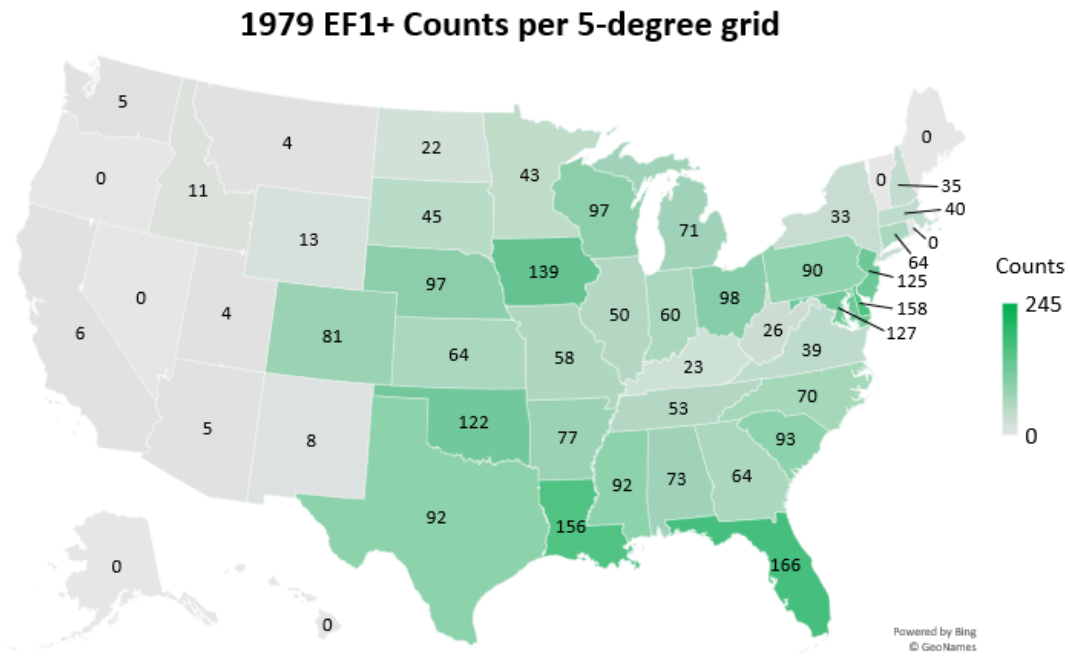

Figure 202. Normalized statewide mean annual number of EF-1 or greater tornado reports in 1979 using values along a best-fit line from SPC's Storm Reports database on a 5-degree grid.

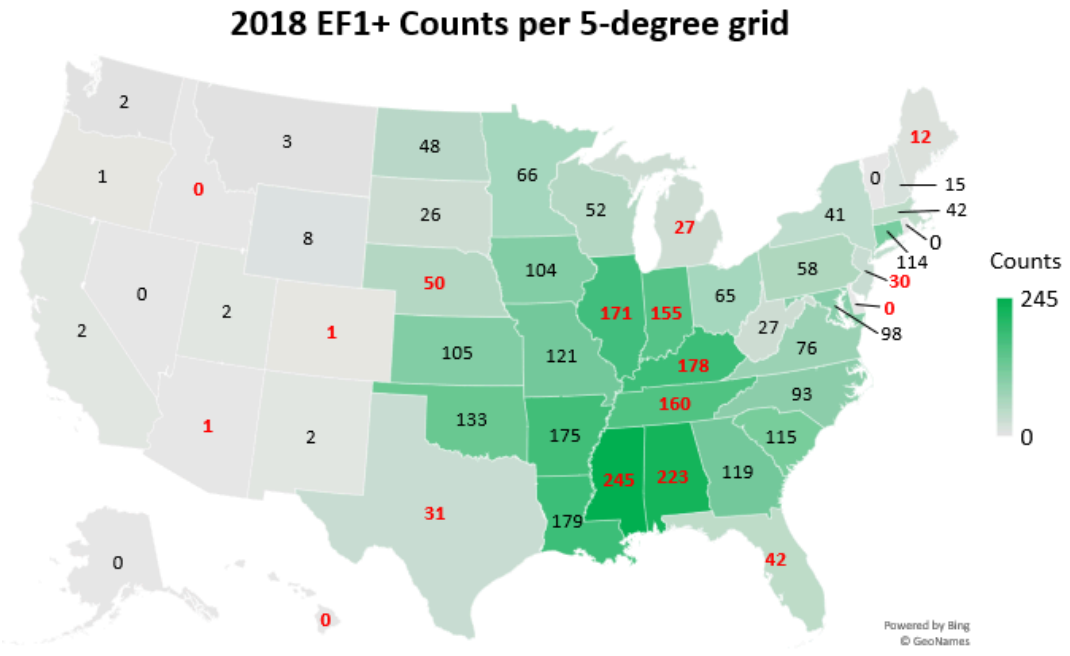

Figure 203. Normalized statewide mean annual number of EF-1 or greater tornado reports in 2018 using values along a best-fit line from SPC's Storm Reports database on a 5-degree grid.
The red numbers represent statistically-significant changes from 1990 to 2018, as determined by a two-sided t-test with a confidence of 95%.

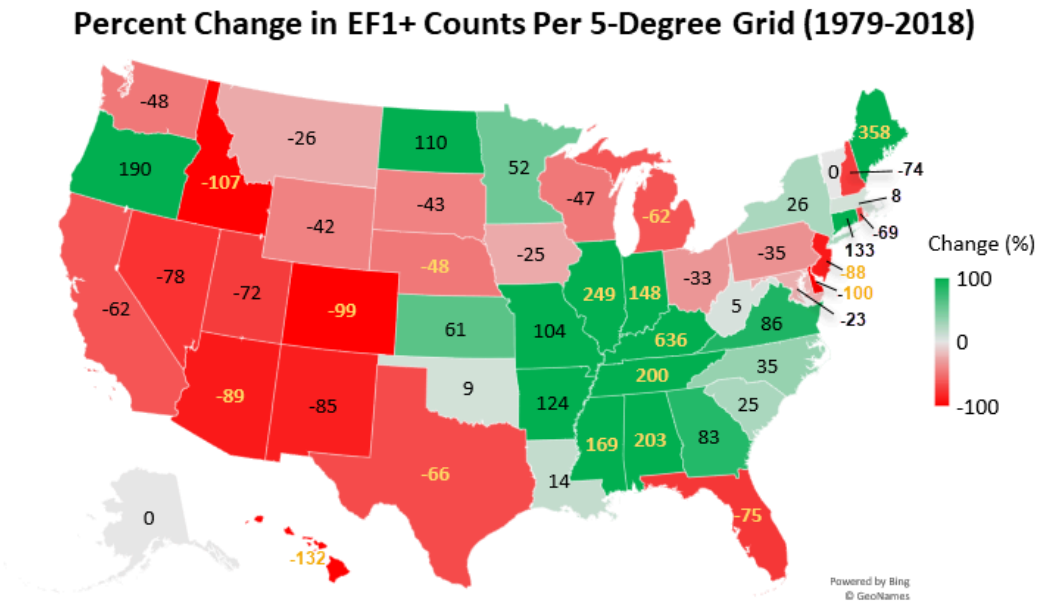

Figure 204. Normalized percent change in statewide mean annual EF-1 or greater tornado reports between 1979 and 2018 using values along a best-fit line from SPC's Storm Reports database on a 5-degree grid.
The yellow numbers represent statistically-significant changes from 1990 to 2018, as determined by a two-sided t-test with a confidence of 95%.

One possible explanation for the increased tornado activity over much of the Southeast since 1979 may be related to changes in the El Niño–Southern Oscillation (ENSO), particularly to La Niña. ENSO quantifies the degree to which the central to eastern equatorial Pacific Ocean temperatures are warmer or cooler than normal, smoothed out over several months. ENSO is in its positive phase during La Niña events and in its negative phase during El Niño events. The presence of La Niña results in an atmospheric environment favorable for tornado outbreaks in the Southeast, irrespective of climate change (Lee et al., 2016). Some studies (e.g., Wang et al., 2019) suggest that climate change has and will continue to increase the frequency and intensity of ENSO events. In fact, comparing two consecutive 20-year periods, 1979-1998 and 1999-2018, of ENSO activity (i.e., 3-month periods where the ENSO index ≥ 0.5°C) using the NINO 3.4 index[86] shows 15% more ENSO activity during the latter 20-year period.

Historical trends in straight-line wind activity

Similar to hail and tornadoes, convective straight-line wind reports are skewed by population biases. Some of these biases can be removed by analyzing wind days instead of individual wind reports. In addition, although damaging winds can be identified by Doppler weather radar, the U.S. nationwide archived data from these radars are only available for a relatively short historical time period. This time period is too short to be able to identify with certainty

[86] Historical ENSO data are available on CPC's website at: https://origin.cpc.ncep.noaa.gov/products/analysis_monitoring/ensostuff/ONI_v5.php

if and to what extent climate change plays a role in any temporal trends in straight-line wind frequency and/or intensity seen in the observed data. In addition, despite being the most-frequently occurring of the three sub-perils associated with severe convective storms, widespread severe straight-line wind events are rare. As a result, there are far fewer published studies about potential climate change impacts on convective straight-line wind temporal and spatial trends than on potential hail and tornado climate-related changes (Gensini et al., 2020).

Verisk researchers analyzed a subset of extreme straight-line wind events produced by severe thunderstorms in the U.S. that were officially classified as derechos (i.e., straight-line winds that produce over a 240-mi damage swath with wind gusts of at least 58 mph (50 kts) along most of its length) in SPC's Storm Reports database from 1990 to 2019. As evident in Figure 205, results show that U.S. nationwide derecho frequency has increased over the last three decades. However, the criteria for classifying a derecho is heavily dependent on the number and density of severe straight-line wind reports. Any non-meteorological changes in reporting will likely impact derecho identification, so it is not clear if this trend has a meteorological cause.

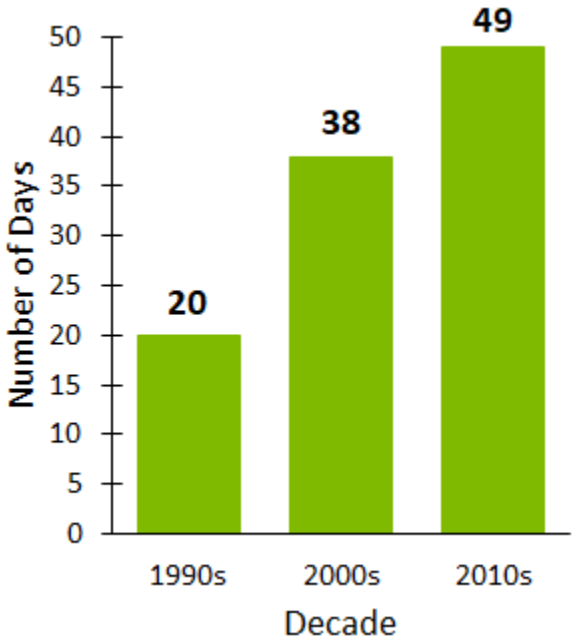

Figure 205. Number of days per decade in which a derecho occurred in the U.S. based on SPC's Storm Reports database

In addition, Verisk researchers analyzed a time series of annual 58-mph (50-kt) or greater convective straight-line wind gust days in the U.S. (i.e., number of days when at least one straight-line wind gust report of 58 mph or greater was reported in the U.S.) based on SPC's Storm Reports database along with U.S. population from 1979 to 2018 (Figure 206). Wind gust days were once again used instead of individual wind reports to reduce population biases in the observed data. Results show that annual severe straight-line wind days have been fairly stable despite the increase in U.S. population during this 40-year time

period. These results suggest that 1) by using wind days instead of individual wind reports, population biases in the data have been greatly reduced, and 2) no statistically-significant trends in severe straight-line wind frequency have occurred on a countrywide level between 1979 and 2018.

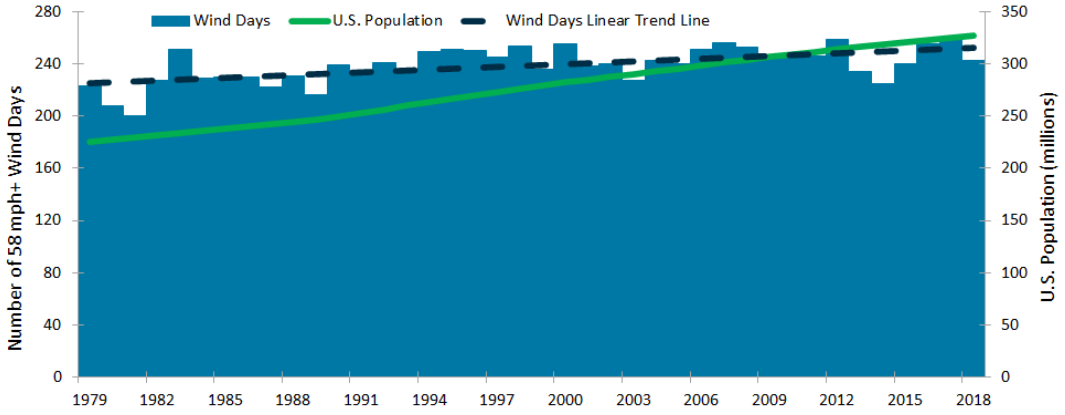

Figure 206. Number of 58-mph or greater straight-line wind gust days across the contiguous U.S. based on SPC's Storm Reports database (blue bars), linear best fit straight-line wind trend line (dark blue dashed line), and U.S. population (green line) from 1979 to 2018.

Next, Verisk researchers used a slightly higher wind threshold to analyze the mean annual number of 63-mph (55-kt) or greater convective straight-line wind gust days in 1990 and in 2018, by state (Figure 207 and Figure 208, respectively), which were calculated using a best-fit curve through the 1990-2018 time series of SPC reports in each state. Comparing the two figures, notable statistically-significant increases are seen, especially across New Mexico, Oklahoma, Minnesota, Wisconsin, Illinois, and much of the Southeast U.S., where straight-line wind days have increased severalfold. It is difficult to attribute these increases entirely to population increases, although some states (e.g., Mississippi and Georgia) exhibit a more significant population bias beginning in the early 2000's (not shown). However, it is equally difficult to quantify the extent to which climate change has impacted severe straight-line wind activity in this area (Gensini et al, 2020).

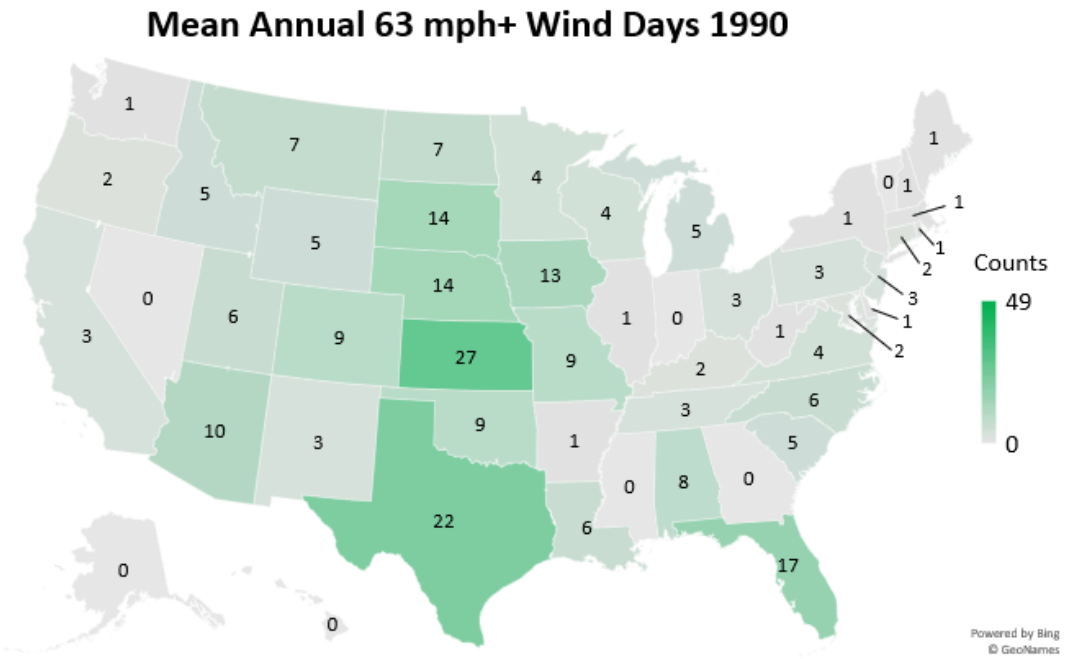

Figure 207. Mean annual number of 63-mph or greater straight-line wind days in 1990 based on values along a best-fit line through the 1990-2018 times series of SPC reports in each state.

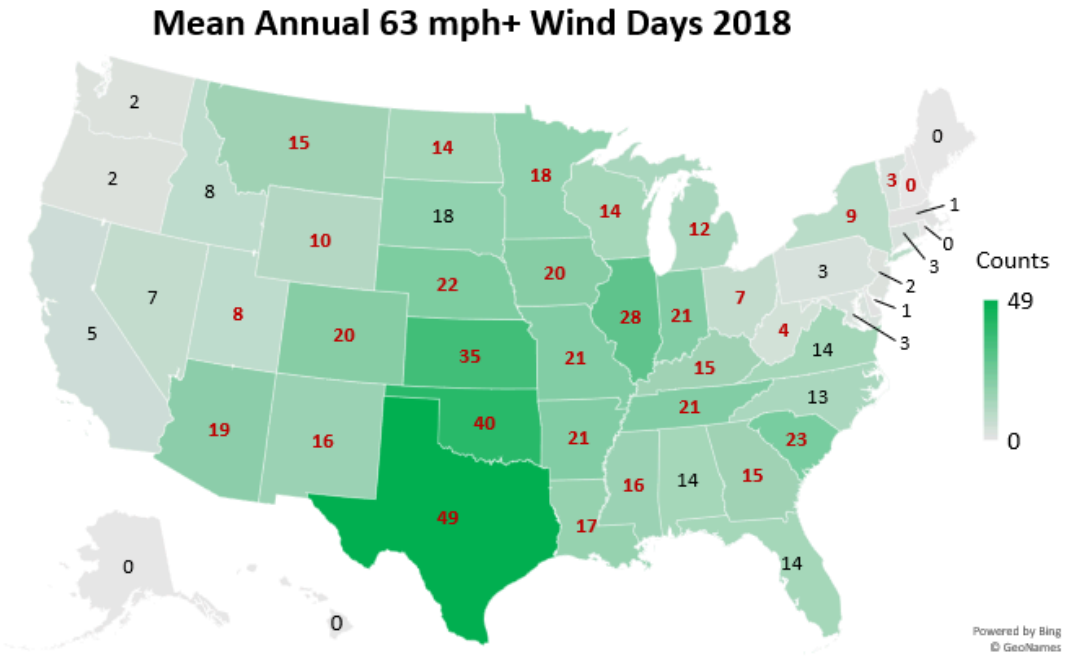

Figure 208. Mean annual number of 63-mph or greater straight-line wind days in 2018 based on values along a best-fit line through the 1990-2018 times series of SPC reports in each state.
The red numbers represent statistically-significant changes from 1990 to 2018, as determined by a two-sided t-test with a confidence of 95%.

Summary of historical trends

While Verisk researchers and various other studies have found no nationwide statistically-significant temporal trends in severe thunderstorm frequency attributable to climate change in the U.S. overall, they have identified statistically-significant regional trends in the occurrence frequency of both severe thunderstorms and the environmental conditions favorable for severe thunderstorm development. Both occurrence frequencies have increased across much of the eastern half to two-thirds of the U.S. and have decreased across much of the western third to one-half of the U.S. The extent and amount of these changes vary by season. In addition, while the nationwide observed tornado frequency has not significantly changed, observed tornado-specific occurrence variability (e.g., a longer and earlier start to the tornado season, decreased number of tornado days but a growing number of tornado days with numerous tornadoes) has increased since the 1970s. Looking forward, various GCMs project the frequency of favorable severe thunderstorm environments will increase by the late 21st century, especially across the eastern half to two-thirds of the U.S. Similar to observed trends, this increase is projected to vary by season.

Despite these noted trends in severe thunderstorm activity and a physically-plausible explanation as to why climate change would increase severe convective weather activity (i.e., a warming climate would add more moisture to the air and enhance instability needed for thunderstorm development), other factors limit our ability to isolate the amount to which these changes can be attributed to anthropogenic climate change alone. These factors include a limited historical dataset affected by population and reporting biases, inherent uncertainties associated with the numerical modeling component of GCMs, and the amount of influence other recurring climate patterns (e.g., ENSO) have on severe thunderstorm development. As a result, researchers express modest confidence that the noted severe thunderstorm activity changes can be attributed to anthropogenic climate change.

Verisk's overall assessment is that climate change may be impacting U.S. severe thunderstorm activity and more attention should be given to the recent climatology (e.g., last 20 years) than to the climatology of the distant past (e.g., prior to 1998). Observed data from the last century should not be completely ignored but, rather, these data should be used to define aspects of interannual variability rather than conveying absolute numbers for frequency and intensity. Verisk's assessment is supported by existing literature, Verisk's own analyses, a physically-plausible explanation for changes in some aspects of severe convective weather, changes observed in SPC's Storm Reports database, and historical resimulations from many GCMs.

7.3 Model and catalog development

The Verisk Severe Thunderstorm Model for the United States' stochastic catalog is built based on detailed information from NOAA's SPC and NCEI storm reports, NCEP's CFSR, and NOAA's Next Generation Radar (NEXRAD) Level III radar data. Verisk's stochastic catalog was last updated in 2020 to leverage 8 years of additional data along with new datasets available since the catalog was previously updated. Particular focus was given to more closely match

hailstone frequency and intensity climatology by incorporating additional historical data and geographically-varying hailstorm event generation methodologies.

Verisk researchers correct for reporting biases in the SPC data by employing a combination of statistical and physical methods (e.g., additional observational datasets, atmospheric severe weather indices, smart smoothing, population growth detrending, and generalized additive models). Stability is an important aspect of any catastrophe model, as well as its ability to reflect the current climate. Thus, Verisk researchers focus on implementing a robust stochastic catalog that reflects both the 1979-2018 mean and the longer-term variability about the mean, adjusted to account for climate-based trends so it represents the current climate, as discussed below. The stochastic catalog includes severe thunderstorm-modeled event frequency, starting location, storm track direction, storm length and width, and intensity information specific to the sub-peril (i.e., hail, straight-line wind, or tornado).

One of the most important data sources for developing the model is the local storm reports database maintained by the SPC. These reports represent point observations of severe weather by trained storm spotters, emergency management, and the general public. While this dataset contains valuable information about severe thunderstorm events, there are also several types of reporting biases in these data. Since this dataset is composed of observed reports, these reports tend to be clustered around population centers and major roads. There is also a general noticeable increase in the number of reports with time. Potentially contributing non-meteorological factors to this increase include population growth (more possible observers), metropolitan expansion into previous rural areas, greater interest in severe weather, storm chasing, and expansion of cell phone networks and social media, making reporting easier. Climate variability and change may also be contributing factors. Since these potential signals contributing to the trend are inseparable from each other, Verisk researchers take an agnostic approach to detrend the historical storm reports data. This approach corrects any under-reporting in early years of the record and accounts for climate-related impacts to create a near-present view of the hazard.

The first step in detrending SPC data is to correct for over-reporting. For example, two reports separated by only a few miles and minutes are likely to be separate observations of the same storm. Hail and windstorm reports are spatially-clustered on a daily time scale to create a set of reported storms from the storm reports. After the over-reporting is accounted for by clustering, the second step corrects the upward trend in annual reported severe days. A severe day is a day that results in one or more severe storm reports. This upward trend in severe days appears to level off around 1998. The earlier years likely had severe weather on more days than were reported. A piecewise model is fit to the observed data that assumes a positive linear trend in early years and no trend in more recent years. Then, this model is used to make the mean severe day frequency consistent with recent years. Even after accounting for the upward trend in severe days, there is still a positive trend in the annual count of severe storm reports. The annual counts are detrended in the same manner as the annual severe days, using the mean of years 2010 and later as the baseline. The mean frequency of the model is based on the most recent years, removing any non-meteorological trends and accounting for the current climate. This process is performed for the hail and wind sub-perils. Tornadoes of EF-1 intensity and greater have no notable trend.

The Verisk model employs a daily simulation method where stochastic days are based on historical days. Each stochastic day has a similar number and location of storms as the respective historical day. The annual detrending factors developed for the SPC reports are used to inflate the historical number of microevents (storms) to produce a modeled frequency that has a consistent frequency, no matter the historical year used as the basis for simulation.

Simulated microevents have unique attributes describing their footprints: length, width, and intensity. In creating the stochastic catalog, each microevent's attributes are randomly drawn from probability distributions. The wind and tornado distributions are created from storm reports, and hail distributions are from a blend of storm reports and radar-based storm footprints. Due to the growth in storm reports over time, distributions are implicitly weighted toward more recent years. Additionally, the radar data used is from 1996 and later, so the same implicit weighting is present there as well. While there is no clear signal in storm attributes over time, any potential changes would be mostly accounted for by using more recent data.

7.4 Model validation

The Verisk Severe Thunderstorm Model for the United States has been validated against recent severe thunderstorm frequency and intensity observations to show that Verisk's stochastic catalog reflects the most recent severe thunderstorm climatology. A common method to measure severe thunderstorm frequency uses the days unit. A location or area experiences a severe day if there is one or more report(s) of severe weather on that given day. The observed and model-average annual number of severe days are both calculated for the time period of interest. The model-average annual severe days is validated by state and sub-peril against observed average annual severe days derived from clustered SPC reports.

As described previously, there is a significant growth in storm reports over time. Thus, validating model frequency against all reports would bias the observed frequency low. As a result, years 2000-2018 were selected for validation because the number of reported severe days stabilizes in the late 1990s, and this time period represents the near-present climate. Note that Verisk researchers used the 10K all-events catalog as opposed to the 10K cat-only catalog for these validations. Using the all-events catalog is a more stringent test because it includes all severe weather events as opposed to only those macroevents that result in gross insurable loss of at least 25 million USD.

See Also

Average Annual Days

Hail validation

Figure 209 and Figure 210 compare Verisk-modeled versus observed average annual severe (1-in. or greater) hail days, for each state. Similarly, Figure 211 and Figure 212 compare Verisk-modeled versus observed average annual significant (2-in. or greater) hail days, for each state. For hail, there are two sets of observations: SPC reports (2000-2018) and radar-

based swaths (for the periods 1996-2002 and 2005-2017; 2003 and 2004 are missing). The Verisk model compares very well with both sets of observations for severe hail days. However, there are differences between model-simulated and observed significant hail days that can be explained by known biases in the two observational data sets.

The Verisk model simulates a greater number of significant hail days than the number of observed days in the SPC Storm Reports database. Since SPC reports are point observations and are dependent upon someone actually observing and then reporting hail correctly, it is likely that the maximum hail size produced by a given storm often goes underreported (or not reported at all). As a result, it is not surprising that Verisk model-simulated significant hail days are more numerous than the observed hail days generated from SPC data.

The Verisk model simulates a slightly lower number of significant hail days compared to radar-based observed significant hail days. The radar-based hail days may be a better prediction of the actual maximum hail size than SPC reports because radars spatially sample the entire storm. However, radars, like other observational datasets, have their limitations. The presence of hail and maximum hail size are both radar-derived quantities, not actual observations, and do not necessarily represent ground truth. For example, the maximum estimated hail size radar algorithm is known to have a slight high bias (Wilson et al. 2009), which is not present in the Verisk model.

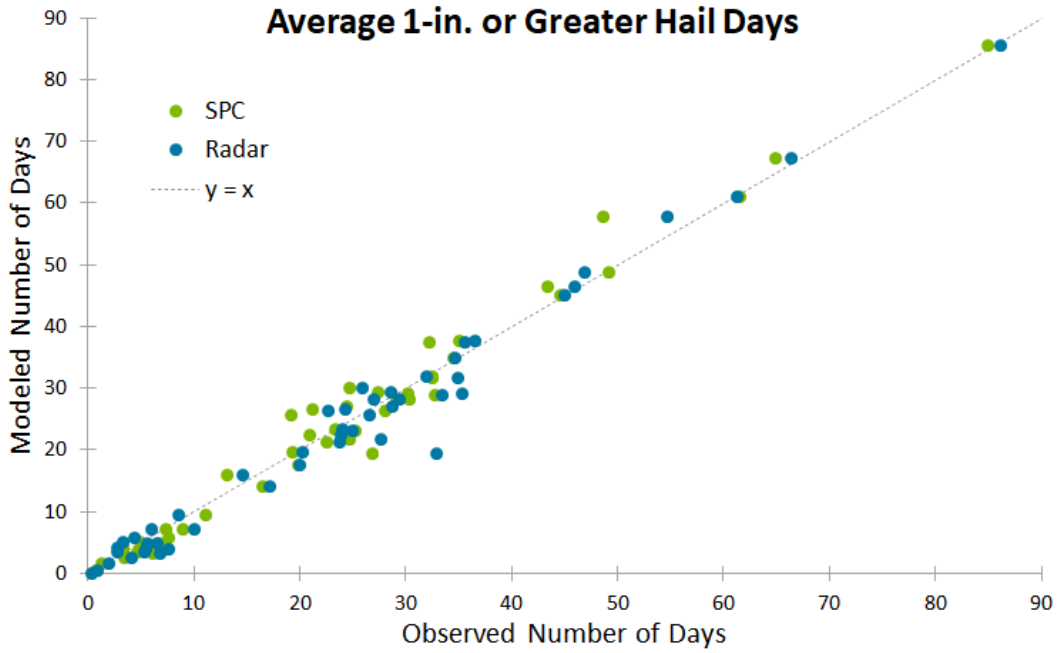

Figure 209. Verisk-modeled versus SPC (2000-2018; green dots) and radar (1996-2002 and 2005-2017; blue dots) observed average annual severe (1-in. or greater) hail days, by state
Note: Each state's annual average value is represented by a dot.

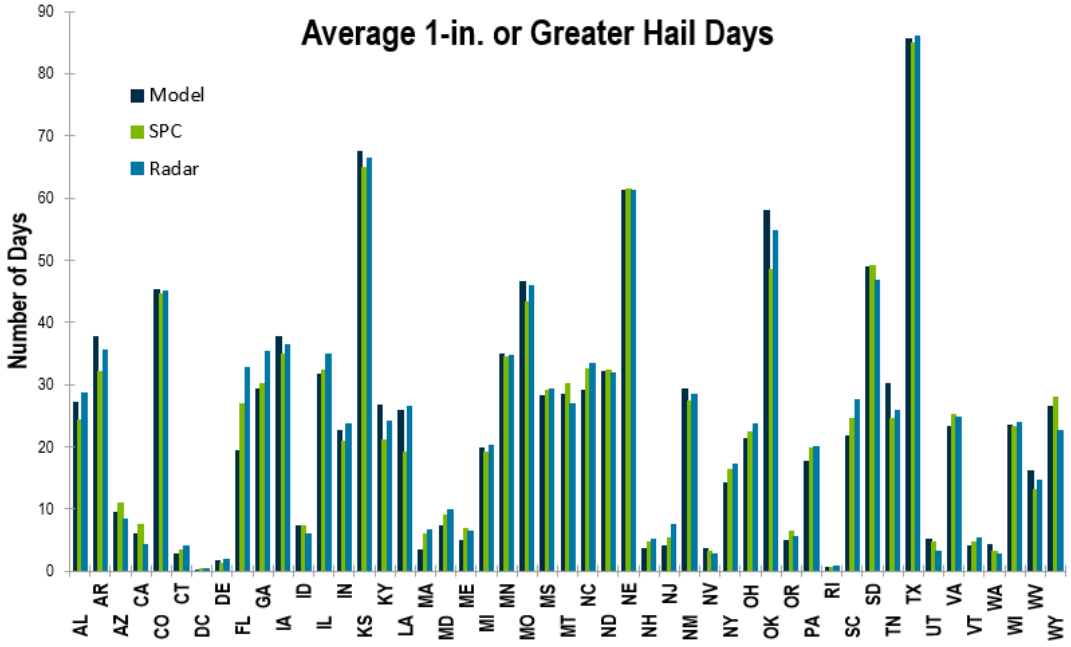

Figure 210. Verisk-modeled (dark blue bars), SPC-observed (2000-2018; green bars), and radar-indicated (1996-2002 and 2005-2017; blue bars) average annual severe (1-in. or greater) hail days, by state

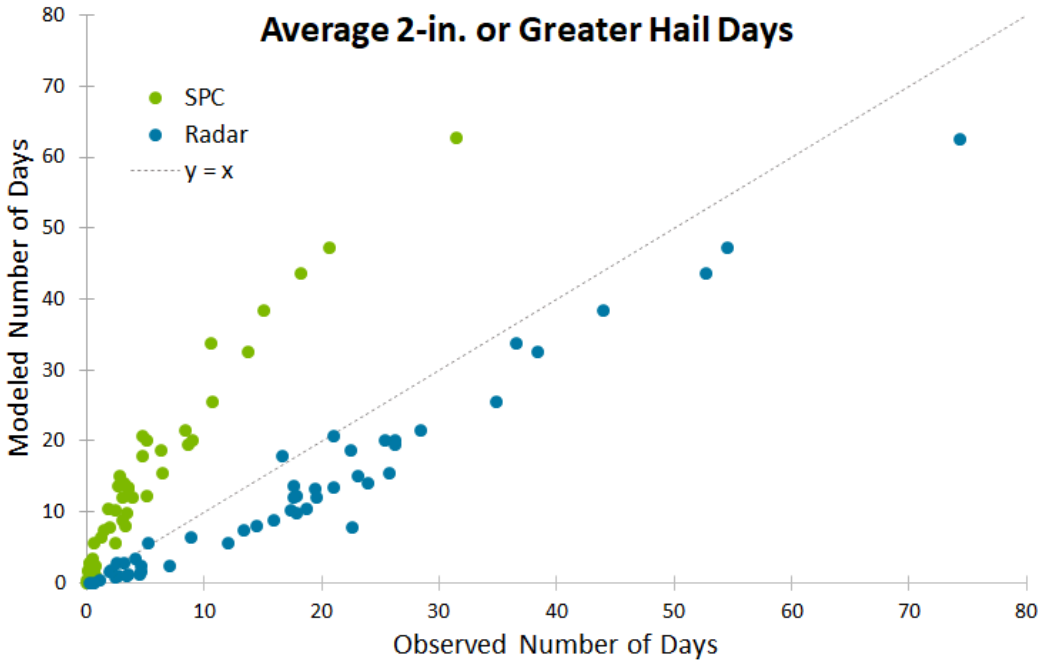

Figure 211. Verisk-modeled versus SPC (2000-2018; green dots) and radar (1996-2002 and 2005-2017; blue dots) observed average annual significant (2-in. or greater) hail days, by state
Note: Each state's annual average value is represented by a dot.

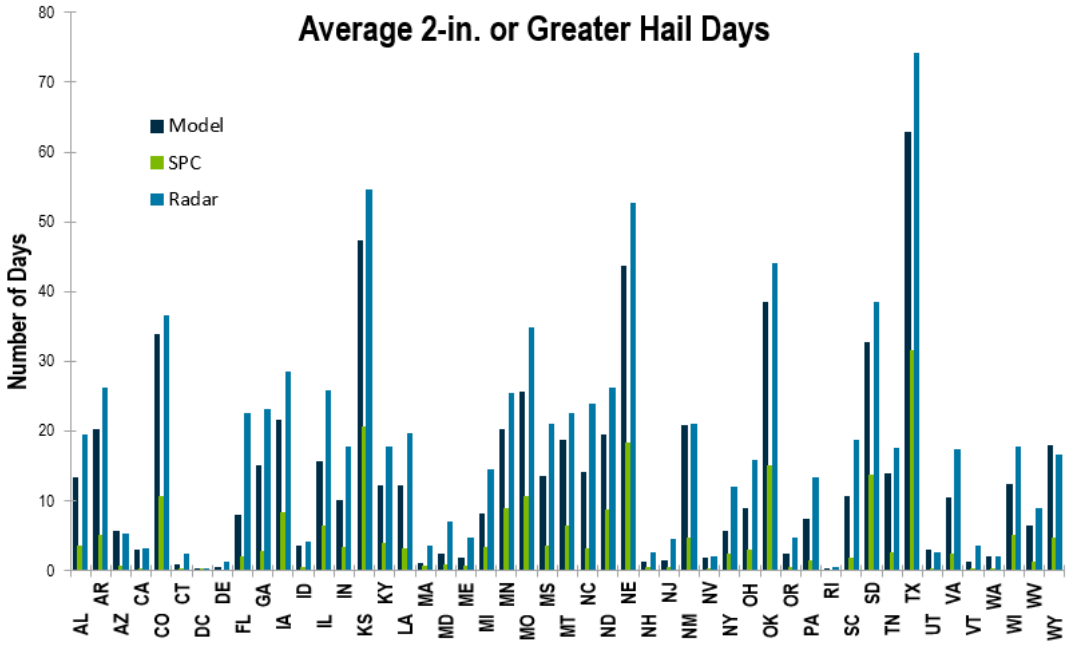

Figure 212. Verisk-modeled (dark blue bars), SPC-observed (2000-2018; green bars), and radar-indicated (1996-2002 and 2005-2017; blue bars) average annual significant (2-in. or greater) hail days, by state

Tornado validation

Verisk model-simulated average annual tornado days are validated using the SPC storm reports database from 2000 to 2018 in the same manner as average annual severe hail days. Figure 213 and Figure 214 compare Verisk-modeled versus observed average annual EF-1 or greater tornado days, for each state. Similarly, Figure 215 and Figure 216 compare Verisk-modeled versus observed average annual EF-3 or greater (i.e., significant) tornado days, for each state. It is evident that Verisk-modeled EF-1 or greater tornado days compare well with observed frequencies from SPC, while Verisk-modeled EF-3 or greater tornado days are higher, on average, than observed. Since SPC's intensity is rated based on damage, tornadoes that occur in rural areas devoid of well-built structures may have their intensities underestimated by damage surveys because there is no evidence of tornado damage to support a stronger classification. For example, a characteristic of violent tornadoes (EF-4 and 5) that distinguishes them from weaker tornadoes is their ability to destroy strong structures. So, a violent tornado that only affects a cornfield is unlikely to be classified as an EF-5. In Verisk's model, however, intensity is rated based exclusively on wind speed, irrespective of damage, so a cornfield could be struck by an "EF-5." For this reason, it is not surprising that the observed significant tornado frequency is lower than the Verisk-modeled frequency, and this difference is an expected result in order for the Verisk Severe Thunderstorm Model for the United States to properly reflect the recent tornado climatology.

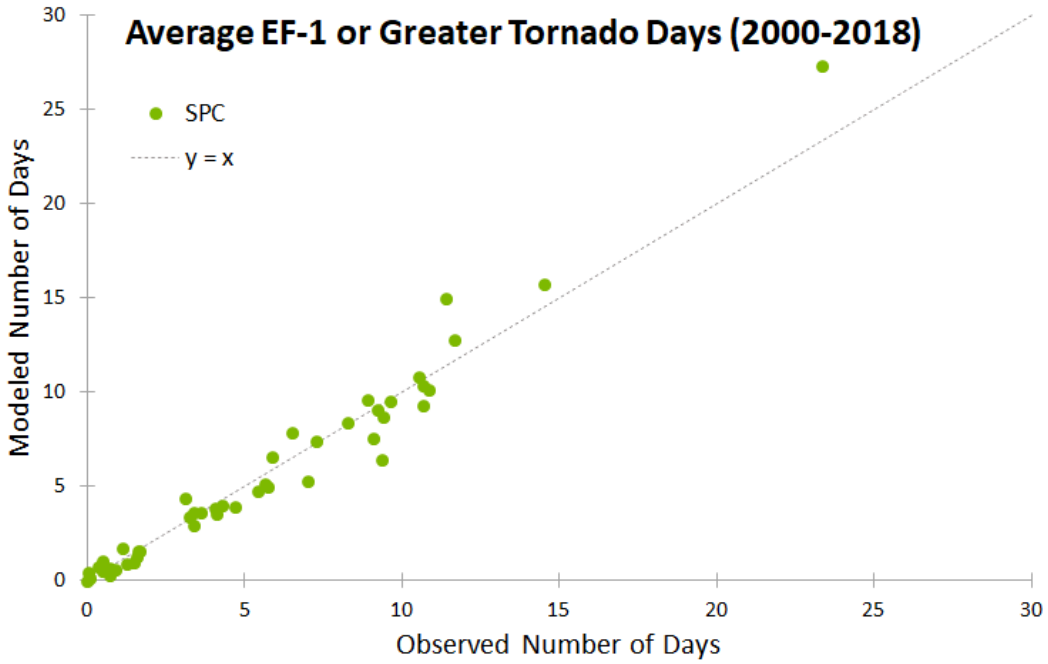

Figure 213. Verisk-modeled versus SPC-observed average annual EF-1 or greater tornado days from 2000-2018, by state
Note: Each state's annual average value is represented by a dot.

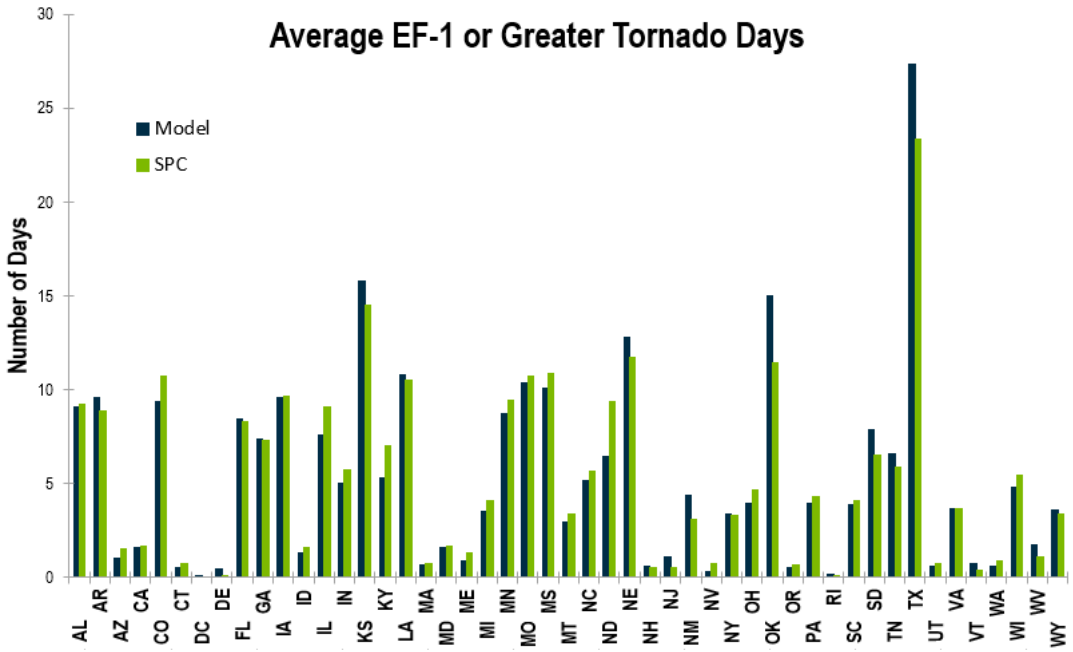

Figure 214. Verisk-modeled (dark blue bars) and SPC-observed (green bars) average annual EF-1 or greater tornado days from 2000-2018, by state

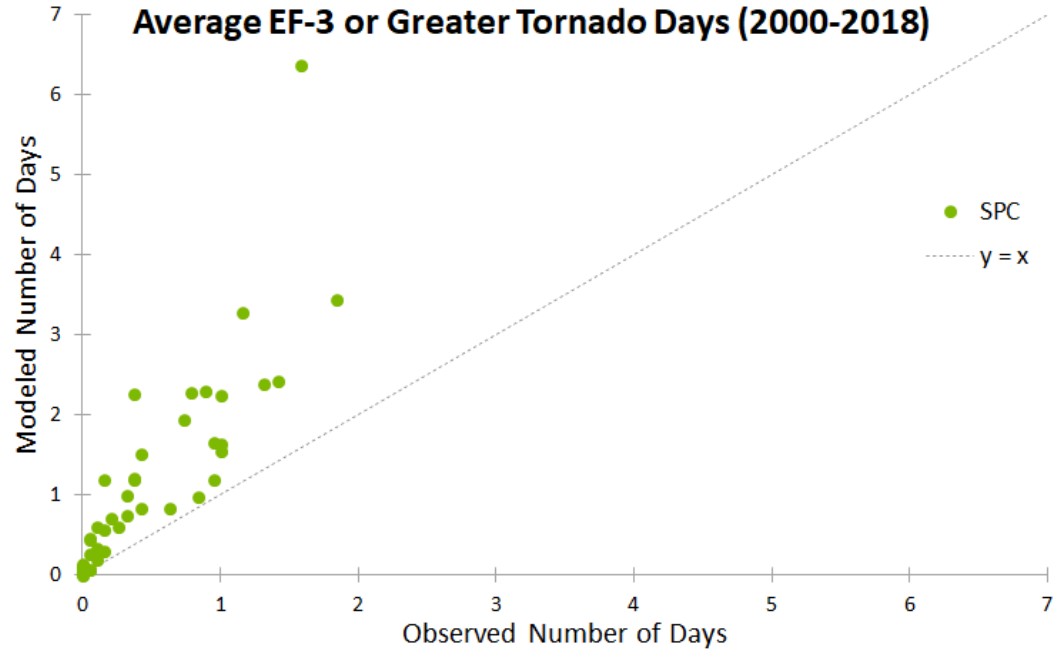

Figure 215. Verisk-modeled versus SPC-observed average annual significant (EF-3 or greater) tornado days from 2000-2018, by state
Note: Each state's annual average value is represented by a dot.

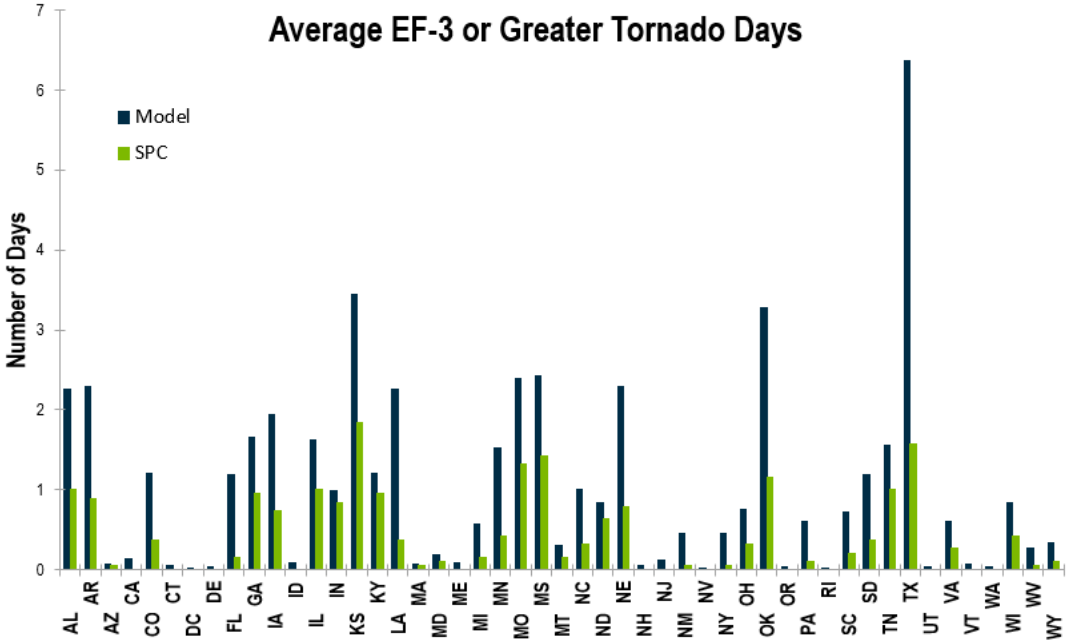

Figure 216. Verisk-modeled (dark blue bars) and SPC-observed (green bars) average annual significant (EF-3 or greater) tornado days from 2000-2018, by state

Straight-line wind validation

Figure 217 and Figure 218 compare Verisk-modeled versus observed average annual 58-mph or greater convective straight-line wind gust days, for each state. Similarly, Figure 219 and Figure 220 compare Verisk-modeled versus observed average annual 75-mph or greater convective straight-line wind gust days, for each state. Verisk-modeled severe straight-line wind gust days are lower, on average, than observed days calculated from SPC's Storm Reports (2000-2018). Many severe wind reports in the SPC database have unknown or estimated wind speed. In addition, human-estimated wind speeds may suffer from a high bias because the observer often reports a higher wind speed than the actual wind speed (Edwards et al. 2018). Thus, the SPC-based observed frequency is likely an overestimate of the true frequency of severe wind events, assuming other reporting biases are minimal during the range of years used (2000-2018). For this reason, it is not surprising that the observed severe wind speed frequency is higher than the Verisk-modeled frequency, and this difference is an expected result in order for the Verisk Severe Thunderstorm Model for the United States to properly reflect the most recent severe convective straight-line wind climatology.

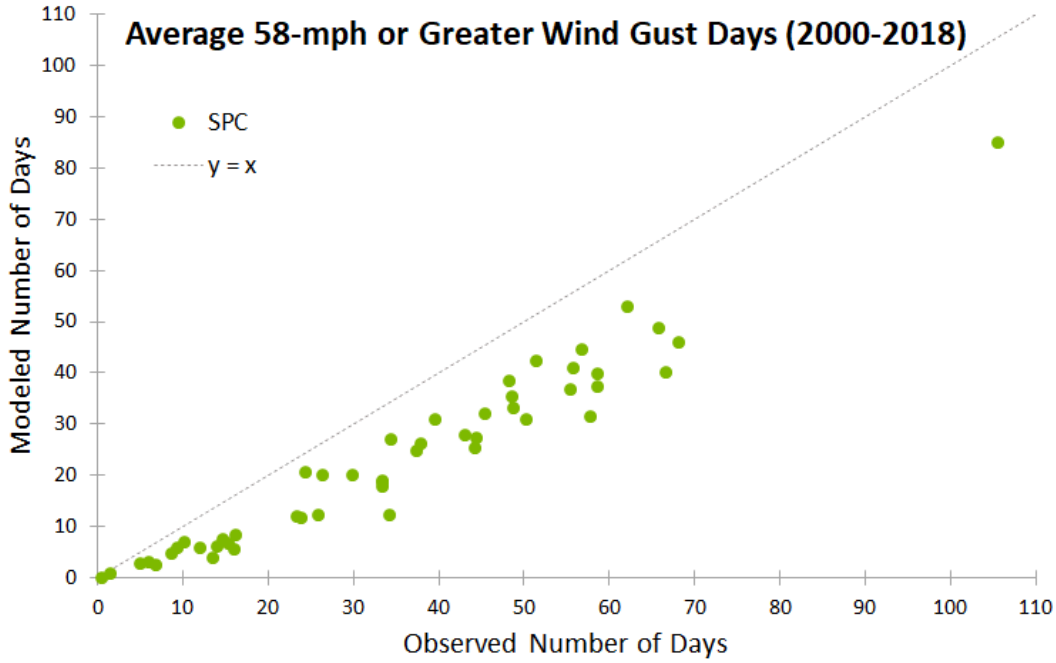

Figure 217. Verisk-modeled versus SPC-observed average annual 58-mph or greater convective straight-line wind gust days from 2000-2018, by state
Note: Each state's annual average value is represented by a dot.

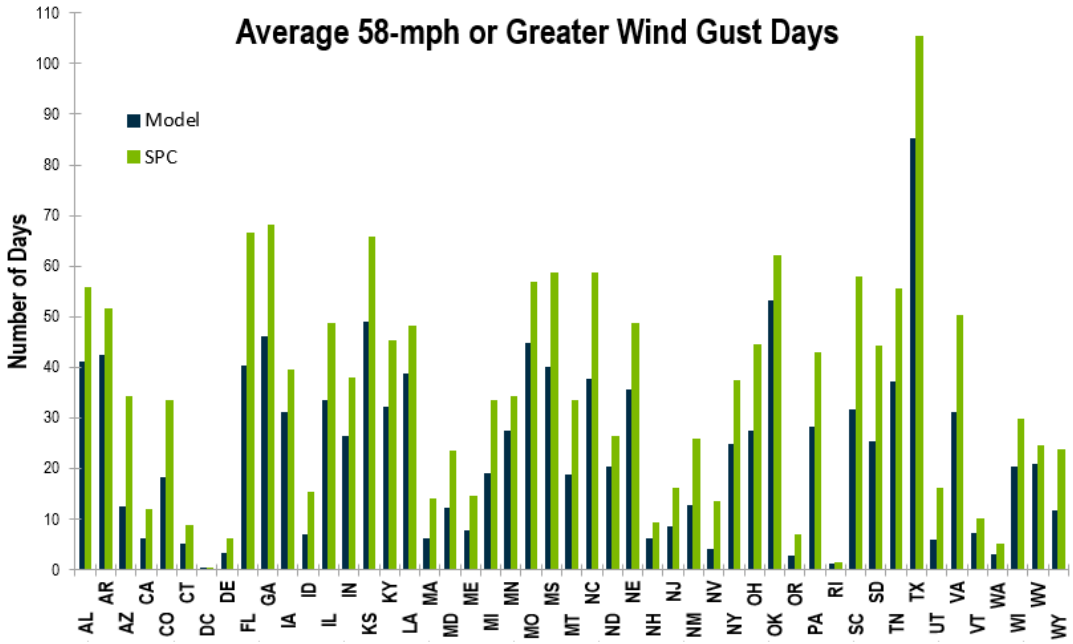

Figure 218. Verisk-modeled (dark blue bars) and SPC-observed (green bars) average annual 58-mph or greater convective straight-line wind gust days from 2000-2018, by state

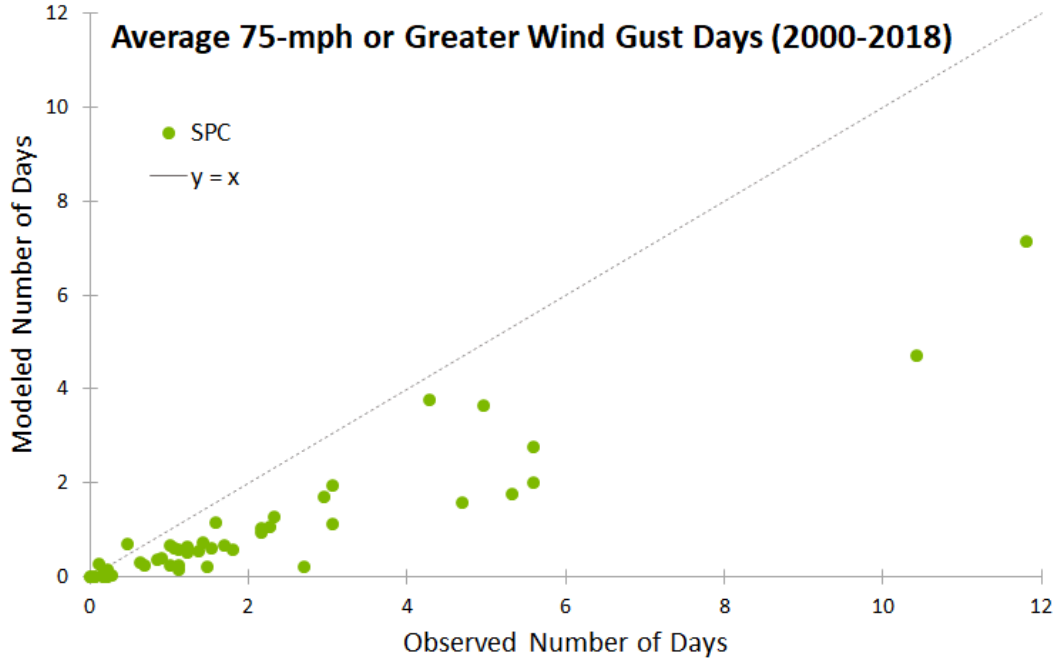

Figure 219. Verisk-modeled versus SPC-observed average annual 75-mph or greater convective straight-line wind gust days from 2000-2018, by state
Note: Each state's annual average value is represented by a dot.

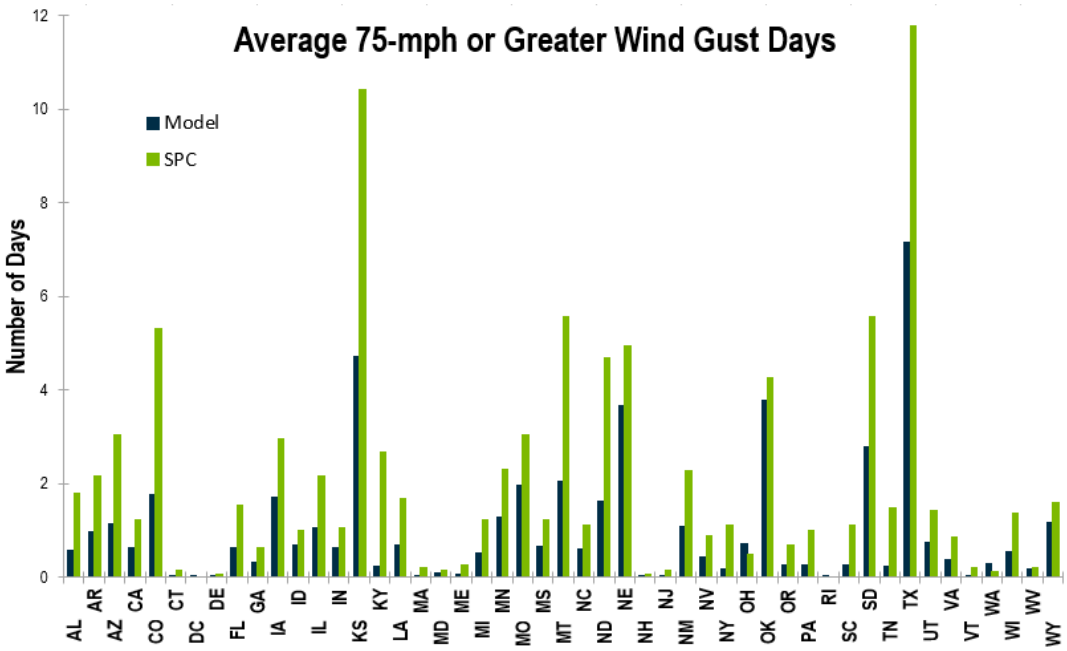

Figure 220. Verisk-modeled (dark blue bars) and SPC-observed (green bars) average annual 75-mph or greater convective straight-line wind gust days from 2000-2018, by state

Summary

While there are no overall **nationwide** temporal trends in historical severe thunderstorm event frequency or intensity, regional trends have been observed during the last 20-30 years, as reported in the published literature. Given the biases that exist in the observational datasets, it is difficult to determine the extent to which anthropogenic climate change has played a role in these trends, even though, in some instances, the physical understanding is consistent with the observed changes. Thus, researchers express modest confidence that the observed severe thunderstorm activity changes can be attributed to anthropogenic climate change as opposed to natural variability that may not be indicative of a long-term trend. As a result, Verisk researchers gave more attention to the recent climatology (e.g., last 20 years) than to the climatology of the distant past (e.g., prior to 1998) when developing Verisk's stochastic catalog. Therefore, the updated Verisk Severe Thunderstorm Model for the United States represents the current severe thunderstorm risk.

8 Verisk Severe Thunderstorm Model for the United States in Touchstone and Touchstone Re

8.1 Available catalogs

Touchstone supports six varieties of stochastic catalogs and a historical event set in the Verisk Severe Thunderstorm Model for the United States. Touchstone Re supports one stochastic catalog and a historical event set in this model.

Stochastic catalog

Touchstone

Touchstone supports the following stochastic catalogs:

- All-events catalogs of simulated severe thunderstorms in the United States,[87] which reflect severe thunderstorm risk, regardless of how much industry loss they cause, under average climate conditions. These catalogs include:
  - 10,000-year (10K) all-events catalog
  - 50,000-year (50K) all-events catalog
  - 100,000-year (100K) all-events catalog
- Cat-only catalogs of simulated severe thunderstorms in the United States, which reflect severe thunderstorm risk that result in gross insurable loss greater than or equal to USD 25 million under average climate conditions. These catalogs include:
  - 10K cat-only catalog
  - 50K cat-only catalog
  - 100K cat-only catalog

See Also

Stochastic catalog

Touchstone Re

Touchstone Re supports the following stochastic catalog:

[87] The all-events catalogs are contained within the standard event sets in Touchstone.

- 10K cat-only catalog of simulated severe thunderstorms in the United States, which reflects severe thunderstorm risk that result in gross insurable loss greater than or equal to USD 25 million under average climate conditions.[88]

See Also

Stochastic catalog

Historical event set

In the Verisk Severe Thunderstorm Model for the United States, both Touchstone and Touchstone Re support a marquee event set, consisting of 35 historical events. These 35 events are comprised of 5 variations of the 7 historical events. The 5 realizations of each event contain the same number of microevents by sub-peril and are of the same duration. They do, however, differ in terms of modeled variables, such as starting location, length, width, storm track direction, and intensity, with the amount of perturbation depending upon the degree of uncertainty. Table 32 lists the model's 35 historical events and event IDs that are available in both Touchstone and Touchstone Re.

Table 32. Historical events available in Touchstone and Touchstone Re for the Verisk Severe Thunderstorm Model for the United States

Event ID	PCS ID	Historical Event	Event ID	PCS ID	Historical Event
1	13	May 10, 2010	21	46	April 22 - 28, 2011
2	13	May 10, 2010	22	46	April 22 - 28, 2011
3	13	May 10, 2010	23	46	April 22 - 28, 2011
4	13	May 10, 2010	24	46	April 22 - 28, 2011
5	13	May 10, 2010	25	46	April 22 - 28, 2011
6	14	May 12 - 16, 2010	26	48	May 20 - 27, 2011
7	14	May 12 - 16, 2010	27	48	May 20 - 27, 2011
8	14	May 12 - 16, 2010	28	48	May 20 - 27, 2011
9	14	May 12 - 16, 2010	29	48	May 20 - 27, 2011
10	14	May 12 - 16, 2010	30	48	May 20 - 27, 2011
11	18	June 10 - 16, 2010	31	83	June 28 - July 2, 2012
12	18	June 10 - 16, 2010	32	83	June 28 - July 2, 2012
13	18	June 10 - 16, 2010	33	83	June 28 - July 2, 2012
14	18	June 10 - 16, 2010	34	83	June 28 - July 2, 2012
15	18	June 10 - 16, 2010	35	83	June 28 - July 2, 2012
16	31	October 4 - 6, 2010			
17	31	October 4 - 6, 2010			

[88] The Touchstone Re stochastic catalog contains industry losses for cat-only events and zero industry loss placeholders for non-cat events to support losses from detailed company loss files/company loss association files (CLF/CLA) that may include these non-cat events. They will not produce industry loss but will produce loss for non-cat events if they are present in the CLF/CLA.

Event ID	PCS ID	Historical Event	Event ID	PCS ID	Historical Event
18	31	October 4 - 6, 2010			
19	31	October 4 - 6, 2010			
20	31	October 4 - 6, 2010			

See Also

Historical event set

Modeled losses for historical severe thunderstorms

Significant historical U.S. severe thunderstorms

8.2 Verisk Severe Thunderstorm Model for the United States in Touchstone

Supported geographic resolutions

The following geographic resolutions are supported for the Verisk Severe Thunderstorm Model for the United States in Touchstone:

- County
- ZIP Code
- Complete Address (including the street, city, and state)
- User specified latitude/longitude

Modeling aggregate data

Disaggregation, the process by which Touchstone distributes aggregate exposure data from a coarse geographic resolution to a fine geographic resolution more suitable for detailed catastrophe modeling, is supported in the Verisk Severe Thunderstorm Model for the United States. Touchstone supports the disaggregation of exposure data in the United States from a source resolution level of county, city, or ZIP Code to a target resolution level of 1-km grid cells.

The Average Properties feature, which specifies how Touchstone applies physical properties (e.g., soil type and land use/land cover data) during a loss analysis, is not supported in the Verisk Severe Thunderstorm Model for the United States.

Construction and occupancy classes, year built and height bands, and relative vulnerabilities

A structure's vulnerability depends on its construction and occupancy class combination, age, height, and gross area/square footage. With the goal of enabling clients to code their exposure data as specifically as possible, the Verisk Severe Thunderstorm Model for the United States supports 140 construction classes and 112 occupancy classes, of which 62

are occupancy classes for large industrial facilities.[89] The model also supports several height and age bands, which are defined separately for different construction classes, as well as the ability to incorporate the effect of square footage for high-value homes for wind and tornado, and for the majority of the residential and commercial risks for hail.

Verisk has compiled all the supported construction and occupancy class information, along with relative vulnerabilities, into the *Verisk Severe Thunderstorm Model for the United States Supplement*. This supplement is available with login on the Client Portal.

The Verisk Severe Thunderstorm Model for the United States Supplement contains the following information:

- Complete lists of supported construction and occupancy classes
- Supported hail, straight-line wind, and tornado construction/occupancy class combinations
- Supported hail, straight-line wind, and tornado height bands
- Supported hail, straight-line wind, and tornado secondary risk characteristics
- Relative hail, straight-line wind, and tornado vulnerabilities for select construction and occupancy class combinations, for Coverages A, C, and D
- Relative hail, straight-line wind, and tornado vulnerability comparisons for the 400-series occupancy classes relative to a wood frame/general industrial facility (101/321), for Coverages A, C, and D
- Relative hail, straight-line wind, and tornado vulnerabilities for buildings (Coverage A) by year built, for select years
- Relative hail, straight-line wind, and tornado vulnerabilities for buildings (Coverage A) by height
- Relative hail, straight-line wind, and tornado vulnerabilities of each secondary risk characteristic option

Note that detailed descriptions of the supported construction and occupancy classes are available in the *Touchstone Exposure Data Validation Reference*, which can be accessed from www.unicede.com.

Supported secondary risk characteristics

The Verisk Severe Thunderstorm Model for the United States contains a hail damage framework and a wind damage framework, which identify key building features that may significantly exacerbate or mitigate losses (i.e., secondary risk characteristics). These frameworks were developed based on structural engineering expertise and building damage observations made in the aftermath of severe storms. Touchstone supports the following secondary risk characteristics for the Verisk Severe Thunderstorm Model for the United States.

[89] The industrial facilities set of occupancy classes refers to the 400-series, which include structures that are very different from the 300-series as they represent large, complex facilities comprised of many components. Small facilities (300-series) consist of mostly buildings and some machinery.

Straight-line wind and tornado damage	27
Hail damage	13

Table 33 and Table 34 provide a description of the secondary risk characteristics supported in the model for straight-line winds, tornadoes, and hail.

Table 33. Secondary risk characteristics supported in Touchstone for straight-line winds and tornadoes

Secondary Risk Modifier	Description
Appurtenant Structures	Components of a property that are not an integral part of the main building and are not connected to it. Appurtenant structures may require a different treatment in analysis from the main building.
Average Adjacent Building Height	Average height of buildings adjacent to the building of interest.
Building Condition	A building's overall general condition of the external cladding and maintenance, based on a visual inspection.
Building Foundation Connection	Connection type between the structure and its foundation. This connection transfers the vertical and lateral wind loads on the building to the foundation.
Certified Structures (IBHS)	Fortification standards developed by the Insurance Institute for Business and Home Safety (IBHS) to help strengthen residential and commercial buildings through retrofitting and new construction standards to improve the home's strength and resistance to natural perils. Residential single- and multi-family homes (occupancy types 301, 302, and 303) of wood, masonry, concrete, or steel that meet IBHS criteria for load resistance are eligible for gold, silver, or bronze certification, which represents the level of disaster protection or mitigation. In addition, commercial buildings including, but not limited to, hotels, group institutional housing, condominiums, general commercial buildings, retail stores, and wholesale stores (occupancy types 304, 305, 306, 311, 312, 313+) that meet the IBHS fortification standards set forth for commercial buildings are eligible for this feature.
Exterior Doors	Nature of the exterior doors of a building. Exterior doors and their frames are weak in resisting wind loads. They deflect considerably under high wind loads and thus fail.
Floor of Interest	Floor of concern if insurance coverage is not for the entire building.
Glass Percentage	The percentage of the wall that is covered by glass. Generally, a higher percentage of glass means higher vulnerability.
Glass Type	Type of glass used in the building. Different glass types have varying degrees of resistance to wind loads and debris impact.

Secondary Risk Modifier	Description
Large Missile	Indicates if materials within a 100-foot radius of the property may, during high winds, become large missiles capable of damaging the property. Examples include garden furniture and wood planks that dislodge from nearby buildings.
Roof Anchorage	Connections that secure the roof support system to the walls. Roof anchorage transfers wind loads from roof to walls.
Roof-Attached Structures	Any equipment attached to the roof, mechanical or otherwise. Attached structures are often more vulnerable than the main building.
Roof Covering	Material used to cover the roof. Damage to the roof covering can allow water to damage the building's interior.
Roof Covering Attachment	Connections that secure the roof covering to the underlying roof deck. An improper attachment can increase the vulnerability of the roof.
Roof Deck	Material and construction type of the roof deck. Roof decks transfer the roof loads to the underlying joists and purlins. Damage to the roof deck allows breaching of the building envelope, which can lead to significant damage.
Roof Deck Attachment	Nature of the connections used to secure the roof deck to the underlying roof support system.
Roof Geometry	Shape of the roof, which affects the wind pressure intensity and the uplift resistance.
Roof Pitch	The roof slope. Low pitch roofs experience greater uplift forces during high winds as compared to high pitch roofs.
Roof Year Built	The year the roof was built or had a major renovation. With age, roofs lose their ability to resist wind loads.
Seal of Approval	The level of professional engineering attention given to the design of a structure.
Small Debris	Indicates if any small debris within a 200-foot radius of the property may, during high winds, become small missiles capable of breaking window glass. Small debris can be carried to all heights of the building. Examples are roof gravel, trash bins, and tree branches.
Terrain Roughness	Describes the terrain conditions whether they be a large city, urban/suburban areas, open terrain with scattered obstructions, or flat, unobstructed areas.
Tree Exposure	The tree hazard around the building. Trees may snap in strong winds and damage nearby buildings.
Wall Attached Structure	Nonintegral components of a property that are physically attached to the main building. Attached structures are often more vulnerable than the main building.

Secondary Risk Modifier	Description
Wall Siding	Materials to protect walls from weathering, which affects the resistance to wind damage. A breach in the wall siding can expose walls to wind and rain, resulting in damage and the buildup of internal pressure.
Wall Type	Materials used for external walls of the building. These materials affect the resistance to wind-induced lateral loads. A breach in an external wall can result in damage and buildup of internal pressure.
Window Protection	Window protection can reduce the potential damage to a building.

Table 34. Secondary risk characteristics supported in Touchstone for hail

Secondary Risk Modifier	Description
Certified Structures (IBHS)	Fortification standards developed by the Insurance Institute for Business and Home Safety (IBHS) to help strengthen residential and commercial buildings through retrofitting and new construction standards to improve the home's strength and resistance to natural perils. Residential single- and multi-family homes (occupancy types 301, 302, and 303) of wood, masonry, concrete, or steel that meet IBHS criteria for load resistance are eligible for gold, silver, or bronze certification, which represents the level of disaster protection or mitigation. In addition, commercial buildings including, but not limited to, hotels, group institutional housing, condominiums, general commercial buildings, retail stores, and wholesale stores (occupancy types 304, 305, 306, 311, 312, 313+) that meet the IBHS fortification standards set forth for commercial buildings are eligible for this feature.
Glass Percentage	The percentage of the wall that is covered by glass. Generally, a higher percentage of glass means higher vulnerability.
Glass Type	Type of glass used in the building. Different glass types have varying degrees of resistance to hail impact.
Roof Attached Structure	Any equipment attached to the roof, mechanical or otherwise. Attached structures are often more vulnerable than the main building.
Roof Covering	Material used to cover the roof. Damage to the roof covering can allow water to damage the building's interior.
Roof Deck	Material used for the roof deck. A damaged roof deck results in a breached building envelope, which can cause building and contents damage.
Roof Geometry	A roof's shape, which has an effect on its vulnerability to hail damage.

Secondary Risk Modifier	Description
Roof Hail Impact Resistance (Impact-Resistance A, B, C, D)	Class A: Lowest impact resistance (shingles withstand up to 1.25” diameter ice ball impact twice in the same spot). Class B: Shingles withstand up to 1.5” diameter ice ball impact twice in the same spot. Class C: Shingles withstand up to 1.75” diameter ice ball impact twice in the same spot. Class D: Highest impact resistance (shingles that can withstand up to 2” diameter ice ball impact twice in the same spot).
Roof Pitch	The roof slope, which has an effect on its vulnerability to hail damage.
Roof Year Built	The year the roof was built or had a major renovation. With age, roofs lose their strength and become more vulnerable to hail damage.
Wall Attached Structure	Any object physically attached to a building's exterior walls that are not an integral part of the main building structure (e.g., carport, garage, porch, balcony). These attached structures are often more vulnerable to hail damage than the main building.
Wall Siding	Materials to protect walls from weathering, which affects the resistance to hail damage. A breach in the wall siding can expose walls to water intrusion, resulting in damage.
Window Protection	The type of protection system (if any) a building has for its windows. Window protection can reduce the potential hail damage to a building if it is installed just prior to the event.

For more information on wind and hail SRCs, please see the *Secondary Risk Characteristics* webpage available, with login, on the Client Portal.

See Also

Accounting for hail Secondary Risk Characteristics
Accounting for wind Secondary Risk Characteristics

Damage functions for unknown characteristics

In the Verisk Severe Thunderstorm Model for the United States, building, contents, and time element damage functions are available for unknown construction, occupancy, and building-height classes. In these cases, Touchstone uses a composite damage function based on Verisk's Industry Exposure Database.

The damage functions for unknown construction, occupancy, and height classes are exposure-weighted averages of the damage functions corresponding to all values of the unknown parameters, with weights determined by the relative share of the total insurable value of each class. Different damage functions are used depending on how many variables, and which ones, are unknown.

For example, the damage function for a specific exposure of known construction and occupancy, but unknown height, would be a weighted average of the damage functions, for the same construction and occupancy classes, corresponding to all the different height classes. The damage function for a specific exposure of known occupancy but unknown construction and height would be a weighted average of the damage functions for the same occupancy class corresponding to all combinations of construction and height classes.

See Also

Damage functions for buildings with unknown primary characteristics

Supported policy terms

The financial module in Touchstone allows for the application of a wide variety of location, policy, and reinsurance conditions. Location terms may be specified to include limits and deductibles by site or by coverage. Supported policy terms include blanket and excess layers, minimum and maximum deductibles, and sublimits. Reinsurance terms include facultative certificates and various types of risk-specific and aggregate treaties with occurrence and aggregate limits.

For more information about policy terms for a given year, please see the Verisk publication *Industry Deductible Assumptions* for the appropriate year. This document is available with login through the Client Portal.

8.3 Verisk Severe Thunderstorm Model for the United States in Touchstone Re

Resolution of analysis results

Modeled loss estimates for the Verisk Severe Thunderstorm Model for the United States are reported at the state and county levels in Touchstone Re.

Verisk Industry Exposure Database

The Industry Exposure Database is an integral and highly valuable component of Touchstone Re. This database contains estimates of insured and insurable property exposure data at a high degree of resolution, including the number of risks, their replacement values (broken down by line of business, coverage, occupancy, and construction type), building attributes, and information regarding standard policy terms and conditions. These underlying data are aggregated to the county level by Line of Business (LOB) in Touchstone Re.

Verisk uses a variety of public and private sources to estimate industry exposures, including government data, commercially-available demographic information, and other industry data. Verisk's Industry Exposure Database is extensively validated via comparison against values obtained from various insurance industry and governmental sources.

The Industry Exposure Database implemented in the Verisk Severe Thunderstorm Model for the United States is current through the end of 2019. For more details about the Industry

Exposure Database for this model, see the document *Verisk Industry Exposure Databases for the United States* (available with login from the Client Portal), which provides further details about the Industry Exposure Database for this region and peril including:

- How the Industry Exposure Database was developed
- The data sources used to develop the Industry Exposure Database
- Maps detailing the total exposure for the modeled region
- Share of Industry Exposure by LOB
- Construction splits by LOB
- Coverage splits by LOB
- Height band splits by LOB
- Assumed take-up rates
- Policy condition assumptions

Lines of business for reporting model losses

The Verisk Severe Thunderstorm Model for the United States supports the following lines of business for reporting modeled losses in Touchstone Re.

Residential	Residential Building, Contents, and Time Element
Manufactured (Mobile) Home	Manufactured Home Building, Contents, and Time Element
Commercial/ Industrial	Commercial and Industrial Buildings, Contents, and Time Element
Automobile	Personal and Commercial

Supported take-up rates and policy conditions

Take-up rate information can be found in the Verisk publication *Industry Take-Up Rates* for the appropriate year. Deductible information is available in the Verisk Publication *Industry Deductible Assumptions* for the appropriate year. Both publications are available with login through the Client Portal.

A Analysis Settings

The following settings were used in Verisk's Research Model (Table 35), Touchstone 10.0 (Table 36), and Touchstone Re 10.0 (Table 37) to produce the loss results provided in this document. For information on take-up rate assumptions, see the Verisk publication *Industry Take-Up Rates* for the appropriate year, available with login on the Client Portal.

Table 35. Analysis settings for the Verisk Severe Thunderstorm Model for the United States in Verisk's Research Model

Setting	Options
Perils Modeled	• Hail • Straight-line winds • Tornadoes • Hail, straight-line winds, and tornadoes combined
Catalogs	• Unfiltered 10,000-year (10K) All-events • Unfiltered 10K Cat-only
Industry Exposure Vintage	2019
Average Properties	N/A
Demand Surge	N/A
Disaggregation	Off

Table 36. Analysis settings for the Verisk Severe Thunderstorm Model for the United States in Touchstone 10.0

Setting	Options
Perils Modeled	• Hail • Straight-line winds • Tornadoes • Hail, straight-line winds, and tornadoes combined
Catalog	Unfiltered 10K Cat-only
Industry Exposure Vintage[90]	2019
Average Properties	N/A
Demand Surge	On
Disaggregation	Off

[90] Due to the 90-m resolution of the database, coupled with the high model resolution and number of events, Verisk ran a random 10% sample of the Industry Exposure Database, without any location or line of business bias.

Table 37. Analysis settings for the Verisk Severe Thunderstorm Model for the United States in Touchstone Re 10.0

Setting	Options
Perils Modeled	Hail, straight-line winds, and tornadoes combined
Catalog	Filtered 10K Cat-only[91]
Industry Exposure Vintage	2019
Take-Up Rates	2021 Take-up Rates[92]
Demand Surge	On

[91] The Touchstone Re stochastic catalog contains industry losses for cat-only events and zero industry loss placeholders for non-cat events to support losses from detailed company loss files/company loss association files (CLF/CLA) that may include these non-cat events. They will not produce industry loss but will produce loss for non-cat events if they are present in the CLF/CLA.

[92] For specific take-up rates, see the *2021 Industry Take-Up Rates,* available with login on the Client Portal.

B Temporal Vulnerability Changes

Table 38 shows the temporal vulnerability changes for modeled states and counties for engineered and non-engineered structures in the Verisk Severe Thunderstorm Model for the United States.

Table 38. Temporal vulnerability changes by region and construction type

		Vulnerability Changes for Non-Engineered Structures			Vulnerability Changes for Engineered Structures		
State	**Counties**	**None***	**Changes Annually**	**None**	**None**	**Changes Annually**	**None**
Alabama	Autauga, Calhoun, Etowah, Monroe, Tuscaloosa	≤ 1994	1995-2012, 2013-2015	≥ 2016	≤ 1994	1995-2007, 2008-2015	≥ 2016
	Baldwin	≤ 1994	1995-2007, 2008-2011, 2012-2014	≥ 2015	Same as Non-Engineered		
	Chilton, Houston, Montgomery, Shelby	≤ 1994	1995-2012, 2013-2014	2015-2016, ≥ 2017	≤ 1994	1995-2007, 2008-2014	2015-2016, ≥ 2017
	Dale, Jackson, Pike, Walker	≤ 1994	1995-2012, 2013-2014	2015-2017, ≥ 2018	≤ 1994	1995-2007, 2008-2014	2015-2017, ≥ 2018
	Jefferson	≤ 1994	1995-2012, 2013-2014	≥ 2015	≤ 1994	1995-2007, 2008-2014	≥ 2015
	Mobile	≤ 1994	1995-2001, 2002-2014	≥ 2015	≤ 1994	1995-2007, 2008-2014	≥ 2015
	Wilcox	≤ 1994	1995-2012, 2013-2014	≥ 2015	≤ 1994	1995-2007, 2008-2014	2015-2017, ≥ 2018
	Rest of the State	≤ 1994	1995-2012, 2013-2014	≥ 2015	≤ 1994	1995-2007, 2008-2014	≥ 2015
Arizona	Apache	≤ 1994	1995-2003, 2004-2014	2015-2018, ≥ 2019	Same as Non-Engineered		
	Cochise	≤ 1994	1995-2004, 2005-2014	≥ 2015	Same as Non-Engineered		
	Coconino, Santa Cruz	≤ 1994	1995-2006, 2007-2013, 2014	≥ 2015	Same as Non-Engineered		
	Gila	≤ 1994	1995-2006, 2007-2014	≥ 2015	Same as Non-Engineered		
	Graham	≤ 1994	1995-2014	≥ 2015	Same as Non-Engineered		

		Vulnerability Changes for Non-Engineered Structures			Vulnerability Changes for Engineered Structures		
State	**Counties**	**None***	**Changes Annually**	**None**	**None**	**Changes Annually**	**None**
	Greenlee, Navajo	≤ 1994	1995-2004, 2005-2014	2015-2018, ≥ 2019	Same as Non-Engineered		
	La Paz	≤ 1994	1995-2009, 2010-2014	≥ 2015	Same as Non-Engineered		
	Maricopa	≤ 1994	1995-2004, 2005-2012, 2013-2014	≥ 2015	Same as Non-Engineered		
	Mohave	≤ 1994	1995-2008, 2009-2014	≥ 2015	Same as Non-Engineered		
	Pima	≤ 1994	1995-2000, 2001-2012, 2013-2014	≥ 2015	Same as Non-Engineered		
	Pinal	≤ 1994	1995-2006, 2007-2012, 2013-2014	≥ 2015	Same as Non-Engineered		
	Yavapai	≤ 1994	1995-2007, 2008-2014	≥ 2015	Same as Non-Engineered		
	Yuma	≤ 1994	1995-2005, 2006-2012, 2013-2014	≥ 2015	≤ 1994	1995-2003, 2004-2012, 2013-2014	≥ 2015
Arkansas	All	≤ 1994	1995-2014	≥ 2015	Same as Non-Engineered		
California	All	≤ 1994	1995-2007, 2008-2013, 2014	≥ 2015	Same as Non-Engineered		
Colorado	Adams	≤ 1994	1995-2006, 2007-2014	≥ 2015	Same as Non-Engineered		
	Alamosa	≤ 1994	1995-2007, 2008-2014	2015-2016, ≥ 2017	Same as Non-Engineered		
	Arapahoe	≤ 1994	1995-2005, 2006-2014	2015-2016, ≥ 2017	Same as Non-Engineered		
	Boulder	≤ 1994	1995-2002, 2003-2012, 2013-2014	≥ 2015	Same as Non-Engineered		
	Broomfield, Eagle	≤ 1994	1995-2003, 2004-2014	2015-2016, ≥ 2017	Same as Non-Engineered		
	Chaffee	≤ 1994	1995-2006, 2007-2014	2015-2017, ≥ 2018	Same as Non-Engineered		
	Clear Creek	≤ 1994	1995-2011, 2012-2014	2015-2017, ≥ 2018	Same as Non-Engineered		
	Delta, Las Animas	≤ 1994	1995-2004, 2005-2014	≥ 2015	Same as Non-Engineered		
	Denver	≤ 1994	1995-2003, 2004-2015	≥ 2016	Same as Non-Engineered		

		Vulnerability Changes for Non-Engineered Structures			Vulnerability Changes for Engineered Structures		
State	**Counties**	**None***	**Changes Annually**	**None**	**None**	**Changes Annually**	**None**
	Douglas	≤ 1994	1995-2005, 2006-2012, 2013-2014	≥ 2015	Same as Non-Engineered		
	Elbert, Mesa	≤ 1994	1995-2014	2015-2018, ≥ 2019	Same as Non-Engineered		
	Fremont, Logan, Otero	≤ 1994	1995-2008, 2009-2014	≥ 2015	Same as Non-Engineered		
	Garfield, Gilpin, Hinsdale	≤ 1994	1995-2015	≥ 2016	Same as Non-Engineered		
	Grand	≤ 1994	1995-2010, 2011-2014	2015-2017, ≥ 2018	Same as Non-Engineered		
	Gunnison	≤ 1994	1995-2009, 2010-2014	≥ 2015	Same as Non-Engineered		
	Jefferson	≤ 1994	1995-2001, 2002-2013, 2014	≥ 2015	Same as Non-Engineered		
	Lake	≤ 1994	1995-2004, 2005-2012, 2013-2014	≥ 2015	Same as Non-Engineered		
	La Plata	≤ 1994	1995-2004, 2005-2014	2015-2017, ≥ 2018	Same as Non-Engineered		
	Larimer	≤ 1994	1995-2004, 2005-2013, 2014	≥ 2015	Same as Non-Engineered		
	Lincoln, Moffat, Rio Blanco, Rio Grande	≤ 1994	1995-2007, 2008-2014	≥ 2015	Same as Non-Engineered		
	Montezuma	≤ 1994	1995-2012, 2013-2014	2015-2017, ≥ 2018	Same as Non-Engineered		
	Montrose	≤ 1994	1995-2014	2015, ≥ 2016	Same as Non-Engineered		
	Morgan, San Miguel	≤ 1994	1995-2010, 2011-2014	≥ 2015	Same as Non-Engineered		
	Ouray	≤ 1994	1995-2009, 2010-2014	≥ 2015	Same as Non-Engineered		
	Park	≤ 1994	1995-2013, 2014-2015	≥ 2016	Same as Non-Engineered		
	Pitkin	≤ 1994	1995-2009, 2010-2014	2015-2016, ≥ 2017	Same as Non-Engineered		
	Pueblo	≤ 1994	1995-2014	≥ 2015	Same as Non-Engineered		

		Vulnerability Changes for Non-Engineered Structures			Vulnerability Changes for Engineered Structures		
State	**Counties**	**None***	**Changes Annually**	**None**	**None**	**Changes Annually**	**None**
	Routt	≤ 1994	1995-2014	2015-2017, ≥ 2018	≤ 1994	1995-2005, 2006-2014	2015-2017, ≥ 2018
	Teller	≤ 1994	1995-2007, 2008-2014	2015-2016, ≥ 2017	Same as Non-Engineered		
	Weld	≤ 1994	1995-2011, 2012-2014	≥ 2015	Same as Non-Engineered		
	Rest of State	≤ 1994	1995-2014	≥ 2015	Same as Non-Engineered		
Connecticut	All	≤ 1994	1995-2005, 2006-2014	2015-2016, ≥ 2017	Same as Non-Engineered		
Delaware	Kent, New Castle	≤ 1994	1995-2001, 2002-2013, 2014	≥ 2015	Same as Non-Engineered		
	Sussex	≤ 1994	1995-2005, 2006-2013, 2014	≥ 2015	Same as Non-Engineered		
District of Columbia (Washington D.C.)	All	≤ 1994	1995-2001, 2002-2013, 2014	≥ 2015	Same as Non-Engineered		
Florida	All	≤ 1994	1995-2001, 2002-2011, 2012-2014	≥ 2015	Same as Non-Engineered		
Georgia	All	≤ 1994	1995-2002, 2003-2013, 2014	≥ 2015	Same as Non-Engineered		
Idaho	All	≤ 1994	1995-2001, 2002-2013, 2014	≥ 2015	≤ 1994	1995-2001, 2002-2014	2015-2016, ≥ 2017
Illinois	Boone	≤ 1994	1995-2003, 2004-2014	≥ 2015	Same as Non-Engineered		
	Brown, Champaign	≤ 1994	1995-2006, 2007-2014	≥ 2015	Same as Non-Engineered		
	Carroll	≤ 1994	1995-2004, 2005-2014	≥ 2015	≤ 1994	1995-2010, 2011-2014	≥ 2015
	Coles	≤ 1994	1995-2011, 2012-2014	≥ 2015	Same as Non-Engineered		
	Cook	≤ 1994	1995-2014	2015, 2016-2018, ≥ 2019	≤ 1994	1995-2014	2015-2018, ≥ 2019
	DeKalb, Sangamon	≤ 1994	1995-2009, 2010-2014	≥ 2015	Same as Non-Engineered		

		Vulnerability Changes for Non-Engineered Structures			Vulnerability Changes for Engineered Structures		
State	**Counties**	**None***	**Changes Annually**	**None**	**None**	**Changes Annually**	**None**
	DuPage, Kendall, Lake, Lawrence, McLean, Tazewell, Vermilion	≤ 1994	1995-2013, 2014	≥ 2015	Same as Non-Engineered		
	Effingham, Stephenson	≤ 1994	1995-2014	2015-2017, ≥ 2018	Same as Non-Engineered		
	Fayette	≤ 1994	1995-2008, 2009-2014	≥ 2015	Same as Non-Engineered		
	Franklin	≤ 1994	1995-2014	≥ 2015	≤ 1994	1995-2014	2015, ≥ 2016
	Grundy, Williamson	≤ 1994	1995-2010, 2011-2014	≥ 2015	Same as Non-Engineered		
	Jersey	≤ 1994	1995-2007, 2008-2014	≥ 2015	Same as Non-Engineered		
	Kane	≤ 1994	1995-2012, 2013-2014	≥ 2015	Same as Non-Engineered		
	Kankakee	≤ 1994	1995-2008, 2009-2014	2015-2016, ≥ 2017	Same as Non-Engineered		
	Knox	≤ 1994	1995-2006, 2007-2011, 2012-2014	≥ 2015	Same as Non-Engineered		
	LaSalle, St. Clair	≤ 1994	1995-2006, 2007-2014	2015-2016, ≥ 2017	Same as Non-Engineered		
	Madison	≤ 1994	1995-2014	≥ 2015	Same as Non-Engineered		
	McHenry, Ogle	≤ 1994	1995-2014	2015, ≥ 2016	Same as Non-Engineered		
	Peoria	≤ 1994	1995-2011, 2012-2014	≥ 2015	Same as Non-Engineered		
	Rock Island	≤ 1994	1995-2003, 2004-2013, 2014	≥ 2015	Same as Non-Engineered		
	Will	≤ 1994	1995-2013, 2014	≥ 2015	≤ 1994	1995-2005, 2006-2013, 2014	≥ 2015
	Winnebago	≤ 1994	1995-2004, 2005-2014	≥ 2015	Same as Non-Engineered		
	Rest of State	≤ 1994	1995-2014	≥ 2015	Same as Non-Engineered		

		Vulnerability Changes for Non-Engineered Structures			Vulnerability Changes for Engineered Structures		
State	**Counties**	**None***	**Changes Annually**	**None**	**None**	**Changes Annually**	**None**
Indiana	All	≤ 1994	1995-2000, 2001-2014	≥ 2015	≤ 1994	1995-2002, 2003-2013, 2014	≥ 2015
Iowa	Benton, Jasper	≤ 1994	1995-2003, 2004-2014	2015-2017, ≥ 2018	Same as Non-Engineered		
	Black Hawk, Buena Vista, Lee, Mahaska, Scott, Webster	≤ 1994	1995-2003, 2004-2014	2015-2016, ≥ 2017	Same as Non-Engineered		
	Boone, Linn	≤ 1994	1995-2003, 2004-2013, 2014	≥ 2015	Same as Non-Engineered		
	Bremer, Buchanan, Henry, Warren	≤ 1994	1995-2003, 2004-2012, 2013-2014	≥ 2015	Same as Non-Engineered		
	Clay, Plymouth, Woodbury	≤ 1994	1995-2003, 2004-2015	≥ 2016	Same as Non-Engineered		
	Clinton, Des Moines, Kossuth, Polk	≤ 1994	1995-2003, 2004-2014	≥ 2015	Same as Non-Engineered		
	Dubuque	≤ 1994	1995-2003, 2004-2014	2015-2019, ≥ 2020	Same as Non-Engineered		
	Johnson, Washington	≤ 1994	1995-2003, 2004-2014	2015-2018, ≥ 2019	Same as Non-Engineered		
	Wapello	≤ 1994	1995-2003, 2004-2014	2015-2016, ≥ 2017	≤ 1994	1995-2003, 2004-2015	≥ 2016
	Rest of State	≤ 1994	1995-2003, 2004-2014	≥ 2015	Same as Non-Engineered		
Kansas	Allen, Ottawa, Sedgwick	≤ 1994	1995-2014	≥ 2015	Same as Non-Engineered		
	Barton, Brown, Labette, Miami, Thomas, Trego	≤ 1994	1995-2006, 2007-2014	≥ 2015	Same as Non-Engineered		
	Bourbon, Cowley	≤ 1994	1995-2007, 2008-2014	2015-2017, ≥ 2018	Same as Non-Engineered		

		Vulnerability Changes for Non-Engineered Structures			Vulnerability Changes for Engineered Structures		
State	**Counties**	**None***	**Changes Annually**	**None**	**None**	**Changes Annually**	**None**
	Butler	≤ 1994	1995-2011, 2012-2014	≥ 2015	Same as Non-Engineered		
	Chase	≤ 1994	1995-2014	2015-2016, ≥ 2017	Same as Non-Engineered		
	Cloud, Phillips, Riley	≤ 1994	1995-2012, 2013-2014	≥ 2015	Same as Non-Engineered		
	Crawford	≤ 1994	1995-2006, 2007-2015	≥ 2016	Same as Non-Engineered		
	Dickinson	≤ 1994	1995-2013, 2014	≥ 2015	Same as Non-Engineered		
	Douglas, Reno	≤ 1994	1995-2006, 2007-2013, 2014	≥ 2015	Same as Non-Engineered		
	Ellis	≤ 1994	1995-2006, 2007-2014	2015-2016, ≥ 2017	Same as Non-Engineered		
	Finney, Stevens	≤ 1994	1995-2005, 2006-2014	≥ 2015	Same as Non-Engineered		
	Ford, Lyon	≤ 1994	1995-2009, 2010-2014	≥ 2015	Same as Non-Engineered		
	Franklin	≤ 1994	1995-2006, 2007-2014	≥ 2015	Same as Non-Engineered		
	Geary	≤ 1994	1995-2015	≥ 2016	Same as Non-Engineered		
	Harvey	≤ 1994	1995-2003, 2004-2013, 2014	≥ 2015	Same as Non-Engineered		
	Johnson	≤ 1994	1995-2007, 2008-2012, 2013-2014	≥ 2015	Same as Non-Engineered		
	Kiowa	≤ 1994	1995-2006, 2007-2014	2015-2017, ≥ 2018	Same as Non-Engineered		
	Marion, Marshall, Montgomery, Seward	≤ 1994	1995-2014	2015-2017, ≥ 2018	Same as Non-Engineered		
	McPherson, Neosho	≤ 1994	1995-2012, 2013-2014	≥ 2015	Same as Non-Engineered		
	Meade	≤ 1994	1995-2009, 2010-2014	2015-2017, ≥ 2018	Same as Non-Engineered		
	Mitchell, Norton	≤ 1994	1995-2014	2015, ≥ 2016	Same as Non-Engineered		
	Saline	≤ 1994	1995-2009, 2010-2014	2015-2016, ≥ 2017	Same as Non-Engineered		

		Vulnerability Changes for Non-Engineered Structures			Vulnerability Changes for Engineered Structures		
State	**Counties**	**None***	**Changes Annually**	**None**	**None**	**Changes Annually**	**None**
	Shawnee	≤ 1994	1995-2011, 2012-2014	≥ 2015	≤ 1994	1995-2006, 2007-2014	2015-2017, ≥ 2018
	Sumner	≤ 1994	1995-2010, 2011-2014	2015-2018, ≥ 2019	Same as Non-Engineered		
	Wyandotte	≤ 1994	1995-2004, 2005-2015	≥ 2016	Same as Non-Engineered		
	Rest of State	≤ 1994	1995-2014	≥ 2015	Same as Non-Engineered		
Kentucky	All	≤ 1994	1995-2000, 2001-2013, 2014	≥ 2015	Same as Non-Engineered		
Louisiana	Cameron, Iberia, Jefferson, Lafourche, Orleans, Plaquemines, St. Bernard, St. Mary, St. Tammany, Terrebonne, Vermilion	≤ 1994	1995-2006, 2007-2013, 2014	≥ 2015	≤ 1994	1995-2007, 2008-2013, 2014	≥ 2015
	Rest of the State	≤ 1994	1995-2007, 2008-2013, 2014	≥ 2015	Same as Non-Engineered		
Maine	All	≤ 1994	1995-2004, 2005-2014	2015-2017, ≥ 2018	Same as Non-Engineered		
Maryland	All	≤ 1994	1995-2001, 2002-2011, 2012-2014	≥ 2015	Same as Non-Engineered		
Massachusetts	All	≤ 1994	1995-2008, 2009-2014	2015-2018, ≥ 2019	Same as Non-Engineered		
Michigan	All	≤ 1994	1995-2001, 2002-2013, 2014	≥ 2015	Same as Non-Engineered		
Minnesota	All	≤ 1994	1995-2003, 2004-2014	≥ 2015	Same as Non-Engineered		
Mississippi	Coahoma, DeSoto, Humphreys, Lafayette, Leflore, Marshall, Panola	≤ 1994	1995-2014	≥ 2015	Same as Non-Engineered		

		Vulnerability Changes for Non-Engineered Structures			Vulnerability Changes for Engineered Structures		
State	**Counties**	**None***	**Changes Annually**	**None**	**None**	**Changes Annually**	**None**
	Hancock, Harrison, Jackson	≤ 1994	1995-2006, 2007-2014	≥ 2015	Same as Non-Engineered		
	Hinds, Madison, Rankin, Sharkey, Tate, Tunica, Washington	≤ 1994	1995-2014	≥ 2015	Same as Non-Engineered		
	Pearl River, Stone	≤ 1994	1995-2006, 2007-2014	≥ 2015	Same as Non-Engineered		
	Rest of State	≤ 1994	1995-2014	≥ 2015	Same as Non-Engineered		
Missouri	Boone	≤ 1994	1995-2014	2015-2016, ≥ 2017	Same as Non-Engineered		
	Cass, Jackson	≤ 1994	1995-2010, 2011-2014	≥ 2015	Same as Non-Engineered		
	Christian	≤ 1994	1995-2015	≥ 2016	≤ 1994	1995-2008, 2009-2012, 2013-2014	≥ 2015
	Clay	≤ 1994	1995-2012, 2013-2014	≥ 2015	Same as Non-Engineered		
	Cole	≤ 1994	1995-2003, 2004-2014	≥ 2015	Same as Non-Engineered		
	Greene	≤ 1994	1995-2007, 2008-2012, 2013-2014	≥ 2015	Same as Non-Engineered		
	Jefferson	≤ 1994	1995-2004, 2005-2014	2015-2016, ≥ 2017	Same as Non-Engineered		
	Platte	≤ 1994	1995-2008, 2009-2013, 2014	≥ 2015	Same as Non-Engineered		
	St. Charles	≤ 1994	1995-2010, 2011-2014	2015-2016, ≥ 2017	Same as Non-Engineered		
	St. Louis	≤ 1994	1995-2005, 2006-2014	≥ 2015	Same as Non-Engineered		
	Rest of State	≤ 1994	1995-2014	≥ 2015	Same as Non-Engineered		
Montana	All	≤ 1994	1995-2002, 2003-2014	≥ 2015	Same as Non-Engineered		
Nebraska	All	≤ 1994	1995-2003, 2004-2014	≥ 2015	Same as Non-Engineered		

		Vulnerability Changes for Non-Engineered Structures			Vulnerability Changes for Engineered Structures		
State	**Counties**	**None***	**Changes Annually**	**None**	**None**	**Changes Annually**	**None**
Nevada	Carson City, Humboldt, Washoe	≤ 1994	1995-2007, 2008-2013, 2014	≥ 2015	Same as Non-Engineered		
	Churchill, Storey	≤ 1994	1995-2006, 2007-2014	2015-2018, ≥ 2019	Same as Non-Engineered		
	Clark	≤ 1994	1995-2002, 2003-2013, 2014	≥ 2015	Same as Non-Engineered		
	Douglas	≤ 1994	1995-2013, 2014	≥ 2015	Same as Non-Engineered		
	Elko	≤ 1994	1995-2005, 2006-2014	≥ 2015	Same as Non-Engineered		
	Esmeralda, Eureka	≤ 1994	1995-2014	≥ 2015	Same as Non-Engineered		
	Lander	≤ 1994	1995-2006, 2007-2014	≥ 2015	Same as Non-Engineered		
	Lincoln	≤ 1994	1995-2012, 2013-2014	≥ 2015	Same as Non-Engineered		
	Lyon	≤ 1994	1995-2006, 2007-2013, 2014	≥ 2015	Same as Non-Engineered		
	Mineral	≤ 1994	1995-2014	≥ 2015	Same as Non-Engineered		
	Nye	≤ 1994	1995-2006, 2007-2012, 2013-2014	≥ 2015	Same as Non-Engineered		
	Pershing	≤ 1994	1995-2006, 2007-2014	2015-2016, ≥ 2017	Same as Non-Engineered		
	White Pine	≤ 1994	1995-2007, 2008-2012, 2013-2014	≥ 2015	Same as Non-Engineered		
New Hampshire	All	≤ 1994	1995-2006, 2007-2014	2015-2019, ≥ 2020	Same as Non-Engineered		
New Jersey	All	≤ 1994	1995-2004, 2005-2014	≥ 2015	Same as Non-Engineered		
New Mexico	All	≤ 1994	1995-2004, 2005-2014	2015-2016, ≥ 2017	Same as Non-Engineered		
New York	All	≤ 1994	1995-2003, 2004-2015	≥ 2016	Same as Non-Engineered		
North Carolina	All	≤ 1994	1995-2002, 2003-2014	2015-2018, ≥ 2019	Same as Non-Engineered		
North Dakota	All	≤ 1994	1995-2002, 2003-2014	2015-2016, ≥ 2017	Same as Non-Engineered		

		Vulnerability Changes for Non-Engineered Structures			Vulnerability Changes for Engineered Structures		
State	**Counties**	**None***	**Changes Annually**	**None**	**None**	**Changes Annually**	**None**
Ohio	All	≤ 1994	1995-2013, 2014	2015-2019, ≥ 2020	≤ 1994	1995-2001, 2002-2014	2015-2019, ≥ 2020
Oklahoma	All	≤ 1994	1995-2010, 2011-2014	2015-2016, ≥ 2017	≤ 1994	1995-2012, 2013-2014	≥ 2015
Oregon	All	≤ 1994	1995-2003, 2004-2014	2015-2017, ≥ 2018	≤ 1994	1995-2003, 2004-2013, 2014	≥ 2015
Pennsylvania	All	≤ 1994	1995-2005, 2006-2014	2015-2018, ≥ 2019	Same as Non-Engineered		
Rhode Island	All	≤ 1994	1995-2004, 2005-2012, 2013-2014	≥ 2015	Same as Non-Engineered		
South Carolina	All	≤ 1994	1995-2002, 2003-2012, 2013-2014	≥ 2015	Same as Non-Engineered		
South Dakota	Brookings	≤ 1994	1995-2007, 2008-2015	≥ 2016	Same as Non-Engineered		
	Brown	≤ 1994	1995-2002, 2003-2014	2015-2016, ≥ 2017	≤ 1994	1995-2002, 2003-2012, 2013-2014	≥ 2015
	Hughes	≤ 1994	1995-2008, 2009-2014	≥ 2015	≤ 1994	1995-2009, 2010-2012, 2013-2014	≥ 2015
	Lawrence	≤ 1994	1995-2014	≥ 2015	≤ 1994	1995-2009, 2010-2012, 2013-2014	≥ 2015
	Lincoln, McCook	≤ 1994	1995-2014	2015-2016, ≥ 2017	≤ 1994	1995-2009, 2010-2012, 2013-2014	≥ 2015
	Meade	≤ 1994	1995-2010, 2011-2014	≥ 2015	≤ 1994	1995-2009, 2010-2012, 2013-2014	≥ 2015
	Minnehaha	≤ 1994	1995-2006, 2007-2012, 2013-2014	≥ 2015	≤ 1994	1995-2007, 2008-2012, 2013-2014	≥ 2015
	Pennington	≤ 1994	1995-2012, 2013-2014	≥ 2015	≤ 1994	1995-2009, 2010-2012, 2013-2014	≥ 2015
	Yankton	≤ 1994	1995-2004, 2005-2014	2015-2017, ≥ 2018	≤ 1994	1995-2004, 2005-2012, 2013-2014	≥ 2015

		Vulnerability Changes for Non-Engineered Structures			Vulnerability Changes for Engineered Structures		
State	**Counties**	**None***	**Changes Annually**	**None**	**None**	**Changes Annually**	**None**
	Rest of State	≤ 1994	1995-2014	≥ 2015	≤ 1994	1995-2009, 2010-2012, 2013-2014	≥ 2015
Tennessee	All	≤ 1994	1995-2009, 2010-2014	≥ 2015	≤ 1994	1995-2008, 2009-2014	2015-2016, ≥ 2017
Texas	Anderson, Andrews, Bexar, Brazoria, Howard, Lampasas, Llano, Pecos, Reeves, San Saba, Val Verde, Washington	≤ 1994	1995-2003, 2004-2014	≥ 2015	Same as Non-Engineered		
	Aransas, Camp, Colorado, Denton, Hidalgo, Nolan, Terry, Titus, Travis, Webb, Wharton	≤ 1994	1995-2003, 2004-2012, 2013-2014	≥ 2015	Same as Non-Engineered		
	Bailey, Burnet, Cooke, Dallas, Grimes, Jefferson, Lamar, Madison, Scurry, Stephens, Tarrant	≤ 1994	1995-2003, 2004-2014	2015-2016, ≥ 2017	Same as Non-Engineered		

		Vulnerability Changes for Non-Engineered Structures			Vulnerability Changes for Engineered Structures		
State	**Counties**	**None***	**Changes Annually**	**None**	**None**	**Changes Annually**	**None**
	Bee, Bell, Brazos, Caldwell, Franklin, Gray, Harrison, Hill, Johnson, Lee, Morris, Navarro, Walker, Wilbarger, Wilson	≤ 1994	1995-2003, 2004-2014	2015-2017, ≥ 2018	Same as Non-Engineered		
	Blanco, Calhoun, Cameron, Chambers, Coleman, Deaf Smith, El Paso, Erath, Fort Bend, Galveston, Gonzales, Hardin, Harris, Hays, Hood, Jack, Jasper, Karnes, Lubbock, Matagorda, Maverick, Midland, Potter, Rains, Randall, Rockwall, San Patricio, Wichita, Wise	≤ 1994	1995-2003, 2004-2015	≥ 2016	Same as Non-Engineered		

		Vulnerability Changes for Non-Engineered Structures			Vulnerability Changes for Engineered Structures		
State	**Counties**	**None***	**Changes Annually**	**None**	**None**	**Changes Annually**	**None**
	Bowie, Comanche, Coryell, Gregg, Jim Wells, Rusk, Taylor, Williamson, Wood	≤ 1994	1995-2003, 2004-2013, 2014	≥ 2015	Same as Non-Engineered		
	Comal, DeWitt, Ector, Ellis, Henderson, Uvalde, Victoria	≤ 1994	1995-2003, 2004-2014	2015-2018, ≥ 2019	Same as Non-Engineered		
	Rest of State	≤ 1994	1995-2003, 2004-2014	≥ 2015	Same as Non-Engineered		
Utah	All	≤ 1994	1995-2002, 2003-2012, 2013-2014	≥ 2015	Same as Non-Engineered		
Vermont	All	≤ 1994	1995-2014	≥ 2015	Same as Non-Engineered		
Virginia	All	≤ 1994	1995-2005, 2006-2013, 2014	≥ 2015	Same as Non-Engineered		
Washington	All	≤ 1994	1995-2004, 2005-2012, 2013-2014	≥ 2015	Same as Non-Engineered		
West Virginia	All	≤ 1994	1995-2014	≥ 2015	≤ 1994	1995-2012, 2013-2014	≥ 2015
Wisconsin	All	≤ 1994	1995-2000, 2001-2013, 2014	≥ 2015	≤ 1994	1995-2001, 2002-2014	2015-2017, ≥ 2018
Wyoming	All	≤ 1994	1995-2008, 2009-2013, 2014	≥ 2015	Same as Non-Engineered		

*"None" indicates no changes, or no variation in vulnerability for structures built on or before the year indicated.

C ICC Year Bands

Table 39 details the jurisdiction-specific ICC1 and ICC2 years in the Verisk Severe Thunderstorm Model for the United States.

Table 39. ICC years for modeled areas

Jurisdiction		ICC Year Definitions for Non-Engineered Structures		ICC Year Definitions for Engineered Structures	
State	County	ICC1	ICC2	ICC1	ICC2
Alabama	Autauga, Calhoun, Etowah, Monroe, Tuscaloosa	2013	2016	2008	2016
	Baldwin	2008	2012	2008	2012
	Chilton, Houston, Montgomery, Shelby	2013	2017	2008	2017
	Dale, Jackson, Pike, Walker	2013	2018	2008	2018
	Jefferson	2013	2015	2008	2015
	Mobile	2002	2015	2008	2015
	Wilcox	2013	N/A	2008	2018
	Rest of State	2013	N/A	2008	N/A
Arizona	Apache	2004	2019	2004	2019
	Cochise	2005	2015	2005	2015
	Coconino, Santa Cruz	2007	2014	2007	2014
	Gila	2007	2015	2007	2015
	Graham	N/A	N/A	N/A	N/A
	Greenlee, Navajo	2005	2019	2005	2019
	La Paz	2010	N/A	2010	N/A
	Maricopa	2005	2013	2005	2013
	Mohave	2009	2015	2009	2015
	Pima	2001	2013	2001	2013
	Pinal	2007	2013	2007	2013
	Yavapai	2008	2015	2008	2015
	Yuma	2006	2013	2004	2013
Arkansas	All	N/A	N/A	N/A	N/A
California	All	2008	2014	2008	2014
Colorado	Adams	2007	2015	2007	2015

Jurisdiction		ICC Year Definitions for Non-Engineered Structures		ICC Year Definitions for Engineered Structures	
State	County	ICC1	ICC2	ICC1	ICC2
	Alamosa	2008	2017	2008	2017
	Arapahoe	2006	2017	2006	2017
	Boulder	2003	2013	2003	2013
	Broomfield, Eagle	2004	2017	2004	2017
	Chaffee	2007	2018	2007	2018
	Clear Creek	2012	2018	2012	2018
	Delta, Las Animas	2005	N/A	2005	N/A
	Denver	2004	2016	2004	2016
	Douglas	2006	2013	2006	2013
	Elbert, Mesa	N/A	2019	N/A	2019
	Fremont, Logan, Otero	2009	N/A	2009	N/A
	Garfield, Gilpin, Hinsdale	N/A	2016	N/A	2016
	Grand	2011	2018	2011	2018
	Gunnison	2010	2015	2010	2015
	Jefferson	2002	2014	2002	2014
	Lake	2005	2013	2005	2013
	La Plata	2005	2018	2005	2018
	Larimer	2005	2014	2005	2014
	Lincoln, Moffat, Rio Blanco, Rio Grande	2008	N/A	2008	N/A
	Montezuma	2013	2018	2013	2018
	Montrose	2016	N/A	2016	N/A
	Morgan, San Miguel	2011	N/A	2011	N/A
	Ouray	2010	N/A	2010	N/A
	Park	2014	2016	2014	2016
	Pitkin	2010	2017	2010	2017
	Pueblo	N/A	2015	N/A	2015
	Routt	2015	2018	2006	2018
	Teller	2007	2017	2007	2017
	Weld	N/A	2012	N/A	2012
	Rest of State	N/A	N/A	N/A	N/A

Jurisdiction		ICC Year Definitions for Non-Engineered Structures		ICC Year Definitions for Engineered Structures	
State	County	ICC1	ICC2	ICC1	ICC2
Connecticut	All	2006	2017	2006	2017
Delaware	Kent, New Castle	2002	2014	2002	2014
	Sussex	2006	2014	2006	2014
District of Columbia (Washington D.C.)	All	2002	2014	2002	2014
Florida	All	2002	2012	2002	2012
Georgia	All	2003	2014	2003	2014
Idaho	All	2002	2014	2002	2017
Illinois	Boone	2004	N/A	2004	N/A
	Brown, Champaign	2007	N/A	2007	N/A
	Carroll	2005	N/A	2011	N/A
	Coles	2012	N/A	2012	N/A
	Cook	2015	2019	N/A	2019
	DeKalb, Sangamon	2010	N/A	2010	N/A
	DuPage, Kendall, Lake, Lawrence, McLean, Tazewell, Vermilion	N/A	2014	N/A	2014
	Effingham, Stephenson	N/A	2018	N/A	2018
	Fayette	2009	N/A	2009	N/A
	Franklin	N/A	N/A	N/A	2016
	Grundy, Williamson	2011	N/A	2011	N/A
	Jersey	2008	N/A	2008	N/A
	Kane	N/A	2013	N/A	2013
	Kankakee	2009	2017	2009	2017
	Knox	2007	2012	2007	2012
	LaSalle, St. Clair	2007	2017	2007	2017
	Madison	N/A	2015	N/A	2015
	McHenry, Ogle	N/A	2016	N/A	2016
	Peoria	N/A	2012	N/A	2012
	Rock Island	2004	2014	2004	2014
	Will	N/A	2014	2006	2014

Jurisdiction		ICC Year Definitions for Non-Engineered Structures		ICC Year Definitions for Engineered Structures	
State	County	ICC1	ICC2	ICC1	ICC2
	Winnebago	2005	N/A	2005	N/A
	Rest of State	N/A	N/A	N/A	N/A
Indiana	All	2001	N/A	2003	2014
Iowa	Benton, Jasper	2004	2018	2004	2018
	Black Hawk, Buena Vista, Lee, Mahaska, Scott, Webster	2004	2017	2004	2017
	Boone, Linn	2004	2014	2004	2014
	Bremer, Buchanan, Henry, Warren	2004	2013	2004	2013
	Clay, Plymouth, Woodbury	2004	2016	2004	2016
	Clinton, Des Moines, Kossuth, Polk	2004	2015	2004	2015
	Dubuque	2004	2020	2004	2020
	Johnson, Washington	2004	2019	2004	2019
	Wapello	2004	2017	2004	2016
	Rest of State	2004	N/A	2004	N/A
Kansas	Allen, Ottawa, Sedgwick	N/A	2015	N/A	2015
	Barton, Brown, Labette, Miami, Thomas, Trego	2007	N/A	2007	N/A
	Bourbon, Cowley	2008	2018	2008	2018
	Butler	2012	N/A	2012	N/A
	Chase	N/A	2017	N/A	2017
	Cloud, Phillips, Riley	N/A	2013	N/A	2013
	Crawford	2007	2016	2007	2016
	Dickinson	2014	N/A	2014	N/A
	Douglas, Reno	N/A	2014	N/A	2014
	Ellis	2007	2017	2007	2017
	Finney, Stevens	2006	N/A	2006	N/A
	Ford, Lyon	2010	N/A	2010	N/A

Jurisdiction		ICC Year Definitions for Non-Engineered Structures		ICC Year Definitions for Engineered Structures	
State	County	ICC1	ICC2	ICC1	ICC2
	Franklin	2007	2015	2007	2015
	Geary	N/A	2016	N/A	2016
	Harvey	2004	2014	2004	2014
	Johnson	2008	2013	2008	2013
	Kiowa	2007	2018	2007	2018
	Marion, Marshall, Montgomery, Seward	N/A	2018	N/A	2018
	McPherson, Neosho	2013	N/A	2013	N/A
	Meade	2010	2018	2010	2018
	Mitchell, Norton	2016	N/A	2016	N/A
	Saline	2010	2017	2010	2017
	Shawnee	2012	N/A	2007	2018
	Sumner	2011	2019	2011	2019
	Wyandotte	2005	2016	2005	2016
	Rest of State	N/A	N/A	N/A	N/A
Kentucky	All	2001	2014	2001	2014
Louisiana	Cameron, Iberia, Jefferson, Lafourche, Orleans, Plaquemines, St. Bernard, St. Mary, St. Tammany, Terrebonne, Vermilion	2007	2014	2008	2014
	Rest of State	2008	2014	2008	2014
Maine	All	2005	2018	2005	2018
Maryland	All	2002	2012	2002	2012
Massachusetts	All	2009	2019	2009	2019
Michigan	All	2002	2014	2002	2014
Minnesota	All	2004	2015	2004	2015
Mississippi	Coahoma, DeSoto, Humphreys, Lafayette, Leflore, Marshall, Panola	N/A	2015	N/A	2015
	Hancock, Harrison, Jackson	2007	2015	2007	2015

Jurisdiction		ICC Year Definitions for Non-Engineered Structures		ICC Year Definitions for Engineered Structures	
State	County	ICC1	ICC2	ICC1	ICC2
	Hinds, Madison, Rankin, Sharkey, Tate, Tunica, Washington	2015	N/A	2015	N/A
	Pearl River, Stone	2007	N/A	2007	N/A
	Rest of State	N/A	N/A	N/A	N/A
Missouri	Boone	N/A	2017	N/A	2017
	Cass, Jackson	2011	N/A	2011	N/A
	Christian	2009	2016	2009	2013
	Clay	N/A	2013	N/A	2013
	Cole	2004	N/A	2004	N/A
	Greene	2008	2013	2008	2013
	Jefferson	2005	2017	2005	2017
	Platte	2009	2014	2009	2014
	St. Charles	2011	2017	2011	2017
	St. Louis	2006	N/A	2006	N/A
	Rest of State	N/A	N/A	N/A	N/A
Montana	All	2003	2015	2003	2015
Nebraska	All	2004	2015	2004	2015
Nevada	Carson City, Humboldt, Washoe	2008	2014	2008	2014
	Churchill, Storey	2007	2019	2007	2019
	Clark	2003	2014	2003	2014
	Douglas	N/A	2014	N/A	2014
	Elko	2006	N/A	2006	N/A
	Esmeralda, Eureka	N/A	N/A	N/A	N/A
	Lander	2007	N/A	2007	N/A
	Lincoln	N/A	2013	N/A	2013
	Lyon	2007	2014	2007	2014
	Mineral	N/A	2015	N/A	2015
	Nye	2007	2013	2007	2013
	Pershing	2007	2017	2007	2017
	White Pine	2008	2013	2008	2013
New Hampshire	All	2007	2020	2007	2020

Jurisdiction		ICC Year Definitions for Non-Engineered Structures		ICC Year Definitions for Engineered Structures	
State	County	ICC1	ICC2	ICC1	ICC2
New Jersey	All	2005	2015	2005	2015
New Mexico	All	2005	2017	2005	2017
New York	All	2004	2016	2004	2016
North Carolina	All	2003	2019	2003	2019
North Dakota	All	2003	2017	2003	2017
Ohio	All	2014	2020	2002	2020
Oklahoma	All	2011	2017	2013	2015
Oregon	All	2004	2018	2004	2014
Pennsylvania	All	2006	2019	2006	2019
Rhode Island	All	2005	2013	2005	2013
South Carolina	All	2003	2013	2003	2013
South Dakota	Brookings	2008	2016	2008	2013
	Brown	2003	2017	2003	2013
	Hughes	2009	N/A	2010	2013
	Lawrence	N/A	2015	2010	2013
	Lincoln, McCook	N/A	2017	2010	2013
	Meade	2011	N/A	2010	2013
	Minnehaha	2007	2013	2008	2013
	Pennington	N/A	2013	2010	2013
	Yankton	2005	2018	2005	2013
	Rest of State	N/A	N/A	2010	2013
Tennessee	All	2010	N/A	2009	2017
Texas	Anderson, Andrews, Bexar, Brazoria, Howard, Lampasas, Llano, Pecos, Reeves, San Saba, Val Verde, Washington	2004	2015	2004	2015
	Aransas, Camp, Colorado, Denton, Hidalgo, Nolan, Terry, Titus, Travis, Webb, Wharton	2004	2013	2004	2013

Jurisdiction		ICC Year Definitions for Non-Engineered Structures		ICC Year Definitions for Engineered Structures	
State	County	ICC1	ICC2	ICC1	ICC2
	Bailey, Burnet, Cooke, Dallas, Grimes, Jefferson, Lamar, Madison, Scurry, Stephens, Tarrant	2004	2017	2004	2017
	Bee, Bell, Brazos, Caldwell, Franklin, Gray, Harrison, Hill, Johnson, Lee, Morris, Navarro, Walker, Wilbarger, Wilson	2004	2018	2004	2018
	Blanco, Calhoun, Cameron, Chambers, Coleman, Deaf Smith, El Paso, Erath, Fort Bend, Galveston, Gonzalas, Hardin, Harris, Hays, Hood, Jack, Jasper, Karnes, Lubbock, Matagorda, Maverick, Midland, Potter, Rains, Randall, Rockwall, San Patricio, Wichita, Wise	2004	2016	2004	2016
	Bowie, Comanche, Coryell, Gregg, Jim Wells, Rusk, Taylor, Williamson, Wood	2004	2014	2004	2014
	Comal, DeWitt, Ector, Ellis, Henderson, Uvalde, Victoria	2004	2019	2004	2019
	Rest of State	2004	N/A	2004	N/A
Utah	All	2003	2013	2003	2013
Vermont	All	N/A	N/A	N/A	N/A
Virginia	All	2006	2014	2006	2014
Washington	All	2005	2013	2005	2013
West Virginia	All	N/A	N/A	N/A	2013
Wisconsin	All	2001	2014	2002	2018

Jurisdiction		ICC Year Definitions for Non-Engineered Structures		ICC Year Definitions for Engineered Structures	
State	County	ICC1	ICC2	ICC1	ICC2
Wyoming	All	2009	2014	2009	2014

Selected References

Listed below are selected references used in the development of the Verisk Severe Thunderstorm Model for the United States.

Agee, E., Larson, J., Childs, S., & Marmo, A. (2016). Spatial Redistribution of U.S. Tornado Activity between 1954 and 2013. *Journal of Applied Meteorology and Climatology,* 55(8), 1681-1697.

Allen, J. T. (2018). Climate Change and Severe Thunderstorms. *Oxford Research Encyclopedia of Climate Science*, 67pp.

Allen, J. T., & Tippett, M. K. (2015). The characteristics of United States hail reports: 1955–2014. *Electronic Journal of Severe Storms Meteorology,* 10(3), 1-31.

Allen, J. T., Tippett, M. K., & Sobel, A. H. (2015a). An empirical model relating U.S. monthly hail occurrence to large-scale meteorological environment. *Journal of Advances in Modeling Earth Systems,* 7(1), 226-243.

Allen, J. T., Tippett, M. K., & Sobel, A. H. (2015b). Influence of the El Niño/Southern Oscillation on tornado and hail frequency in the United States. *Nature Geosciences,* 8, 278-283.

Allen, J. T., Tippett, M. K., Kaheil, Y., Sobel, A. H., Lepore, C., Nong, S., & Muehlbauer, A. (2017). An extreme value model for U.S. hail size. *Monthly Weather Review,* 145, 4501–4519.

Andrews, K., & Blong, R. J. (1997). Hailstorm Damage in Sydney, Australia, March 1990. *Natural Hazards,* 16, 113-125.

Auer, A. H. (1972). Distribution of graupel and hail with size. *Monthly Weather Review*, 100(5), 325-328.

Bentley, M. L., & Mote, T. L. (1998). A Climatology of Derecho-Producing Mesoscale Convective Systems in the Central and Eastern United States, 1986-95. Part I: Temporal and Spatial Distribution. *Bulletin of the American Meteorological Society*, 79(11), 2527-2540.

Bobby, S., Johnson, T., Kordi, B., Moghim, F., & Ramanathan, K. (2017). The Impact of Temporal and Spatial Variation in Building Codes on the Hurricane Wind Vulnerability of Residential Single Family Homes. *Structures Congress 2017*, Denver, CO, April 6-18, 2017.

Boruff, B. J., Easoz, J. A., Jones, S. D., Landry, H. R., Mitchem, J. D., & Cutter, S. L. (2003). Tornado Hazards in the United States. *Climate Research*, 24(2), 103-117.

Brooks, H. E. (2004). On the Relationship of Tornado Path Length and Width to Intensity. *Weather and Forecasting,* 19, 310-319.

Brooks, H. E., Carbin, G. W., & Marsh, P. T. (2014). Increased variability of tornado occurrence in the United States. *Science,* 346(6207), 349-352.

Brooks, H. E., & Doswell III, C. A. (2001). Normalized Damage from Major Tornadoes in the United States: 1890-1999. *Weather and Forecasting,* 16, 168-176.

Brooks, H. E., & Doswell III, C. A. (2001). Some Aspects of the International Climatology of Tornadoes by Damage Classification. *Atmospheric Research,* 56, 191-201.

Brooks, H. E., Doswell III, C. A., & Kay, M. P. (2003). Climatological Estimates of Local Daily Tornado Probability for the United States. *Weather and Forecasting,* 18, 626-640.

Brooks, H. E., Lee, J. W., & Craven, J. P. (2003). The spatial distribution of severe thunderstorm and tornado environments from global reanalysis data. *Atmospheric Research*, 67, 73-94.

Brown, T. M., & Pogorzelski., W. H. (2014). *Claims Analysis Study of May 24, 2011 Hailstorms in Dallas-Fort Worth*. Applied Climatology, 94th American Meteorology Society Annual Meeting, Atlanta, Georgia, February 4, 2014.

Bunkers, M. J., Klimowski, B. A., Zeitler, J. W., Thompson, R. L., & Weisman, M. L. (2000). Predicting Supercell Motion Using a New Hodograph Technique. *Weather and Forecasting,* 15(1), 61–79.

Changnon, S. A. (1970). Hailstreaks. *Journal of Atmospheric Science,* 27(1), 109-125.

Changnon, S. A. (1977). The Scales of Hail. *Journal of Applied Meteorology,* 16, 626-648.

Changnon, S. A. (1999). Data and Approaches for Determining Hail Risk in the Contiguous United States. *Journal of Applied Meteorology,* 38, 1730-1739.

Changnon, S. A., & Burroughs, J. (2003). The Tristate Hailstorm: The Most Costly on Record. *Monthly Weather Review,* 131, 1734-1739.

Changnon, S. A., & Changnon, D. (1998). Record-High Losses for Weather Disasters in the United States during the 1990s: How Excessive and Why? *Natural Hazards,* 18, 287-300.

Changnon, S. A., Changnon, D., & Hilberg, S. D. (2009). Hailstorms Across the Nation: An Atlas About Hail and its Damages. *Illinois State Water Survey.*

Cintineo, J. L., Smith, T. M., Lakshmanan, V., Brooks, H. E., & Ortega, K. L. (2012). An objective high-resolution hail climatology of the contiguous United States. *Weather and Forecasting*, 27(5), 1235-1248.

Concannon, P. R., Brooks, H. E., & Doswell III, C. A. (2000). *Climatological risk of strong and violent tornadoes in the United States*. Preprints, 2nd Symposium on Environmental Applications, Long Beach, California, American Meteorological Society, 9.4, 212-219, January 13, 2000.

Coniglio, M. C., & Corfidi, S. F. (2006). *Forecasting the speed and longevity of severe mesoscale convective systems*. Symposium on the Challenges of Severe Convective Storms, American Meterological Society, P1.30, February 1, 2006.

Coniglio, M. C., & Stensrud, D. J. (2004). Interpreting the climatology of derechos. *Weather and forecasting,* 19(3), 595-605.

Corfidi, S. F., Weiss, S. J., Kain, J. S., Corfidi, S. J., Rabin, R. M., & Levit, J. J. (2010). Revisiting the 3-4 April 1974 Super Outbreak of Tornadoes. *Weather and Forecasting,* 25(2), 465-510.

Crenshaw, V., & Koontz, J. D. (2001). Simulated Hail Damage and Impact Resistance Test Procedures for Roof Coverings and Membranes. *Engineering,* January 2001.

Dagnew, A., Luo, J., & Kafali, C. (2013). *Insights into Building Damage and Vulnerability from the Recent Severe Thunderstorm Outbreaks: Analyses of Postdamage Surveys and Insurance Claims Data*. Structures Congress 2014, Boston, Massachusetts, April 3-5, 2013.

Dagnew, A., & Stransky, S. (2013). Insights into damage and vulnerability from Verisk's Moore tornado survey team. *AIR Currents,* June 27, 2013.

David O. P., van de Lindt, J. W., Back, E. W., Graettinger, A. J., Pei, S., Coulbourne, W., Gupta, R., James, D. & Agdas, D. (2012). Making the Case for Improved Structural Design: Tornado Outbreaks of 2011. *Leadership and Management in Engineering,* 12(4), 254–270.

Dee, D. P., Balmaseda, M., Balsamo, G., Engelen, R., Simmons, A. J., & Thépaut, J.-N. (2014). Toward a Consistent Reanalysis of the Climate System. *Bulletin of the American Meteorological Society*, 95(8), 1235-1248.

Diffenbaugh, N. S., Scherer, M., & Trapp, R. J. (2013). Robust increases in severe thunderstorm environments in response to greenhouse forcing. *Proceedings of the National Academy of Sciences of the United States of America*, 110(41), 16361-16366.

DNV/Risø (2002). *Guidelines for Design of Wind Turbines*. Det Norske Veritas, Copenhagen, and Wind Energy Department, Risø National Laboratory.

Doswell III, C. A., Brooks, H. E., & Kay, M. P. (2005). Climatological estimates of daily local nontornadic severe thunderstorm probability for the United States. *Weather and forecasting,* 20(4), 577-595.

Doswell III, C. A., & Burgess, D. W. (1988). On Some Issues of United States Tornado Climatology. *Monthly Weather Review,* 116, 495-501.

Dotzek, N., Grieser, J., & Brooks, H. E. (2003). Statistical modeling of tornado intensity distributions. *Atmospheric research,* 67, 163-187.

Edwards, R., Allen, J. T., & Carbin, G. W. (2018). Reliability and Climatological Impacts of Convective Wind Estimations. *Journal of Applied Meteorology and Climatology,* 57(8), 1825-1845.

Efron, B., & Tibshirani, R. J. (1993). *An Introduction to the Bootstrap.* Chapman & Hall, New York, New York.

Extreme Optimization, The Transformed Beta Distribution (2004-2016).

Federal Emergency Management Agency (1999). *Midwest Tornadoes of May 3, 1999: Observations, Recommendations, and Technical Guidance*. FEMA Mitigation Directorate 342, Washington, D.C., BPAT, October 1999.

Feuerstein, B., Dotzek, N., & Grieser, J. (2005). Assessing a Tornado Climatology from Global Tornado Intensity Distributions. *Journal of Climate,* 18, 585-596.

Fujita, T. T. (1971). *Proposed Characterization of Tornadoes and Hurricanes by Area and Intensity*. SMRP Research Report 91, Department of Geophysical Science, University of Chicago, Chicago, Illinois.

Giammanco, I. M., & DeCiampa C. (2018). Performance of Radar-Based Hail Detection and Size Estimation Part I: National Weather Service Radar Hail Detection Outputs. *Insurance Institute for Business and Home Safety Technical Report.*

Gensini, V. A., & Brooks, H. E. (2018). Spatial trends in United States tornado frequency. *npj Climate and Atmospheric Science,* 1(38).

Gensini, V. A., Haberlie, A. M., & March, P. T. (2020). Spatial trends in United States tornado frequency. *Bulletin of the American Meteorological Society,* 101(8), E1259-E1278.

Haan Jr., F. L., Balaramudu, V. K., & Sarkar, P. P. (2010). Tornado-Induced Wind Loads on a Low-Rise Building. *Journal of Structural Engineering,* 136(1).

Herzog, R. F., Morrison, S. J., Patnode, S. A., & Green, J. R. (2012). Ice Ball Impact Testing of Siding. *27th RCI International Convention and Trade Show,* Dallas, TX, March 15-20, 2012, 142-146.

Hohl, R., Schiesser, H., & Aller, D. (2002). Hailfall: the relationship between radar-derived hail kinetic energy and hail damage to buildings. *Atmospheric Research,* 63(3-4), 177-207.

Hohl, R., Schiesser, H., & Knepper, I. (2002). The Use of Weather to Estimate Hail Damage to Automobiles: An Exploratory Study in Switzerland. *Atmospheric Research,* 61(3), 215-238.

Hoogewind, K. A., Baldwin, M. E., & Trapp, R. J. (2017). The Impact of Climate Change on Hazardous Convective Weather in the United States: Insight from High-Resolution Dynamical Downscaling. *Journal of Climate,* 30(24), 10081-10100.

Institute for Business and Home Safety (IBHS; 2004). Investigation into insured losses and damages to single-family homes resulting from the April 5, 2003 North Texas hailstorms, *Institute for Business and Home Safety,* Tampa, Florida.

International Renewable Energy Agency (IRENA; 2012). Renewable Energy Cost Analysis - Wind Power, Volume 1: Power Sector. IRENA, 1(5), June 2012.

Johns, R. H., & Hirt, W. D. (1987). Derechos: Widespread Convectively Induced Windstorms. *Weather and Forecasting,* 2, 32-49.

Kaplan, E. L., & Meier, P. (1958). Nonparametric Estimation from Incomplete Observations. *Journal of the American Statistical Association,* 53(282), 457–481.

Keegan, M., Nash, D. H., & Stack, M. (2013). *Numerical Modelling of Hailstone Impact on the Leading Edge of a Wind Turbine Blade*. EWEA Annual Wind Energy Event 2013, Vienna, Austria, February 4 - 7, 2013.

Kelly, D. L., Schaefer, J. T., & Doswell III, C. A. (1985). Climatology of Nontornadic Severe Thunderstorms Events in the United States. *Monthly Weather Review,* 113(11), 1997-2014.

Khanduri, A. C., & Morrow, G. C. (2003). Vulnerability of Buildings to Windstorms and Insurance Loss Estimation. *Journal of Wind Engineering and Industrial Aerodynamics,* 91(4), 455-467.

Koch, E., Koh, J., Davison, A. C., Lepore, C., & Tippett, M. K. (2021). Trends in the Extremes of Environments Associated with Severe U.S. Thunderstorms. *Journal of Climate,* 34(4), 1259-1272.

Kordi, B., Ramanathan, K., Johnson, T., & Bobby, S. (2017). *Hurricane Risk in Florida as it Relates to the Evolution of Building Codes,* 2017 Americas Conference on Wind Engineering, Gainesville, FL, May 21-24, 2017.

Lee, S.-K., Wittenberg, A. T., Enfield, D. B., Weaver, S. J., Wang, C., & Atlas, R. (2016). US regional tornado outbreaks and their links to spring ENSO phases and North Atlantic SST variability. *Environmental Research Letters,* 11(4).

Leigh, R., & Kuhnel, I. (2001). Hailstorm Loss Modeling and Risk Assessment in the Sydney Region, Australia. *Natural Hazards,* 24, 171-185.

Letchford, C. W., Norville, H. S., & Bilello, J. (2000). *Damage Survey and Assessment of Fort Worth Tornado, 28 March 2000*. Report from Texas Tech University, Wind Science and Engineering Center, submitted to the National Institute for Standards and Technology, August 2000.

Liu, H., Saffir, H. S., & Sparks, P. R. (1989). Wind Damage to Wood-Framed Houses: Problems, Solutions, and Research Needs. *Journal of Aerospace Engineering,* 2(2), 57-70.

Long, J. A., & Stoy, P. C. (2014). Peak tornado activity is occurring earlier in the heart of "Tornado Alley". *Geophysical Research Letters,* 41(17), 6259-6264.

Lu, M., Tippett, M., & Lall, U. (2015). Changes in the seasonality of tornado and favorable genesis conditions in the central United States. *Geophysical Research Letters,* 42(10), 4224-4231.

MacDonald, H., Infield, D., Nash, D. H., & Stack, M. (2016). Mapping hail meteorological observations for prediction of erosion in wind turbines. *Wind Energy,* 19(4), 777-784.

Marshall, T. P. (2002). Tornado Damage Survey at Moore, Oklahoma. *Weather and Forecasting,* 17(3), 582-598.

Marshall, T. P., Herzog, R., Morrison, S. J., & Smith, S. R. (2002). *Hail Damage Threshold Sizes for Common Roofing Materials*. The 21st Conference on Severe Local Storms, American Meteorological Society, San Antonio, Texas, August 2002.

Marshall, T. P. & McDonald, J. R. (1983). *Storm Observations and Damage Survey of the Tornado Outbreak Near Pampa, Texas on May 19, 1982*. Report from Texas Tech University, Institute for Disaster Research, Lubbock, Texas, June 1983.

McDonald, J. R., & Mehta, K. C. (2006). *The Enhanced Fujita Scale*. Report from Texas Tech University, Wind Science and Engineering Center, submitted to the National Weather Service, October 10, 2006.

Meyer, C. L., Brooks, H. E., & Kay, M. P. (2002). *A Hazard Model for Tornado Occurrence in the United States*. 16th Conference of Probability and Statistics, American Meteorological Society, Orlando, Florida, January 13-17, 2002, J88-J95.

Minor, J. E. (2005). Lessons Learned from Failures of the Building Envelope in Windstorms. *Journal of Architectural Engineering,* 11(1), 10-14.

Minor, J. E., & Beason, W. L. (1976). Window Glass Failures in Windstorms. *Journal of the Structural Division,* 102(1), 147-160.

Nateghi, A. F. (1996). Assessment of Wind Speeds That Damage Buildings. *Natural Hazards,* 14, 73-84.

Nisi, L., Hering, A., Germann, U., & Martius, O. (2018). A 15-year hail streak climatology for the Alpine region. *Quarterly Journal of the Royal Meteorological Society,* 144(714), 1429-1449.

National Oceanic and Atmospheric Administration (NOAA) National Centers for Environmental Information (NCEI; 2021). *U.S. Billion-Dollar Weather and Climate Disasters (2021)*. https://www.ncdc.noaa.gov/billions/

Ortega, K. L., Smith, T. M., Manross, K. L., Scharfenberg, K. A., Witt, A., Kolodziej, A. G., Gourley, J. J. (2009). The Severe Hazards Analysis and Verification Experiment. *Bulletin of the American Meteorological Society,* 90(10), 1519-1530.

Ospina, R., & Ferrari, S. L. P. (2010). Inflated beta distributions. *Statistical Papers,* 51(111).

Pan, K., Montepellier, P., & Masoud, Z. (2002). Engineering Observations of 3 May 1999 Oklahoma Tornado Damage. *Weather and Forecasting,* 17(3), 599-610.

Paterson, D. A., & Sankaran, R. (1994). Hail Impact on Building Envelopes. *Journal of Wind Engineering and Industrial Aerodynamics,* 53(1-2), 229-246.

Petty, S., Petty, M., & Kasberg, T. (2009). Evaluation of hail-strike damage to asphalt shingles based on hailstone size, roof pitch, direction of incoming storm, and facing roof elevation. *RCI Interface,* RCI Inc., Raleigh, NC, May/June 2009, 4-10.

Prevatt, D. O., van de Lindt, J. W., Back, E. W., & Graettinger, A. J. (2012). Making the Case for Improved Structural Design: Tornado Outbreaks of 2011. *Leadership and Management in Engineering,* 12(4), 254-270.

Rasmussen, E. N. (2003). Refined supercell and tornado forecast parameters. *Weather and Forecasting,* 18(3), 530-535.

Roofing Industry Committee On Weather Issues (RICOWI; 2012). Hailstorm Investigation Report, Dallas/Fort Worth TX, May 24, 2011. *Roofing Industry Committee on Weather Issues,* Clinton, OH, May 4, 2012.

RICOWI (2016). Hailstorm Investigation Report, North Texas - April 11, 2016. *Roofing Industry Committee on Weather Issues,* Clinton, OH, April 30, 2017.

Saha, S., Moorthi, S., Pan, H.-L., Wu, X., Wang, J., Nadiga, S., Tripp, P., Kistler, R., Woollen, J., Behringer, D., Liu, H., Stokes, D., Grumbine, R., Gayno, G., Wang, J. Hou, Y.-T., Chuang, H., Juang, H.-M. H., Sela, J, … Goldberg, M. (2010). The NCEP Climate Forecast System Reanalysis. *Bulletin of the American Meteorological Society,* 91(8), 1015-1058.

Saha, S., Moorthi, S., Wu, X., Wang, J., Nadiga, S., Tripp, P., Behringer, D., Hou, Y.-T., Chuang, H., Iredell, M., Ek, M., Meng, J., Yang, R., Mendez, M. P., van den Dool, H., Zhang, Q., Chen, M., & Becker, E. (2014). The NCEP Climate Forecast System Version 2. *Journal of Climate,* 27(6), 2185-2208.

Schaefer, J. T. & Edwards, R. (1999). *The Storm Prediction Center Tornado/Severe Thunderstorm Database*. Preprints, 11th Conference on Applied Climatology, American Meteorological Society, Dallas, Texas, January 10-15, 1999, 215-220.

Schmidlin, T. W., King, P. S., Hammer, B. O., & Ono, Y. (1998). Behavior of Vehicles during Tornado Winds. *Journal of Safety Research,* 29(3), 181-186.

Schneider, R., Brooks, H. E., & Schaefer, J. T. (2004). *Tornado Outbreak Day Sequences: historic events and climatology (1875-2003)*. 22nd Conference on Severe Local Storms, American Meteorological Society, October 3, 2004.

Schultz, L. A., & Cecil, D. J. (2009). Tropical cyclone tornadoes, 1950-2007. *Monthly Weather Review,* 137(10), 3471-3484.

Schuster, S. S., Blong, R. J., & McAneney, K. J. (2006). Relationship between radar-derived hail kinetic energy and damage to insured buildings for severe hailstorms in Eastern Australia. *Atmospheric research,* 81(3), 215-235.

Sills, D. M. L., Cheng, V., Rousseau, B., McCarthy, P. J., Waller, J., Klaassen, J., & Auld, H. (2012). *Using tornado, lightning, and population data to identify tornado prone areas in Canada*. Preprints, 26th Conference on Severe Local Storms, American Meteorological Society, Nashville, Tennessee, November 5, 2012.

Sparks, P. R., Liu, H., & Saffir, H. S. (1989). Wind Damage to Masonry Buildings. *Journal of Aerospace Engineering,* 2(4), 186-198.

Speheger, D. A., Doswell III, C. A. & Stumpf, G. J. (2002). The Tornadoes of 3 May 1999: Event Verification in Central Oklahoma and Related Issues. *Weather and Forecasting,* 17(3), 362-381.

Stott, P. (2016). How climate change affects extreme weather events. *Science,* 352(6293), 1517-1518.

Summers, P. W., & Wojtiw, L. (1971). *The Economic Dependence of Hail Damage in Alberta, Canada and its Dependence on Various Hail fall Parameters.* 7th Conference on Severe Local Storms, American Meteorological Society, Kansas City, Kansas, October 5-7, 1971, 158-163.

Taher, R. (2007). Design of Low-Rise Buildings for Extreme Wind Events. *Journal of Architectural Engineering,* 13(1), 54-62.

Tang, B. H., Gensini, V. A., & Homeyer, C. R. (2019). Trends in United States large hail environments and observations. *npj Journal of Climate and Atmospheric Science,* 2(45).

Thompson, K. S. (1990). Adaptive Cluster Sampling. *Journal of the American Statistical Association,* 85(412), 1050-1059.

Thompson, R. L., Edwards, R., Hart, J. A., Elmore, K. L., & Markowski, P. (2003). Close proximity soundings within supercell environments obtained from the Rapid Update Cycle. *Weather and forecasting,* 18(6), 1243-1261.

Tippett, M. K. (2014). Changing volatility of U.S. annual tornado reports. *Geophysical Research Letters,* 41(19), 6956-6961.

Tippett, M. K., Allen, J. T., Gensini, V. A., & Brooks, H. E. (2015). Climate and Hazardous Convective Weather. *Current Climate Change Reports,* 1, 60-73.

Tippett, M. K., & Cohen, J. E. (2016). Tornado outbreak variability follows Taylor's power law of fluctuation scaling and increases dramatically with severity. *Nature Communications,* 7(10668).

Tippett, M. K., Lepore, C., & Cohen, J. E. (2016). More tornadoes in the most extreme U.S. tornado outbreaks. *Science,* 354, 1419-1423.

Tippett, M. K., Sobel, A. H., & Camargo, S. J. (2012). Association of US tornado occurrence with monthly environmental parameters. *Geophysical Research Letters,* 39(2).

Tippett, M. K., Sobel, A. H., Camargo, S. J., & Allen, J. T. (2014). An Empirical Relation between U.S. Tornado Activity and Monthly Environmental Parameters. *Journal of Climate,* 27(8), 2983-2999.

Trapp, R. J., Diffenbaugh, N. S., Brooks, H. E., Baldwin, M. E., Robinson, E. D., & Pal, J. S. (2007). Changes in severe thunderstorm environment frequency during the 21st century caused by anthropogenically enhanced global radiative forcing. *Proceedings of the National Academy of Sciences of the United States of America,* 104(50), 19719-19723.

Trenberth, K. E., Fasullo, J. T., & Mackaro, J. (2011). Atmospheric Moisture Transports from Ocean to Land and Global Energy Flows in Reanalyses. *Journal of Climate,* 24(18), 4907-4924.

Twisdale, L. A. (1988). Probability of Facility Damage from Extreme Wind Effects. *Journal of Structural Engineering,* 114(10), 2190-2209.

van de Lindt, J. W., Pei, S., Dao, T. N., Graettinger, A. J., Prevatt, D. O., Gupta, R., & Coulbourne, W. L. (2013). Dual-Objective-Based Tornado Design Philosophy. *Journal of Structural Engineering,* 139(2), 251–263.

Velden, C., Lewis, W. E., Bresky, W., Stettner, D., Daniels, J., & Wanzong, S. (2017). Assimilation of High-Resolution Satellite-Derived Atmospheric Motion Vectors: Impact on HWRF Forecasts of Tropical Cyclone Track and Intensity. *Monthly Weather Review,* 145, 1107-1125.

Venter, G. (1983). Transformed beta and gamma distributions and aggregate losses. *Proceedings of the Casualty Actuarial Society, LXX*.

Venter, G. (2003). Effects of Parameters of Transformed Beta Distributions. Casualty Actuarial Society Winter Forum.

Verbout, S. M., Brooks, H. E., Leslie, L. M., & Schultz, D. M. (2006). Evolution of the U.S. Tornado Database: 1954-2003. *Weather and Forecasting,* 21(1), 86-93.

Wang, B., Luo, X., Yang, Y.-M., Sun, W., Cane, M. A., Cai, W., Yeh, S.-W., & Liu, J. (2019). Historical change of El Niño properties sheds light on future changes of extreme El Niño. *Proceedings of the National Academy of Sciences,* 116(45), 22512-22517.

Wang, W., Xie, P., Yoo, S.-H., Xue, Y., Kumar, A., & Wu, X. (2010). An assessment of the surface climate in the NCEP climate forecast system reanalysis. *Climate Dynamics,* 37, 1601-1620 (2011).

Willis Limited/Willis Re, Inc. (2013). May 2013 Tornadoes in Texas and Oklahoma - Damage Survey Report, June 2013.

Wilson, D. S., Ortega, K. L., & Lakshmanan, K. O. (2009). Evaluating multi-radar, multi-sensor hail diagnosis with high resolution hail reports. *Preprints, 25th Conference on Interactive Information Processing Systems,* Phoenix, AZ, American Meteorological Society, P2.9.

Yeo, S., Leigh, R., & Kuhne, I. (1999). The April 1999 Sydney Hailstorm. *Australian Journal of Emergency Management,* 14(4), 23-25.

About Verisk

Verisk Analytics (Verisk) provides risk modeling solutions that make individuals, businesses, and society more resilient to extreme events. In 1987, a Verisk subsidiary founded the catastrophe modeling industry and today models the risk from natural catastrophes, terrorism, pandemics, casualty catastrophes, and cyber incidents. Insurance, reinsurance, financial, corporate, and government clients rely on Verisk's advanced science, software, and consulting services for catastrophe risk management, insurance-linked securities, longevity modeling, site-specific engineering analyses, and agricultural risk management. Verisk (Nasdaq:VRSK) is headquartered in Jersey City, New Jersey with many offices throughout the United States and around the world. For information on our office locations, visit https://www.verisk.com/about/locations/.

Contact Information

Verisk Analytics
Lafayette City Center, 2nd Floor
Two Avenue de Lafayette
Boston, MA 02111
USA

Tel: (617) 267-6645
Fax: (617) 267-8284

Verisk welcomes feedback on its documentation. If you need assistance in using the software or understanding the information in this document, please email us at DocumentationFeedback@verisk.com.